The Generation of Flexible Antibody Constructs for the Diagnosis and Targeted Treatment of Pancreatic Cancer.

Aoife Crawley B.Sc

A thesis submitted for the degree of Ph.D.

Based on research carried out at the,

School of Biotechnology,

Dublin City University.

Under the supervision of Professor Richard O'Kennedy

and

Dr Michael Freeley (Co-supervisor)

Jan 2019

Declaration

I hereby certify that this material, which I now submit for assessment on the programme of study leading to the award of Ph.D. is entirely my own work, and that I have exercised reasonable care to ensure that the work is original, and does not to the best of my knowledge breach any law of copyright, and has not been taken from the work of others save and to the extent that such work has been cited and acknowledged within the text of my work.

Signed: _____ ID No.:___59508121_____ Date: _____

Dedication

This thesis is dedicated to my Dad and to Shane for their constant optimism and support.

"Do. Or do not. There is no try"- Master Yoda

Acknowledgments

Firstly, I would like to thank Prof. Richard O'Kennedy, his patience support and guidance have made these last four years and this thesis possible. I will never be able to thank him enough for allowing me to stay in the lab until PhD funding finally came through.

To all of the Applied Biochemistry Group who helped me in so many ways and who brazenly stole my supplies every chance they got, if nothing else we made it interesting for each other. To the boys, Johnny, Dan and Ivan, your constant teasing and abuse have prepared me for the outside world so thanks for the thick skin. To Jenny and Arabelle, a special thanks goes out to you two. I could never have done any of this without your help, the endless science advice from Jenny and frantic meetings with Arabelle after to find out if she had any notion what Jenny just said to us, to all the coffees, laughs, panicked texts and most importantly, the memes. This wouldn't have been the same or possible without you two to keep me sane and make it all bearable. I have to give a second thanks to Jen, you went over and beyond to help me in any way that you could. It was so much appreciated and I can never thank you enough!

To my family and my second family the Quinns, while most of you had no clue what I did for the past four years and continually asked me when my exams were you always assured me I could do it and that everything was going to be ok. You always asked about my work and happily listened to my rants even if you could have cared less about the science. I will always be so grateful for the unconditional support.

To my closest friend Ali, thanks for all the trips and girls nights which were a much-needed respite and helped keep me sane.

Finally to Shane, I can't thank you enough. You have been there for me through the entire process and done everything in your power to make it as easy for me as possible. You always believed in me and I will never be able to repay you for all the ways you have supported me over the last four years. None of this would have been possible without you.

List of Figures

Chapter 1

Chapter 2

Chapter 3

Chapter 4

Chapter 5

Chapter 8

List of Tables

Chapter 1

Chapter 2

Chapter 3

Chapter 4

Chapter 5

Chapter 8

Abbreviations:

Ab	–	Antibody
Abs	–	Absorbance
Ag	–	Antigen
ADCC	–	Antibody-dependent-cell-mediated cytotoxicity
AGR2	–	Anterior Gradient 2
bp	–	Base Pair
BM	–	Bone marrow
BMI	–	Body mass index
BSA	–	Bovine serum albumin
BsAb	–	Bispecific antibody
BiTE	–	Bispecific T-Cell Engager
CA 19-9	–	Carbohydrate Antigen 19-9
cDNA	–	Complementary deoxyribonucleic acid
CDR	–	Complementarity-determining region
cfu	–	Colony forming units
CGM	–	Complete growth media
C_H	–	Constant heavy chain of an antibody molecule
C_L	–	Constant light chain of an antibody molecule
conc	–	Concentration
DMSO	–	Dimethyl sulfoxide
DNA	–	Deoxyribonucleic acid
dNTP	–	Deoxyribonucleic triphosphate
DPBS	–	Dulbecco's phosphate buffer
E. coli	–	*Escherichia coli*
EDTA	–	Ethylenediaminetetra-acetic acid
ELISA	–	Enzyme-linked Immunosorbent Assay
Fab	–	Antigen-binding fragment
FACS	–	Fluorescence- Activated Cell Sorting
FBS	–	Fetal Bovine Serum
Fc	–	Constant region of an antibody molecule
FCA	–	Freund's Complete Adjuvant
FDA	–	Food and Drugs Administration

FICA	–	Freund's Incomplete Adjuvant
Fv	–	Fragment variable of an antibody molecule
HRP	–	Horse radish peroxidase
HEK293	–	Human embryonic kidney
IgG	–	Immunoglobulin class G
IHC	–	Immunohistochemistry
IMAC	–	Immobilized Metal Affinity chromatography
IMDM	–	Iscove's Modified Dulbecco's Medium
IMS	–	Industrial Methylated Spirits
IP	–	Immuoprecipitation
IPTG	–	Isopropyl-β-D glactopyranoside
kDA	–	Kilo-dalton
LB	–	Luria broth
Log	–	Logarithmic
mAb	–	Monoclonal antibody
MHC	–	Major Histocompatibility Complex
MOPS	–	(3 (N-Morpholino)) propanesulfonic acid
mRNA	–	Messenger RNA
MSLN	–	Mesothelin
MUC1	–	Mucin 1
MW	–	Molecular Weight
NTA	–	Nitrilotriacetic acid
NK	–	Natural Killer cells
OD	–	Optical Density
O/N	–	Overnight
pAb	–	Polyclonal antibody
PAGE	–	Polyacrylamide gel electrophoresis
PBS	–	Phosphate buffered saline
PBST	–	Phosphate buffered saline Tween
PCR	–	Polymerase chain reaction
PDAC	–	Pancreatic Ductal Adenocarcinoma
PEG	–	Polyethylene glycol
pH	–	Log of the hydrogen ion concentration

POC	–	Point-of-care
PTM	–	Post-translational modification
rAb	–	Recombinant antibody
rBsAb	–	Recombinant bispecific antibody
RNA	–	Ribonucleic acid
RPM	–	Revolutions per minute
RMPI 1640	–	Roswell Park Memorial Institute 1640 Medium
RT	–	Room temperature
SB	–	Super broth
scAb	–	Single-chain antibody fragment
scFv	–	Single-chain fragment variable
SDS	–	Sodium dodecyl sulphate
SOC	–	Super optimal catabolites
SOE	–	Splice-by-overlap-extension
SPR	–	Surface plasmon resonance
T	–	Tween
TCR	–	T-cell receptor
TAA	–	Tumor associated antigen
TAE	–	Tris-acetate-EDTA
TB	–	Terrific broth
TMB	–	Tetramethylbenzidine dihydrochloride
UV	–	Ultraviolet
V_H	–	Variable Heavy chain of an antibody molecule
V_L	–	Variable Light chain of an antibody molecule
V	–	Volume
WB	–	Western Blot
WHO	–	World Health Organisation
	–	

Units:

µg	–	Microgram
µL	–	Microliter
µM	–	Micromoles
(k)Da	–	(kilo) Dalton
°C	–	Degrees Celsius
cm	–	Centimetre
g	–	Gram
kg	–	Kilogram
L	–	Litre
m	–	Metre
M	–	Molar
mg	–	Milligram
min	–	Minute
mL	–	Millilitre
mm	–	Millimetre
nM	–	Nano-molar
pg	–	Pictogram
rpm	–	Revolutions per minute
RU	–	Response Units
Sec	–	Seconds
V	–	Volts
v/v	–	Volume per unit volume
x *g*	–	Centrifugal force expressed in units of gravity
w/v	–	Weight per unit volume

Publications and presentations:

Presentations:

Crawley, A., O'Kennedy, R. (2015) The Generation of Flexible Antibodies for the Diagnosis and Targeted Therapy of Pancreatic Cancer (Pa). The School of Biotechnology. Dublin City University. Friday 30th of January 2015.

Crawley, A., O'Kennedy, R. (2015) The Generation of Flexible Antibodies for the Diagnosis and Targeted Therapy of Pancreatic Cancer (Pa). Biomedical Diagnostic Institute (BDI). Thursday 18th of December 2015.

Crawley, A., O'Kennedy, R. (2016) Generating recombinant anti-AGR2 antibodies for the improved targeted treatment of pancreatic cancer. The School of Biotechnology. Dublin City University. Friday 29th of January 2016.

Crawley, A., O'Kennedy, R. (2016) The Generation of an anti-AGR2 x CD3ε bispecific T-cell engager (BiTE) for the targeted therapy of pancreatic cancer (Pa). PEGs Europe, Epic SANA Hotel, Lisbon, Portugal. 3rd-4th of November 2016.

Crawley, A., O'Kennedy, R. (2017) The Generation of a bispecific T-cell engager (BiTE) for the targeted therapy of pancreatic cancer (Pa). The School of Biotechnology. Dublin City University. Friday 27th of January 2017.

Crawley, A., O'Kennedy, R. (2018) Construction of a Bispecific T-cell Engager. The School of Biotechnology. Dublin City University. Friday 26th of January 2018.

Publications:

Crawley, A., O'Kennedy, R. (2015) The need for effective Pancreatic Cancer detection/ management – A biomarker-based strategy. *Expert Rev Mol Diagn.* **15** (10), 1339-1353.

Murphy, C., Byrne, H., **Crawley, A.,** Kara Moran, Fitzgerald, J., O'Kennedy, R. (2017) Optical Signal Transduction with an Emphasis on the Application of Surface Plasmon

Resonance (SPR) in Antibody Characterization: Development, Applications and Future Trends. *Pan Stanford Publishing Pte. Ltd.* 1st Edition, Chapter 11, 125- 149.

Sharma, S., **Crawley, A.,** O'Kennedy, R. (2017) Strategies for overcoming challenges for decentralised diagnostics in resource-limited and catastrophe settings. *Expert Rev Mol Diagn.* **17,** 109-118.

McPartlin, D., Loftus, J., **Crawley, A.,** Silke, J., Murphy, C., O'Kennedy, R. (2017) Biosensors for the monitoring of harmful algal blooms. *Curr Opin Biotechnol.* **45,** 164-169.

O'Kennedy., R., Fitzgerald, J., Cassedy, A., **Crawley, A.,** Zhang X., Carrara, S. (2018) Applications of Antibodies in Microfluidics-based Analytical Systems: Challenges and Strategies for Success. *J. Micromechanics Microengineering.* **28** (6), 1-13.

Hayes, B., Murphy, C., **Crawley, A.,** O'Kennedy, R. (2018) Developments in Point-of-Care Diagnostic Technology for Cancer Detection. *Diagnostics.* **8** (2) 39; doi:10.3390/diganostics8020039. *This publication was chosen as the cover for /Diagnostics/, Volume 8, Issue 2 June 2018. A cover image was designed and published , see appendix A .*

Crawley, A., Fitzgerald, J., O'Kennedy, R. (2018) The use of a flexible method for the creation of an anti-HER2 x anti-CD3ε Bispecific T-cell Engager (BiTE). (Manuscript currently under review).

Conferences, Courses Attended and Scholarships

PROSENSE 2013. Dublin City University, Dublin Ireland. (2^{nd}-4^{th} July, 2013)

Laboratory Animal Science and Training (LAST) Animal Handling Training Course for Ireland and UK License. Trinity College Dublin, Ireland. (17^{th} -18^{th} June, 2014).

GS601: IP and Commercialisation – BioAT module. Dublin City University, Dublin Ireland (December, 2014 – February, 2015)

BE532: Introduction to Proteomics and Mass Spectrometry– BioAT module. Dublin City University, Dublin Ireland (19^{th} -20^{Th} February, 2015)

BioAT Writing Module with Claire O'Connell. Dublin City University, Dublin Ireland (February – March, 2016)

Irish Research Council 2014 Government of Ireland Postgraduate Scholarship Scheme (Science, Technology, Engineering & Mathematics (STEM)) 48-Month Structured PhD Scholarship Recipient, Dublin City University. (October, 2014)

PEGs Europe 2016. Epic SANA Hotel , Lisbon, Portugal (2^{nd} – 4^{th} November, 2016)

Abstract

The Generation of Flexible Antibody Constructs for the Diagnosis and Targeted Treatment of Pancreatic Cancer.

Aoife Crawley

This research project exploits the design flexibility of recombinant antibodies (rAbs) coupled with selective biomarkers to improve diagnosis and treatment approaches of the most common pancreatic cancer, known as pancreatic ductal adenocarcinoma (PDAC). PDAC is a malignancy with almost a 100% mortality rate, as a result of resistance to chemotherapy and very inadequate diagnostic methods. A panel of recombinant scFv antibody fragments, specific for the selected biomarkers, anterior gradient 2 (AGR2), mesothelin (MSLN), and mucin 1 (MUC1) were generated for use to improve the diagnosis of PDAC. Additionally, a bispecific T-cell engager was created for potential targeted treatment.

Initially, a murine-derived Capan-1 specific scFv library with a serum antibody titre of 1/200,000 was generated, following immunisation with the pancreatic cancer cell line, Capan-1, which expressed the biomarkers of interest. Library screening was carried out using MSLN expressed in HEK293 cells, following transfection with a MSLN-containing plasmid, and a MSLN-specific scFv was successfully isolated. The resulting scFv were characterised as a immunohistochemistry-based antibodies for the detection of MSLN in tumour tissue and found to have a working concentration of 1/500 when analysed by western and dot blots.

The human naïve library, Tomlinson I and J, was employed for the isolation of scFv specific to MUC1 and AGR2. Functional specific scFv for both antigens were found through panning with purified MUC1 and AGR2 proteins.

A CD3ε-specific scFv with a limit of detection of 20 pg/mL was isolated from an available library derived from an appropriately immunised avian host.

A bispecific T-cell engager (BiTE) was constructed using the anti-CD3ε scFv and a previously generated anti-HER2 scFv with the ability to detect down to 10pg/mL of HER2 in human serum. Two proof-of-concept methods of BiTE construction, employing PCR and cloning techniques are described. The binding abilities of the BiTE to each antigen individual and in dual format was evaluated. The generated BiTE successfully showed the ability to bind to both antigens simultaneously in ELISA format .

Chapter 1

Introduction

1.1 Introduction to Antibodies

Antibodies are a class of glycoproteins that are created by the body's immune system as defence against invading foreign objects such as bacteria and viruses. They are also known as immunoglobulins (Ig) and are produced by plasmocytes in order to attack, eliminate and destroy/neutralize invading pathogens. The general structure of an Ig consists of four polypeptide chains held together by disulphide bonds that form a "Y"-shaped molecule. These four chains are composed of two sets of identical chains, the heavy chains and the light chains. An antibody can have one of two types of light chains; kappa (κ) or lambda (λ) and the heavy chain can be of 5 different classes, IgA/M/D/E/G, the most common of which is an IgG (***Figure 1.1***). Structurally, the light chains of an IgG are composed of a variable region and a constant region and the heavy chain is composed of a variable domain and three constant domains (Janeway *et al.,* 1999).

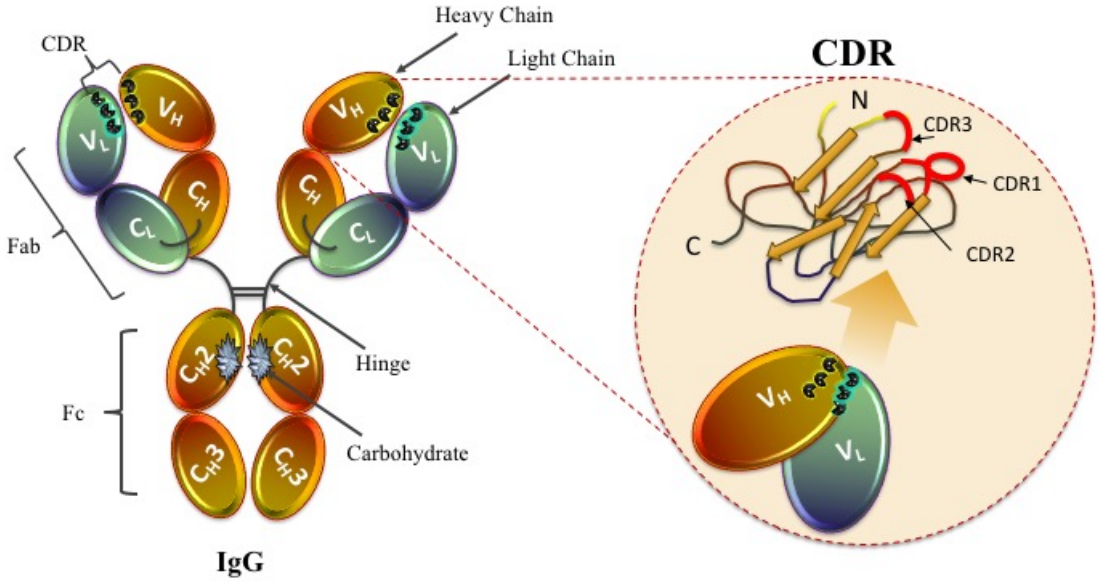

Figure 1.1 Diagrammatic representation of a full IgG antibody

An IgG antibody is composed of beta proteins consisting of four polypeptide chains, two known as the heavy and two termed the light chains that are linked by disulphide bonds. Each polypeptide chain possesses variable V_H and V_L regions. Within these variable domains is the CDR regions that confer the specificity of the antibody for a particular antigen. It is within this site that the antigen-antibody binding event occurs. There are six hypervariable loops in the variable domains, three within the light and three within the heavy chain. The conserved framework β-sheets support these hypervariable loops which when folded are brought together to create the antigen binding site (Sela-Culang et al., 2013).

1.2 Antibody structure

Antibodies are extremely diverse, achieved through unique genetic mechanisms (simplified in ***Figure 1.2***) and can bind to almost an infinite number of antigens. The variable regions house the complimentary-determining regions (CDR) where there is the greatest variability. They are responsible for the recognition of foreign invaders as they form regions that are complementary to the structure of the antigen epitopes (Conroy *et al.,* 2009). The variation in the amino acid sequence within the CDR confers the antigen specificity. In particular, the CDRH3 shows the greatest variability and so, in combination with the CDRL3, is the most significant region for determining an antibody's specificity and affinity. While somatic recombination shown below, is known to be responsible for the diversity of the antibodies generated, there are not enough variable regions to account for the almost unlimited diversity noted of antibodies. Further diversity is achieved by new nucleotides being added during VDJ recombination. The gene segments are flanked by motifs known as the recombination signal sequences (RSS) which are either 12 or 23 base pairs. Recombination can only occur between a 12 and a 23 bp motif, known as the 12/23 rule. These motifs are bound and brought together by RAG recombinase (Parkinson *et al.,* 2015). Furthermore, additional mutations are added by the enzyme activated-induced cytidine deaminase (AID). Cumulatively, these mechanisms are responsible for antibodies to generated against a diverse range of antigens. The Fc region, separated from the Fab region by a flexible 'hinge' region, consists of the three constant heavy regions and is essential for mediating effector functions. These include, the complement system, antibody-dependent phagocytosis and antibody-dependent cell-mediated cytotoxicity (ADCC). This region is mostly conserved with only small variations found between classes.

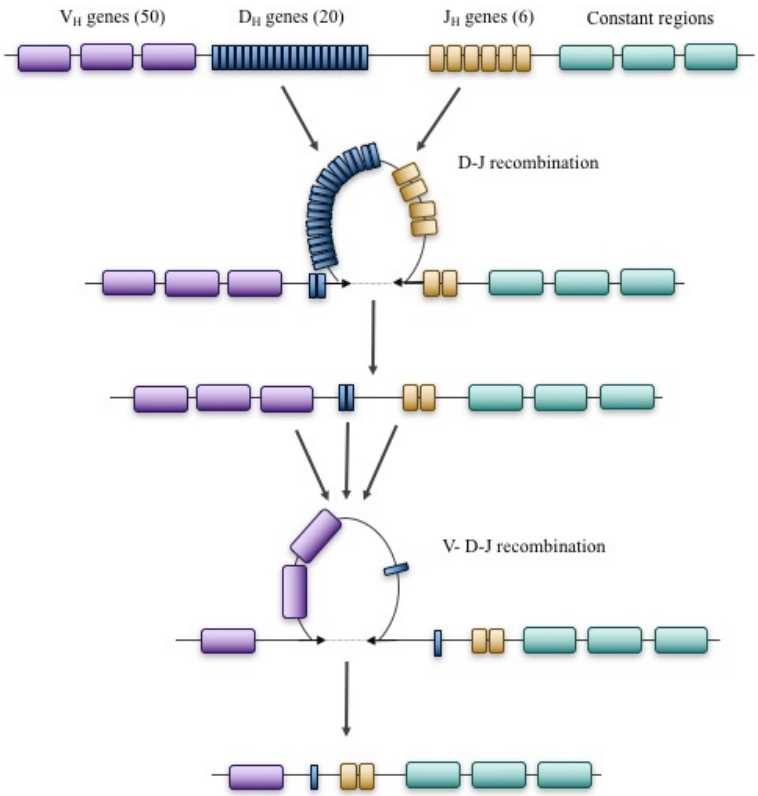

Figure 1.2 Simplistic schematic representation of the recombination events that facilitate antibody diversity.

V(D)J recombination is the process whereby antibodies acquire their diversity. It occurs during B-cell development and results in a highly diverse repertoire of immunoglobulins. Both the H-chain and the L-chain are encoded by the variable and joining gene segments, however, the H-chain is also encoded by the diversity gene segments. During this process, one variable heavy gene is randomly selected along with one diversity gene and one constant gene for translocation. Subsequently for the L-chain, a κ or λ gene group is selected with one variable and one joining gene for translocation. Initially, the diversity and joining regions are brought into close contact and the DNA intervening is looped out and the remaining termini are re-joined. The process is repeated and the variable regions undergo recombination with the D-J regions with intervening DNA being precisely removed. These steps determine the specificity of the antibody and the constant domains control the class/isotype of the antibody (Sadofsky, 2001; Stengel et al., 2017).

Due to the almost unlimited antigen detection capacity of antibodies they are now used for a wide range of applications, from disease therapeutics and diagnostics, to standard use in immunoassay detection techniques. Such immunoassays are very sensitive,

specific and robust. The only limitation is the availability of high quality antibodies. Köhler and Milstein reported the first method of generating monoclonal antibodies in 1975. This hybridoma technology produced monoclonal antibodies of a defined specificity in large quantities by immortalizing the antibody-producing cells by fusing them with tumour cells (Köhler and Milstein, 1975). While much success was achieved with this method, as seen with the first anti-tumour mAb, rituximab, over time the limitations of monoclonal antibodies were uncovered (Chames *et al.,* 2009; Coulson *et al.,* 2014). Most importantly, their clinical applications were hindered by their murine origin, which resulted in a human anti-mouse antibody (HAMA) response (Ahmad *et al.,* 2012). They also suffered from drawbacks such as, short serum half-life, insufficient activation of human effector functions and competition with circulating IgG (Laffly *et al.,* 2005; Chames *et al.,* 2009). In order to improve the specificity and immunogenicity of antibodies and to achieve design flexibility tailored to specific needs, recombinant antibodies were produced by genetic engineering techniques.

1.3 Recombinant antibodies (rAb)

The engineering of antibodies facilitates the generation of antibody fragments of a desired size that have a defined single or dual specificity and affinity towards target molecules. The extensive design flexibility associated with rAbs allows alterations to all aspects of the antibody such as, size, affinity and specificity and they can be generated from a variety of species such as mice, rabbits, and chickens. These antibodies can be generated either by amplifying the variable domains from the cDNA of an immunised source or by directly cloning the variable regions from a monoclonal antibody-producing hybridoma cell. These recombinant antibodies vary in size but the smallest fragment that retains operational binding ability is a single chain variable fragment (scFv). This is comprised of the V_L and V_H domains connected by a glycine-serine linker $(Gly_4Ser)_3$ and is ~30kDa in size. The linker peptide has a hydrophilic sequence incorporated to eliminate any intercalation that may occur between the variable regions or during the folding of the protein (Ahmad *et al.,* 2012; Vu *et al.,* 2017). A wide variety of recombinant antibody formats exist, however, this research focuses on the scFv format (***Figure 1.3***).

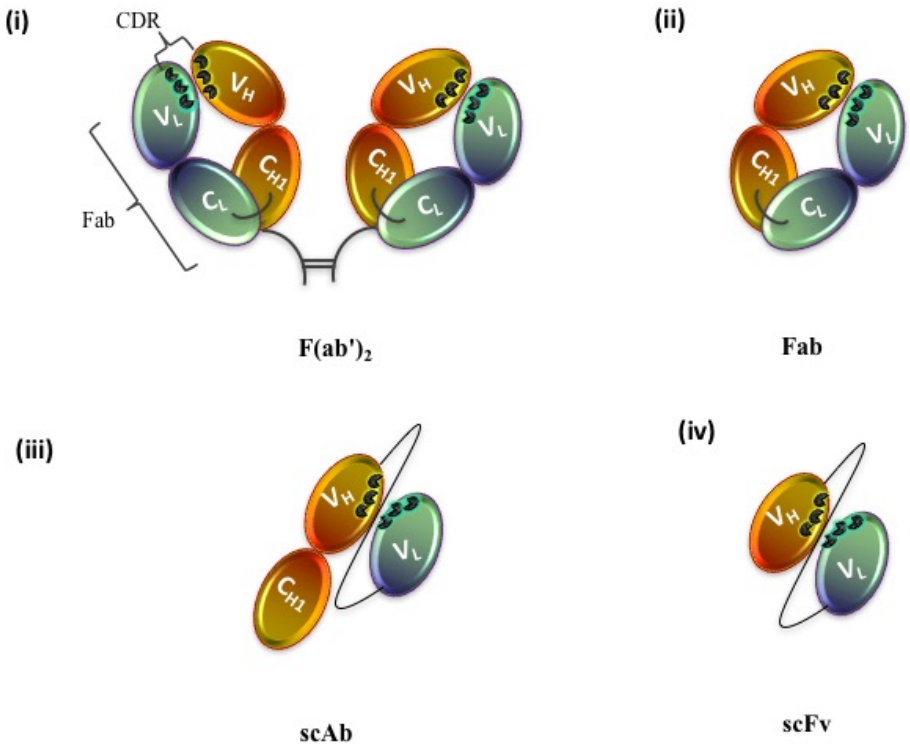

Figure 1.3 Diagrammatic representations of various recombinant antibody formats. ***(i)*** *F(ab')$_2$ is composed of two antigen binding Fab that are linked by disulfide bonds.* ***(ii)*** *Fragment antigen binding (Fab) is the binding region of an antibody made up of a constant and variable domain of the heavy and light chains.* ***(iii)*** *A single-chain antibody (scAb) is an scFv with an additional constant region from the heavy chain.* ***(iv)*** *A single-chain variable fragment (scFv) is a fusion protein that links the variable heavy and light chain with a flexible linker*

Recombinant antibody technology has allowed for a reduction in antibody size while retaining the antigen binding site and thus the antibody affinity and specificity for a given antigen. The smaller size confers numerous advantages clinically, such as superior tumour penetration, reduced immunogenicity and faster blood clearance. In particular, the smaller recombinant antibody fragments are applicable for cancer treatments as they allow an even and rapid penetration to tumours and their microenvironments. Additionally, their reduced size results in more rapid blood clearance and thus are applicable for coupling with drugs, that if retained, could be damaging to surrounding healthy tissue (Ahmad *et al.,* 2012). Conversely, this small molecular mass is concurrently a disadvantage, in that it results in rapid elimination from the body . Another substantial application of recombinant antibodies is as diagnostic reagents. Specifically

designed scFv antibodies can be generated against an almost infinite amount of proteins, and as such renders them incredibly useful in the detection of a large variety of diseases.

1.3.1 Bispecific Antibodies

Bispecific antibody (bsAb) formats may be able to overcome many of the issues associated with the use of monoclonal antibodies as therapeutic agents due to their ability to target a variety of entities directly to cancer cells. Notably, in the last 10 years, two bsAbs were approved for therapeutic use, catumaxomab in 2009 and blinatumomab in 2014. It is predicted that by the year 2024, the market of BsAbs will grow by $5.8 billion per year (Sedykh *et al.,* 2018). Using bsAbs to direct effector cells to cancer cells was originally demonstrated in the 1980's, with clinical studies emerging in the early 90's. However, there were difficulties in producing large volumes of homogenous bsAb. There are three techniques for generating bsAb; (i) chemical conjugation of antibodies with different specificities, (ii) fusion of hydridomas and (iii) use of molecular approaches to engineer the required antibody-derived structures. Chemical conjugation relies on oxidative re-association but this was found to be inefficient. Current methods focus on the use of the homo- or hetero-bifunctional crosslinking reagents. The fusion of two hybridoma cell lines produces a hybrid-hybridoma (See ***Figure 1.4***), which secretes heterogeneous antibodies in addition to the required bispecific antibody (Kontermann, 2012; Byrne *et al.,* 2013). BsAb produced by methods (i) and (ii) had a number of issues such as batch-to-batch variation and difficulties in large-scale production.

Recombinant techniques, created by advancements in protein engineering, allowed for the generation of many formats of bsAb that overcame the shortcomings of methods (i) and (ii). The ability of bsAbs to bind simultaneously to an antigen of interest and a detection moiety makes them excellent candidates as immunoprobes in diagnostics assays while their ability to bind simultaneously to an antigen of interest on tumour cells and to effector cells renders them ideal as therapeutic agents (Nolan and O'Kennedy, 1990). Certain bsAb formats have the ability to induce cytotoxicity and phagocytosis and deliver therapeutic molecules such as drugs to tumour cells. Numerous bispecific formats can now be generated including diabodies and tetrabodies, with the majority of current studies focusing on the BiTE, homodimeric 'knob-in-hole' Abs and trifunctional BsAbs formats (Byrne *et al.,* 2013; Sedykh *et al.,* 2018). The research described in this thesis focuses on the bsAb format known as a bispecific T-cell engager (BiTE).

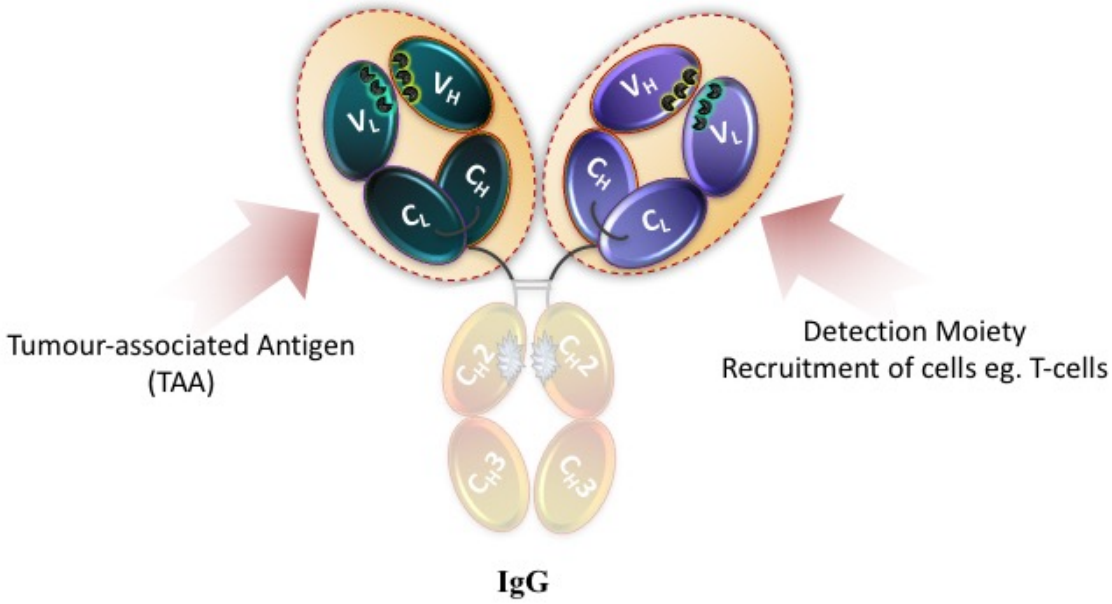

Figure 1.4 An IgG bispecific antibody.

The antibody has two arms with specificities to two different antigens. In addition to its ability to bind to two antigens, a bispecific antibody may be bifunctional, with each arm conferring a different function. For example, as a diagnostic antibody, one arm may be specific to an antigen on a cancer cell while the other binds to a detection enzyme or label. Therapeutically, one arm may be specific for a tumour associated antigen (TAA) while the other is to a T-cell or another effector cell surface marker.

1.3.2 Bispecific T-cell engager (BiTE)

Cytotoxic T-cells are potent killer cells of the immune system. They possess many desirable qualities sought after for cancer therapeutics as they are abundant, infiltrate tumours, proliferate once activated and have the capability to kill more than once. Markers on T-cells are desirable targets for bispecific antibody therapeutics as the 'normal' anti-tumour response of T-cells is often insufficient as cancer cells have the ability to evade T-cell mechanisms (Stieglmaier *et al.,* 2015). BsAbs have been developed to promote destruction of tumor cells by antigen binding against the CD3 receptor (Sedykh *et al.,* 2018). A bispecific T-cell engager is a tandem scFv (~55-60kDa) made by fusing an anti-CD3 scFv to an anti-tumour associated antigen (TAA) scFv using a five-residue peptide linker (GGGGS). The BiTE provides a strategy for targeted killing of tumor cells by directly linking T-cells to the tumor cells (Papayannidis and Martinelli, 2017). The small size of the BiTE ensures that the T-cell is in close proximity to the target

tumour cell. The linker facilitates the free rotation of the two arms and forms a link between the T-cell and the TAA. Once the link between the T-cell and tumour cell is achieved the immunological synapse is formed. This induces the T-cell to release proteins, such as perforins and granzymes, which enter the tumour cell and ultimately cause apoptosis. This activation is independent of the presence of MHC I or any co-stimulation (Yuraszeck *et al.,* 2017) (***Figure 1.5***).

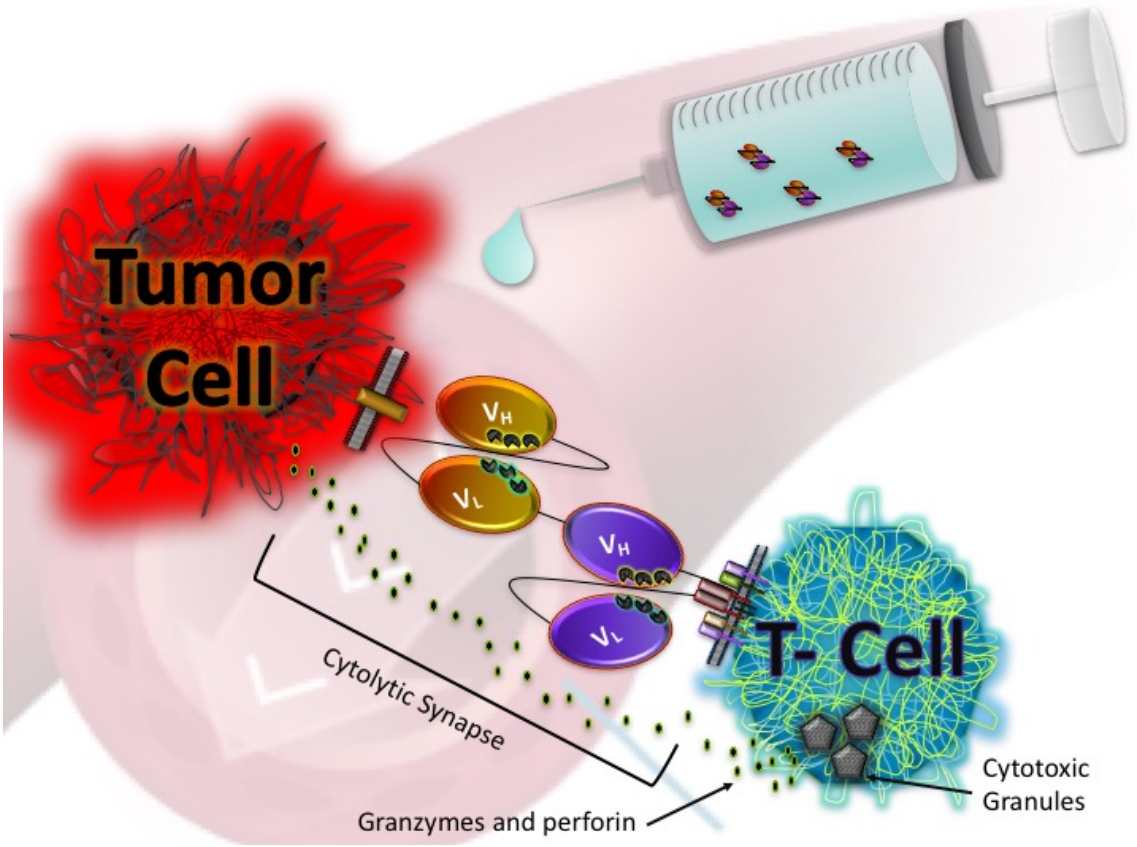

Figure 1.5 The mechanism of action of a BiTE.

The BiTE directs the T-cell to the tumour cell through binding to a TAA on the tumour cell. This results in activation of the T-cell without co-stimulation and produces a cytolytic synapse between the two cells. In turn, the cytolytic granules in the activated T-cell result in the production and release of granzymes and perforin, subsequently causing cell lysis of the tumour cell and ultimately cell death.

The potential for these antibodies was demonstrated in the early 1990's, when a tandem scFv targeting EpCAM and CD3 was developed, as was an anti-CD19xCD3 antibody. Over the years, remarkable data on the properties of BiTEs have accumulated. Impressively, only a very low concentration of BiTE is required to induce tumour cell lysis and research into the effector to target ratio has indicated that BiTEs can kill more

than once (Chames *et al.,* 2009). The first BiTE that was approved by the US FDA was blinatumomab, which targets CD19, expressed on B-cells, both healthy and neoplastic (Papayannidis and Martinelli, 2017; Krishnamurthy and Jimeno, 2018). A shortcoming of blinatumomab is a short half-life of approximately 2 hours, which prevented uninterrupted drug exposure. This issue was circumvented by continuous intravenous administration of the drug (Stieglmaier *et al.,* 2015). Other work, carried out by Goyos *et al,* (2018), presented work on a B-cell maturation antigen (BCMA) half-life extended (HLE)- BiTE that indicated a weekly dose was suitable in mouse xenografts and non-human primates for potent and effective induction of cytotoxicity of target cells. Consequently this BiTE is under evaluation in humans. The tumor targeting properties of BiTEs was investigated by labelling the AMG211 BiTE, which binds to CEA and CD3, with zirconium-89. The study successfully illustrated AMG211 *in vivo* behaviour for tumor targeting and localisation in mice with CEA+ xenografts (Waaijer *et al.,* 2018).

To date, a variety of BiTEs have been developed that are currently in various stages of clinical trials (***Table 1.1***). Moreover, BiTEs have even been employed for treatment of other diseases with promising results. For example, a study by Brozy *et al,* (2018) recently used a BiTE construct for targeting HIV. The results indicated the possible therapeutic and curative potential of a BiTE for HIV treatment as data obtained illustrated inhibition of HIV by the administered BiTE. BiTEs represent a therapeutic approach that can produce a level of precision that the standard chemotherapy or radiotherapy is unable to achieve. As PDAC often responds poorly to chemotherapy, a BiTE is an attractive alternative approach. A promising study has been performed showing the potential of the BiTE antibody as a targeted therapy for PDAC. A BiTE that binds to MSLN and CD3 (MG1122) was developed and the *in vivo* functions of the antibody analysed. This work showed the BiTE successfully activated T-cells in the presence of tumor cells expressing MSLN and effectively resulted in the death of these cells when tested using human PDAC cell lines (Park *et al.,* 2018).

Table 1.1: Examples of BiTEs as cancer therapeutics currently in clinical development

	Antigen	*Target Disease*	*Reference*
Blinatumomab (AMG 103/ MT103)	CD19	B-cell malignancies / Leukemia	Krishnamurthy and Jimeno, 2018
AMG 330	CD33	Myeloid Leukemia / Acute non-lymphoblastic Leukemia	Trivedi *et al.,* 2017
AMG 211/ MT111	CEA	Colorectal cancer / Gastrointestinal adenocarcinoma	Trivedi *et al.,* 2017
BAY2010112, AMG 212	PSMA	Prostate neoplasms	Trivedi *et al.,* 2017
Solitomab (AMG 110/ MT110)	EpCAM	Epithelial-derived neoplasms / Solid tumours	Huehls *et al.,*2015
bscEphA2 x CD3	HER2/EphA2	Multiple solid tumours	Huehls *et al.,* 2015
MCSP-BiTE	MCSP	Melanoma	Huehls *et al.,*, 2015
A300E	ADAM17/PSCA	Prostate cancer	Huehls *et al.,*2015

1.4 Antibody Phage display

A particular challenge in producing recombinant antibodies is the selection process, to isolate and enrich antigen-specific antibody fragments from a large repertoire of non-functional and non-specific antibody fragments. Phage display is a technique that was developed by George Smith (Smith, 1985) and has evolved into the most effective method for the display and selection of recombinant antibodies (Smith, 1985; Bazan *et al.,* 2012; Rami *et al.,* 2017). This molecular diversity technique employs non-lytic filamentous bacteriophage to present ligands on the surface of their phage coat. The technology is based on the fact that phage phenotype and genotype are linked. As the antibody genes are fused to the phage genes this results in the expression of the antibody on the phage surface as a functional protein (Pansri *et al.,* 2009; Hammers and Stanley, 2014). The overall aim of the approach is to select and isolate phage that display antibodies of high affinity binding to the antigen of interest and to remove any non-specific binders. Panning by phage display can isolate significant and rare clones from a large library repertoire (Ahmad *et al.,* 2012). Phage display is advantageous in that it has the ability to screen multiple clones easily. It can screen up to 10^{12} phage to select those with the desired antigen binding capacity. However, it is not without limitations in that it is a complicated and time-consuming procedure. Additionally, the phage library may not fully represent the full repertoire of antibodies due to issues with phage assembly and earlier complications such as poor RNA recovery and sub-optimal construction of the DNA library (Hammers *et al.,* 2014).

Simply put, the phage display technique is based on ligation of the PCR products into the phagemid vector (a plasmid containing a phage-derived origin of replication in addition to its plasmid of origin replication), repeated rounds of selection against a specific antigen is performed, followed by phage propagation. Phagemids, such as the pComb3X, contain the required packaging signal and cloning sites and have high transformation efficiencies, beneficial for generating large antibody repertoires (***Figure 1.6 (i)***). These phagemids consist of DNA encoding an scFv, which is fused to the gene that encodes the phage proteins pIII or pVIII (***Figure 1.6 (ii)***). The vector also includes necessary features such as antibiotic resistance, an origin of replication, a promoter region and affinity tags like poly-histidine for use in subsequent antibody purification. However, the phagemid does not encode all of the necessary genes for full bacteriophage replication and, therefore,

helper phage, such as M13K07, is added to supply the missing structural proteins (Hammers *et al.,* 2014; Rami *et al.,* 2017).

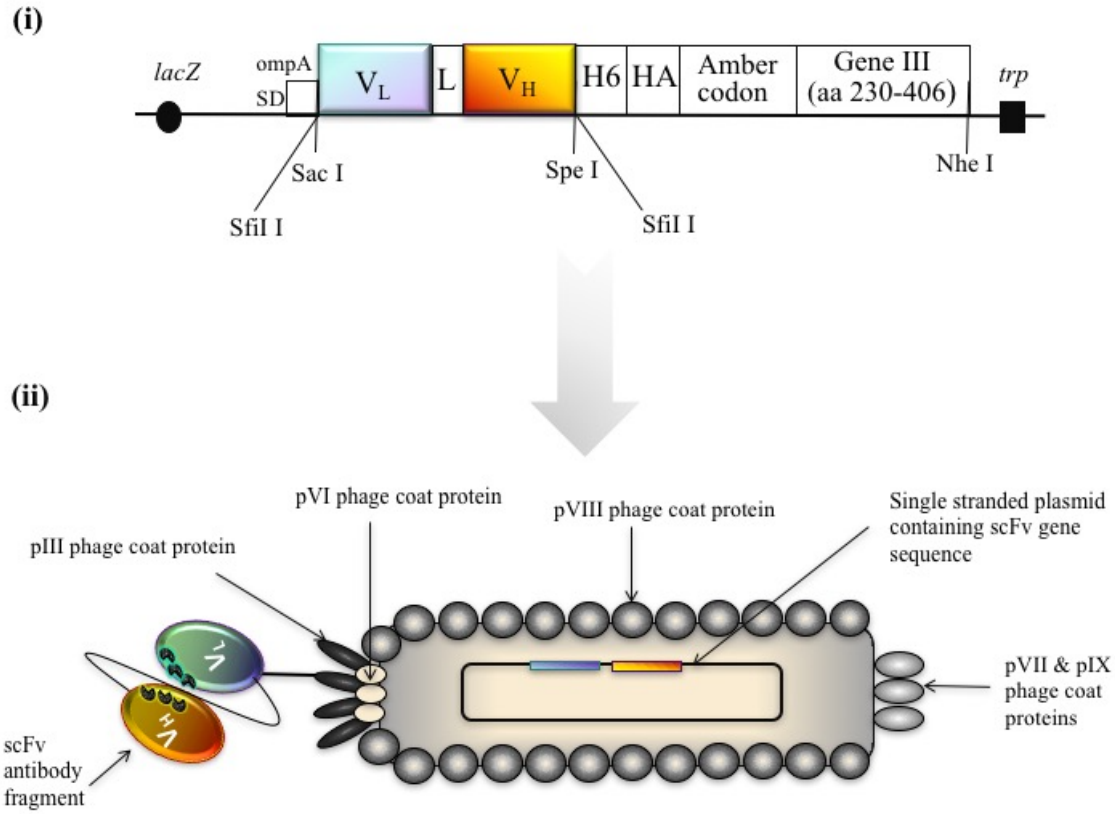

Figure 1.6 The pComb3XSS phagemid vector and expression of an scFv protein on a filamentous phage

(i) Map of the pComb3 phagemid vector. *The lacZ promoter allows for the expression of the heavy and the light chains of the antibody. The Shine Dalgarno (SD) is a ribosome-binding sequence that initiates protein synthesis. The leader sequence ompA directs the expression of the antibody and fusion gene III protein coat. The amber codon is present between the 3' SfiI restriction site and the 5' end of the gene III which permits soluble protein expression in non-suppressor strains of bacteria. The SfiI sites allow for directional cloning of the protein for phage display. The six-histidine tag allows for purification and the HA tag can be used for detection using an anti-HA antibody. The terminator trp provides transcription termination (Andris-Widhopf et al., 2000). Full pComb3XSS vector map can be found in Appendix C.* ***(ii) Representation of the filamentous phage structure****. PIII, PVIII, PVII and PIX are the proteins of the phage coat. The scFv is displayed on the PIII/PVII (Barbas et al., 2001).*

1.4.1 Panning of antibody phage display libraries

Panning is a cyclic affinity selection technique, performed on antibodies expressed on filamentous phage, for the selection and isolation of antigen-specific clones. It consists of multiple rounds of filamentous phage binding to an immobilised antigen, followed by, washing, elution, re-infection and subsequent re-amplification of the antigen binding phage. The selection process is outlined in ***Figure 1.7.*** Generally 3 to 5 rounds of selection are required to obtain highly specific binding clones (Hammers *et al.,* 2014).

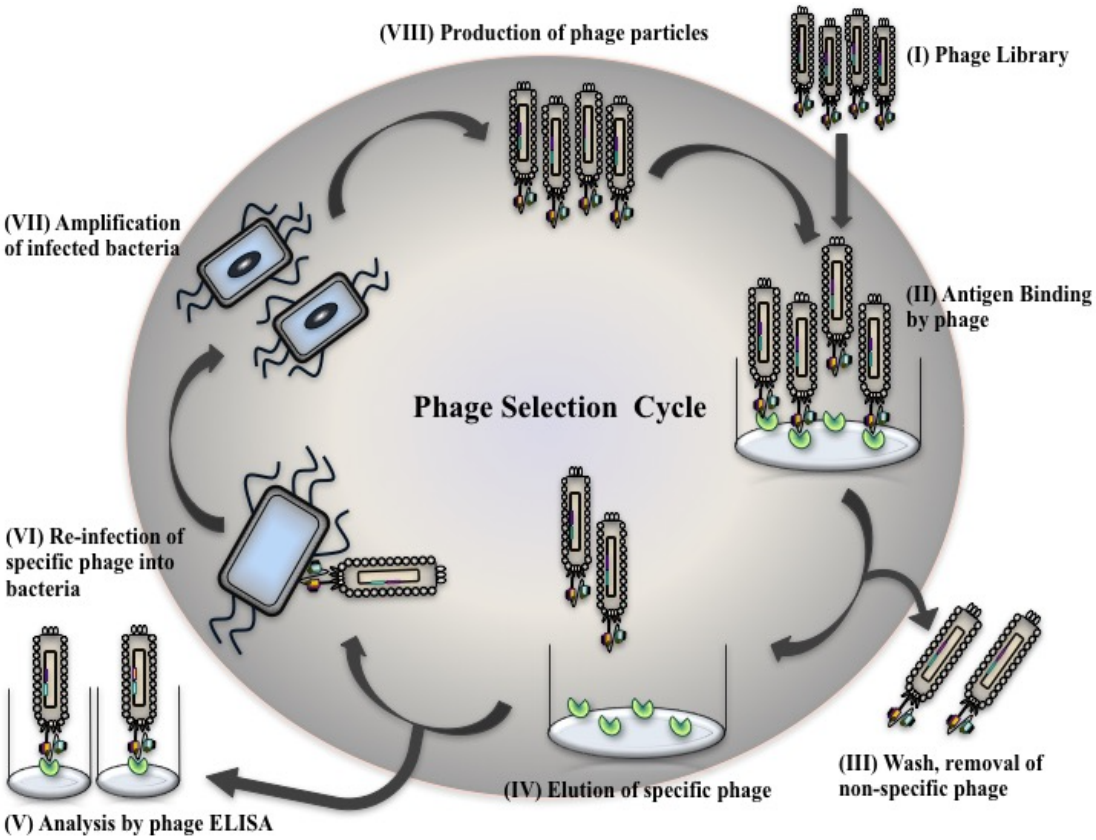

Figure 1.7 A schematic of the phage display cycle for panning of an antibody library*. There are a variety of steps involved in this process; (I) The construction of the phage library; (II) Binding of the phage to the target antigen that is immobilised onto an immunotube/ 96-well plate; (III) Removing unbound phage through washing; (IV) Recovering of antigen-specific phage; (V) Analysis of antigen-specific phage via ELISA; (VI) Re-infection of specific-phage into bacteria; (VII) Amplification of antigen-specific phage by infection of E. coli and; (VIII) Production of enriched phage against the specific target.*

The specific phage are then solubly expressed by infection into a non-suppressor *E. coli* strain, such as Top10F, to allow the scFv to be secreted without the phage particle. The phage pools from each round of panning are tested by ELISA, whereby the phage are detected by an antibody directed against the major capsid protein. Screening of the enriched library is then carried out by analysing single colonies to determine each clone's specificity in a monoclonal ELISA. This process is employed numerous times throughout the work described in this thesis to isolate antibodies for applications in the diagnosis and treatment of pancreatic cancer .

1.5 Introduction to Pancreatic Cancer

The pancreas is an organ that has both endocrine and exocrine functions and is involved in the digestion and maintenance of blood sugar levels (***Figure 1.8***). It is well known that cancers associated with the pancreas are infamously chemoresistant with very short survival time expectations. Pancreatic cancer is a potentially lethal malignancy with a 5-year survival rate of less than 9%, of which the most common form is pancreatic ductal adenocarcinoma (PDAC) (~90% of cases) (Güngör *et al.,* 2014; Xu *et al.,* 2014; Kenner, 2018). It is one of the most aggressive solid malignancies (Wang *et al.,* 2017). Approximately 15-20% of patients present with resectable cancer and undergo pancreatectomy as a curative treatment, whilst 53% present with metastatic disease (Jazieh *et al.,* 2014; Goel *et al.,* 2015; Spadi *et al.,* 2016). Unfortunately, many who have undergone surgery will suffer from further metastasis (about half within the first year) accounting for the high mortality rate (Bissolati *et al.,* 2015). While it has a relatively low incidence rate, PDAC is the 4th leading cause of cancer-related deaths in the US, resulting in almost 40,000 annually, with proportional numbers recorded in most developed countries (Fong *et al.,* 2012; Siegel *et al.,* 2014; Li *et al.,* 2015; Kikuyama *et al.,* 2018). Numbers of deaths from pancreatic cancer across Europe and the US for 2020 are estimated at 146,063 (Klein *et al.,* 2018). This disease is infamous for its poor outcomes due to delayed diagnosis, absence of highly effective screening methods, disease aggression and therapeutic resistance (Goel *et al.,* 2015).

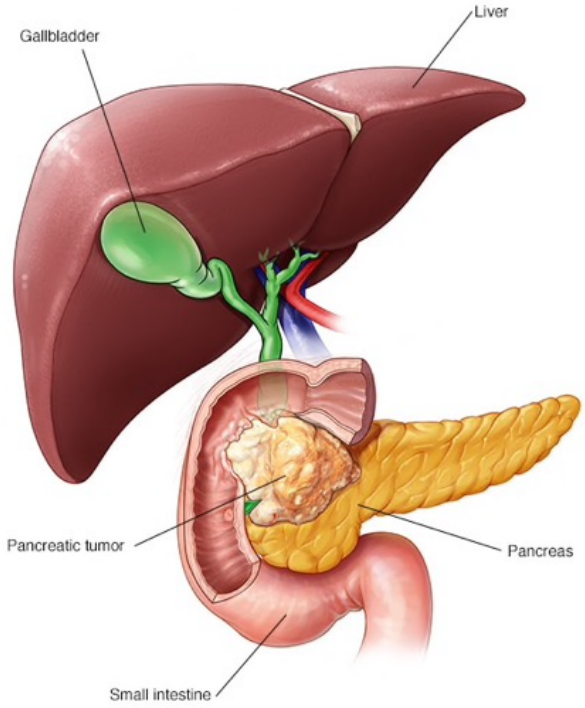

Figure 1.8 Illustration of the location of the pancreas with an associated tumor

The pancreas is approximately 6 inches long and is located within the abdomen lying horizontally behind the stomach. The head of the pancreas is connected via the pancreatic duct to the duodenum, which is a section of the small intestine. The pancreas has both endocrine and exocrine functions. The endocrine portion is composed of islet of Langerhans that secretes numerous hormones for regulation of blood sugar (Gittes, 2009). The exocrine portion of the pancreas is approximately 85% percent of the organ which aids in digestion. Picture taken from : https://www.mayoclinic.org/diseases-conditions/pancreatic-cancer/symptoms-causes/syc-20355421

The objective of this research was to generate a variety of pancreatic cancer-specific recombinant antibodies (rAbs) to improve the diagnosis and treatment of pancreatic cancer. The following sections will describe, in-depth, the issues surrounding the current methods of pancreatic cancer detection and treatment and how exploiting rAbs could alleviate these problems.

1.6 PDAC-associated risk factors

PDAC is an age-dependent disease with incidence levels growing due to the increasing life longevity. However, this disease has numerous environmental and hereditary risk factors. The most common PDAC-associated risk is smoking which is attributed to almost

25% of cases. Smokers have a 2.2-fold increased risk of developing PDAC over non-smokers (Wang *et al.,* 2014; Andersson *et al.,* 2016; Maisonneuve and Lowenfels, 2018). Additional environmental and lifestyle factors include occupational exposures, heavy alcohol intake, pancreatitis, poor diet, ABO blood type, increased BMI, infection with hepatitis B/C and type-2 diabetes (which is also a potential early sign of PDAC onset) (Fiorino *et al.,* 2013; Wolfgang *et al.,* 2013; Liu *et al.,* 2018). Interestingly, about 5-10% of pancreatic cancers occur as a result of genetic susceptibility (Maisonneuve *et al.,* 2010; Stoita *et al.,* 2011; Saiki *et al.,* 2014). Those with first-degree relatives that have PDAC or those with known cancer-causing mutations are at a much higher risk of developing the disease (Lucas *et al.,* 2014; Carrera *et al.,* 2017).

1.7 Biological mechanism of PDAC

While the exact initiation factors for PDAC remain elusive, certain aspects of the biological mechanisms involved have been identified. The genetic diversity within PDAC is substantial as research has shown that pancreatic cancer cells have genetic alterations such as deletions, frameshifts and amplifications. Several genes are universally disrupted in PDA while some are infrequent or inherited. In common with most malignancies, PDAC arises from the accumulation of mutations in various oncogenes and tumour suppressor genes including, but not limited to, *KRAS, p16, TP53* and *SMAD4* (Wolfgang *et al.,* 2013; Güngör *et al.,* 2014; Kleeff *et al.,* 2016). As *KRAS* is found to be mutated in more than 90% of pancreatic cancers, clinical studies are underway to investigate its potential as a prognostic and predictive PDAC biomarker. Moreover, *TP53* is the tumor suppressor that is mutated in 70% of pancreatic cancers and, additionally has shown some promising prognostic abilities (Cicenas *et al.,* 2017). Sequencing of these genes is currently used to identify mutations with prognostic features and potential therapeutic capacity.

Recently, significant efforts have been made by a variety of consortiums such as, Pancreatic Cancer Case-Control Consortium (PanC4), Pancreatic Cancer Cohort Consortium (PanScan) and PANcreatic Disease ReseArch (PANDoRA) consortium to use genome-wide (GWAS) association studies and meta-analysis to try to identify novel regions of the genome associated with pancreatic cancer susceptibility. Klein *et al.* (2018) carried out the largest pancreatic cancer GWAS to date in a bid to identify common

susceptibility alleles. The data indicated that *NOC2L* could be a possible pancreatic susceptibility gene.

PDAC is associated with precursor lesions that increase in grades within the ductal epithelium and progress to fully invasive pancreatic cancer (Wang *et al.,* 2015; Yu *et al.,* 2018). There are numerous pre-malignant lesions that are associated with PDAC development including pancreatic intraepithelial neoplasia (PanIN), intrapancreatic mucinous neoplasia (IPMN) and mucinous cystic neoplasia (MCN) (Stoita *et al.,* 2011; Saiki *et al.,* 2014; Patra *et al.,* 2017). The varying grades or subclasses of these lesions are dependent upon the degree of disease. For example, the best characterised of the lesions, PanIN, are classed from PanIN-1 to PanIN-3 (Regel *et al.,* 2012). It could be beneficial to identify different markers associated with each lesion stage, which would assist lesion detection and treatment before its progression into fully invasive cancer. Of particular interest for the PanIN lesions is the marker MUC1 that is exclusively overexpressed in higher grade PanIN lesions (PanIN-2/PanIN-3) and can be linked to invasive PDAC (Distler *et al.,* 2014). As lesions progress the accumulation of genetic mutations rise (Li *et al.,* 2015). Genetically, the inactivation of *p16/CDKN2A* is already detectable in the early PanIN stages while inactivation of *TP53* and *SMAD4/DPC4* is associated with the latter stages (Distler *et al.,* 2014; Hosoda *et al.,* 2017).

1.7.1 Desmoplastic reaction

The lack of blood supply to tumours is an architectural hallmark of PDAC (Li *et al.,* 2015). PDAC tumours are poorly defined and extend beyond the main tumour location (Maitra *et al.,* 2008; Xu *et al.,* 2014;). These tumours are surrounded by a fibrous stroma known as the desmoplastic reaction which arises from gene alterations (Goel *et al.,* 2015; Aghamaliyev *et al.,* 2016). The desmoplastic reaction creates a tumour stromal environment that promotes tumour growth and metastasis as well as forming a barrier to chemotherapy (Hidalgo *et al.,* 2010; Merika *et al.,* 2012; de Sousa Cavalcante *et al.,* 2014). Desmoplasia occurs when the pancreas is injured and involves increased proliferation of fibroblasts resulting in the deposition of extracellular matrix components (EMCs) (Gore *et al.,* 2014; Matsusaki *et al.,* 2017). This results in increased elasticity of the tumour tissue and increased intestinal fluid pressure, in turn, decreasing the penetration abilities of therapeutic agents (Habisch *et al.,* 2010; Whatcott *et al.,* 2012). Interestingly, this stroma accounts for almost 80% of the tumour mass, with malignant

epithelial cells accounting for the remaining 20% (Lin and Lin, 2017). As such, large-scale identification and validation of stroma-specific markers may allow for more effective therapeutic modalities to be determined.

1.8 Current diagnosis and treatment

Pancreatic cancer cases present asymptomatically or with generic symptoms indicative of less concerning pancreatic diseases with the most common including indigestion, abdominal pain or discomfort, weight loss, back pain and nausea (Li *et al.,* 2015; Kikuyama *et al.,* 2018). Consequently, the disease is often at a late stage when identified and possibly distant metastasis will already have occurred. Specific symptoms of the disease tend to manifest only after the tumour has grown and invaded other organs or obstructed the bile duct (Moniaux *et al.,* 2004). Current diagnosis relies heavily on scans such as ultrasonic B, magnetic resonance cholangiopancreatography (MRCP), computed tomography (CT) or endoscopic ultrasound scan (EUS), in conjunction with a tumour biopsy and tumour marker analysis. However, these scans suffer a plethora of disadvantages (Herreros-Villanueva *et al.,* 2013).

The CT scan is the most widely used and available method for imagining of PDAC. Yet while a CT scan is a first line modality with a 96% sensitivity and accuracy rates of up to 86.8%, it cannot be used as a screening tool as it is extremely costly, and involves exposing the patients to ionising radiation (Chu *et al*., 2017). The EUS scans are less invasive, however the localisation of the pancreas means it cannot be visualised particularly well. To circumvent this the EUS is often combined with fine needle aspiration (FNA) of tumour tissue, however, this also involves a level of invasion and with it a possibility of complications (Kim & Ahuja*,* 2015). It also suffers from a limited ability to detect distant metastasis. While screening for PDAC is not sufficient using the available diagnostic techniques, it is known that close to 10% of cases occur as a result of genetic mutations and thus it is advisable that individuals over the age of 50 in high-risk populations undergo yearly screening by EUS and MRI (Zhang *et al.,*2018).

Staging of a pancreatic cancer tumour is assessed by the ‘tumour-node-metastasis’ (TNM) classifications in accordance with the most recent American Joint Committee on

Cancer (AJCC) staging system effective January 2018 (***Table 1.2***) (Edge *et al.,* 2010; Tamm *et al.,* 2012).

Table 1.2: The TNM staging details for pancreatic cancer

Stage	**I**			**II**	**III**	**IV**
	IA	**IB**	**IIA**	**IIB**		
T	T1	T2	T3	T1-T3	T4	Any T
N	No Regional Lymph Nodes [N0]			Regional Lymph Nodes [N1]	Any N	
M	No Distant Metastasis [M0]					Distant Metastasis [M1]
RS	Potential for Resection				Borderline	Un-resectable
T	T0 – No evidence of primary tumour T1 – Tumour contained within the pancreas at a size of ≤ 2cm T2 – Still contained in the pancreas at a size of >2cm T3 – Extends outside of the pancreas but not involving any of the large blood vessels (celiac axis & superior mesenteric artery) T4 – Tumour has spread to the large blood vessels					
N	N0 – Has not metastasized to lymph nodes N1 – Has metastasized to lymph nodes					
M	M0 – No distant metastasis present M1 – Has metastasized to distant organs					

T-Tumour grade, N- Regional lymph nodes, M- Distant metastases, RS- Resectable stages.
(Table created based on information obtained from Tamm et al., 2012 and Edge et al., 2010)

If the disease is resectable, curative care can still be given. Unfortunately, recurrence is common and thus survivors of the disease are in need of constant surveillance. For invasive disease, treatment options are primarily palliative and are mostly based upon gemcitabine, with or without other therapeutic combinations. Gemcitabine (2',2'-difluorodeoxycytidine) is an analog of deoxycytidine. It works by incorporating itself into the DNA which inhibits necessary DNA processes and results in cell death (Plunkett *et al.,* 1995). Gemcitabine, and its cocktails (e.g. gemcitabine plus nab-paclitaxel, which is most applicable to the older population (Kaltsas *et al.,* 2014)), or FOLFIRINOX are considered the standard first-line treatments (Michl *et al.,* 2013; Saif, 2013 & 2014; Buchsbaum *et al.,* 2014). FOLFIRNOX is a combined therapy consisting of, 5-fluorouracil, leucovorin, irinotecan and oxaliplatin (Attard *et al.,* 2014).While FOLFIRINOX has shown improvement in overall survival (OS), it is linked to severe toxicity and so is advised only for patients who have an overall better 'health status' (Goel

et al., 2015; Spadi *et al.,* 2016). These chemotherapies confer limited benefits by prolonging life and controlling symptoms thus improving the overall quality of life (Chames *et al.,* 2010). Investigations are under-way to expand the uses of gemcitabine and to determine potential improvements using treatment adjuvants (Heinemann *et al.,* 2012).

Currently, there is a wide range of gemcitabine-based and FOLFIRINOX-based treatment regimens under consideration. Work carried out in 2011 found that a combination of FOLFIRNOX with leucovorin, fluorouracil and irinotecan showed an increase in overall survival when compared to gemcitabine alone, however, the toxicity related to FOLFOIRNOX was a reported issue (Spadi *et al.,* 2016). Consequently, FOLFIRNOX regimes are a promising alternative for treatment of patients under the age of 75. GEMCAP, a combination of gemcitabine and capecitabine (a fluoropyrimidine), showed a promising OS rate improvement from 22.0% (gemcitabine alone) to 24.3% (combination) (Cunningham *et al.,* 2009). Outside of gemcitabine, other treatment options have been explored. In Japan, a combination of tegafur, gimeracil and octeracil was well tolerated by PDAC patients and was approved for first-line treatment (Taieb *et al.,* 2017). More recently, a study by Yang *et al.,* 2018 developed an antibody fragment-conjugated gemcitabine and paclitaxel-loaded liposome system that has shown some potential in improving the therapeutic efficacy in pancreatic cancers. Regardless of these recent findings, the incidence of high mortality from lack of effective treatment options remains a pertinent issue.

1.9 Biomarkers

Numerous biomarker-focused studies have been conducted to enhance the diagnosis and treatment of PDAC, but with minimal success to date. However, there is potential for diagnostic improvement by exploiting sets of existing and newly discovered biomarkers in multiplexed formats. The FDA defines a biomarker as "A characteristic that is objectively measured and evaluated as an indicator of normal biologic processes, pathogenic processes, or biological response to a therapeutic intervention. A biomarker can be physiologic, pathologic, or an anatomic characteristic or measurement that is thought to relate to some aspect of normal or abnormal biologic function or process. Biomarkers measured in patients prior to treatment may be used to select patients for

inclusion in a clinical trial. Changes in biomarkers following treatment may predict or identify safety problems related to a drug candidate or reveal a pharmacological activity expected to predict an eventual benefit from treatment". A particularly relevant application of biomarkers is their ability to be applied for screening high-risk populations. It is not financially feasible to screen groups incessantly and the requirement for an easy-to-use point-of-care (POC) device is badly needed to alleviate the demands on health-care systems. Biomarkers have the capacity to indicate the presence of a particular cancer and the source of the cancer even after metastasis. For therapeutics, biomarkers can aid in determining the ideal course of treatment, since within a given type of cancer, characteristics are not uniform, and all cancer patients may not respond identically to a given treatment. Their use offers potentially less invasive, less costly and swifter methods of disease monitoring and surveillance (Malati, 2007). A given tumour marker can be regularly monitored for any elevations that could indicate disease recurrence. Additionally, expression levels of certain markers can predict survival (Fitzgerald *et al.,* 2013).

Biomarkers can be detected in a multitude of bodily fluids, from blood and urine to organ-specific fluids like pancreatic juice (Selleck *et al.,* 2017). Markers can be broadly segregated as diagnostic, prognostic and predictive. A diagnostic marker detects the presence of the disease, its extent and, occasionally, post-resection relapses. Prognostic markers indicate the history of disease progression and are utilised for identification of treatment options and surveillance. Predictive markers are used to predict the response of the disease to treatment (Winter *et al.,* 2013; Jones *et al.,* 2017).

The ideal biomarker is one that has the ability to screen cancer in a blood test or perhaps, more ideally, in saliva/urine when there are mild symptoms (Ballehaninna *et al.,* 2012). It would offer information on the cancer type, size, aggression and sensitivity to different available treatments and have the ability to generate this data in a cost-effective manner on a large-scale (Sharma, 2009; Sharma *et al.,* 2017). Dependence on a single biomarker for all the aforementioned capabilities has unfortunately found to be futile and it is essential that the concept of using a panel of markers for each cancer and stage be adopted. Biomarkers can be viewed as a fingerprint of the tumour rather than as a signal of its

presence. While confirmation by biopsies may always be necessary, tumour markers have the ability to refine and discriminate between benign and malignant disease.

1.9.1 Biomarkers for PDAC

The most widely used and validated marker for the routine management of PDAC is CA19-9 (Duffy *et al.,* 2013; Winter *et al*., 2013; Lee *et al*., 2018). It was first discovered in 1979 and in 1981 was found to be produced by pancreatic carcinoma rendering it the most used biomarker for pancreatic ductal adenocarcinoma (Poruk *et al*., 2015). It is beneficial in its analytical ability to monitor and detect post-treatment recurrence. However, the limitations are numerous, indicating elevated levels in benign disease, and its restrictions to diagnose small/early tumours (Duffy *et al.,* 2010; Passerini *et al.,* 2012; Poruk *et al.,* 2013). Most concerning of all, CA19-9 is a sialylated Lewis (Le^{ab}) blood group antigen, and 6%-22% of the population in the US are Le^{a-b-} and thus do not generate the specific antigen. Consequently, CA19-9 is a false negative for this population, rendering it useless (Poruk *et al*., 2015). Studies have all shown poor results when exploring the utility of CA19-9 as a screening marker in early and asymptomatic cases (Kim *et al.,* 2004). Its median sensitivity is in the range of 79-81%, with a median specificity of 70-92%. The specificity is reduced due to the co-existence of jaundice at presentation and the existence of elevated levels in non-malignancy-associated jaundice (Huang *et al.,* 2014). It has potential as a post-operative marker due to its ability to detect disease progression post-resection. For example, should levels fail to normalise after approximately 3-6 months it could infer poor survival (Hernandez *et al.,* 2009). Interestingly, Lee *et al.,* (2018) recently showed that combining CA19-9 with CEMIP resulted in improved pancreatic cancer diagnosis over CA19-9 alone. This indicates that, despite its limitations, CA19-9 could be useful in a multi-marker setting.

Work is underway to identify novel markers and validate recognised markers (***Table 1.3***) in a multitude of bodily fluids from serum to pancreatic tissue/juice, stool and saliva (Zhang *et al.,* 2010). A meta-analysis-, carried out by Chen *et al.,* (2018), identified that increased levels of platelets in post-surgical resection patients act as a very promising prognostic marker, indicating poor overall survival. Other work has explored the use of miRNA as prognostic markers, Shi *et al.,* (2018) analysed The Cancer Genome Atlas

(TCGA) RNA-seq data and their findings suggest that a signature of five miRNAs could potentially be used as a pancreatic cancer prognostic marker.

Within this research, three biomarkers, anterior gradient 2 (AGR2), mesothelin (MSLN) and mucin 1 (MUC1), were chosen. In combination, these markers may generate diverse information on tumour protein expression, facilitating personalised therapies and aid in diagnosis. The following sections will give a brief background on each of these markers and compare their behaviours in normal tissue to their roles in PDAC cells. The subsequent chapters contain a more in-depth discussion on each marker.

Table 1.3: Comprehensive list of PDAC markers

Biomarker	Serum marker	Tissue Marker	Reference
Anterior gradient 2 (AGR2)	+	+	Dumartin *et al.,* 2017
BCl-2	-	+	Duffy *et al.,* 2010
CA 19-9	+	-	Winter *et al.,* 2013; Loosen *et al.,* 2017
CA 50	+	-	Rückert *et al.,* 2010
CA 72-4	+	-	Loosen *et al.,* 2017
CA 125	+	-	Winter *et al.,* 2013; Loosen *et al.,* 2017
CA 242	+	-	Duffy *et al.,* 2010; Zhang *et al.,* 2015
CA 494	+	-	Li *et al.,* 2015
Carcinoembryonic Antigen (CEA)	+	-	Zhang *et al.,* 2015; Loosen *et al.,* 2017
Claudin 4 & 18	-	+	Chames *et al*., 2010; Wöll *et al*., 2014
D-Dimer (DD)	+	+	Li *et al.,* 2015
DUPAN2	+	+	Herreros-Villanueva *et al.,* 2013
Epidermal Growth Factor Receptor (EGFR)	-	+	Saif, 2013; Chiramel *et al.,* 2017
Epithelial Cell Adhesion Molecule (EpCAM)	-	+	Saif, 2013; Wang *et al.,* 2018
Fibrinogen (FIB)	+	-	Li *et al.,* 2015
Hippocalcin-like 1 protein (HPCAL1)	-	+	Chen *et al.,* 2014

Human Epidermal Growth Factor Receptor 2 (HER2)	-	+	Dodson *et al.,* 2011
Human CNT3	-	+	Yu and Cheung, 2018
Human Equilibrative Nucleoside Transporter – 1 (hENT1)	-	+	Goel *et al.,* 2015; Yu and Cheung, 2018
HuR	-	+	Winter *et al.,* 2013
Insulin-like Growth Factor 1 receptor (IGF-1R)	-	+	Humar *et al.,* 2017
Integrin β1	-	+	Pan *et al.,* 2018
Mesothelin (MSLN)	+	+	Winter *et al.,* 2013
MicroRNA -21	+	-	Loosen *et al.,* 2017
Minimolecular Pancreatic Antigen (MPOA)	+	-	Li *et al.,* 2015
MUCIN 1/3/4/5AC	-	+	Winter *et al.,* 2013; Root *et al.,* 2018
Nonspecific Cross-reacting Antigen (NCA)	+	-	Saif, 2013
Osteopontin (OPN)	+	+	Chang *et al.,* 2017; Loosen *et al.,* 2017
PAM4	+	-	Loosen *et al.,* 2017
Pancreatic Cancer-Specific Antigen (PCAA)	+	-	Li *et al.,* 2015
Tissue polypeptide antigen (TPA)	+	-	Duffy *et al.,* 2010
Tissue polypeptide-specific antigen (TPS)	+	-	Duffy *et al.,* 2010; Herreros-Villanueva *et al.,* 2013
Vascular Endothelial Growth Factor (VEGF)	-	+	Dodson *et al.,* 2011; Saif, 2014

1.9.2 MUCIN

The 'mucins' are a large family of multifunctional, highly glycosylated, proteins. They can be either membrane-bound or extracellularly located on epithelial surfaces of numerous organs (Torres *et al.,* 2012). This family of proteins has a range of roles in homeostasis and the formation and progression of cancer. Mucins are expressed in >85% of invasive pancreatic cancer cases and can be used as an early disease biomarker, or for staging purposes (Felder *et al.,* 2014).

MUC1, a membrane-bound glycoprotein, is overexpressed in almost 90% of pancreatic cancer tumours (Park *et al.,* 2015). MUC1 is normally expressed on the apical surface of most epithelial cells and provides a barrier of protection against pathogens. This barrier is created by the *O*-glycosylation which form a mucus-type gel on the cell surface. Structurally, MUC1 consists of an N-terminal domain and a C-terminal domain which consists of a small extracellular portion and a cytoplasmic tail (***Figure 1.9***). The C-terminal is highly conserved and by phosphorylation of the cytoplasmic tail MUC1 activates various intracellular signalling by interactions with a myriad of proteins. In cancerous cells, increased phosphorylation of the cytoplasmic tail results in increased interactions of MUC1 with these proteins which can be aberrantly expressed. The cytoplasmic tail brings together kinases and various proteins that lead to increased cell proliferation and reduced apoptosis (Nath *et al.,* 2013). The N- and C- terminals are bound through hydrogen bonds, however, MUC1 can be cleaved into serum which is often associated with cancers such as pancreatic cancer (Cascio & Finn 2016). This increases the internalisation of MUC1 and alters the signals in cancer cells. Furthermore, the glycosylation patters of MUC1 are altered with under glycosylated forms are highly expressed in pancreatic cancer and has been associated with the invasiveness of cancerous cells.

In PDAC, over-expression of a differentially glycosylated from of MUC1 is associated with disease development and progression. MUC1 overexpression is evident during the earlier developmental stages of pancreatic cancer (Herreros-Villanueva *et al.,* 2013). In terms of biological function, MUC1 is thought to play a role in maintaining the lumina of ductal epithelial cells. In cancer, it is thought to aid in the vascular spread of carcinoma cells (Levi *et al.,* 2004). It is overexpressed primarily in the high-grade PanIN stages and thus is a possible aggressive late-stage PDAC marker. The PanIN lesion is related to

mucin expression and levels of MUC1 increase with the progression of PanIN lesions (Lowery *et al.,* 2011; Rao *et al.,* 2016). Most importantly, overexpression of MUC1 in cancerous cells is linked to chemo resistance (Nath *et al.,* 2013). As MUC1 is associated with pancreatic tumor invasiveness by increasing proliferation and reducing apoptosis, as well as playing a role in the chemoresistance of pancreatic cancer, this is an attractive biomarker to target (Hinoda *et al.,* 2003).

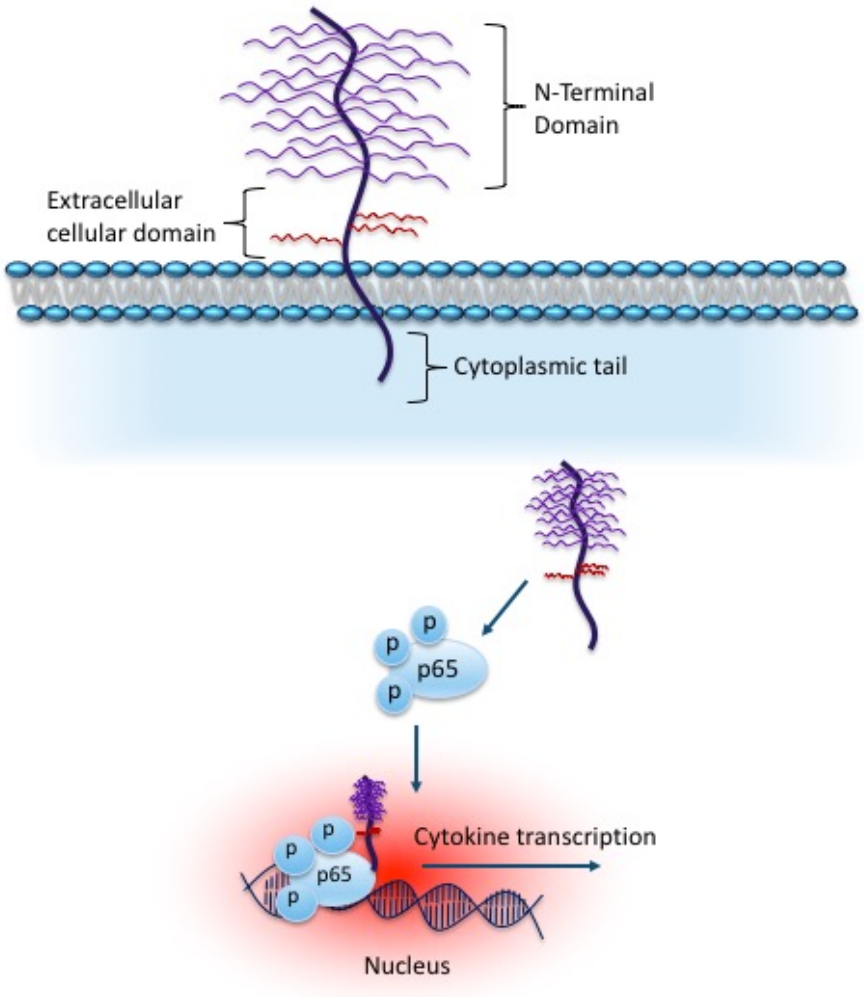

Figure 1.9 Cytokine activation by MUC1 in cancer cells

When the cancer cell is stimulated with TNF-alpha, the hypoglycosylated MUC1 accumulates within the cytosol of the cell. MUC1 then associates with the activated p65 and translocates to the nucleus. Within the nucleus it associates with the promoter of pro-inflammatory cytokines, such as interleukin 6 (IL-6) known to be involved cell proliferation and survival, and controls the transcription of these pro-inflammatory cytokines. (Taken and amended from Cascio & Finn, 2016)

1.9.3 Mesothelin (MSLN)

Mesothelin (MSLN) is a cell-surface glycoprotein found in nearly 100% of pancreatic cancer tissues but is absent from surrounding non-cancerous tissues. As such, MSLN is not cancer-specific but is a differentiation antigen (Hassan *et al.,* 2005; White *et al.,* 2018). Importantly, normal MSLN expression is limited to mesothelial cells, which are expendable making it a highly attractive target as a therapeutic and diagnostic marker (Hassan *et al.,* 2016).

MSLN is synthesized as a ~71kDa precursor protein that is cleaved to release the megakaryocyte potentiating factor (MPF) whilst the mature MSLN, now ~41kDa, remains bound to the cell membrane (Hassan *et al.,* 2016). Whilst its exact biological function remains unclear, many studies have attempted to identify its possible functions by silencing MSLN. Silencing resulted in decreased cell proliferation and migration and inhibited tumour growth *in vivo,* indicating a role in cancer cell migration, proliferation and tumour progression (Tang *et al.,* 2013; Zervos *et al.,* 2016). Investigations into MSLNs role in pancreatic cancer progression have involved determining the role of MSLN exerting its effects by STAT3. STAT3 is a transcription factor that when phosphorylated dimerises and translocates to the nucleus enabling gene transcription. When constitutively activated it was found to be involved in pancreatic cancer cell proliferation. Additional analysis has been carried out by blocking MSLN expression which resulted in inhibited cell progression with decrease in cyclin levels. Cyclin-dependent kinases are involved in the progression of cells through the cell cycle. Moreover it was fond that high cyclin E expression can be linked to poor prognosis (Bharadwai *et al.,* 2008). Numerous analysis has been carried out in a bit to elucidate the various biological pathways in which MSLN promotes pancreatic cancer progression (***Figure 1.10***).

In addition, MSLN has a role in chemo-resistance. Thus, $MSLN^+$ tumours may indicate if chemotherapy is a viable option (Chang *et al.,* 2009). A high expression level of MSLN is a strong indicator of poor survival rates and $MSLN^+$ tumours require highly aggressive and rapid treatment (Chen *et al.,* 2013). In the pancreas, the MSLN protein is only found on cancerous tissue. No other pancreatic disease, such as chronic pancreatitis, results in the expression of MSLN. Therefore, this marker could be valuable for immunohistochemistry analyses on pancreatic adenocarcinoma tumours. Additionally, it

was found that there is a limited amount of MSLN that is shed into the serum, and it can be detected in patients with pancreatic disease (Johnston *et al.,* 2009; Kendrick *et al.,* 2014). MSLNs overexpression in malignant cells and limited expression in normal cells makes it a potential target for immunotherapeutics (Johnston *et al.,* 2009). MSLN can be used as a signal to identify a tumour for specific types of treatment, or as a target for drugs through the use of antibody-based approaches.

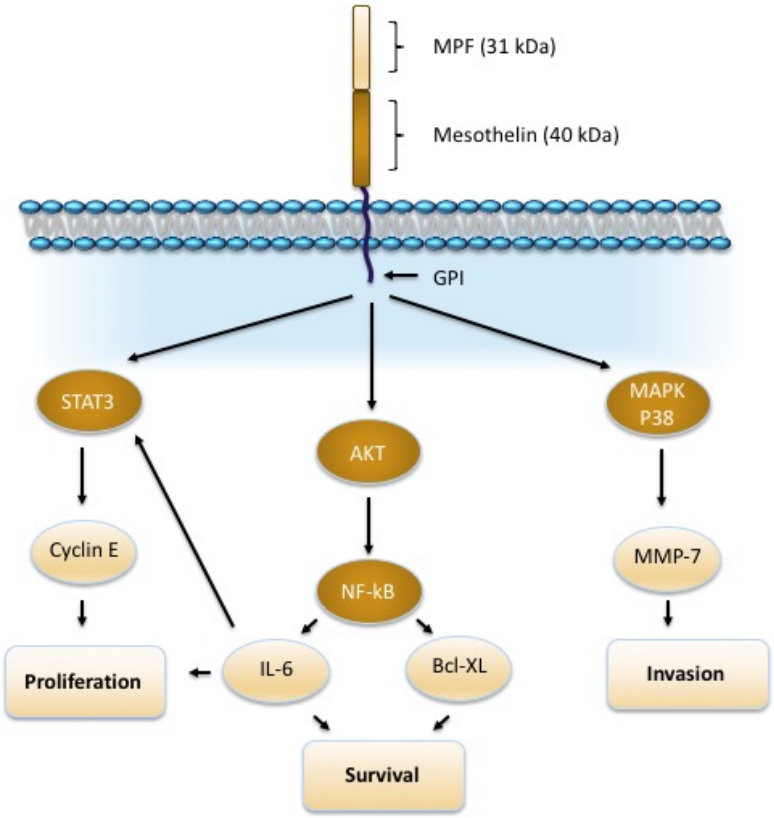

Figure 1.10 Associated pathways of MSLN in pancreatic cancer

MSLN is thought to have roles in cancer cell progression, survival and invasion. Evidence has shown that activation of NK-kappa B is associated with poor survival. It has also been shown to result in constitutive Akt activation leading to upregulation of anti-apoptotic proteins such as Bcl-XL. Furthermore, activation of MMP-7 through the p38 MAPK-dependent pathway is related to increased cancer cell mobility (Zhang et al., 2016).

1.9.4 Anterior Gradient 2 (AGR2)

Anterior gradient 2 (AGR2) is a member of the protein disulphide isomerase family of endoplasmic reticulum-resident proteins (Brychtova *et al.,* 2011). AGR2 is the human orthologue of XAG-2, the *Xenopus Laevis* protein. XAG-2 acts in the regulation of embryonic molecules. The role of AGR2 in humans, while not yet fully clear, is thought to have conserved roles in development and tissue regeneration. It is strongly expressed in numerous tissues that contain mucus-secreting cells such as the lung and colon and is noted to have higher expression in female patients (Riener *et al.,* 2009).

As mentioned, AGR2 is an endoplasmic reticulum-resident protein.The endoplasmic reticulum has been identified to be heavily involved in tumour growth. It is involved in controlling the secretion of proteins by a variety of molecular systems such as protein synthesis and folding. The proteins involved in these molecular mechanisms can contribute to the development and progression of cancers. One such protein is AGR2, which has also been shown to play intracellular roles such as regulation of p53 (Chevet *et al.,* 2013). It is linked to a variety of human cancers such as hormone-dependent, breast, prostate, hormone-independent, colorectal and pancreatic cancers (Brychtova *et al.,* 2011). AGR2 is known to be overexpressed in a diverse range of cancers and can be secreted and detected which makes it a very attractive marker for pancreatic cancer diagnosis.

AGR2 is a metastasis-associated protein (when silenced there was a significant reduction in invasiveness) that is upregulated in various cancers and is often associated with poor prognosis (Brychtova *et al.,* 2014). While its exact role in pancreatic cancer is poorly understood, it was determined that the overexpression of AGR2 attenuates p53 which may indicate that AGR2 acts as a survival factor by inhibiting p53 (Ramachandran *et al.,* 2008) (***Figure 1.11***). The degree of AGR2 expression is proportional to the invasiveness of pancreatic cancer cells. AGR2 appears to stimulate growth, invasiveness, survival *in vitro,* tumour growth and sensitivity to chemotherapy *in vivo*. Thus, it may be beneficial in diagnosis and development of therapeutic approaches (Ramachandran *et al.,* 2008) .AGR2 is potentially a highly exploitable biomarker. While absent from normal tissue, it is highly expressed in the earliest developmental stages of precancerous pancreatic lesions (PanIN) (Dumartin *et al.,* 2017). This elevation was seen in the pancreatic juice of patients with pre-malignant conditions (Chen *et al.,* 2010; Norris *et al.,* 2013).

Furthermore, a study uncovered a 2- to 10-fold elevation of AGR2 in PanIN3 juice samples, indicating this marker could potentially be beneficial as a pancreatic juice biomarker for the early detection of pancreatic cancer (Chen *et al.,* 2010). Moreover, AGR2 is involved in drug resistance and thus may be used to evaluate the potential response to gemcitabine treated tumours (Brychtova *et al.,* 2011).

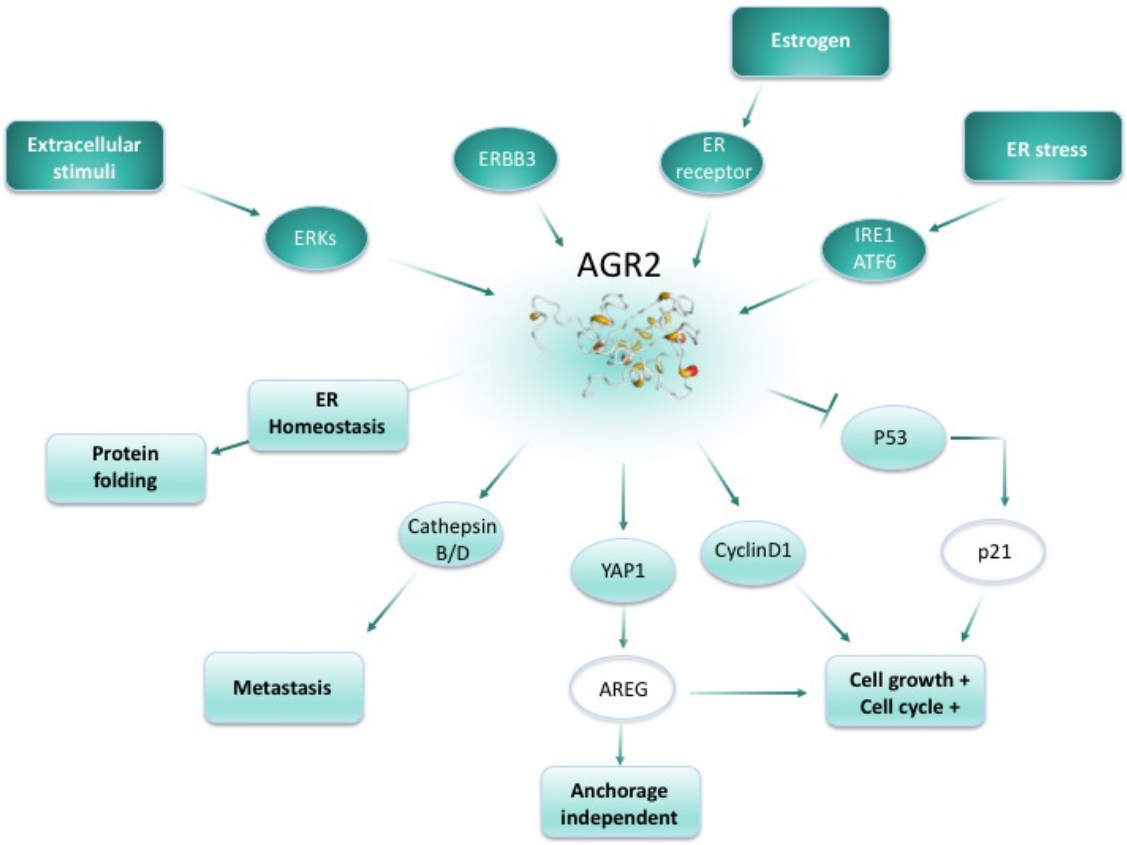

Figure 1.11 Anterior gradient 2 biological pathways.

This diagram represents known and potential AGR2 biological pathways. The pathways that regulate AGR2 expression are in dark green and functions that are AGR2-dependent are shown in light green with the resulting effects on cancer progression shown in light green boxes. Taken and adapted from Chevet et al., 2013.

1.9.5 Biomarkers and antibodies

Antibodies play a major role in the clinical diagnosis and treatment of many cancers. Their ability to detect a diverse range of proteins makes them ideal for biomarker detection. While the production of antibodies for cancer treatment and diagnosis is well established, certain cancers have been relatively overlooked in this area. Pancreatic cancer is a crucial example and few antibodies exist for the biomarkers of this cancer.

Thus, there is a niche for generating antibodies for both diagnostic and therapeutic applications. A major component of this project is the development of recombinant scFv antibodies against the three previously described PDAC biomarkers, namely, mucin 1 (MUC1), mesothelin (MSLN) and anterior gradient 2 (AGR2). Each of these markers can be used as indicators of different stages and characteristics of pancreatic cancer, thus, when incorporated into a multiplex format, may aid in the diagnosis and staging of PDAC and generate valuable information for personalised treatment.

1.10 Thesis outline and project aims

The main aims of this project are two-fold, namely, to tackle both the diagnostic- and therapeutic-associated issues relating to pancreatic cancer by exploiting the design flexibility of recombinant antibodies.

This work proposes a multi-pancreatic cancer marker panel that would generate crucial information about disease, stage, potential progression, and susceptibility to therapeutics. Chapter three and four detail the work carried out to produce the components for the proposed diagnostic panel.

Chapter three describes the generation of an anti-Mesothelin scFv using a biased murine immune library. In order to isolate an anti-MSLN specific scFv, the MSLN antigen was expressed from transfected HEK293 cells. The successfully isolated MSLN-specific scFv was subsequently characterized using ELISA and Dot Blotting.

Chapter 4 focuses on isolating the final scFv of the diagnostic panel, using Mucin 1 and AGR2 antigens expressed in *E. coli* systems, from the naïve human Tomlinson I & J library. Two scFvs , specific to each antigen, were successfully isolated and employed in the generation of validated ELISA assays.

Chapter 5 outlines the production, selection and characterization of an anti-CD3ε scFv from an avian immune library and its subsequent incorporation into a bispecific antibody. It details a ‘proof of concept’ method for the generation of a bispecific T-cell engager and dual-functionality testing of the resulting antibody.

Chapter 2

Materials & Methods

2.1 Equipment

Apparatus	Supplier
Chyo-Model JK-180 Mettler Model-PJ300 Orion 3 star-pH meter Pierce™ G2 Fast Blotter Airstream® Class II Type A2 biological safety cabinet Gen 3 (E-Series) Scrilogex MX-S Vortex mixer Scrilogex D1008 Mini centrifuge	Medical Supply Company Ltd., Damastown, Mulhuddart, Dublin 15, Ireland.
Nikon Diaphot Inverted Tissue Culture Microscope	Nikon Instruments, Inc., 1300 Whitman Road, Melville, New York 11747-3064, USA.
ImageMaster® VDS	GE Healthcare Life Sciences, Amersham Place, Little Chalfont, Buckinghamshire, HP7 9NA, UK.
Mini-PROTEAN® Tetra Cell	Fannin House, South County Business Park, Leopardstown, Dublin 18, Ireland.
Bio-Rad Gene Pulser Xcell Bio-Rad PowerPac™ Basic DNA Gel Apparatus Bio-Rad (Wide-Mini-Sub® Cell GT)	Alpha Technologies, The Leinster Technology Centre, Blessington Industrial Estate, Blessington, Co.Wicklow, Ireland.
Hermle Z233M-2 Air-cooled version Microcentrifuge	Hermle Labortechnik GmbH, 25 Siemensstrasse, Wehingen,

	78564, Germany.
Homogeniser Ultra Turrax	Janke & Kunkel IKA-Werk Ultra-Turrax, Staufen, 79129, Germany.
New Brunswick Scientific-Excella® Incubator Shaker Type E24 Eppendorf 5810r Benchtop Centrifuge	Mason Technologies, Greenville Hall, 228 South Circular Road, Dublin 8, Ireland.
Biometra $T_{GRADIENT}$ Thermal Cycler	Biometra GmbH, Rudolf-Wissell-Str. 30, D-37079 Göttingen, Germany.
NanoDrop™ ND-1000 Spectrophotometer	NanoDrop Technologies, Inc., 3411 Silverside Rd 100BC, Wilmington, DE19810-4803, USA.
IKA® MTS 2/4 Digital Microtitre Plate Shaker STR6 Ohaus Pioneer 210g x 1mg Balance	Lennox, John F. Kennedy Drive, Naas Road, Dublin 12, Ireland.
Branson Digital Sonifier®	ABG Scientific Ltd., Dublin Industrial Estate, Glasnevin, Dublin 9, Ireland.
Eppendorf ™ Centrifuge with swing-bucket rotor (A-4-62) and fixed angle rotor (F-45-30-11)	Eppendorf UK Ltd., Endurance House, Vision Park Histon, Cambridge CB24 9ZR, UK.
SSM4 see-saw Rocker	Fisher Scientific Ireland, Suite 3, Plaza 212,

Thermo Forma Series II 3110 water-jacketed CO_2 incubator	Blanchardstown Corporate Park 2, Ballycoolin, Dublin 15, Ireland.
VAPOUR-Line^{eco} 50 Autoclave	VWR International Ltd., Orion Business Park, North West Business Park, Ballycoolin, Dublin, Ireland.
Sigma Laborzentrifugen Model 2K15	SIGMA Laborzentrifugen GmbH, Osterode am Harz, Lower Saxony 37507, Germany.
DarkReader® Transilluminator	Clare Chemical Research, 995 Railroad Ave, Unit E, Dolores, CO 81323, USA.
Tecan Safire^2 Plate reader	Tecan Group Ltd., Seestrasse 103, CH-8708 Männedorf, Switzerland.
Thermostatic Water Bath Model Y6	Grant Instruments (Cambridge) Ltd., 29 Station Road, Shepreth, Royston, Herts., SG8 6PZ, UK.
ÄKTA Pure Instrument Superdex® 75 10/300 GL column	GE Healthcare Bio-Sciences AB, Danmarksgatan 41, M5, 75184 Uppsala, Sweden.

2.2 Reagents

All reagents were of analytical grade and purchased from Sigma-Aldrich Ireland Ltd. (Dublin, Ireland), unless otherwise stated.

Reagent	Supplier
Acetic acid Agarose Carbenicillin Glycerol Kanamycin Molecular grade water Precept tablets Sodium chloride PageRuler Plus pre-stained protein ladder Pierce™ 1-step transfer buffer	Fisher Scientific Ireland, Suite 3 Plaza 212, Blanchardstown Corporate Park 2, Ballycoolin, Dublin 15, Ireland.
Superscript III cDNA synthesis kit TriZol® SYBR® Safe M13K07 Helper Phage Glycogen SOC media 3M Sodium Acetate RNAlater™ RNA zap	Biosciences Ltd., 3 Charlemont Terrace, Crofton Road, Dun Laoghaire, Ireland.

Bacteriological Agar Tryptone Powder Yeast Extract Powder	Cruinn Diagnostics Ltd., Hume Centre, Parkwest Business Park, Nangor Road, Dublin 12, Ireland.
PCR Primers	Integrated DNA Technologies, Interleuvenlaan 12A, B-3001 Leuven, Belgium.
Restriction digest enzymes Amylose Resin Factor Xa protease	New England Biolabs, Hitchin, Hertfordshire, SG4 0TY, England.
HyperLadder™ 1Kb HyperLadder™ Plus 1Kb	Bioline USA Inc, 305 Constitution Drive, Taunton, MA 02780, USA.
1,5-Dansyl-Glu-Gly-Arg Chloromethyl Ketone, Dihydrochloride	Merck Chemicals Ltd., Boulevard Industrial Estate, Padge Road, Nottingham, NG9 2JR, UK.
Instant*Blue* ™ Ni-NTA His Bind® Resin	MyBio, Kilkenny Research and Innovation Centre, St. Kieran's College Road, Kilkenny, Ireland.
Virkon	Lennox Laboratory Supplies Ltd, John F. Kennedy Drive, Naas Road, Dublin 12, D12 FP79, Ireland.
SureBlue ™ TMB Microwell peroxidase substrate	Insight Biotechnology Ltd., PO Box 520, Wembley,

	Middlesex, HA9 7YN, UK.
IMDM with 25mM HEPES with L-Glutamine (500mL) RPMI-1640 with 25mM HEPES with UltraGlutamine I (500mL) DMEM with L-Glutamine DPBS (1X) without Ca^{++} or Mg^{++} (500ml) Antarctic Phosphatase enzyme T4 DNA Ligase	Brennan and Company, Unit 61, Birch Ave, Stillorgan Industrial Park, Stillorgan, Co. Dublin, Ireland.

2.2.1 PCR Polymerases

Polymerase	Supplier
Platinum® *Taq* DNA Polymerase High Fidelity	Biosciences Ltd., 3 Charlemont Terrace, Crofton Road, Dun Laoghaire, Ireland.
My*Taq*™ Red Mix	Medical Supply Company Ltd., Damastown, Mulhuddart, Dublin 15, Ireland
Dream*Taq*® DNA Polymerase High Fidelity Thermo Scientific™ Phusion High-Fidelity DNA Polymerase	Fisher Scientific Ireland, Suite 3 Plaza 212, Blanchardstown Corporate Park 2, Ballycoolin, Dublin 15, Ireland.

2.3 Cells

2.3.1 Mammalian cell lines

Cells	Supplier
Capan-1 cell line (ATCC® HTB-79™) Jurkat E6.1 Clone (ATCC® TIB-152™) 293 [HEK-293] (ATCC® CRL-1573™)	LGC Standards, Queens Road, Teddington, Middlesex TW11 0LY, UK.

2.3.2 Bacterial cells used in cloning and protein expression

Cells	Genotype	Supplier
XL1-Blue Electroporation-competent cells *E. coli*	*rec*A1 *end*A1 *gyr*A96 *thi*-1 *hsd*R17 *sup*E44 *rel*A1 *lac* [F' *pro*AB *lac*I^{q}ZΔM15 Tn*10*(Tet^t)]	Agilent Technologies, 5301 Stevens Creek Blvd., Santa Clara, CA 95051, United States.
TOP10 F' strain *E. coli* One Shot® BL21(DE3) Chemically-competent *E. coli*	F' {*lac*I^q, Tn*10*(Tet^R)} *mcr*A Δ(*mrr-hsd*RM-*mcr*BC) Φ80*lac*ZΔM15 Δ*lac*X74 *deo*R *rec*A1 *ara*D139 Δ(*ara-leu*)7697 *gal*U *gal*K *rps*L (Str^R) *end*A1 *nup*G F$^-$ *ompT hsdS*B (rB mB) *gal dcm* (DE3)	Biosciences Ltd., 3 Charlemont Terrace, Crofton Road, Dun Laoghaire, Ireland.

2.4 Culture media formulations

Media / Media components	Formulation	
Luria Bertani Broth (LB) medium	Tryptone Yeast Extract NaCl	10 g/L 5 g/L 5 g/L
Super Broth (SB) medium	MOPS Tryptone Yeast Extract	10 g/L 30 g/L 20 g/L
Terrific Broth (TB) medium	Tryptone Yeast Extract Glycerol (0.04% ; v/v) KH_2PO_4 K_2HPO_4	12 g/L 24 g/L 4 mL/L 0.017 M 0.072 M

Solid media was made by the addition of 15 g/L bacteriological agar to the aforementioned formulations.		
Auto-Induction Media	Broth 1M $MgSO_4$, 0.01% (v/v) 50 X 5052, 2% (v/v) 20 X NPS, 5% (v/v)	928 mL/L 1 mL/L 20 mL/L 50 mL/L
2 X Tryptone and Yeast Extract (TY) medium	Tryptone Yeast Extract NaCl	16 g/L 10 g/L 5 g/L
1M $MgSO_4$	$MgSO_4$	24.65 g/100 mL
100X 505 (50% glycerol, 5% glucose)	Glycerol, 50% (v/v) Glucose, 5% (w/v)	50 mL/ 100mL 5 g / 100mL
50X 5052 (0.5% glycerol, 0.05% glucose, 0.2% α- lactose)	Glycerol, 0.5% (v/v) Glucose, 0.05% (w/v) α- lactose, 0.2% (w/v)	25 g/100 mL 2.5 g/100 mL 10 g/100 mL
20X NPS	$(NH_4)_2SO_4$ KH_2PO_4 Na_2HPO_4	6.6 g/100 mL 13.6 g/100 mL 14.2 g/100 mL
Complete Growth Media (CGM) for Capan-1 cells	IMDM, 80% (v/v) FBS, 20% (v/v)	800 mL/L 200 mL/L
CGM for HEK 293 cells	DMEM, 90% (v/v) FBS, 10% (v/v) Penicillin-Streptomycin, (10,000 U /mL) (v/v)	900 mL/L 100 mL/L 10 mL/L
CGM for Jurkat cells	RMPI 1640, 90% (v/v) FBS 10%, (v/v)	900 mL/L 100 mL/L
Freezing media for mammalian cell line cryopreservation	CGM, 95% (v/v) DMSO, 5% (v/v)	4.75 mL 250 µL

2.4.1 Antibiotics

Antibiotic	Formulation	
Carbenicillin, 100 mg/mL	Carbenicillin salt Molecular grade water	500 mg 5 mL
Kanamycin, 60 mg/mL	Kanamycin Molecular grade water	300 mg 5 mL
Tetracycline, 5 mg/mL	Tetracycline Molecular grade ethanol	25 mg 5 mL
Chloramphenicol, 25 mg/mL	Chloramphenicol Molecular grade ethanol	125 mg 5 mL

2.5 Buffer Compositions

2.5.1 General Buffers

Buffer	Composition	
Phosphate Buffered Saline (PBS)	NaCl Na_2HPO_4 NaH_2PO_4	5.84 g/ L 4.72 g/ L 2.64 g/ L Final pH 7.4 Reagents were dissolved in ultra-pure H_20. The required pH was adjusted by titration with the appropriate acid or base.
PBS-Tween 20 (0.05%, v/v) (PBS-T)	PBS Tween 20	1X 0.05% (v/v)
(Milk Marvel / BSA) PBS-T	PBS Milk Marvel / BSA	1X 5% / 3% (w/v)

2.5.2 Buffers for sodium dodecyl sulfate-polyacrylamide gel electrophoresis

Buffer	Composition	
10X Electrophoresis Buffer	50 mM Tris, pH 8.3 196 mM Glycine 0.1% (w/v) SDS dH_20	30g / L 144 g / L 10 g / L Up to 1L
4.5% stacking gel (1 gel)	1 M Tris-HCl, pH 6.8 30% (w/v) Acrylagel 2% (w/v) Bis-Acrylagel	300 µL 375 µL 150 µL

	Deionised H_2O 10% (w/v) SDS 10% (w/v) APS Tetramethlylethylenediamine (TEMED)	1.625 mL 24 µL 24 µL 2 µL
12.5% separating gel (1 gel)	1 M Tris-HCl, pH 8.8 30% (w/v) Acrylagel 2% (w/v) Bis-Acrylagel Deionised H_2O 10% (w/v) SDS 10% (w/v) APS Tetramethlylethylenediamine (TEMED)	1.5 mL 2.5 mL 1.0 mL 934 µL 30 µL 30 µL 6 µL

2.5.3 Protein Purification Buffers for amylose resin

Buffer	Composition and pH
Column Buffer	20 mM Tris-HCl 200 mM NaCl 1 mM EDTA pH 7.4
Elution Buffer	Column Buffer plus: 10 mM Maltose pH 7.4

2.5.3 Gel Filtration buffers for size exclusion chromatography (SEC)

Buffer	Composition
SEC Buffer	1 X PBS containing protease inhibitor tablets
The buffer was prepared, sterile filtered through 0.2 µM filtered and degassed before use.	

2.5.5 Protein Purification Buffers for Ni^2-NTA resin

Buffer	Composition and pH
Lysis Buffer	50 mM NaH_2PO_4 300 mM NaCl 10 mM Imidazole pH 8.0
Equilibration buffer	50 mM NaH_2PO_4 100 mM NaCl

	10 mM Imidazole pH 8.0
Wash Buffer A	1X PBS 150 mM NaCl 30 mM Imidazole pH 8.0
Wash Buffer B	1X PBS 150 mM NaCl 40 mM Imidazole pH 8.0
Elution Buffer	1X PBS 300 mM Imidazole pH 8.0

2.6 Commercially sourced kits

Kit	Source
Superscript III® Reverse Transcriptase Kit	Biosciences Ltd., 3 Charlemont Terrace, Crofton Road, Dun Laoghaire, Ireland.
NucleoSpin® Gel and PCR Clean up Kit NucleoSpin® Plasmid mini prep Kit NucleoSpin® Xtra midi plasmid Kit	Fisher Scientific Ireland, Suite 3, Plaza 212, Blanchardstown Corporate Park 2, Ballycoolin, Dublin 15, Ireland.
ViraPack Transfection Kit	Agilent Technologies, 5301 Stevens Creek Blvd. Santa Clara, CA 95051, United States.

2.7 Commercially sourced antibodies

Antibody	Dilution	Source
Peroxidase-labelled rat anti-HA (Human Influenza virus hemagglutinin) antibody (Cat. No: 12013819001)	1: 2,000	Sigma-Aldrich Ireland Limited, Vale Road, Arklow, Wicklow, Ireland.
Peroxidase-labelled goat anti-mouse IgG antibody (Cat. No: A4416)	1: 10,000	
Peroxidase-labelled mouse monoclonal anti-polyHistidine antibody (Cat. No: A7058)	1: 2,000	
Mouse monoclonal anti-AGR2 antibody (Cat. No: WH0010551M3)	1: 2,000	
Peroxidase-labelled rabbit anti-chicken IgY (IgG) whole molecule antibody (Cat. No: A9046)	1: 30,000	
Peroxidase-labelled mouse anti-maltose binding protein antibody (Cat. No: ab49923)	1: 2,000	Abcam, 330 Cambridge Science Park, Cambridge, CB4 0FL, UK.
Peroxidase-labelled mouse anti-M13 antibody (Cat. No: ab50370)	1: 20	
Rabbit monoclonal antibody to Mesothelin (Human) (Cat. No: ab134109)	1: 2,000	
Peroxidase-labelled rabbit polyclonal antibody to Myc (Cat No: ab1236)	1: 40,000	
Mouse anti-MUC1 (Human) antibody (Cat No: 36690)	1: 5,000	
Mouse anti-CD3 epsilon (Human) antibody (Cat No: 134408)	1: 2,000	

2.8 Commercially sourced proteins

Protein	Source
CD3ε epsilon (CD3-TCR Complex) protein (His-Tagged)	Antibodies-online GmbH, Schloss-Rahe-Str. 15, 52072 Aachen, Germany.

2.9 Commercially sourced vectors/plasmids

Vector/Plasmid	Source
Mesothelin (MSLN) Protein Vector (Human) (pPB-N-His) Mucin 1 (MUC1) Protein Vector (Human) (pPB-N-His)	NBS Biologicals Ltd, 14 Tower Square, Huntington PE29 7DT, UK.
pAdEasy-Msln-iCre-HA-Flag	A gift from William Pu (Addgene plasmid # 18097) Addgene, 75 Sidney Street, Suite 550A, Cambridge, MA 02139, USA.
pMAL-Anterior Gradient 2 (AGR2)	A gift from Ronny Drapkin (Addgene plasmid # 18097) Addgene, 75 Sidney Street, Suite 550A, Cambridge, MA 02139, USA.
pET-26b(+)	Novagen, Merck KGaA, Darmstadt, Germany.
pComb3XSS phagemid vector	Sourced from the Applied Biochemistry Group (ABG) laboratory.

2.10 General Lab Techniques

2.10.1 Agarose Gel Electrophoresis

Agarose gel electrophoresis is an effective method for the separation, identification and purification of DNA fragments. Various percentage gels (typically between 0.6-1.5% (w/v)) were prepared by weighing out the required percentage in grams of agarose. The agarose was then dissolved in 1 X Tris-Acetate-EDTA (TAE) buffer (typically 50-100 mL) by heating in the microwave for approximately 1-2 min. SYBR safe (0.001% (v/v)) was added to the cooling gel and swirled. The SYBR safe stains the DNA and allows it to be visualised under U.V light. The gel was then poured into the gel cast, the comb inserted and allowed to set. The gel was placed into the gel apparatus and 1 X TAE was used as the running buffer. To facilitate the loading of samples that are in colourless buffers, a tracker dye was added (2 µL dye + 10 µL sample). Gels were run between 85-100 V for 1 hour. Gels were visualized on a UV transilluminator and photographed using a UV image analyser.

2.10.2 SDS-PAGE

SDS-PAGE is a common method to electrophoretically separate proteins for analysis. This procedure utilises the reducing agent β-mercaptoethanol and heat to dissociate the proteins. The denatured proteins bind to SDS and become negatively charged. The amount of SDS that binds is proportional to the molecular mass of the polypeptides (MacPhee, 2010). The gels were composed as listed in *Section 2.5.2.* The separation gel (12.5% (w/v)) was poured into glass plates held together using Bio-rad gel holder cassettes. The stacking gel (4.5% (w/v)) was then added directly on top of the separation gel. A plastic comb was placed into this gel to create wells for sample loading. Once fully polymerised, the gels were placed into the electrophoresis chamber. The comb was removed and the chamber and wells were submerged in 1 X electrophoresis buffer. The samples were prepared with 4 X SDS sample and heat was applied for 5 min at 95°C to dissociate the proteins into individual polypeptides. Ten µL of PageRuler Plus protein ladder was loaded into a well in each gel for identification of the molecular mass of the proteins. A sample volume of 20 µL was then added to the remaining wells. The gel was run at 140 V until the samples had reached the bottom of the gel. The separated proteins were then visualized by the addition of Instant Blue^{TM} to the gel for 1- 2 hours.

2.10.3 Western Blotting

Western blotting is a technique that transfers a replica of the separated proteins from the polyacrylamide gel onto a nitrocellulose membrane, followed by qualitative detection of a specific protein (MacPhee, 2010). Before transferring the gel onto the nitrocellulose membrane, the gel, filter paper and nitrocellulose membrane were soaked in Thermo Scientific™ Pierce™ 1-Step Transfer Buffer for 15 min to dissociate the SDS from the proteins and improve the adsorption of protein to the membrane (MacPhee, 2010). The proteins were transferred to the membrane using the Pierce™ G2 Fast Blotter at 25V for 7 min. The resulting membrane was then blocked (to block any non-specific binding sites on the membrane and to promote the renaturation of antigenic sites (MacPhee, 2010)) using 50 mL PBS containing 3% (w/v) BSA O/N at 4°C with gentle agitation. The membrane was washed 3 times with PBS and PBS-T 0.05% (v/v). Ten mL of the primary antibody, at the dilution advised by the manufacturer (typically 1/1,000-1/2,000 dilution), was prepared in PBS-T 0.05% (v/v) containing 1% (w/v) BSA and was added on top of the membrane for 1 hour at RT with gentle agitation. The membrane was washed thoroughly as before. If necessary, a secondary antibody was prepared and added identically to addition of the primary antibody and then washed. TMB peroxidase substrate was added to the blot. The TMB forms an insoluble blue precipitate when it comes in contact with the HRP label on the antibody making the protein bands visible.

2.10.4 Quantification of proteins/nucleic acids on the NanoDrop™1000 Spectrophotometer

The NanoDrop™ 1000 spectrophotometer was pre-set to the correct parameters for the sample to be quantified. When measuring protein, the absorbance is 280nm and when measuring DNA, the absorbance is 260nm. The NanoDrop™ was initialised by adding 1 μL of H_2O to the pedestal. This initialization step generates a reading equivalent to a blank reading. It includes any external sources of signal that could react with the detector, and this reading is then removed from all sample, standard and reference readings that are subsequently taken. The machine was then blanked by the addition of the sample buffer. One μL of the sample to be quantified was pipetted onto the pedestal and the measurement was taken in triplicate to ensure accuracy. The pedestal was then blotted clean for the next measurement.

2.10.5 LB Agar plate preparation

The necessary components (*See Section 2.4*) were weighed out into a 1L bottle and autoclaved. The agar was cooled to ~50°C. The appropriate concentration of the necessary antibiotic was added, and the solution was inverted a few times to mix. The agar was then poured into 10 cm polystyrene petri dishes and the plates were allowed to cool with the lids on, until solid. The plates were then labelled and sealed using parafilm and stored at 4°C until needed.

2.10.6 Preparation of bacterial cell stocks

Small-scale cultures (10 mL media supplemented with the relevant antibiotic), containing a single colony from an agar plate, or a scraping from a glycerol stock, were grown O/N at 37°C at 220rpm. In 1.5 mL tubes, bacterial stocks were made to a final volume of 1 mL (500 µL of 50% (v/v) glycerol and 500 µL of overnight culture). These bacterial stocks were stored at -80°C for long-term storage.

2.10.7 Plasmid propagation and purification using NucleoBond® Xtra high-copy plasmid purification

An overnight 10 mL culture, supplemented with the relevant antibiotic, was inoculated with a single colony from an agar plate or glycerol stock and then incubated O/N at 37°C, and 220 rpm. The culture was centrifuged at 11,000*g* (Hermle Z233M-2 Air-cooled version Microcentrifuge) for 10 min at 4°C to pellet the cells. The plasmid was then purified using the NucleoBond® Xtra Midi, as per the manufacturer's guidelines (manufacturers protocol can be found in Appendix D). The purified plasmid was eluted in 30 µL of molecular grade H_2O and quantified using the NanoDrop™ at 260nm.

2.10.8 Optimisation of recombinant protein expression

Optimisation of recombinant protein expression was performed depending on the attributes of the antibody/analyte of interest. Various concentrations of isopropyl β-D-1-thiogalactopyranoside (IPTG), for induction of protein expression, temperatures and media types were evaluated. This section describes a generic protocol for expression studies, with any refinements, deviations or modifications noted in the relevant sections. An 10 mL culture, containing a single colony from a plate or using a bacterial glycerol stock, supplemented with the relevant antibiotic, was grown O/N at 37°C at 220rpm. The following day, subcultures were inoculated and grown at 37°C at 220rpm until an $O.D_{600}$

of ~0.6 was reached. The cultures were then induced with varying concentrations of IPTG and grown at different temperatures (25°C, 30°C and 37°C) O/N at 220rpm. The next day the samples were removed and centrifuged at 11,000*g* (Hermle Z233M-2 Air-cooled version Microcentrifuge) for 30 min. The pellets were resuspended in 200 µL of 1 mg/mL lysozyme in 1X PBS. The lysozyme breaks down the peptidoglycan in the bacterial cell wall resulting in bacterial cell lysis. The samples were then alternated from -80°C for 10 min, to 37°C for 10 min, for a minimum of 3 times to ensure complete cell lysis. The cellular debris was collected by centrifugation of the samples at 11,000*g* (Hermle Z233M-2 Air-cooled version Microcentrifuge) for 45 min at 4°C. The supernatant was collected and prepared for analysis by SDS-PAGE and WB.

2.11 Mammalian cell culture methods

All methods described below were performed aseptically in a laminar flow hood.

2.11.1 Preparation of Complete Growth Media (CGM) for mammalian cell lines

CGM preparation was carried out aseptically in a laminar hood. The media and FBS were pre-warmed in a 37°C water bath for 30 min. Any cell-line dependent additives, 10-20% (v/v) FBS and 1 mL of 10,000 I.U./mL Penicillin-10,000 (µg/mL) Streptomycin were added, at the appropriate concentration, to the media specified for each cell line, as per S*ection 2.4*. The media mixture was swirled and stored at 4°C until further use. FBS is a supplement that is a mixture of necessary growth promoting and inhibiting biomolecules that aid in cell growth, metabolism and stimulate proliferation (Brunner *et al.,* 2010) whereas, penicillin-streptomycin is added to reduce the chances of microbial contamination.

2.11.2 Thawing and propagation of mammalian cell stocks

The appropriate CGM was placed in the 37°C bath for 30 min. A cryovial was removed from the liquid nitrogen (LN_2) carefully, using gloves and protective face-wear. The vial was thawed quickly with gentle agitation in a water bath with the lid kept above water to avoid contamination. Once thawed, the 1mL cell solution was removed and suspended in 9mL of pre-warmed CGM. The cells were then spun down at 125*g* for 5 min (Sigma Laborzentrifugen Model 2K15). The supernatant was removed and discarded, and the cell pellet was resuspended in 10 mL of CGM and placed in a T-25cm^2 cell culture flask. The

flask was incubated in the 37°C/ 5% CO_2 for the cells to recover and propagate. After ~72 hours the cells were subcultured to maintain optimum propagation conditions.

2.11.3 Subculturing of adherent mammalian cells

The CGM and sterile 'Ca^{2+} - and Mg^{2+} - free' (Ca^{2+} and Mg^{2+} promote cell adherence thus they can hinder the removal of adherent cells from the flaks surface) DPBS were pre-warmed in the 37°C water bath for 30 min. The media within the flask of cells was removed and discarded. DBPS was carefully added to avoid dislodgment of the adherent cells. Using a gentle rocking motion the cells were rinsed and the DPBS was discarded to remove any dead or loosely bound cells. Warm CGM was added to the flask and a rubber policeman employed to gently lift adherent cells from the surface of the flask. One mL of the detached cell suspension was removed for cell counting and determination of cell viability, as detailed in *Section 2.11.4.* The cell suspension was centrifuged at 125*g* for 5 min (Sigma Laborzentrifugen Model 2K15) and the supernatant was discarded. The pellet was resuspended in the appropriate volume of CGM and added to a new flask with fresh CGM. The flask of cells was then placed in the 37°C/ 5% CO_2 incubator to allow the cells to propagate.

2.11.3.1 Subculturing of Jurkat E6.1 clone cells

This protocol was performed as outlined in *Section 2.11.3*

Protocol Deviations:

I. The Jurkat E6.1 cell line is a T-lymphocyte suspension cell line and did not require a wash using DBPS or scraping. The Jurkat E6.1 clone cells/CGM mix was removed from the flask and then centrifuged at 125 *g* for 5 min (Sigma Laborzentrifugen Model 2K15). The supernatant was discarded and the pellet was resuspended in fresh pre-warmed CGM and added to a flask of fresh CGM at a concentration of $1 \times 10^5 – 1 \times 10^6$ cells in a T-75cm flask.

2.11.4 Counting mammalian cells

Cell viability counts were performed using the trypan blue exclusion method. This method is based on the concept that viable cells will not be stained by the membrane impermeable trypan blue stain but permeable dead cells will. This leaves the non-viable cells stained blue under the microscope and the live cells remain unstained (Louis *et al.,*

2011). One hundred µL of cell suspension was mixed with 150 µL PBS and 250 µL of trypan blue (0.4% v/v) and left at RT for 2 min. Ten µL was added to each side of a disposable C-Chip hemocytometer and examined under the 10 X objective using the Nikon Diaphot Inverted Tissue Culture Microscope. Viable cells within the central grid were counted and calculated using the following formula: Cell/mL = N x 5 x 10^4 (N = average viable cells counted, 5 = dilution factor, 10^4 = constant).

2.11.5 Harvesting of mammalian cells for cryopreservation of cell stocks

Cryopreservation is the process by which living cells are cooled to sub-zero temperatures to effectively stop any enzymatic or chemical activity that could be damaging (Pegg, 2007). Cells were harvested from 90% confluent flasks. The cells were washed using DPBS, removed from the flask and centrifuged as described in *Section 2.11.3.* The pellet was resuspended in freezing media (95% (v/v) CGM and 5% (v/v) DMSO) to create a cell suspension of ~1-2 x 10^6 viable cell / mL. The aliquots were placed in a Mr. Frosty freezing container and filled with ice cold isopropanol, at -80°C for 12 hours. The cell aliquots were then stored in LN_2 indefinitely.

2.11.6 Cell authentication and mycoplasma testing for mammalian cells

In order to determine the authenticity of cell lines, short tandem repeat (STR) analysis was performed by investigating a number of highly polymorphic unlinked loci. Furthermore, a DNA PCR mycoplasma test that screens for 19 contaminant species was performed. This cell line authentication and mycoplasma testing was carried out on all cell lines employed herein, using the DDC Medical DNA collection card kit. In accordance with the kit instructions, 1 x 10^6 cells were spotted onto the suppled sample collection card and allowed to dry. The card was subsequently shipped to DCC where STR and mycoplasma analysis was carried out and results were later provided via email.

2.12 Expression and purification of a recombinant AGR2 protein

2.12.1 Streaking of pMAL-AGR2 plasmid to obtain single colonies

LB agar plates supplemented with 100 µg/mL carbenicillin were made as outlined in *Section 2.10.5.* Using an inoculation loop, the plasmid was streaked onto 4 separate plates and incubated inverted at 37°C O/N. The colony-covered plates were then stored at 4°C.

2.12.2 Small-scale expression studies of the fusion protein AGR2-MBP

A 10 mL culture, containing a single colony from a plate or using a bacterial glycerol stock supplemented with 100 µg/mL of carbenicillin, was grown O/N at 37°C at 220rpm. The next day, 10 mL auto-induction media with various broth bases, supplemented with 100 µg/mL carbenicillin, were inoculated with the overnight culture. These cultures were grown O/N at 37°C and 30°C at 220rpm. A one mL sample from each of the cultures was removed and centrifuged at 11,000*g* (Hermle Z233M-2 Air-cooled version Microcentrifuge) for 30 min. The supernatant was discarded and the pellets were retained and stored at -80°C.

2.12.3 Lysis of *E. coli* for analysis of protein expression

The protein pellets were thawed at 37°C in a water bath and resuspended in 200 µL of 1 mg/mL lysozyme in 1 X PBS. The samples were alternated from -80°C for 10 min to 37°C for 10 min for a minimum of 3 times. The cellular debris created by lysis was collected by centrifuging the samples at 11,000*g* (Hermle Z233M-2 Air-cooled version Microcentrifuge) for 45 min at 4°C. The supernatant was collected and prepared for SDS-PAGE and WB.

2.12.4 Large-scale expression of AGR2-MBP fusion protein

A 10 mL culture containing a single colony from a plate or using a bacterial glycerol stock, supplemented with 100 µg/mL of carbenicillin, was grown O/N at 37°C at 220rpm. One litre of auto-induction media in TB broth was made, as described in *Section 2.4,* and split into 5 x 200mL sterile flasks, supplemented with 100 µg/mL carbenicillin, and inoculated with 200 µL of the 10 mL overnight culture. The 5 x 200 mL flasks were grown O/N at 37°C at 220rpm. The entire 1L culture was then centrifuged at 4,000*g* (Eppendorf ™ Centrifuge fixed angle rotor (F-45-30-11)) for 20 min and the pellets were retained and stored at -80°C.

2.12.5 Sonication of *E. coli* cells prior to purification of selected proteins

The large-scale AGR2-MBP fusion protein expression pellets were resuspended in 10mL of column buffer and incubated on ice *(Section 2.5.3)*. The sonicator was set to the following conditions: 25% amplitude, 2 sec on pulse, 2 sec off pulse for 2 min. After sonication, the samples were centrifuged at 11,000*g* (Eppendorf ™ Centrifuge fixed angle rotor (F-45-30-11)) for 30 min at 4°C. The supernatant was collected and filtered using a

0.2 µM filter. This 'filtered lysate' was applied to the amylose resin column for protein purification.

2.12.6 Purification of the fusion protein AGR2-MBP by amylose resin

Amylose resin is an affinity resin used in a gravity flow column for the purification of proteins that are fused to maltose binding protein (MBP) (Neissi *et al.,* 2013). Three mL of the amylose resin slurry (Brennan & Co.) was added to the column. Once settled, the resin was equilibrated with 30 mL of ice-cold column buffer. The filtered lysate was diluted 1:6 with column buffer and applied to the column. A 30 µL sample was retained and marked as 'Flow-through 1'. This flow-through was then re-applied to the column and a second sample was taken and marked as 'Flow-through 2'. The column was then washed three times, each with 10 mL of column buffer. With each wash a sample was taken to identify any protein loss during the wash steps. The bound protein was eluted with 8 mL of elution buffer (column buffer & 10 mM maltose). This was collected in 8 x 1 mL fractions. All the samples taken were analysed on an SDS-PAGE and WB to determine the AGR2-MBP fusion protein-containing fractions. Protein-containing fractions were concentrated using a Vivaspin 50,000 MW 'cut-off' column.

2.12.7 Protease cleavage of MBP from AGR2 protein

Cleavage of AGR2 from MBP was carried out using the protease Factor Xa. It cleaves after the arginine residue in its preferred site IIe-(Glu or Asp)-Gly-Arg. One µg of Factor Xa was added per 50 µg of fusion protein and incubated O/N at RT. The Factor Xa was inactivated by the addition of 1,5-Dansyl-Glu-Gly-Arg Chloromethyl Ketone Dihydrochloride (EMD Millipore) to a final concentration of 2 µM. Following cleavage, the mixture was buffer exchanged into 1 X PBS, pH 7.4, using a Vivaspin column.

2.12.8 Gel filtration of AGR2 protein on an ÄKTA pure system

Gel filtration (also referred to as size exclusion chromatography) is a basic chromatographic technique that separates proteins based on differences in molecular size and shape as they pass through a gel filtration medium in a packed column, and it is often used as a final polishing purification step (Kim *et al*., 2011). A Superdex 75 10/300 GL column gel filtration column (GE Healthcare) was equilibrated with 1 X PBS, pH 7.4, (1CV = 50 mL). The cleaved AGR2-MBP mixture was applied to the column at a flow rate of 0.5 mL/min. Fractions were collected after 0.4 CV until 1 CV was reached. Protein

was monitored online by A_{280} using the dedicated Unicorn control and evaluation software (GE Healthcare). Protein peaks were analysed by SDS-PAGE/WB and quantified using the NanoDrop™. Protein-containing fractions were concentrated to 500 µL.

2.13 Expression and purification of a recombinant MUC1 protein

2.13.1 Heat-shock transformation of Mucin 1 (MUC1) Protein Vector (Human) (pPB-N-His) into One Shot® BL21 (DE3) *E. coli* chemically competent cells

LB agar plates supplemented with 50 µg/mL of kanamycin were pre-warmed in a 37°C incubator. A 50 µL aliquot of One Shot® BL21 (DE3) *E. coli* of chemically competent cells (Invitrogen) was thawed on ice for 5 min. One µL of plasmid at a concentration of 10 ng/µL was added to the cells. These were mixed by gentle tapping and left on ice for 30 min. The competent cell/plasmid mix was placed in a 42°C water bath for 45 sec and then incubated on ice for 2 min. The cells were recovered by adding 150 µL of pre-warmed SOC media and then incubated at 37°C at 240 rpm for 1 hour. This step allows the bacteria to generate the antibiotic resistance proteins to ensure they can grow on the agar plates. The recovered cells were spread onto LB plates, containing 50 µg/mL of kanamycin in various dilutions, to obtain single colonies. The plates were inverted and incubated at 37°C O/N.

2.13.2 Optimisation of expression of recombinant MUC1 protein

This protocol was performed as outlined in *Section 2.10.8.*

2.13.3 Large-scale expression of recombinant MUC1 protein

This protocol was performed as outlined in *Section 2.12.4.*

2.13.4 Sonication of *E. coli* cells for purification

This protocol was performed as outlined in *Section 2.12.5.*

Protocol deviations:

I. For buffers used for lysis, see *Section 2.5.4.*

2.13.5 Purification of recombinant proteins using Ni^2-NTA resin

The lysate supernatant was collected and filtered using a 0.2 µM filter to remove residual cells debris. Three mL of Ni^2-NTA resin slurry (Novagen) was added to the column and allowed to settle. The resin was equilibrated with 10 mL of equilibration buffer. The lysate was applied to the column and allowed to flow through the resin; a sample of this was retained and marked as 'Flow-through 1'. This flow-through was then re-applied to the column and a second sample was taken and marked as 'Flow-through 2'. The column was washed with 10 mL of wash buffer A, followed by 10 mL of wash buffer B to remove any loosely bound proteins. With each wash, a sample was taken to determine if there was any protein loss during the wash steps. The bound HIS-tagged protein was then eluted with 8 mL of elution buffer in 1 mL fractions. The eluted fractions containing the antibody were then buffer exchanged against filtered PBS (with 0.02% (w/v) NaN_3) using a Vivaspin™ 6 column with the appropriate molecular weight 'cut-off'. The purified sample was then analysed on the NanoDrop™ 1000 and stored at -20°C. The efficiency of the purification was evaluated using SDS-PAGE and Western-blotting as per *Sections 2.10.2* and *2.10.3.*

2.14 Mammalian Expression of a recombinant MSLN protein

2.14.1 Preparation of adenoviral DNA for transfection by digestion of pAdEasy-Msln-iCre-HA-Flag vector

The bacterial stab of DH5aplha *E. coli* cells containing the pAdEasy-Msln-iCre-HA-Flag vector was streaked onto an LB agar plate supplemented with 60 µg/mL kanamycin to obtain single colonies. A single colony was used to inoculate a 10 mL culture of SB media supplemented with 60 µg/mL kanamycin and incubated while shaking at 220rpm at 37°C O/N. The plasmid was purified from the culture (as per *Section 2.10.6*) and linearized using the *Pac*I enzyme acquired from NEB using the NEB CutSmart® buffer.

Table 2.1: Components for PacI linearization of adenoviral DNA

Component	Concentration/Volume
Purified pAdEasy-Msln-iCre-HA-Flag	1 µg
*Pac*I (10,000 units /mL)	1 U
CutSmart® Buffer (10X)	5 µL
Molecular grade H_2O	Up to 50 µL

The digestions were incubated at 37°C for 1 hour and de-activated at 65°C for 20 min. The digested vector was analysed on a 0.6% (w/v) agarose gel with non-digested vector acting as a control.

2.14.2 Mammalian Expression of recombinant MSLN

Transfection of the pAdEasy-Msln-iCre-HA-Flag was achieved using the ViraPack Transfection Kit (Agilent). This is based on a modified $CaPO_4$ method of DNA transfection into HEK293 cells. The $CaPO_4$ forms a precipitate resulting in transfection by enhancing the adsorption of DNA to cell membranes and thus, DNA uptake by the mammalian cells. Additionally, the $CaPO_4$ precipitate limits the digestion of the DNA by DNase associated with mammalian cells (Ling *et al.,* 2017).

Twenty-four hours prior to transfection, HEK293 cells were plated at 1 x 10^5 cells / well (in 5 mL CGM) in a 6-well 60-mm tissue culture plate. The cells were incubated at 37°C/ 5% CO_2 O/N. The following day 5 µg of digested plasmid was added to 450 µL sterile H_2O. The transfection was completed as per the manufacturer's guidelines for the ViraPack Transfection Kit. Briefly, the DNA was incubated with a $CaCl_2$/ BBS (N-bis-2-hydroxyethyl)-2-aminoethanesulfonic acid and buffered saline) solution. Concurrently, the CGM was removed from the HEK293 cells. The cells were then washed twice with DPBS and 5 mL of DMEM containing 6% (v/v) modified bovine serum (MBS) was added. The DNA solution was slowly added in a circular dropwise motion and the flask swirled gently to ensure even distribution of the DNA in the culture plate. The tissue culture plates were then incubated for 3 hours at 37°C/ 5% CO_2. The supernatant was removed and the cells washed 3 times with DPBS. Fresh CGM was added to the tissue

culture plates and left at 37°C/ 5% CO_2. Six -days post-transfection the cells and supernatant were harvested for MSLN protein purification.

2.14.3 Gel filtration of MSLN protein on an ÄKTA pure system

This protocol was performed as outlined in *Section 2.13.8.*

2.15 Generation of a murine anti-Capan-1 scFv library

2.15.1 Immunisation of BALB/c mice using Capan-1 pancreatic cancer cell line

This cell line was selected as the literature confirmed that it positively expressed the three markers that antibodies were generated against. A group of six female BALB/c mice aged 5-8 weeks, were each initially immunised with 1 x 10^6 Capan-1 cells in a 1:1 ratio of sterile PBS and Freund's complete adjuvant to a final volume of 200 µL/per mouse. Freund's complete adjuvant contains heat-killed mycobacteria, which attracts cells such as macrophages to the injection site enhancing the immune response (Billiau *et al.,* 2001). The solution was injected into the peritoneal cavity. Four subsequent boosts (days 14, 28, 42 and 56) were performed using the same volume of cells in a 1:1 ratio with Freund's incomplete adjuvant. Freund's incomplete adjuvant lacks the mycobacteria resulting in minimal side effects and consequently is used for boosting (Billiau *et al.,* 2001). A bleed was taken from the mice facial vein 7 days after each injection and was employed to determine the antibody titre against Capan-1 cells. Once a high titre response was reached, the mice were given a final boost into the peritoneal cavity and then sacrificed 7 days later.

2.15.2 Analysis of immune response to Capan-1 cells

Nunc MaxiSorp™ immunoplates were coated with 1 x 10^5 cells/well in 105 µL CGM and 10 µL of FBS. The plate was incubated O/N at 37°C / 5% CO_2. The plate was blocked with 200 µL /well of PBS containing 3% (w/v) BSA for 1 hour at 37°C / 5% CO_2. The plate was washed 3 times with PBS-T (0.05% (v/v)) and PBS. Serial dilutions of each of the mice anti-serum in PBS-T (0.05% (v/v)) containing 1% (w/v) BSA were added to the wells (100 µL/well) and incubated at 37°C / 5% CO_2 for 1 hour. The plate was washed as before. A 1 in 2,000 dilution of HRP-labelled goat anti-mouse IgG antibody in PBS-T (0.05% (v/v)) containing 1% (w/v) BSA was added to each well (100 µL/well) and incubated for 1 hour at 37°C / 5% CO_2. The plate was then washed as before and TMB substrate was added (100 µL/well). The plate was incubated at 37°C for 30 min, after

which the reaction was stopped by the addition of 10% (v/v) HCl (50 µL/well). The absorbance was read at 450nm on a Tecan Safire2™ platereader.

2.15.3 Extraction and isolation of total RNA from mouse spleens

The following preparatory steps were taken before the RNA extraction was carried out; Oakridge tubes were decontaminated using Virkon®, washed with 'Rnase-free' water, sprayed with RnaseZap® and left O/N to ensure complete eradication of remaining Rnases. The homogenizer was incubated in Precept™, washed with 'Rnase free' water, autoclaved and then baked in a 60°C oven O/N. The 75% (v/v) ethanol was prepared using 'Rnase-free' water in 'Rnase-free' tubes and stored until needed at -20°C. The laminar flow hood was de-contaminated with 70% (v/v) IMS and RnaseZap.

The mice were sacrificed by cervical dislocation. Four of the six mouse spleens were removed, submerged in RNAlater in 'Rnase-free' tubes and stored at -80°C. The remaining two spleens were placed in 10 mL of ice-cold TriZol® reagent (Sigma) and homogenized. TriZol® is a phenol and guanidine isothiocyanate-based solution that solubilises biological material and denatures protein. During homogenization TriZol® retains the integrity of the RNA while disrupting cells and cell components (Rio *et al.,* 2010). The homogenized spleen / TriZol® mix was then centrifuged at 1575*g* (Sigma Laborzentrifugen Model 2K15) for 10 min at 4°C. The supernatant was removed into a 85 mL Oakridge tube containing 2 mL of ice-cold chloroform. This was mixed well by shaking and let stand at RT for 15 min. The supernatant containing chloroform was then centrifuged at 17,500*g* (Eppendorf ™ Centrifuge fixed angle rotor (F-45-30-11)) for 20 min at 4°C. The addition of chloroform causes phase separation resulting in 3 layers. Protein is extracted to the lower organic layer, DNA resolves at the interface and RNA remains in the upper aqueous layer (Rio *et al.,* 2010). The upper aqueous layer was very carefully removed, taking the utmost care to not disrupt the other layers. The upper aqueous layer was added to a fresh 85 mL Oakridge tube with 5mL of isopropanol for precipitation of RNA. The sample was mixed and let stand at RT for 10 min. The sample was then centrifuged at 17,500*g* (Eppendorf ™ Centrifuge fixed angle rotor (F-45-30-11)) for 20 min at 4°C. The resulting supernatant was carefully removed and discarded without disrupting the pellet. The RNA pellet was washed by adding 10 mL of 75 % (v/v) ethanol and centrifuging at 17,500*g* (Eppendorf ™ Centrifuge fixed angle rotor (F-45-30-11)) for 10 min at 4°C. The supernatant was again carefully removed and discarded.

The pellet was the allowed to air dry in the laminar flow hood for 10 min. Once dry, the pellet was resuspended in 250 µL of 'Rnase-free' molecular grade water (Sigma) and transferred into a 2 mL 'Rnase-free' tube and stored on ice. The RNA was quantified on the NanoDrop™ and cDNA synthesis was immediately performed.

2.15.4 cDNA synthesis

The RNA obtained from the murine spleens was transcribed to cDNA by reverse transcription PCR. The cDNA serves as a template for the amplification of the variable heavy and light chain gene fragments for antibody library building. The cDNA synthesis reaction was performed using a Superscript III first strand cDNA synthesis kit (Invitrogen). This kit was used as it includes a polymerase is a version of Moloney Murine Leukemia Virus Reverse Transcriptase (M-MLV RT) which is superior to other superscripts due to its reduced Rnase H activity and full enzymatic activity at 50°C. The reaction components were as follows:

Table 2.2: Mixture 1 components

Mixture 1	Volume
Total RNA	X µL
Oligo dT (50µM)	20 µL
dNTPs 10mM	20 µL
MgH_2O	Up to 200 µL
Total	**200 µL**

Table 2.3: Mixture 2 components

Mixture 2	Volume
10x RT Buffer	40 µL
25mM $MgCl_2$	80 µL
0.1M DTT	40 µL
RNase Out (40U/µL)	20 µL
Superscript III RT (200U/µL)	20 µL
Total	**200 µL**

Mixture 1 was dispensed into 8 tubes (25 µL/tube) and incubated at 65°C in the thermal cycler (Biometra $T_{Gradient}$ PCR machine). The samples were then placed on ice for 1 min. Mixture 2 was then dispensed into the 8 tubes (25 µL/tube) and incubated at 50°C for 50 min followed by 85°C for 5 min. The tubes were placed on ice for 3 min and 5 µL of RNase H was added to each. The RNase H was added last as the presence of RNase H during the first-strand synthesis digests the template mRNA reducing the sensitivity of the PCR. The tubes were then incubated at 37°C for 20 min. Once complete, the 8 x 50 µL tubes were combined and stored at -20°C. The cDNA was then quantified using the NanoDrop™.

2.15.5 PCR primers for amplification of mouse scFv (pComb3XSS vector)

All primers were synthesized by IDT.

Vκ5' Sense Primers

MSCVK-1	5' GGG CCC AGG CGG CCG AGC TCG AYA TCC AGC TGA CTC AGC C 3'
MSCVK-2	5' GGG CCC AGG CGG CCG AGC TCG AYA TTG TTC TCW CCC AGT C 3'
MSCVK-3	5' GGG CCC AGG CGG CCG AGC TCG AYA TTG TGM TMA CTC AGT C 3'
MSCVK-4	5' GGG CCC AGG CGG CCG AGC TCG AYA TTG TGY TRA CAC AGT C 3'
MSCVK-5	5' GGG CCC AGG CGG CCG AGC TCG AYA TTG TRA TGA CMC AGT C 3'
MSCVK-6	5' GGG CCC AGG CGC CCC AGC TCG AYA TTM AGA TRA MCC AGT C 3'
MSCVK-7	5' GGG CCC AGG CGG CCG AGC TCG AYA TTC AGA TGA YDC AGT C 3'
MSCVK-8	5' GGG CCC AGG CGG CCG AGC TCG AYA TYC AGA TGA CAC AGA C 3'
MSCVK-9	5' GGG CCC AGG CGG CCG AGC TCG AYA TTG TTC TCA WCC AGT C 3'
MSCVK-10	5' GGG CCC AGG CGG CCG AGC TCG AYA TTG WGC TSA CCC AAT C 3'

MSCVK-11 5’ GGG CCC AGG CGG CCG AGC TCG AYA TTS TRA TGA CCC ART C 3’

MSCVK-12 5’ GGG CCC AGG CGG CCG AGC TCG AYR TTK TGA TGA CCC ARA C 3’

MSCVK-13 5’ GGG CCC AGG CGG CCG AGC TCG AYA TTG TGA TGA CBC AGK C 3’

MSCVK-14 5’ GGG CCC AGG CGG CCG AGC TCG AYA TTG TGA TAA CYC AGG A 3’

MSCVK-15 5’ GGG CCC AGG CGG CCG AGC TCG AYA TTG TGA TGA CCC AGW T 3’

MSCVK-16 5’ GGG CCC AGG CGG CCG AGC TCG AYA TTG TGA TGA CAC AAC C 3’

MSCVK-17 5’ GGG CCC AGG CGG CCG AGC TCG AYA TTT TGC TGA CTC AGT C 3’

Vκ3’ Reverse Primers

MSCJK12-BL 5’ GGA AGA TCT AGA GGA ACC ACC CCC ACC ACC GCC CGA GCC ACC GCC ACC AGA GGA TTT KAT TTC CAG YTT GGT CCC 3’

MSCJK4-BL 5’ GGA AGA TCT AGA GGA ACC ACC CCC ACC ACC GCC CGA GCC ACC GCC ACC AGA GGA TTT TAT TTC CAA CTT TGT CCC 3’

MSCJK5-BL 5’ GGA AGA TCT AGA GGA ACC ACC CCC ACC ACC GCC CGA GCC ACC GCC ACC AGA GGA TTT CAG CTC CAG CTT GGT CCC 3’

Vλ5’ Sense Primer

MSCVL-1 5’ GGG CCC AGG CGG CCG AGC TCG ATG CTG TTG TGA CTC AGG AAT C 3’

Vλ3' Reverse Primer

MSCJL-BL 5' GGA AGA TCT AGA GGA ACC ACC CCC ACC ACC GCC CGA GCC CGA GCC ACC GCC ACC AGA GGA GCC TAG GAC AGT CAG TTT GG 3'

VH5' Sense Primers

MSCVH1 5' GGT GGT TCC TCT AGA TCT TCC CTC GAG GTR MAG CTT CAG GAG TC 3'

MSCVH2 5' GGT GGT TCC TCT AGA TCT TCC CTC GAG GTB CAG CTB CAG CAG TC 3'

MSCVH3 5' GGT GGT TCC TCT AGA TCT TCC CTC GAG GTC CAG CTG AAG SAS TC 3'

MSCVH4 5' GGT GGT TCC TAT AGA TCT TCC CTC GAG GTC CAR CTG CAA CAR TC 3'

MSCVH5 5' GGT GGT TCC TCT AGA TCT TCC CTC GAG GTY CAG CTB CAG CAR TC 3'

MSCVH6 5' GGT GGT TCC TCT AGA TCT TCC CTC GAG GTY CAR CTG CAG CAG TC 3'

MSCVH7 5' GGT GGT TCC TCT AGA TCC TCC CTC GAG GTC CAC GTG AAG CAG TC 3'

MSCVH8 5' GGT GGT TCC TCT AGA TCT TCC CTC GAG GTG AAS STG GTG GAA TC 3'

MSCVH9 5' GGT GGT TCC TCT AGA TCT TCC CTC GAG GTG AWG YTG GTG GAG TC 3'

MSCVH10 5' GGT GGT TCC TCT AGA TCT TCC CTC GAG GTG CAG SKG GTG GAG TC 3'

MSCVH11 5’ GGT GGT TCC TCT AGA TCT TCC CTC GAG GTG CAM CTG GTG GAG TC 3’

MSCVH12 5’ GGT GGT TCC TCT AGA TCT TCC CTC GAG GTG AAG CTG ATG GAR TC 3’

MSCVH13 5’ GGT GGT TCC TCT AGA TCT TCC CTC GAG GTG CAR CTT GTT GAG TC 3’

MSCVH14 5’ GGT GGT TCC TCT AGA TCT TCC CTC GAG GTR AAG CTT CTC GAG TC 3’

MSCVH15 5’ GGT GGT TCC TCT AGA TCT TCC CTC GAG GTG AAR STT GAG GAG TC 3’

MSCVH16 5’ GGT GGT TCC TCT AGA TCT TCC CTC GAG GTT ACT CTR AAA GWG TS 3’

MSCVH17 5’ GGT GGT TCC TCT AGA TCT TCC CTC GAG GTC CAA CTV CAG CAR CC 3’

MSCVH18 5’ GGT GGT TCC TCT AGA TCT TCC CTC GAG GTG AAC TTG GAA GTG TC 3’

MSCVH19 5’ GGT GGT TCC TCT AGA TCT TCC CTC GAG GTG AAG GTC ATC GAG TC 3’

VH3’ Reverse Primers

MSCG1ab-B 5’ CCT GGC CGG CCT GGC CAC TAG TGA CAG ATG GGG STG TYG TTT TGG C 3’

MSCG3-B 5’ CCT GGC CGG CCT GGC CAC TAG TGA CAG ATG GGG CTG TTG TTG T 3’

MSCM-B	5’ CCT GGC CGG CCT GGC CAC TAG TGA CAT TTG GGA AGG ACT GAC TCT C 3’

SOE Sense Primer

RSC-F	5’ GAG GAG GAG GAG GAG GAG GCG GGG CCC AGG CGG CCG AGC TC 3’

SOE Reverse Primer

RSC-B	5’ GAG GAG GAG GAG GAG GAG CCT GGC CGG CCT GGC CAC TAG TC 3’

Note: Avian primers employed are outlined in Appendix B.

2.15.6 Amplification of antibody variable domain genes using pComb series primers

The PCR reaction components and conditions were as follows:

Table 2.4 Components and volumes for variable domain PCR

Component	Concentration/Volume
cDNA	0.5 µg
2x MyTaq Reaction Buffer	25 µL
Forward Primer	2 µM
Reverse Primer	2 µM
Molecular grade H_2O	Up to 50 µL
Total	**50 µL**

The amplification of the variable regions was performed in the Biometra $T_{Gradient}$ PCR machine under the following conditions:

Table 2.5 PCR thermal cycler conditions

Temperature		Time	
Step 1:	95 °C	5 min	
Step 2:	95 °C	30 sec	30 cycles
	60 °C	30 sec	
	72 °C	45 sec	
Step 3:	72 °C	5 min	

Once the variable regions were successfully amplified, the PCR samples were analysed (10 µL /well) on a 1.5% (w/v) agarose gel with 1kb Hyperladder (Bioline) for DNA size determination (*Section 2.10.1).* The reaction was then carried out large-scale (10-20 X) and the resulting PCR products were pooled and ethanol-precipitated *(Section 2.15.7)*. The products were then purified from a 1.5% (w/v) agarose gel using the using NucleoSpin® PCR Clean-Up Kit and the DNA was quantified by measuring the absorbance on the NanoDrop™ at 260nm.

2.15.7 Ethanol Precipitation of PCR products

The PCR samples were pooled and the following was added:

- 0.1 X 3M Sodium acetate (pH 5.5)
- 2 X 100% (v/v) Ethanol (Ice cold)
- 1 µL Glycogen

The solution was mixed and incubated at -20°C O/N. The DNA was pelleted by centrifugation at 20,000*g* (Hermle Z233M-2 Air-cooled version Microcentrifuge) for 30 min at 4°C. The supernatant was removed and discarded and the DNA pellet was washed with 250 µL of 70% (v/v) isopropanol to remove any excess contaminants such as salts and chelators. This was achieved by centrifugation at 20,000*g* (Hermle Z233M-2 Air-cooled version Microcentrifuge) for 10 min at 4°C. The supernatant was once again removed and discarded and the pellet was allowed to air-dry. Once dry, the pellet was resuspended in 30 µL of pre-warmed molecular grade water.

2.15.8 Purification of the variable region gene fragments using NucleoSpin® PCR Clean-Up Kit

The ethanol-precipitated variable fragments were analysed on an agarose gel. The appropriate DNA band was excised from the gel (~400bp for V_H, ~350bp for V_L chains). The excised gel was weighed and binding buffer (NTI) was added at 200 µL per 100 mg of gel. The excised gel pieces and buffer were incubated in the water bath at 50°C until completely melted. The melted gel was loaded into the provided NucleoSpin® Gel and PCR Clean-up Column and the method was performed according to manufacturer's guidelines. The eluted DNA was then quantified using the NanoDrop ™.

2.15.9 Splice by overlap extension PCR

In the SOE-PCR, the purified variable heavy and variable light chain gene fragments are mixed in equal ratios to generate the overlap product (~800bp) joined by a glycine-serine linker $(G_4S)_4$ incorporated by the primers.

The SOE-PCR components and conditions were as follows:

Table 2.6: SOE-PCR components and volumes

Component	Concentration/Volume
2x MyTaq Reaction Buffer	25 µL
Forward Primer	2 µM
Reverse Primer	2 µM
V_H DNA	100 ng
V_L DNA	100 ng
Molecular grade H_2O	Up to 50 µL
Total	**50 µL**

The amplification of the SOE product was performed in the Biometra $T_{Gradient}$ PCR machine under the following conditions:

Table 2.7: SOE-PCR thermal cycler conditions

Temperature		Time	
Step 1:	95 °C	5 min	
Step 2:	95 °C	30 sec	30 cycles
	60 °C	30 sec	
	72 °C	90 sec	
Step 3:	72 °C	10 min	

2.15.10 Restriction-digest of the purified overlap PCR product and vector DNA

The restriction digest was carried out using *Sfi*I enzyme acquired from NEB using the NEB CutSmart® Buffer.

Table 2.8: Components and volumes for restriction digest

Component	Concentration/Volume
Digestion of the SOE-PCR product:	
Purified SOE-PCR product	10 µg
*Sfi*I (36U per µg of DNA)	360 U
CutSmart® Buffer (10 X)	20 µL
Molecular grade H_2O	Up to 200 µL
Digestion of the vector DNA:	
Purified vector DNA (pComb3XSS)	20 µg
*Sfi*I (6U per µg of DNA)	120 U
CutSmart® Buffer (10X)	20 µL
Molecular grade H_2O	Up to 200 µL

The digests were incubated at 50°C for 5 hours and de-activated at 65°C for 20 min. The pComb3XSS vector was treated with Antarctic Phosphatase for 15 min at 37°C, and de-activated at 70°C for 5 min. The Antarctic Phosphatase catalyses the dephosphorylation of the 5' and 3' ends of DNA which prevents re-ligation of the plasmid. The digested SOE-PCR fragment and digested pComb3XSS vector were ethanol precipitated O/N (*Section 2.15.7*) at -20°C. The digested SOE –PCR fragment was analysed on a 1% (w/v) agarose gel and the pComb3XSS gel on a 0.6% (w/v) gel. The SOE-PCR fragment,

pComb3XSS vector and pComb3XSS stuffer fragment were purified from the gel using NucleoSpin® Gel and PCR Clean-up kit. DNA was quantified using the NanoDrop™ at 260nm.

2.15.11 Ligation of the digested SOE-PCR product with vector DNA

The purified *Sfi*I-digested scFv fragment was cloned into the purified *Sfi*I -digested pComb3XSS vector using T4 DNA ligase. The T4 ligase catalyses the formation of phosphodiester bonds between juxtaposed 5` phosphate end and 3` hydroxyl termini in duplex DNA.

Table 2.9: Components and volumes for ligation reaction

Component	Concentration/Volume
Ligation of the SOE-PCR product into the pComb3XSS vector:	
pComb3XSS (digested and purified)	1.4 µg
SOE-PCR product (digested and purified)	700 ng
T4 DNA Ligase buffer (10X)	40 µL
T4 DNA Ligase	10 µL
Molecular grade H_2O	Up to 400 µL

The ligations were incubated at 16°C O/N at RT and de-activated at 65°C for 20 min. The ligated vector with SOE-PCR insert were then ethanol precipitated (see *Section 2.15.7*.). The DNA pellet was resuspended in 30 µL of MGH_2O and transformed into *E. coli* XL1-Blue electrocompetent cells (BioSciences) by electroporation.

2.16 Antibody phage display and library panning

2.16.1 Transformation of *E. coli* XL1 Blue Electrocompetent cells with ligated pComb3XSS phagemid vector

The electroporation cuvettes were pre-chilled on ice for 10 min. Concurrently, electrocompetent *E. coli* XL1-Blue cells were thawed on ice. The ligation was added to 150 µL of cells. This was gently mixed and transferred into the pre-chilled cuvette and placed on ice for 1 min. The sample was then electroporated in the Gene Pulser xCell Electroporation system (Bio-rad) using the set parameters of 25 µF, 1.25 kV and the gene pulse controller at 200Ω. The cuvette was immediately flushed with 1 mL of pre-warmed

(37°C) SOC medium and then rinsed twice with 2 mL of SOC medium and transferred into a 50 mL polypropylene tube. To rescue the cells, the electroporated sample was incubated for 1 hour at 37°C at 220rpm.

To estimate the titre of the transformed cells, 25 µL of the rescued cells was added to 225 µL of SB media. Serial dilutions down to 10^{-6} were made and plated out on LB plates containing 100 µg/mL carbenicillin and incubated inverted overnight at 37°C. The number of transformants was calculated as follows:

$$\text{Estimated library} = \frac{\text{No. of colonies x culture vol. x total ligation vol.}}{\text{Plating vol. x ligation vol.}}$$

The remaining culture of rescued cells was then spun down for 10 min at 4,000*g* (Sigma Laborzentrifugen Model 2K15). The supernatant was discarded and the pellet resuspended in 600 µL of SB and plated out at 100 µL/plate supplemented with 100 µg/mL carbenicillin. These were labelled stock plates and left to incubate inverted overnight at 37°C.

2.16.2 Rescue and precipitation of scFv-displaying phage

The following day, the stock plates were scraped into 5 mL of SB / plate using a rubber policeman and combined in a sterile 50 mL universal tube. The stock culture was spun down for 10 min at 4,000*g* (Sigma Laborzentrifugen Model 2K15) and the pellet resuspended in 1 mL of SB. Five-hundred µL of the resuspended pellet was added to 250 mL of SB in a baffled conical flask supplemented with 100 µg/mL carbenicillin. The remaining 500 µL of resuspended pellet was mixed with 500 µL of 50 % (v/v) glycerol and stored at -80°C as a glycerol stock of the 'unpanned' library. The culture was grown at 37°C at 220rpm until an $O.D_{600}$ of 0.4-0.6 was reached. The optimal cell density is in the mid-log phase of growth, $O.D_{600}$ is used because the cellular components of bacteria absorb greater light at wavelengths lower than 600 nm. Two-hundred µL of helper phage M13K07 was added and the culture was incubated stationary at 37°C for 30 min. The culture was then incubated at 37°C at 220rpm for 1 hour. Kanamycin was added at a final concentration of 60 µg/mL and the culture was incubated at 30°C O/N at 250rpm.

An immunotube was coated with 500 µL of the appropriate antigen and concentration (the concentration of antigen was reduced in each round of panning, see ***Table 2.10***), covered in parafilm and stored stationary and upright at 4°C. An overnight culture of XL1-Blue *E. coli* cells was also prepared. The next day, the overnight *E. coli* culture was used to inoculate SB media supplemented with 30 µg/mL of tetracycline and left growing at 37°C at 250rpm until an $O.D_{600}$ of 0.4-0.6 was reached.

The overnight phage culture was centrifuged at 11,000*g* (Eppendorf ™ Centrifuge with fixed angle rotor (F-45-30-11)) for 30 min at 4°C. The supernatant was transferred into fresh, sterile, Oakridge tubes and polyethylene glycol (PEG) and NaCl was added at concentrations of 4% (w/v) and 3% (w/v), respectively, and dissolved by gentle shaking. The Oakridge tubes were incubated on ice for 1 hour at 4°C. This resulted in the precipitation of the phage particles. The precipitated phage cultures were centrifuged at 11,000*g* (Eppendorf ™ Centrifuge with fixed angle rotor (F-45-30-11)) for 20 min at 4°C. The supernatant was removed and discarded and the pellet was allowed to air-dry for 10 min. The phage pellet was resuspended in 1 mL of 1% (w/v) BSA in PBS and stored at 4°C. This phage pellet suspension was labelled 'input'.

2.16.3 Enrichment of phage library via biopanning against immobilised antigens

The antigen solution was poured off the coated immunotube and 3% (w/v) BSA/PBS solution was added to the tube filling it to the top to ensure sufficient blocking of immunosorbent sites. The immunotube was then covered with parafilm and left blocking on the bench at RT for 2 hours. The blocking solution was poured out of the immunotube and it was washed once with PBS. Five-hundred µL of the rescued 'input' phage was added to the tube, which was covered with parafilm and incubated a RT on a roller for 2 hours. The remaining phage were labelled and stored at 4°C. Any non-specific phage were removed by washing the tube 5 times with PBS-T (0.05% (v/v)) and PBS (this wash step became increasingly more stringent in each round; see ***Table 2.10***). Antigen-specific phage were eluted by the addition of with 500 µL of 10 mg/mL (w/v) trypsin in PBS. The tube was incubated for 10 min at RT on a roller and the eluted phage (labelled 'output') removed by vigorous pipetting to ensure removal of all bound phage.

Table 2.10: Panning strategy

The required stringency was accomplished by increasing the washes with PBS and PBS-T (0.05% (v/v)) while decreasing the antigen concentration.

Panning round	Antigen Conc.	Wash frequency
Round 1	50 µg/mL	5 X PBS, 5 X PBS-T (0.05% (v/v))
Round 2	25 µg/mL	10 X PBS, 10 X PBS-T (0.05% (v/v))
Round 3	12.5 µg/mL	15 X PBS, 15 X PBS-T (0.05% (v/v))
Round 4	5 µg/mL	15 X PBS, 15 X PBS-T (0.05% (v/v))

2.16.4 Re-infection of *E. coli* XL1-Blue cells with eluted phage and library titre estimation

The XL-1 Blue *E. coli* culture grown to an $O.D_{600}$ of 0.4-0.6 was used to create serial dilutions of the 'input' and 'output' phage pools down to 10^{-9} and 10^{-6} respectively. Three hundred µL of the remaining 'output' phage pool was re-infected into the remaining 4mL XL-1 Blue *E. coli* culture. The dilutions and 'output' infected culture were incubated stationary at 37°C for 30 min. The serial dilutions were plated at 100 µL/ plate on LB plates containing 100 µg/mL carbenicillin plates and incubated inverted overnight at 37°C.

The 'output'- infected XL-1 Blue *E. coli* culture was spun down for 10 min at 4,000 *g* (Sigma Laborzentrifugen Model 2K15). The supernatant was discarded and the pellet resuspended in 400 µL of SB and was plated out 100 µL/ plate supplemented with 100 µg/mL carbenicillin. These were labelled 'stock plates' and left to incubate inverted O/N at 37°C. The following day the stock plates were scraped using a rubber policeman and spun down for 10 min at 4,000 *g* (Sigma Laborzentrifugen Model 2K15). The pellet was resuspended in 1 mL of SB media. Five-hundred µL was used in the next round of panning and the remaining 500 µL was added to 500 µL of glycerol and stored at -80°C. After the final round of panning, the output was re-infected into the non-suppressor strain of *E. coli* Top10F' for soluble scFv expression.

2.16.5 Polyclonal ELISA

To evaluate the success of the panning experiment, phage pools from each round were tested by ELISA. A Nunc MaxiSorp™ 96-well plate was coated with 100 µL/well of 1 µg/mL of antigen diluted in PBS and incubated at 4°C O/N. The plate was washed 3 times

with PBS/ PBS-T (0.05% (v/v)) and blocked with 200 µL/well PBS containing 3% (w/v) BSA for 1 hour at 37°C. Rescued phage inputs from each round of panning were diluted 1:3 in PBS-T (0.05% (v/v)) containing 1% (w/v) BSA and added to the plate in triplicate (100 µL/well). This was incubated for 1 hour at 37°C and washed as before. HRP-labelled anti-M13 rat secondary antibody in PBS-T (0.05% (v/v)) with 1% (w/v) BSA, at a 1 in 1,000 dilution, was added to each well (100 µL) and incubated for 1 hour at 37°C. The plate was washed as before. One hundred µL/well of TMB substrate was added to the plate and was developed for 30 min with gentle agitation. The reaction was stopped using 10% (v/v) HCl (50 µL/well) and the absorbance was read at 450nm on the Tecan Safire2™ platereader.

2.16.6 Colony Pick-PCR

To ensure the vector was harbouring the scFv product, single colonies were randomly selected from the final round of panning and incorporated into a colony-pick PCR. The PCR conditions were the same as those in *Table 2.7.* The colonies were picked from plates using sterile pipette tips. The amplified scFv fragments were analysed by gel electrophoresis on a 1.5% (w/v) agarose gel.

Table 2.11: Volumes of components in colony-pick PCR

Component	Concentration/Volume
2x *MyTaq* Reaction Buffer	25 µL
Forward Primer	2 µM
Reverse Primer	2 µM
Single colony	1 colony
Molecular grade H_2O	Up to 50 µL
Total	**50 µL**

2.16.6.1 Fingerprint analysis of clones by restriction mapping

After the amplified scFv genes from the colony pick PCR were resolved on a 1.5% (w/v) agarose gel, the genes were digested with Alu*I* and BstN*I* to generate a DNA fingerprint for each clone. The digestions were setup as described in *Table 2.12.* The digestions were performed for 2 hours at 37°C for Alu*I* followed by 2 hours at 60°C for BstN*I* and deactivated at 65°C for 20 min. They were resolved on a 3% (w/v) agarose gel.

Table 2.12: Components and volumes for **Alu*I* and BstN*I* digestion**

Component	Concentration/Volume
SOE PCR Product	5 µL
Buffer 2 (10X)	2.5 µL
Alu*I*	5 U
BstN*I*	5 U
Molecular grade H_2O with 1% (w/v) BSA	Up to 25µL
Total	**25 µL**

2.16.7 Monoclonal ELISA for the detection of specific scFv clones

Colonies were selected and placed individually in wells in a 96-well plate containing 150 µL of SB (supplemented with 100 µg/mL carbenicillin) and grown O/N at 220rpm at 37°C. This plate was then sub-cultured into a fresh 96- well plate containing 200 µL SB supplemented with 100 µg/mL carbenicillin, 1 X 505 and 1mM $MgSO_4$. Glycerol stocks were made of the original plate by the addition glycerol to a final concentration of 25% (v/v) and stored at -80°C for long-term storage. The sub-cultured plate was incubated at 37°C at 200rpm until an $O.D_{600}$ of ~0.6 was reached. Expression of the scFv was induced by the addition of IPTG to a final concentration of 1mM. The plate was then incubated O/N at 30°C at 200rpm. The following day, the plate was centrifuged at 3,220*g* (Eppendorf ™ centrifuge with fixed angle rotor (F-45-30-11)) for 20 min at 4°C. The supernatants were removed and discarded and the pellets were resuspended in 100 µL of 1% (w/v) lysozyme in PBS and placed at -80°C for 20 min. The sample plate was thawed for 20 min at 37°C. This free-thaw procedure was repeated 3 times. The plate was then centrifuged at 3,220*g* (Eppendorf ™ Centrifuge with fixed angle rotor (F-45-30-11)) for 20 min at 4°C.

A Nunc MaxiSorp™ 96-well plate was coated with 100 µL/well of 1 µg/mL of antigen and incubated O/N at 4°C. The plate was washed 3 times with PBS/PBS-T (0.05% (v/v)) and blocked with 200 µL/well PBS containing 3% (w/v) BSA for 1 hour at 37°C. The plate was washed as before. The lysate was added to the plate at 100 µL/well and was incubated for 1 hour at 37°C. The plate was washed as before. PBS-T (0.05% (v/v)) with 1% (w/v) BSA containing, a 1 in 1,000 dilution of HRP-labeled anti-HA rat antibody (when detecting an scFv in the pComb3XSS vector), or a 1 in 10,000 dilution of HRP-labeled anti-cMyc antibody (when detecting in the pIT2 vector), was added to the wells

at 100 µL/well and was incubated for 1 hour at 37°C. The plate was washed as before. One hundred µL/well of TMB substrate was added and developed for 30 min with gentle agitation. The reaction was then stopped by the addition of 50 µL/well 10% (v/v) HCl and the absorbance was read at 450nm on the Tecan Safire2™ platereader.

2.16.8 Competitive ELISA for the detection of free antigen

Expressed scFv that positively bound to the immobilised antigen of interest were then subjected to competitive analysis to ensure antigen specificity, by incubation with free antigen. Competition occurs between free antigen and surface immobilised antigen for binding to the scFv. A Nunc MaxiSorp™ 96-well plate was coated with 100 µL/well of 1 µg/mL of antigen and incubated O/N at 4°C. The plate was washed 3 times with PBS/PBS-T (0.05% (v/v)) and blocked with 200 µL/well PBS containing 3% (w/v) BSA for 1 hour at 37°C. The plate was washed as before. Various antigen concentrations were incubated with an equal volume of lysate .The lysate-antigen mixture was then added to the ELISA plate for 1 hour 37°C. The plate was washed as before. PBS-T (0.05% (v/v)) with 1% (w/v) BSA containing, a 1 in 1,000 dilution of HRP-labeled anti-HA rat antibody (when detecting an scFv in the pComb3XSS vector), or a 1 in 10,000 dilution of HRP-labeled anti-cMyc antibody (when detecting in the pIT2 vector), was added to the wells at 100 µL/well and was incubated for 1 hour at 37°C. The plate was washed as before and TMB substrate was added (100 µL/well) and incubated for 30 min at 37°C. The reaction was then stopped by the addition of 50 µL/well 10% (v/v) HCl and the absorbance was read at 450nm on the Tecan Safire2™ platereader.

2.16.9 Sequence analysis of specific clones

Plasmid preparations of the selected clones were carried out as per *Section 2.10.7.* Double stranded DNA Sanger sequencing was carried out by Source Bioscience, Tramore, Ireland using the following primers:

Table 2.13: Primers used for Sanger sequencing of scFv in pComb3XSS and pIT2 vectors

Primer	Sequence
pComb3XSS sequencing primers	
Ompseq (Forward primer)	5` AAG ACA GCT ATC GCG ATT GCA G 3`
gBack (Reverse primer)	5` GCC CCC TTA GCG TTT GCC ATC 3`
pIT2 sequencing primers	
LMB3 (Forward primer)	5` CGA CCC GCC ACC GCC GCT G 3`
pHEN (Reverse primer)	5` CTA TGC GGC CCC ATT CA 3`

The resulting DNA sequence was translated using the ExPASy online translate tool (http://www.expasy.ch/tools/dna.html). The amino acid sequence was then aligned using MultiAlin program to compare the various sequences (http://www.multalin.toulouse.inra.fr/multalin/). The aligned sequences were then analysed using the Kabat rules to identify the heavy and light chain CDRs of the antibody.

2.16.10 Antibody expression and purification

ScFv expression conditions were optimised as described in *Section 2.10.8.* The optimum conditions were then employed for large-scale scFv expression. Ten mL of SB media supplemented with 1% (v/v) glucose and 100 µg/mL carbenicillin was inoculated with the relevant scFv glycerol stock and grown O/N at 37°C at 250rpm. The following day this overnight culture was subcultured into 1 L of SB media containing 1 X 505 and 100 µg/mL carbenicillin. The culture was grown at 37°C at 250rpm until an $O.D_{600}$ of ~0.6 was reached and induced with the optimum concentration of IPTG and incubated O/N at the determined temperature with shaking at 220rpm. The following day, the culture was centrifuged at 4,000*g* (Eppendorf ™ Centrifuge fixed angle rotor (F-45-30-11)) for 30 min at 4°C and the supernatant discarded. The cell pellet was then thoroughly resuspended in 20 mL of lysis buffer and sonicated as per *Section 2.12.5.* The cell debris was removed by centrifuging at 11,000*g* (Hermle Z233M-2 Air-cooled version Microcentrifuge) for 10 min. The supernatant was filtered using a 0.2µM filter.

2.16.11 Purification of scFv antibody fragments by immobilised metal affinity chromatography (IMAC)

This protocol was performed as outlined in *Section 2.13.5.*

2.17 Characterisation of purified scFv antibody

2.17.1 ELISA titre of purified scFv antibody

A Nunc MaxiSorp™ 96-well plate was coated with 100 µL/well of 1 µg/mL antigen and incubated O/N at 4°C. The plate was blocked with 200 µL/well PBS containing 3% (w/v) BSA for 1 hour at 37°C. The plate was washed as before. The purified antibody was serially diluted down to 1 in 1,000,000 in PBS with 1% (w/v) BSA) and added to the plate at 100 µL/well and detected as described in *Section 2.16.7.*

2.17.2 Checkerboard ELISA for the determination of optimal concentration of immobilised antigen and dilution of antibody

A Nunc MaxiSorp™ 96-well plate was coated with varying antigen concentrations (10 µg/mL – 1µg/ mL). Each concentration of antigen was added to a separate row on the ELISA plate. The plate was and blocked with 200 µL/well PBS containing 3% (w/v) BSA for 1 hour at 37°C. One hundred µL samples of purified antibody, serially diluted 1:5 in PBS (0.05% (v/v)) with 1% (w/v) BSA were added to each well and detected as described in *Section 2.16.7.*

2.17.3 Inter/Intra-day variability studies

Intra-day studies were carried out in order to determine the precision and variability within the assay. This was achieved by direct comparison of three replicate samples within the same assay. Nunc MaxiSorp™ 96-well plates were coated with the appropriate concentration of antigen, determined by the checkerboard ELISA, and blocked with 3% (w/v) BSA. Standards of decreasing concentrations of free antigen were prepared in PBS. Fifty µL of each standard was added to an equal volume of antigen-specific scFv at the optimal concentration in PBS containing 1% (w/v) BSA. The antigen-antibody mix was added in triplicate to the plates and incubated for 1 hour at 37°C. The plates were then washed 3 times with PBS and 3 times PBS-T (0.05% (v/v)). Bound antibody was detected following the addition of the appropriate HRP-labelled secondary antibody in PBS-T (0.05% (v/v)) with 1% (w/v) BSA. The plate was incubated and washed as before. TMB

substrate (100 µL/well) was then added and incubated at 37°C for 30 min. The reaction was then stopped by the addition of 10% (v/v) HCl and the absorbance read at 450nm on the Tecan Safire2™ platereader. The inter-assay study was performed using the same conditions on three separate days. This study was used to assess the reproducibility of the assay and overall assay precision and accuracy.

2.17.3.1 Inter/Intra-day variability studies in human serum

In order to mimic the activity of the antibody within physiological conditions, inter and intra studies were performed as per *Section 2.17.3*. However, within these studies, the antigen standards and antibody dilution were performed in normal human serum (Merck Millipore).

2.17.4 Precision assay and determination of analytical limits

An inhibition ELISA was performed to determine the concentration of free antigen that could be accurately distinguished from blank samples with 95% confidence. This was achieved by incubating 20 blank replicas (in normal human serum), 20 replicas of the lowest concentration of antigen and 20 replicas of a higher concentration of free antigen, with the appropriate dilution of antigen-specific scFv. The mixture was added to a coated plate. Here, the free and immobilised antigen compete for binding with the antigen-specific scFv. Binding of the scFv was detected by addition of the appropriate HRP-labelled secondary antibody in 1% (w/v) BSA in PBS-T. After 1 hour of incubation at 37°C the plate was washed as before and TMB substrate (100 µL/well) was added. Following incubation for 30 min at 37°C, the reaction was stopped by the addition of 10% (v/v) HCl and the absorbance read at 450nm. The assay was used to determine the concentration of free antigen that can be detected with 95% confidence, inferring that the scFv has the ability to accurately identify at least 19/20 positive samples when assayed with 20 positive and 20 negative samples. It is the lowest concentration of analyte where a response can be reliably distinguished from the background.

2.17.5 Dot Blot Analysis

The dot blot is a derivative technique of the traditional western blot. It represents a simplified version in that, the protein detected is not denatured prior to analysis nor is it separated by gel electrophoresis. Instead, the protein is applied by pipetting directly onto

the nitrocellulose membrane as a dot. This technique was employed to determine the basic working concentration of the anti-MSLN scFv antibody against the MSLN protein in its native state. The MSLN protein (2.5 µL at a concentration of 5 µg/mL) was directly applied to the membrane in dot format and allowed to dry. The dot blots were then blocked in 3% (w/v) BSA in PBS for 1 hour at RT with gentle agitation. The blots were washed 3 times with PBS and PBS-T 0.05% (v/v). Varying dilutions (1 in 10, 1 in 50, 1 in 100, 1 in 500) of the anti-MLSN scFv clone were prepared in 1% (w/v) BSA in PBS-T 0.05% (v/v)) and used to probe the dot blots for 1 hour at RT. The blots were washed 3 times with PBS and 3 times PBS-T (0.05% (v/v)), and the secondary antibody prepared in 1% (w/v) BSA in PBS-T) at a 1 in 2,000 dilution. The secondary antibody was left on the blots for 1 hour at RT. Once the blot was washed, TMB peroxidase substrate was added, and antibody binding visualised by the depth of the colour change observed.

2.18 Generation of bispecific T-cell engager

As previously mentioned, the bsAb BiTE format consists of one scFv arm that binds to CD3ε on the surface of a T-cell and a second scFv arm specific for a given tumour-associated antigen (TAA). The concept here employs PCR and cloning techniques to insert the two scFv into the pET-26b(+) for expression of a BiTE. Each scFv is amplified using specifically designed primers that incorporate specific restriction sites. These sites allow for directional cloning of both scFv into the pET-26b(+) vector.

The anti-CD3ε scFv was created in the research described in this thesis. Initially, the anti-TAA arm of the BiTE was to be one of the scFv generated for the diagnostic panel as these markers show some therapeutic potential. However, none of these antibodies were generated and characterized at the time work on the BiTE initiated. Additionally, issues were encountered during initial attempts to isolate a murine anti-CD3ε scFv that led to employment of an avian library for anti-CD3ε scFv isolation. Due to primer design, it was necessary for this strategy that both scFv be generated within the same host animal, consequently, an avian anti-HER2 scFv generated and partially characterized in a previous project was selected as the anti-TAA arm (***Figure 2.1***). Therefore the work on this anti-HER2 scFv is only described from inter-/intra-day assays and precision testing to the generation of the BiTE through PCR and cloning techniques.

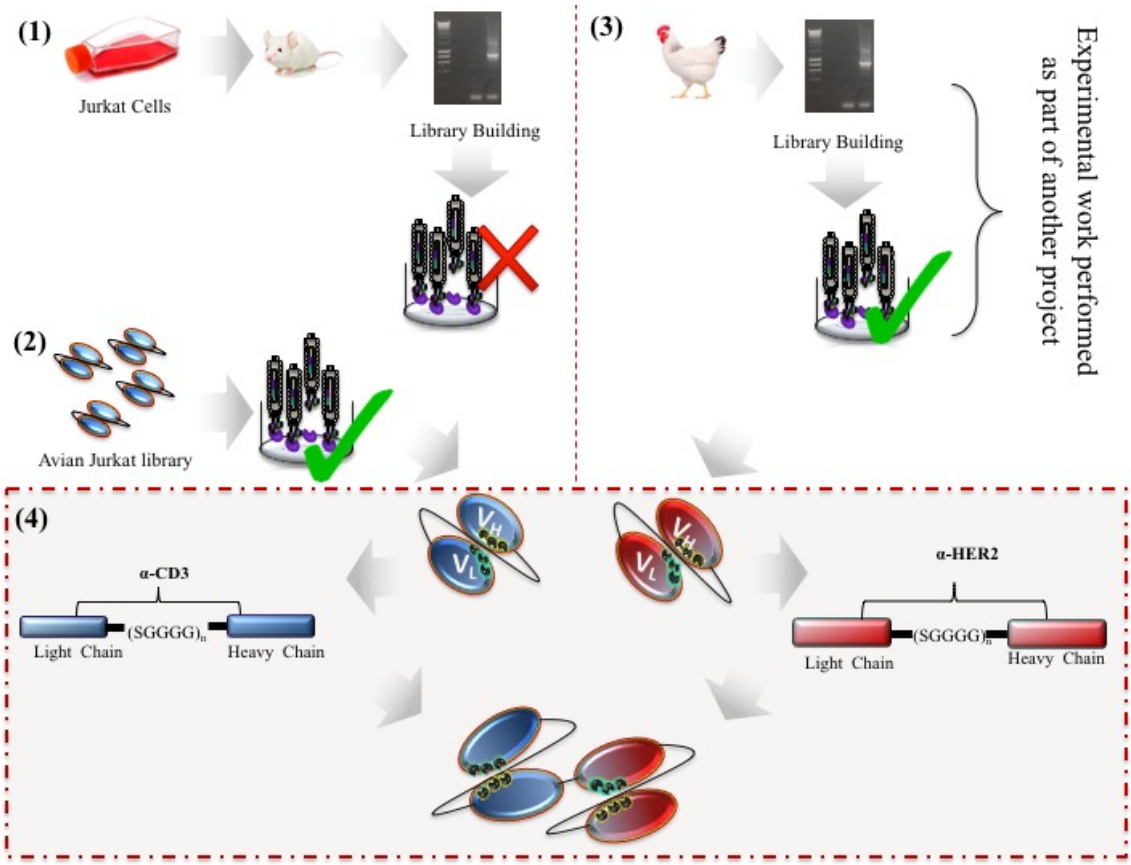

Figure 2.1 Basic illustration showing the origin of each scFv arm of the BiTE construct.

(1) *The anti-CD3ε arm of the BiTE was created within this project. Initial work attempted to isolate an anti-CD3ε specific scFv from a biased murine library but with no success as the immune library generated was too limited to isolated highly specific antibodies (fully elaborated in Chapter 5).* ***(2)*** *A previously generated avian library was used and a CD3ε-specific scFv isolated.* ***(3)*** *The second arm is composed of an anti-HER2 scFv. The work from immunisation of the avian host to initial characterization of this antibody was carried out in a previous project and was included in this work as a part of the 'proof-of-concept' method for BiTE generation.* ***(4)*** *PCR and cloning techniques were employed for the generation of an anti- CD3ε x HER2 BiTE.*

2.18.1 Large-scale expression and purification of anti-CD3ε scFv

Large-scale expression was carried out as described in *Section 2.16.10.* and purified as per *Section 2.13.5.*

2.18.2 Cross reactivity studies of the anti- HER2 and anti-CD3ε scFv

The CD3ε and HER2 scFv were assessed for cross reactivity against HER2 and CD3ε antigens, respectively. Calibration curves were prepared in assay buffer, as per *Section 2.17.3,* using each of the antigens in a concentration range from 10 µg/mL to 1 µg/mL. The IC_{50} values were then compared to the IC_{50} values when the scFv were assessed with their cognate antigen to determine the degree of cross reactivity.

2.18.3 Amplification of the anti-HER2 and anti-CD3ε scFv genes using specifically designed primers

In order to insert the scFv into the pET-26b (+) vector, various digestions sites, found in the pET-26b (+) multiple cloning sites, were added to allow the directional cloning of the two scFv into the vector. For this, specific primers were designed, see *Table 2.14.*

Table 2.14: Primers used for incorporating required digestion sites for directional cloning into pET-26b (+) vector.

Primer	Sequence
scFv -1 (HER2)	
scFv 1 – Forward	5’ AT CCG AAT TCG AGC GGC GCG CCG GTG GCC CAG GCG GCC CTG ACT CAG 3’
scFv 1 – Back	5’ CAT GGC GCA TAC CCG TAC GAC GTT CCG GAC GAC TAC GCT TCT AAG CTT GCG G 3’
scFv -2 (CD3ε)	
scFv 2 – Forward	5’ AT CCG AAT TCG GTA GTG GCC CAG GCG GCC CTG ACT CAG 3’
scFv 2- Back	5’ TCC TCC ACT AGT GGC CAG GCC GGC CAG GGT TCG GGC GCG CCG GTG 3`
scFv 2- Back- Longer linker	5’ TCC TCC TCC TCC GGC GGC ACT AGT GGC CAG GCC GGC CAG GGT TCG GGC GCG CCG GTG 3’

The plasmids containing both antibodies were isolated as per *Section 2.10.7.* The plasmid DNA was incorporated into two separate PCR containing the appropriate primer set. The PCR components and conditions were as follows:

Table 2.15 Components and volumes for addition of restriction enzyme sites

Component	Concentration/Volume
Plasmid DNA	100 ng
2x MyTaq Reaction Buffer	25 µL
Forward Primer	2 µM
Reverse Primer	2 µM
Molecular grade H_2O	Up to 50 µL
Total	**50 µL**

The amplification of the two scFv was performed in the Biometra $T_{Gradient}$ PCR machine under the following conditions:

Table 2.16 PCR thermal cycler conditions

Temperature		Time	
Step 1:	95 °C	5 min	
Step 2:	95 °C	30 sec	30 cycles
	60 °C	30 sec	
	72 °C	90 sec	
Step 3:	72 °C	10 min	

The PCR samples were analysed (10 µL /well) on a 1.5% (w/v) agarose gel with 1kb Hyperladder (Bioline). The products were purified from a 1.5% (w/v) agarose gel using the NucleoSpin® PCR Clean-Up Kit and the DNA was quantified by measuring the absorbance on the NanoDrop™ at 260nm.

2.18.4 Incorporation of the anti-HER2 scFv into the pET-26b (+) vector

The HER2 PCR product now contains restriction-digestion sites, *Asc*I for the directional cloning of the second scFv, and *EcoR*I and *Hind*III for cloning into the vector. The HER2

product and pET-26b (+) vector restriction digest were carried out using the *EcoR*I and *Hind*III enzymes acquired from NEB using the NEB CutSmart® Buffer.

Table 2.17: Components and volumes for restriction digest

Component	Concentration/Volume
Purified HER2 PCR product / pET-26b (+) vector	1 µg
*EcoR*I	1U
*Hind*III – HF®	1U
CutSmart® Buffer (10X)	5 µL
Molecular grade H_2O	Up to 50 µL

The digests were incubated at 37°C for 5 hours and de-activated at 80°C for 20 min. The pET-26b (+) vector was then treated with Antarctic Phosphatase for 15 min at 37°C, and de-activated at 70°C for 5 min. The digested HER2–PCR fragment was analysed on a 1% (w/v) agarose gel and the pET-26b (+) vector on a 0.6% (w/v) gel to ensure digestion had occurred. The HER2-PCR fragment and pET-26b (+) vector were purified from PCR using NucleoSpin® Gel and PCR Clean-up kit. DNA was quantified using the NanoDrop™ at 260nm.

2.18.4.1. Ligation of the digested HER2 SOE product with vector DNA

The purified digested scFv fragment was cloned into the purified digested vector using T4 DNA ligase.

Table 2.18: Components and volumes for ligation reaction

Component	Concentration/Volume
pET-26b (+) vector (digested and purified)	500 ng
HER2 scFv product (digested and purified)	250 ng
T4 DNA Ligase buffer (10X)	20 µL
T4 DNA Ligase	5 µL
Molecular grade H_2O	Up to 200 µL

The ligations were incubated at 16°C O/N at RT and de-activated at 65°C for 20 min. The ligated product was then ethanol precipitated (see *Section 2.15.7.*). The DNA pellet was

resuspended in 30 µL of MGH_2O. The ligated product was then analysed on a 0.6% (w/v) agarose gel to ensure ligation efficiency and quantified using the NanoDrop™ at 260nm.

2.18.5 Incorporation of the anti-CD3ε scFv into the pET-26b (+) vector containing the anti-HER2 scFv

The CD3ε PCR product now contains two restriction-digestion sites, *Asc*I and *EcoR*I. The CD3ε PCR product and pET-26b (+) vector containing HER2 scFv were digested using the *Asc*I and *EcoR*I enzymes acquired from NEB using the NEB CutSmart® Buffer.

Table 2.19: Components and volumes for restriction digest

Component	Concentration/Volume
Purified CD3ε PCR product / pET-26b (+) vector containing HER2 scFv	1 µg
*EcoR*I	1 U
*Asc*I	1 U
CutSmart® Buffer (10X)	5 µL
Molecular grade H_2O	Up to 50 µL

The digests were incubated as described in *Section 2.18.4*. Once digestion was confirmed on agarose gels, the products were ligated as described in *Section 2.18.4.1.*

2.18.6 Transformation of the pET-26b (+) vector containing the BiTE gene into BL21 (DE3) cells

The pET-26b (+) vector containing the HER2 and CD3ε scFv was ethanol precipitated as described in *Section 2.15.7.* Following this, the product was transformed into BL21 (DE3) cells (described in *Section 2.13.1*). The transformation was then plated onto LB agar plates, supplemented with 60 µg/mL kanamycin, to obtain single colonies.

2.18.7 Determination of successful construction of a BiTE antibody

Single colonies were selected from the LB agar plate of transformed colonies. Each colony was first resuspended in 10 µL dH_2O. Five µL was removed and integrated into a colony-pick PCR, with some of the remaining 5 µL used to inoculate a 10 mL LB overnight culture supplemented with 60 µg/mL Kanamycin. The colony-pick PCR was carried out as described in *Section 2.16.6.* The PCR was performed using the same

components outlined in ***Table 2.6*** with the inclusion of the scFv-2 forward primer and scFv-1 back primer from ***Table 2.13***. PCR conditions were those outlined in ***Table 2.7***. The results were analysed on a 1.5% (v/v) agarose gel to determine the presence of a ~1600bp product.

The following day the 10 mL cultures were used to inoculate 10 mL LB cultures supplemented with, 60 µg/mL kanamycin, 1 X 505 and 1mM $MgSO_4$. The cultures were induced using a final concentration of 5mM as described in *Section 2.13.3* and lysed according to *Section 2.13.4.* The lysate was then analysed on WB and SDS-PAGE (*Sections 2.10.2/3).*

2.18.8 Expression and purification of BiTE antibody

The BiTE antibody was expressed and purified as per *Section 2.16.10.*

2.18.9 Indirect ELISA to ensure BiTE binding retention to CD3ε and HER2

The binding capabilities of each arm of the BiTE to its cognate antigen was tested in indirect ELISA format. Half of a Nunc MaxiSorp™ 96-well plate was coated with 100 µL/well of 1 µg/mL of HER2 diluted in PBS and the other half coated with 100 µL/well of 8 µg/mL of CD3ε and incubated at 4°C O/N. The plate was washed 3 times with PBS/ PBS-T (0.05% (v/v)) and blocked with 200 µL/well PBS containing 3% (w/v) BSA for 1 hour at 37°C. Serial dilutions (1:2) of the purified BiTE were made in PBS-T (0.05% (v/v)) containing 1% (w/v) BSA and added 100 µL/well to each half of the plate in duplicate. The plate was incubated for 1 hour at 37°C and washed as before. HRP-labelled rabbit anti-chicken secondary antibody in PBS-T (0.05% (v/v)) with 1% (w/v) BSA at a 1 in 1,000 dilution was added to each well (100 µL) and incubated for 1 hour at 37°C. The plate was washed as before. One hundred µL/well of TMB substrate was added to the plate and was developed for 10 min with gentle agitation. The reaction was stopped using 10% (v/v) HCl (50 µL/well) and the absorbance was read at 450nm on the Tecan Safire2™ platereader.

2.18.10 Investigation into dual binding capabilities of BiTE

A Nunc MaxiSorp™ 96-well plate was coated with 100 µL/well of 1 µg/mL of HER2 diluted in PBS and incubated at 4°C O/N. The plate was washed 3 times with PBS/ PBS-T (0.05% (v/v)) and blocked with 200 µL/well PBS containing 3% (w/v) BSA for 1 hour

at 37°C. A 1:2 dilution of purified antibody was made in PBS-T (0.05% (v/v)) containing 1% (w/v) BSA and added 100 µL added per well. This was performed in triplicate. The plate was incubated for 1 hour at 37°C and washed as before. Eight µg/mL of free CD3ε antigen diluted in PBS was added to the plate, incubated for 1 hour at 37°C and washed as before. A 1 in 2,000 dilution of mouse anti-CD3 epsilon antibody in PBS-T (0.05% (v/v)) with 1% (w/v) BSA was added to each well (100 µL) incubated for 1 hour at 37°C and washed as before. A HRP-labelled anti-mouse secondary antibody in PBS-T (0.05% (v/v)) with 1% (w/v) BSA at a 1 in 1,000 dilution was added to each well (100 µL) and incubated for 1 hour at 37°C. The plate was washed as before. One hundred µL/well of TMB substrate was added to the plate and was developed for 10 min with gentle agitation. The reaction was stopped using 10% (v/v) HCl (50 µL/well) and the absorbance was read at 450nm on the Tecan Safire2™ platereader.

2.18.11 ELISA titre of purified BiTE antibody

A Nunc MaxiSorp™ 96-well plate was coated with 100 µL/well of 1 µg/mL of antigen and incubated O/N at 4°C. The plate was washed 3 times with PBS/PBS-T (0.05% (v/v)) and blocked with 200 µL/well PBS containing 3% (w/v) BSA for 1 hour at 37°C. The plate was washed as before. The purified bispecific antibody was titred in doubling dilutions in PBS-T (0.05% (v/v)) with 1% (w/v) BSA) and added to the plate at 100 µL/well and detected as described in *Section 2.18.10.*

2.19 Licencing

The work within this thesis regarding animals was ethically approved and carried out in accordance with the Department of Health and Children licence number B100/2705. Aoife Crawley has completed the LAST-Ireland program

2.20 Statistical analysis

Any statistical analysis performed herein is calculated as described below.

2.20.1 Limit of blank (LOB) and limit of detection (LOD)

The limit of detection (LOD) is defined by Armbruster *et al* (1994), as the smallest concentration of analyte that produces a signal likely to be reliably distinguished from the limit of the blank (LOB). The limit of blank (LOB) is the highest value observed in a

series of results from a sample that contains no analyte. The LOD and LOB were calculated using the equations below.

$$LOB = \text{mean blank} - 1.645\ (\text{SD blank})$$
$$LOD = LOB - 1.654\ (\text{SD low concentration analyte})$$

2.20.2 Four-parameter logistic model and IC_{50} value

Antibody sensitivity within this work was evaluated by competitive ELISA in PBS and normal human serum for calculation of half maximal inhibitory concentration (IC_{50}) value. This value represents the concentration of free protein that produced 50% inhibition in response. This was calculated as outlined below.

$$50\%\ \text{maximal response} = \text{max response} - (0.5 \times (\text{max response} - \text{min response}))$$

Using the BiaEvaluation™ software sigmoidal curves were plotted in log-scale using a four parameter logistic function. The equation to obtain a four-parameter sigmoidal curves is outlined below.

$$y = A + \frac{B-A}{1 + (x/c)^D}$$

y = normalised response; x = concentration of free protein; A = max normalised response; B= min normalised response; C = point of inflection; D = slope of linear part of the curve.

2.20.3 Coefficient of variance (CV)

The coefficient of variance (CV) is used to determine the variability of an assay and is used preferentially over standard deviation (SD). As standard deviation increase/decreases proportional to the mean the CV represents a standardization of the SD which allows for comparison of variability within the working range of the assay (Reed *et al.,* 2002). The CV was calculated by dividing the standard deviation by the means values multiplied by 100.

$$\%\ CV = (S.D/Mean) \times 100$$

Chapter 3

Generation of both a Capan-1-biased murine immune library and MSLN-specific scFv using a mammalian-expressed antigen

Chapter outline

As previously outlined in *Chapter 1,* this project aims to tackle both diagnostic and therapeutic issues surrounding PDAC. This chapter, in combination with *Chapter 4,* describes the generation of a diagnostic panel encompassing three antibodies for the improved diagnosis of PDAC. Specifically, this chapter focuses on the generation of an anti-MSLN scFv with the generation of the other two scFv addressed in *Chapter 4.*

BALB/c mice were subjected to a typical immunisation schedule with the PDAC cell line, Capan-1. Capan-1 was selected as the immunogen as it expresses the three markers required for the chosen multi-marker panel while simultaneously limiting the number of animals required. It was envisioned that the Capan-1-biased library would concurrently be used for the selection of specific scFv described in both this chapter and *Chapter 4.* Following numerous immunogen boosts, the mice sera were analysed for antigen-specific antibodies by titration against Capan-1 cells. The library was subsequently biopanned against a MSLN antigen to enrich and select for MSLN-specific scFv. The MSLN antigen used in the selection process was recombinantly expressed. Initial attempts to express this antigen in *E. coli* expression systems were unsuccessful. The antigen was subsequently expressed in HEK293 cells with impressive protein yields obtained. Following biopanning, a monoclonal ELISA was performed to identify single clones. The clones were expressed, purified and tested in ELISA formats. The resulting scFv were found to have limited abilities to bind to MSLN in serum, however, both clones identified successfully bound to MSLN in conformational and linear forms suggesting the scFv hold potential as primary antibodies in tissue applications such as IHC.

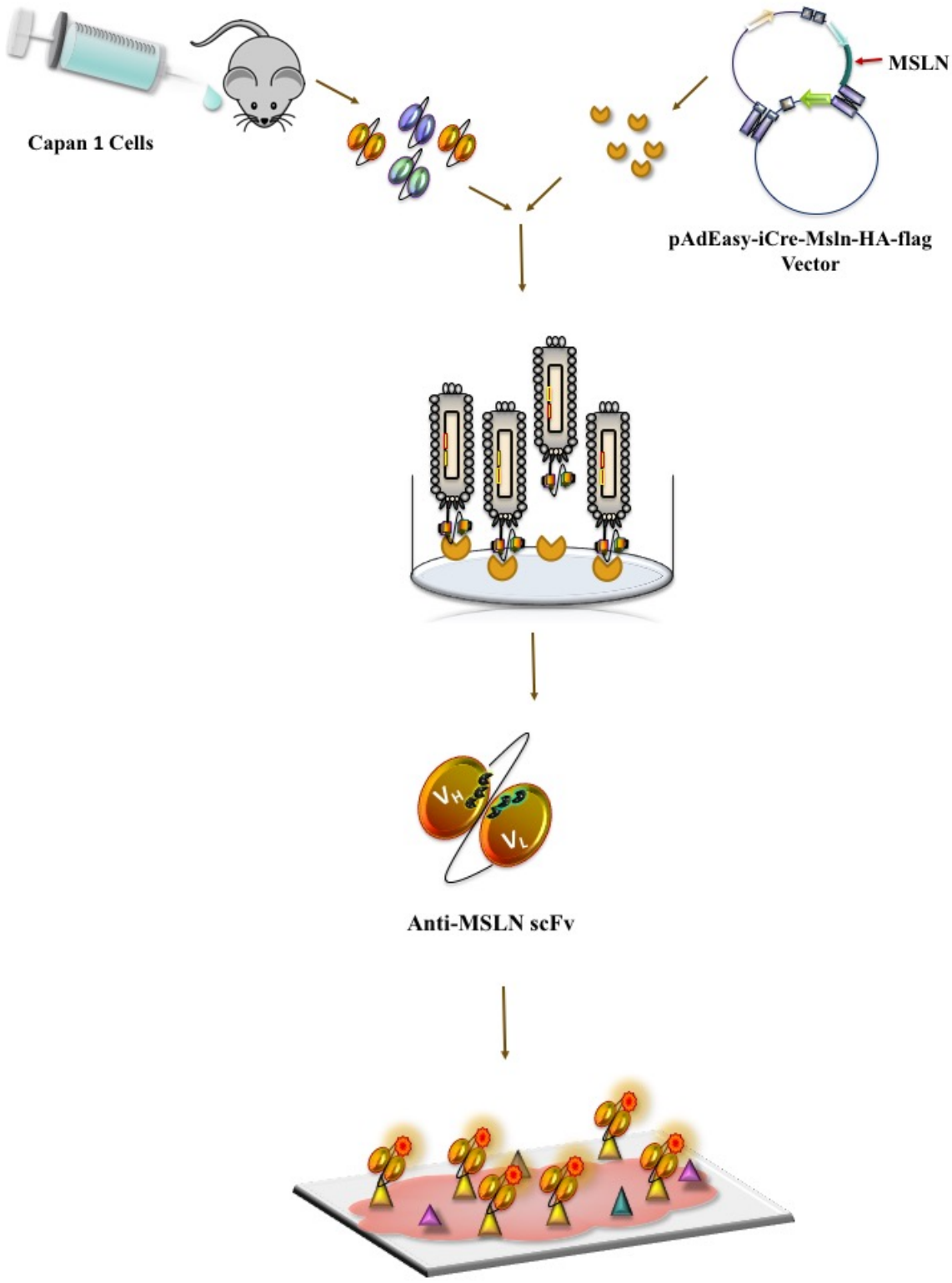

Figure 3.1 Illustrated workflow for Chapter 3

An anti- MSLN scFv antibody was isolated from a murine immune anti-Capan-1 library by panning and phage display using a recombinant MSLN protein expressed in mammalian cells. The scFv was characterized for future application as a tissue diagnostic marker for pancreatic cancer.

3.1 Introduction

The high mortality rate of PDAC is a result of both insufficient curative treatment options and the major issue of late-stage diagnosis. While asymptomatic in early stages, the disease often presents with generic symptoms associated with other pancreatic syndromes (Brenner, 2018). The lack of cancer-specific symptoms means that the majority of cases are missed until late-stage PDAC when distant metastasis has occurred. Current methods of diagnosis include various scans such as EUS, CT and MRI in conjunction with a blood test to detect the biomarker CA19-9. These scans suffer from a several drawbacks, ranging from high cost to poor visualisation (Herreros-Villanueva *et al.,* 2013). The biomarker CA19-9 is the gold standard FDA-approved marker for PDAC diagnosis. However it has low specificity and is non-cancer specific, as it is elevated in other pancreatic diseases such as pancreatitis (Winter *et al.,* 2013). Hence it is imperative that other markers be explored for PDAC diagnosis. Biomarkers offer a wealth of information on malignant processes occurring within body. Their presence, absence, increase or decrease can be a sign of cancer presence, progression, regression or susceptibility to certain treatments. Recently, efforts have focused on identifying new markers of pancreatic cancer to enhance the poor diagnostic methods available. From this, MSLN was flagged as a differentiation marker (specific to a type of tissue) that has the ability to distinguish between benign and malignant pancreatic tissue (Zhang *et al.,* 2018). A meta-analysis performed indicated that while this marker may not possess the ability to screen PDAC, it does have potential diagnostic value. This work supports the theory that one biomarker will not be sufficient for PDAC diagnosis, and the utilisation of combinations of markers may provide the optimal approach (Zhu *et al.,* 2014).

The exploitation of the potential of a multi-marker based diagnostic strategy gave rise to the hypothesis of the research described herein. In 2010, a study carried out by Edgell and colleagues (2010), assessed a multi-marker panel for diagnosis of ovarian cancer, consisting of five ovarian cancer-related biomarkers, CA125, C-reactive protein (CRP), interleukins 6 (IL-6) and 8 (IL-8) and serum amyloid A (SAA). The use of this panel showed significant increase in cumulative diagnostic abilities over the use of CA125 alone. Another study, centred around a multi marker panel for the detection of endometrial cancer, discovered a five-biomarker panel composed of prolactin, GH, Eotaxin, E-selectin and TSH, possessed the ability to distinguish endometrial cancer from

ovarian and breast cancer. This ability indicates the panel may be applicable as a blood-based early detection method for endometrial cancer (Yurkovetsky *et al.,* 2007). A circulating tumour cell (CTC) marker panel was investigated in 2014 by Barbazán and colleagues, that proved to have prognostic and predicative value for metastatic colorectal cancer patients. In 2015, a study utilised four zinc fingers as capture antigens for the detection of autoantibodies in colorectal cancer providing a multiplexed autoantibody assays for detection of colorectal cancer (O'Reilly *et al.,* 2015). Multi-marker research has also been undertaken for pancreatic cancer. A study by Park and colleagues (2017) performed a large-scale multi-centre validation of a multi-marker panel. To construct this panel, they performed measurements on the levels of differentially expressed proteins in healthy groups and those with pancreatic diseases, both benign and malignant. They proposed a three marker panel of LRG1, TTR, and CA19-9 which resulted in significantly improved performance when compared to CA19-9 alone. Another study explored a three marker panel, to discriminate PDAC from healthy and benign controls, that showed significant improvement over use of CA19-9 alone as an early detection strategy (Brand *et al.,* 2011). Research has also found that CA19-9 combined with CA125 and CEA can help to predict the outcome of PDAC patients post-surgery and chemotherapy (Chang and Kundranda, 2017).

This work aims to generate a panel of scFv antibodies against selected PDAC-associated markers that, when combined, would provide information on cancer stage and personalised diagnostics for determination of specific and effective treatment options. The hypothesized approach embraces the idea of multi-marker diagnosis rather than relying on a single marker. It is designed to exploit the cumulative abilities of antibodies to bind to the cognate antigen in serum and on tissue. This is illustrated in ***Figure 3.2.***

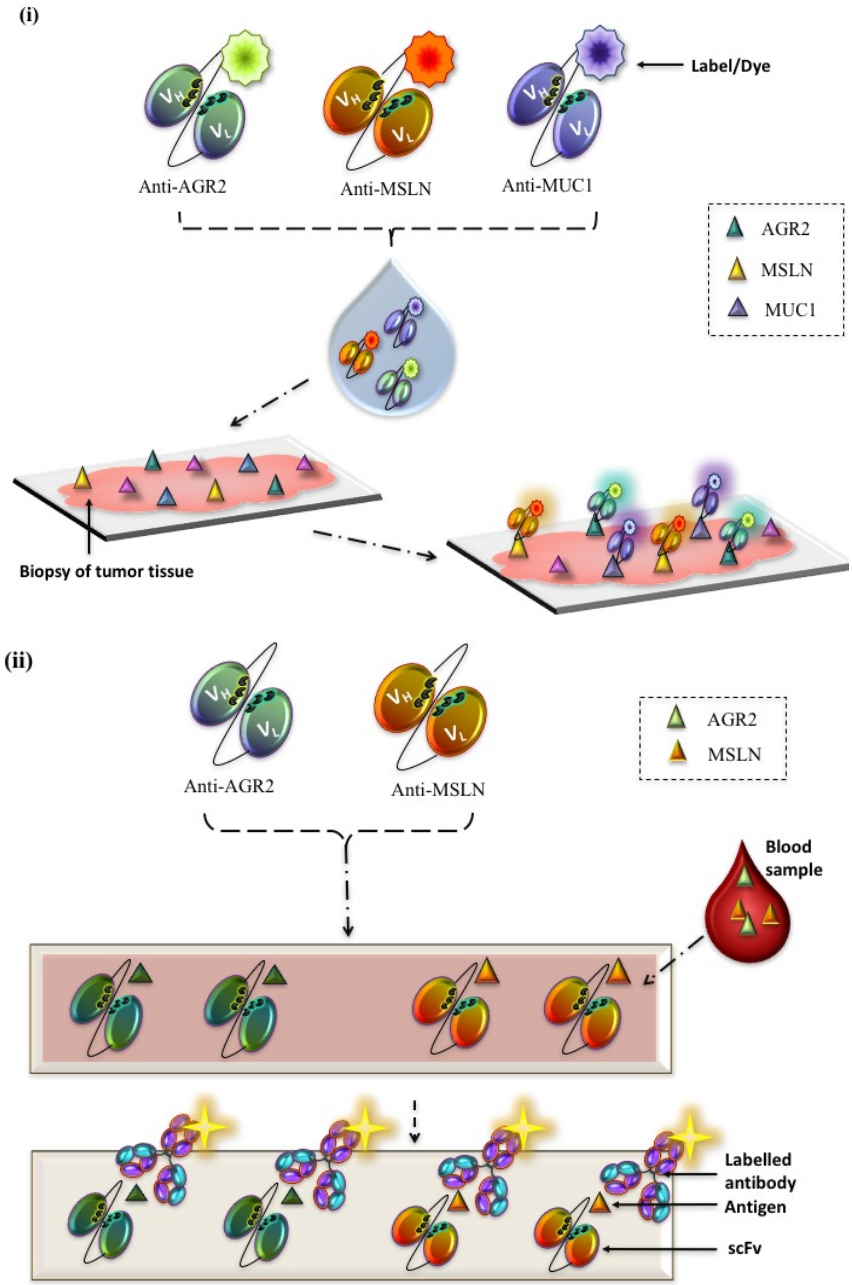

Figure 3.2 Simplified illustration of the potential uses of the envisioned multi-scFv diagnostic panel.

(i) *Multi-marker scFv panel for applications such as IHC. Specific scFv generated against the selected tissue markers found (or upregulated) in pancreatic cancer are coupled to different labels. These scFv can be applied to tumour tissues obtained by a biopsy. Any antigen within the tissue will be detected by the relevant scFv.* ***(ii)*** *This illustration depicts the potential diagnosis of pancreatic cancer using two of the recombinant scFv antibodies generated against serum antigens found in pancreatic cancer. Each antigen provides information crucial to the treatment and prognosis of the disease.*

The selection of the panel of markers was based on the realisation that the evasive nature of PDAC requires the capacity to detect relevant markers in tissue and serum since tissue biopsy may be a requirement for diagnosis. All of the chosen markers are found to be either upregulated or exclusively expressed in PDAC tissue and provide different data on the tumour characteristics. Detection of the marker AGR2 can indicate invasiveness of the disease and provide information for selection of treatment options. Upregulation of the MUC1 marker can indicate the initiation of PDAC, with expression levels providing a means for PDAC staging. MSLN is present only on cancerous tissue Its expression can indicate migration and proliferation of cancer cells and also indicates possible treatment options. A high expression level of MSLN is a strong indicator of poor survival rates and, thus, $MSLN^{+}$ tumours would require highly aggressive and rapid treatment (Chen *et al.,* 2013).

MSLN expression was first identified by Argani and colleagues (2001) as present in pancreatic adenocarcinoma but absent in normal pancreatic cells. By employing serial analysis of gene expression (SAGE), *in situ* hybridization, RT-PCR and IHC, they showed that in 60 pancreatic cancer tumour, all 60 overexpressed MSLN consistently. It is a glycophosphatidylinositol (GPI)-linked differentiation antigen that is expressed in a variety of epithelial cancers. The gene encodes for a ~69kDa precursor protein that is cleaved to produce an N-terminal soluble fragment (MPF) and a C-terminal membrane bound fragment (MSLN). Work has been carried out to investigate whether circulating MSLN could be detected in the sera of pancreatic disease patients and if its levels are elevated in those with pancreatic cancer compared to healthy controls. The findings showed that soluble MSLN levels were increased in those with pancreatic disease, confirming MSLN as a potential biomarker of pancreatic disease, be it benign or malignant (McJohnston *et al.,* 2009). The exact role of MSLN, even in healthy tissues, remains elusive, as mice with MSLN gene inactivation present with no obvious abnormalities (Koyama *et al.,* 2017). Recent studies have shed some light on the unknown molecular mechanisms of MSLN in pancreatic cancer. A study postulated that the oncogenic transcription co-factor YAP1 is involved in the activation of MSLN expression via regulatory CanScript activity. While knocking down the YAP1 expression reduced MSLN expression, overexpression of YAP1 did not turn on MSLN expression, suggesting that it is involved in MSLN expression but is not responsible for it (Ren *et al.,* 2011). Overexpression of MSLN is also thought to possibly be triggered by epigenetic

events as it is found to be hypomethylated in pancreatic adenocarcinoma, while it is methylated in normal pancreatic tissue (Marin-Muller *et al.,* 2012). Other studies have shown that MSLN is associated with increased S-phase cell population and upregulation of growth and survival pathways by growth factors. It results in pancreatic cancer cells becoming resistant to tumour necrosis factor (TNF) - α – induced apoptosis by NF-κB activation (Li *et al.,* 2008).

It is critical for high-affinity antibodies to be selected that are specific for their target biomarkers for successful PDAC diagnosis. In this chapter the development of MSLN-specific murine scFv is reported. Mice are widely used for generating immune libraries as PCR primers are readily available and methods of library construction have been extensively studied (Barbas *et al.,* 2001). The human and mouse antibody repertoires are generated by similar processes, however, the diversity and location of antibody gene loci is far less understood in mice than in humans (Collins *et al,* 2015) .

Due to the high associated costs, MSLN was expressed 'in-house' for the selection of specific scFv. A plasmid containing the MSLN gene was purchased from NBS Biologicals Ltd. (***Figure 3.3***) and transformed into BL21 (DE3) cells for *E. coli*-based expression of the relevant genes. BL21 (DE3) cells are made for high expression of recombinant proteins (Rosano *et al.,* 2014). They carry the lambda DE3 lysogen, ideal for use with plasmids that are bacteriophage T7 promoter-based expression systems. The *E. coli* expression system did not give successful MSLN expression, most likely due to complex post translational modifications that this prokaryotic system cannot perform. It was decided that an attempt to express the protein in a mammalian expression system could potentially have more success.

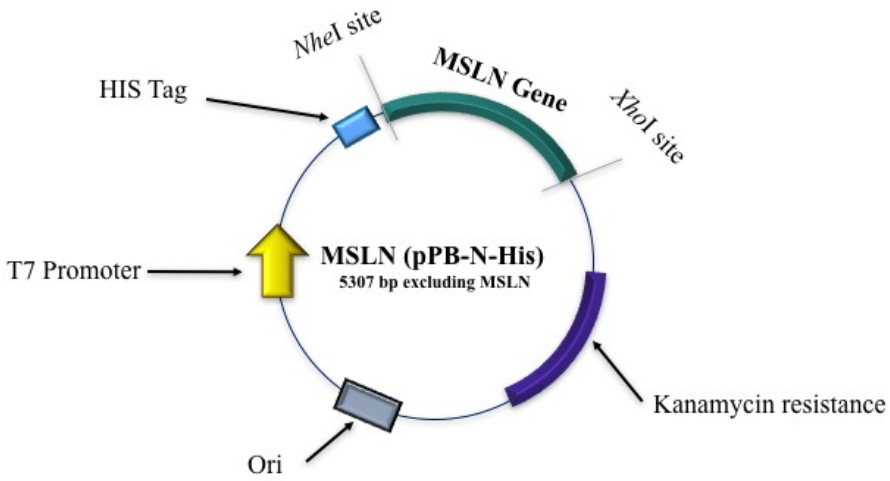

Figure 3.3 Map of MSLN Protein Vector (Human) (pPB-N-His)

This map illustrates the recombinant MSLN gene, with the N-terminal polyhistidine tag and the kanamycin antibiotic resistance gene. Full map available in Appendix C.

For this, the pAdEasy-MSLN-iCre-HA-Flag vector was purchased from Addgene. Recombinant adenoviruses are widely-use gene delivery and expression systems that are capable of infecting a plethora of cell types. The virus is rendered incapable of self-replication as a consequence of deletions in the adenoviral genes. For example, the pAdEasy-1 plasmid has deleted E1 and E3 genes so that it is unable to replicate or produce infectious viral particles. The E1 gene is essential for production of viral particles and is provided in *trans* by HEK293 cells. The most common method of generating recombinant adenoviruses requires cloning the gene of interest into a shuttle vector and transferring the gene into the adenovirus genome by homologous recombination. An improvement in recent years exploits the homologous machinery in *E. coli.* and the recombinant adenovirus is produced by double recombination occurring between co-transformed adenoviral backbone plasmid vector-the pAdEasy vector, and the shuttle vector containing the gene of interest (***Figure 3.4***). This system allows for transient expression of the desired protein with the correct post-translation modifications. Successful expression of MSLN was achieved allowing for selection and characterization of MSLN-specific scFv described in this chapter.

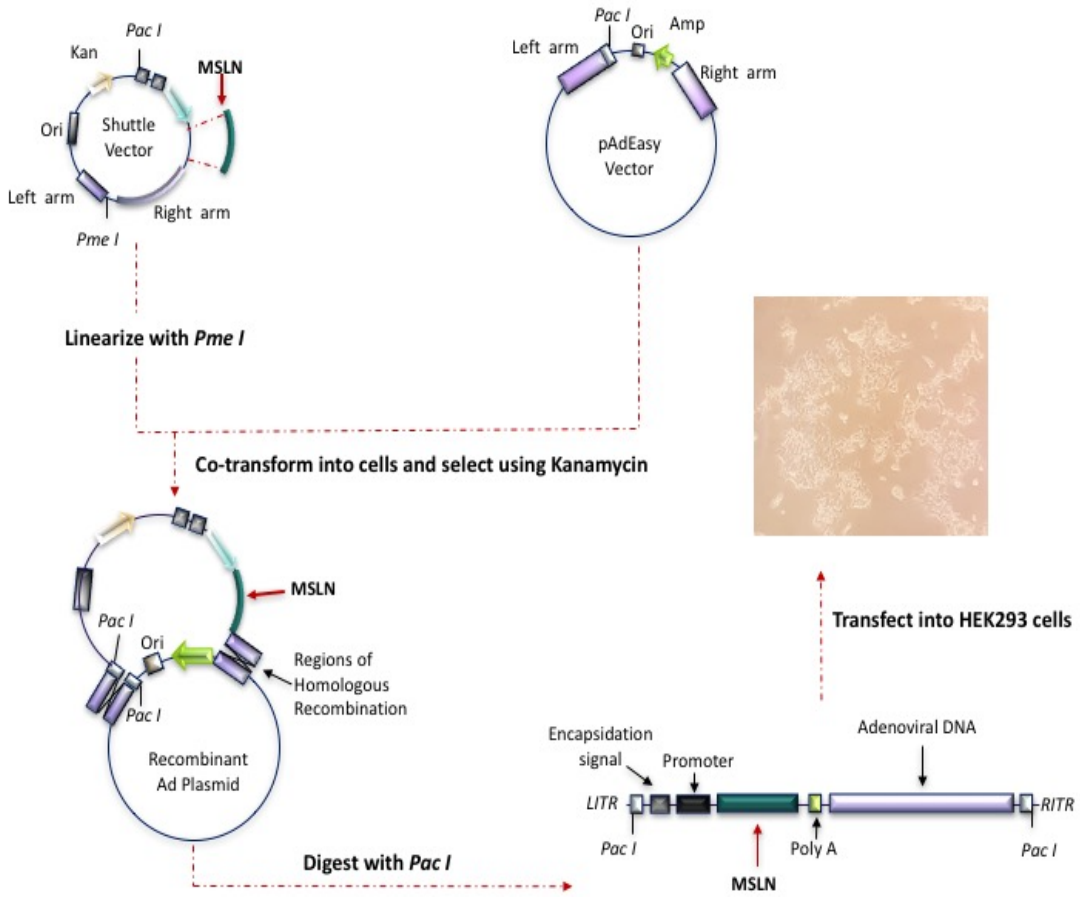

Figure 3.4 Workflow of transfection of pAdEasy MSLN vector into HEK293 cells for expression of a recombinant MSLN protein.

The pAdEasy backbone vector was supplied already co-transformed with the shuttle vector housing the MSLN gene and the kanamycin resistance gene. The plasmid is plated out on LB agar plates containing kanamycin to select for transformants. Single colonies are selected, grown and purified to obtain the recombinant plasmid DNA. The plasmid DNA is linearized with the PacI restriction enzyme and then transformed into HEK293 for expression of the MSLN protein. Full map of the pAdEasy-1 vector can be found in Appendix C.

3.2 Results

3.2.1 Generation of a murine anti-Capan-1 library

3.2.1.1 Propagation of Capan-1 cell line

This approach allowed for minimal animal usage in compliance with the "Three Rs" tenet, Replacement, Reduction and Refinement. This tenet states that animals should only be used if an attempt to find a non-animal alternative has failed. When they are needed the most humane methods are used on the smallest number of animals that would provide valid data (Fenwick *et al.,* 2009).

3.2.1.2 Immunisation of BALB/c mice with Capan-1 cell line

Six BALB /c mice were immunised subcutaneously with equal parts of a suspension composed of Capan-1 cells and Freund's complete adjuvant in PBS. Each mouse received 1 x 10^6 viable cells in sterile 1 X PBS. An initial immunisation was carried out followed by 5 subsequent boosts mixed with Freund's incomplete adjuvant. All boosts contained the same number of viable cells as the initial immunisation. Each boost was administered 14 days apart. After four boosts, an antibody serum titre determination was performed by ELISA against Capan-1 cells.

3.2.1.3 Murine serum antibody titre determination

An ELISA was performed on a Nunc MaxiSorp™ 96-well plate coated with 1 x 10^5 / well Capan-1 cells and probed using varying dilutions of mice serum (1/100 – 1/400,000). A sufficiently high immune response of ~1/200,000 was observed against the cell line after the 3rd boost (***Figure 3.5***). Following administration of the 4th boost, two mice died. The spleens of these two mice were harvested, placed in RNAlater™ and stored indefinitely at -80°C. A bleed was taken from the two mice post-mortem and an antibody serum titre was carried out to determine if RNA extraction of these spleens would be valuable (***Figure 3.6***). Both produced an antibody titre greater than 1:100,000 indicating the murine immune systems had actively responded to the Capan-1 cells. The remaining four mice were culled to harvest the B-cells from the spleens for recombinant antibody generation.

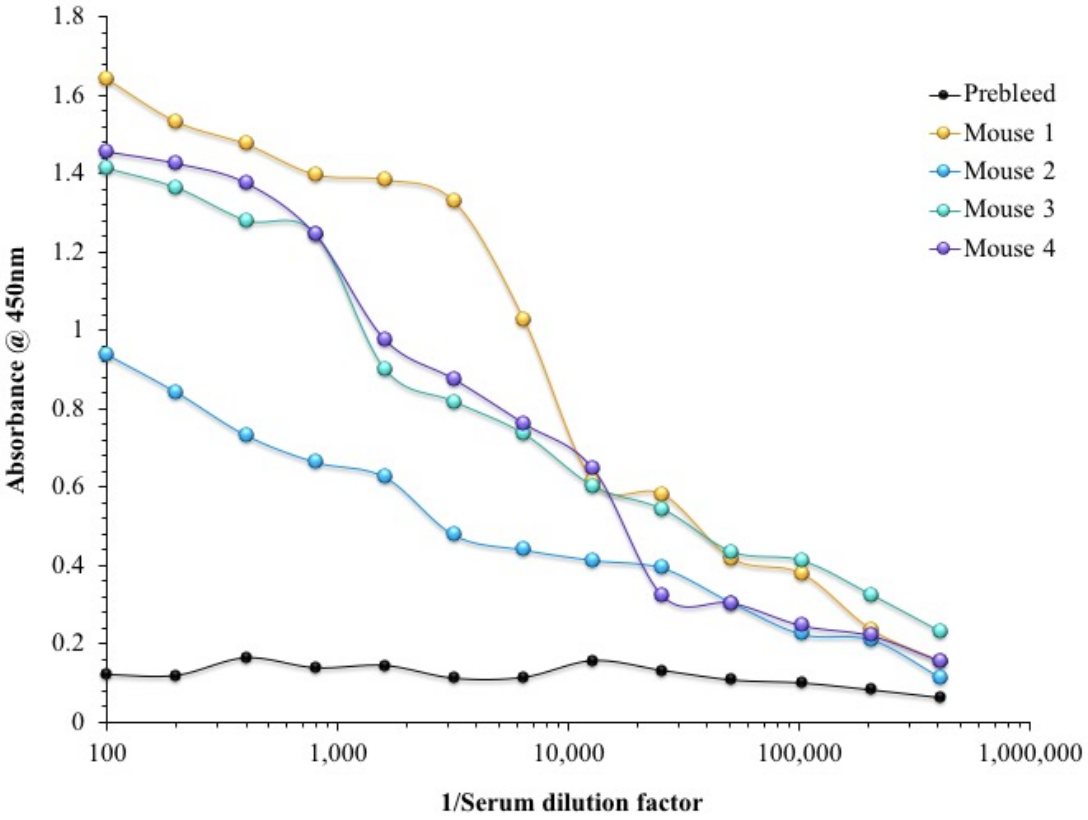

Figure 3.5 Titration of serum antibodies, obtained from mice immunised with Capan-1 cells after 4 boosts, determined by ELISA

The serum was collected from the immunised mice from the facial vein. The response analysis for each of the 4 live mice was analysed on two plates and the results plotted on the graph. A pre-bleed was taken from the mice prior to immunisation. This was used as a control to compare the immune response after exposure. The bound antibodies were detected using a HRP-labelled goat anti-mouse IgG antibody. There was a significant response to Capan-1 cells in the sera from all four mice.

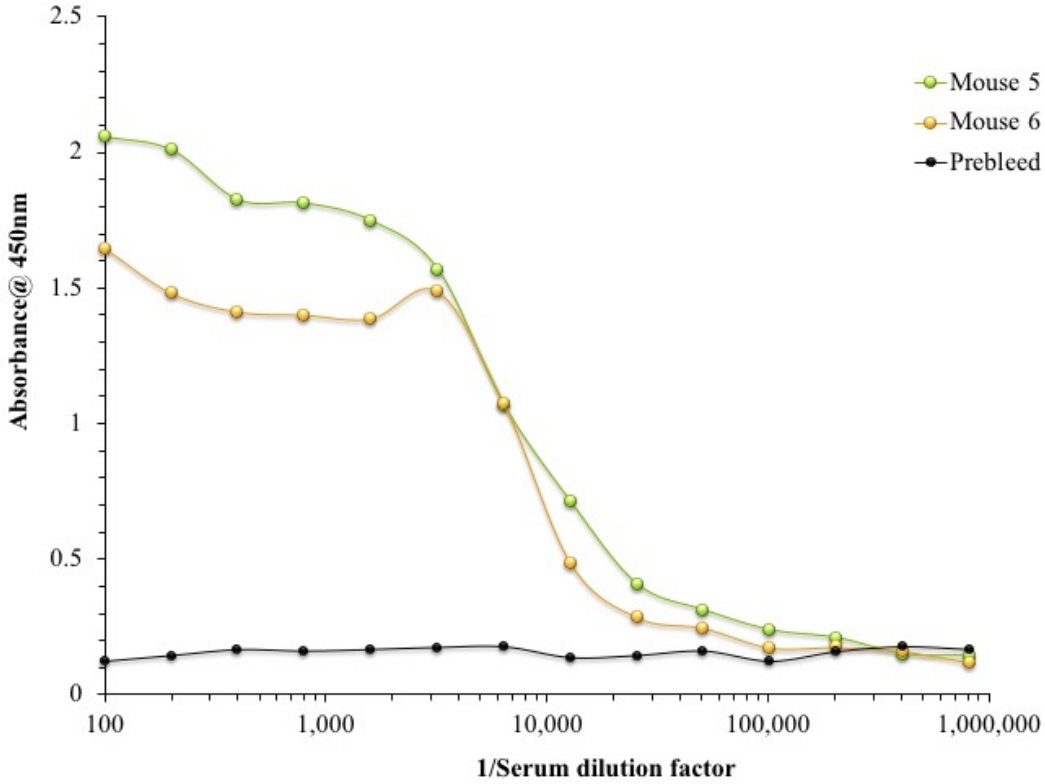

Figure 3.6 Titration of murine serum antibodies by ELISA using sera obtained from the two deceased mice.

The serum was collected immediately post mortem. The antibody titre responses were performed on one ELISA plate and plotted on the graph. A pre-bleed was taken from the mice prior to immunisation. This was used as a control to compare the immune response after exposure. The bound antibodies were detected using a HRP-labelled goat anti-mouse IgG antibody. There was a significant immune response to Capan-1 in the sera collected from the deceased mice.

3.2.1.4 Isolation of RNA from spleen B-cells and cDNA synthesis

The spleens were removed from the mice and homogenised in TriZol. Total RNA was carefully extracted from the homogenized spleen samples and then quantified using the Nanodrop™ ND-1000. First-strand cDNA synthesis was performed by reverse transcription. This cDNA template was then used to amplify the variable light (λ and κ chains) and heavy chain genes.

3.2.1.5 Primer optimisation for the murine variable heavy and light chain genes

A standard PCR protocol using My*Taq*™ Red Mix DNA polymerase was used for the optimisation of the variable heavy (V_H) and light (V_κ) chain genes. Each domain has a wide variety of forward primers and a small number of reverse primers that required optimisation. The reverse primers were mixed and then employed in a single reaction with a different forward primer (***Figure 3.7***). The optimisation of the forward primers for the amplification of the V_κ and V_H chain genes was successful with the majority resulting in sufficient amplification. These primers were mixed in the volumes stated by Barbas *et al.* (2001) and subsequently employed for large-scale amplification of the V_κ and V_H chain genes.

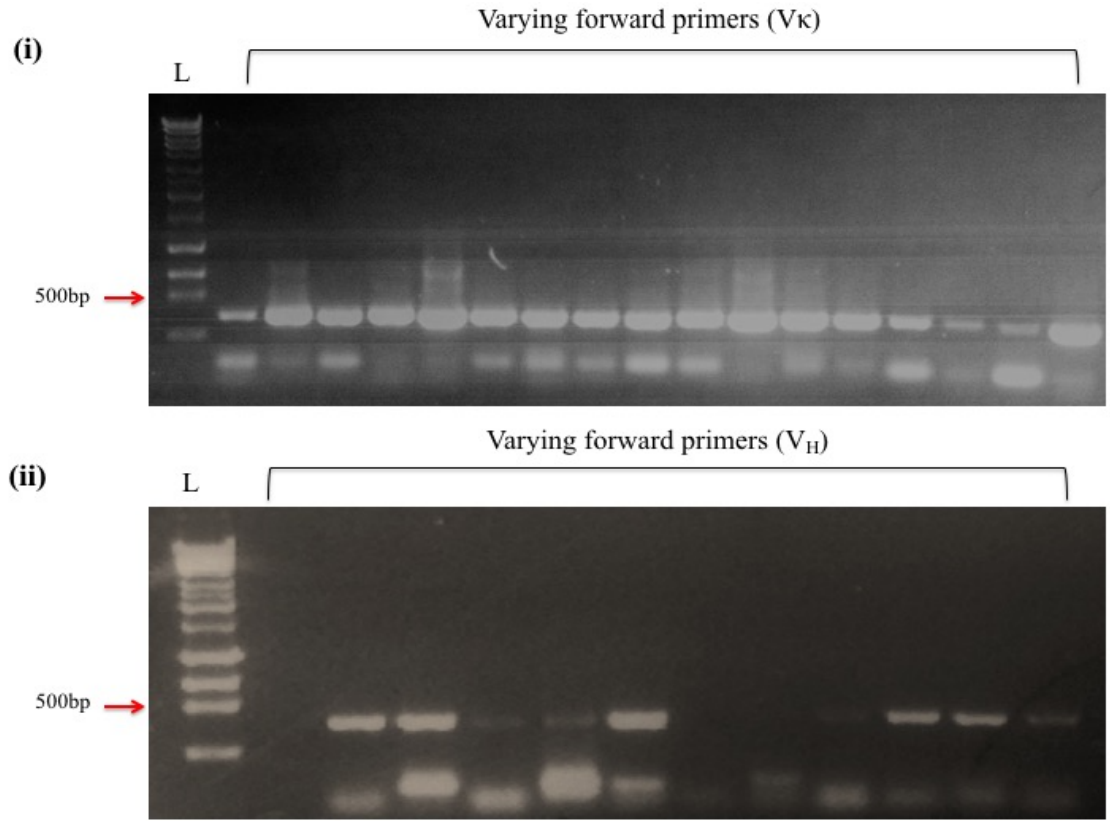

Figure 3.7 Optimisation of primer combinations

(i) *Optimisation of primer combinations to amplify murine V_κ from synthesised cDNA derived from the Capan-1-immunised mice. Each lane represents one forward primer (1-17). Amplification was performed using MyTaq™ Red Mix 2X and the manufacturer's recommended PCR conditions* ***(ii)*** *Optimisation of primer combinations to amplify murine V_H. Each lane represents one forward primer (1-12) The same conditions as those used for the amplification of V_κ were followed. L = 1kb Ladder (Bioline HyperLadder™ Plus).*

3.2.1.6 PCR optimisation for the murine V_H, Vκ and Vλ generation and Splice by overlap extension (SOE) –PCR of the V_H and V_L chains

A standard protocol was used for the large-scale amplification of the variable chain genes from the reverse-transcribed cDNA. All regions amplified successfully with no further optimisation required (***Figure 3.8***). The variable fragments were gel-purified and then linked by splice-by-overlap extension PCR (SOE-PCR). In the SOE-PCR, the variable light and heavy fragments are linked by a glycine-serine linker $(G_4S)_4$ providing the scFv with the necessary flexibility. The thermocycler conditions differ in this PCR to accommodate for the longer product (800bp). The extension time and final extension is doubled to favour the overlap of the variable chains. The initial attempt at the SOE-PCR was performed under the standard conditions for My*Taq*™ Red Mix 2X polymerase, as outlined in *Section 2.15.9,* using equal concentrations of the purified variable domains (100ng each) as the DNA template. This yielded a streaky product with several non-specific products and little amplification at 800bp (***Figure 3.8 (iv)***). This streaky product is most likely caused by an inappropriate annealing temperature resulting in the primers binding non-specifically to the template.

The amplification of the SOE product required investigation for establishing the optimal reaction conditions. The annealing temperature can greatly influence the specificity of primer binding. This temperature is determined by calculating the melting temperature (T_m) of the primers, however, this is an approximation and can be affected by the other components of a PCR, for example the buffer. As such, performing the SOE-PCR at a range of temperatures above and below the calculated T_m should indicate the optimum annealing temperature to amplify the product. The annealing temperature was optimised by carrying out an SOE-PCR at a range of annealing temperatures from 58°C to 62°C and also performing a 'touch-down' SOE-PCR which incrementally reduced the annealing temperature of 62°C by 0.2°C per cycle. The products of these optimisations were resolved on a 1.5% (w/v) agarose gel as show in ***Figure 3.9***. The touch-down PCR did not increase the specificity of the reaction as is evident by the presence of numerous faint bands. The results of the temperature gradient investigation were similar to that observed for the touch-down PCR. However, there is stronger specific amplification at the desired 800bp band. Regardless, this was not sufficient amplification of the 800bp product as non-specific products amplified preferentially.

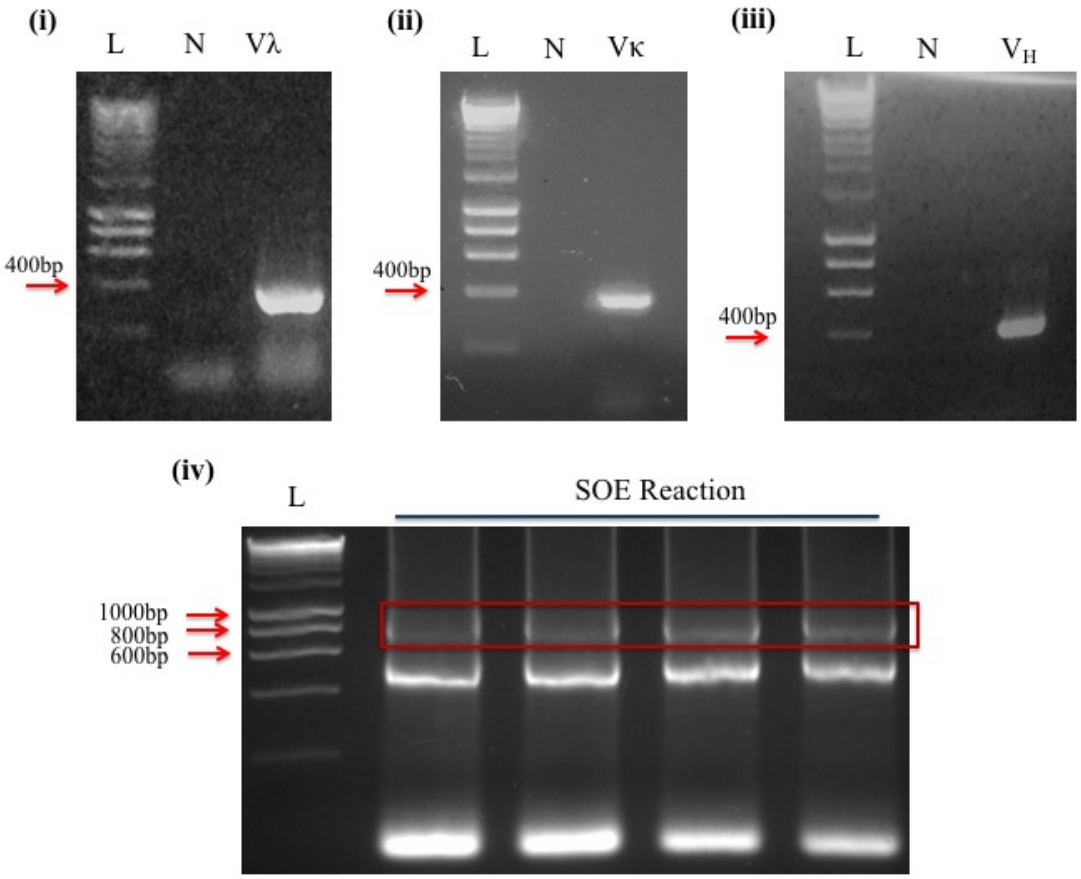

Figure 3.8 Amplification of the variable regions

(i) *Vλ;* ***(ii)*** *Vκ;* ***(iii)*** *V_H from synthesised cDNA. Amplification was performed using MyTaq™ Red Mix 2X using the manufacturer's recommended PCR conditions. L = 1kb Ladder (Bioline HyperLadder™). N = Control lane. This is a sample containing all the components of the PCR without the cDNA template.* ***(iv)*** *Splice by Overlap Extension-PCR of the amplified V_H and V_L fragments. This initial amplification was carried out using the conditions followed when amplifying the variable fragments. The only alteration was the use of a longer final extension time of 10 min instead of the 5 min used for the shorter variable fragments. Non-specific amplification is observed as well as a streaky product and limited amplification. L = 1kb Ladder (Bioline HyperLadder™); N = Control lane without DNA template; SOE = SOE-PCR amplification.*

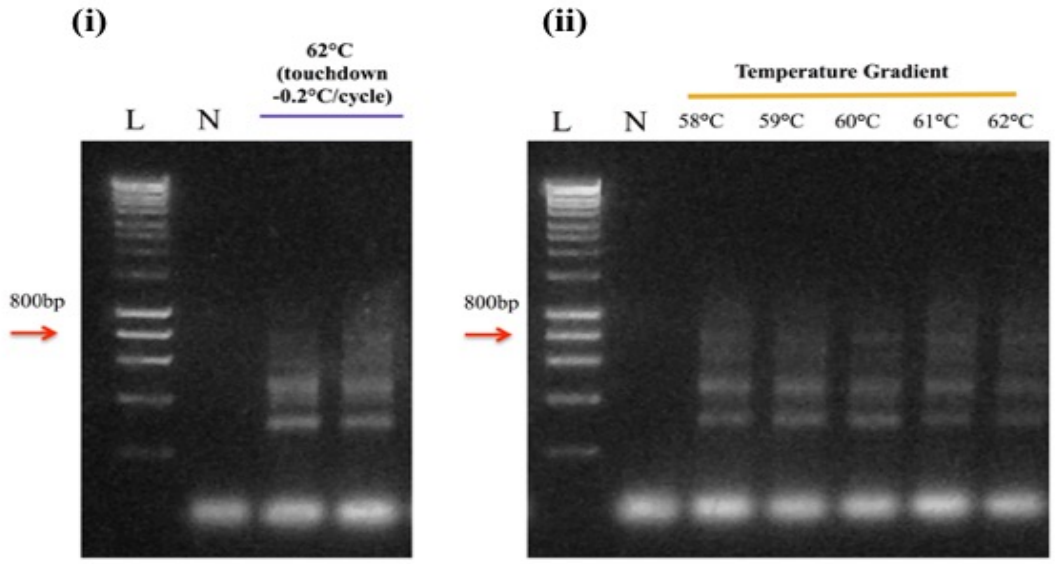

Figure 3.9 Optimisation of the scFv product amplification by temperature variations ***(i)*** *Touch-down SOE-PCR was performed with the initial annealing temperature of 62°C reduced by 0.2°C per cycle.****(ii)*** *SOE-PCR using different annealing temperatures from 58°C to 62°C.Standard SOE-PCR conditions using MyTaq™ Red Mix 2X polymerase were used. L = 1kb Ladder (Bioline HyperLadder™); N = Control sample without DNA template.*

Various *Taq* polymerases can influence the specificity and fidelity of DNA amplification. Due to the consistent presence of non-specific amplification products a different *Taq* polymerase, Phusion DNA polymerase, was tested. This is a high-fidelity polymerase with proof reading capabilities as a result of its 3'-5' exonuclease activity. This polymerase is often recommended when amplifying difficult amplicons. It is essential to optimise the concentration of $MgCl_2$ when using Phusion DNA polymerase. Excessive amounts of $MgCl_2$ can significantly hinder the denaturation of DNA causing non-specific binding. Despite the presence of an additional band at ~600bp, the $MgCl_2$ optimisation using Phusion DNA polymerase yielded a specific 800bp band. The high-fidelity buffer supplemented with 3mM $MgCl_2$ was selected for further optimisation as it resulted in the amplification with the least amount of non-specific product (***Figure 3.10 (i)***).

To improve preferential amplification of the 800bp product, various PCR additives were investigated. Betaine and DMSO are PCR enhancers that can help to increase the yield of the desired product while reducing the production of non-specific products. Betaine (recommended for use at 1M concentration) and DMSO (recommended concentration of

3-10% (v/v)) both aid in DNA strand separation (Jensen *et al.,* 2010). A DMSO gradient using 5% and 10% (v/v) and investigation of Betaine alone and in combination with DMSO was performed using the standard amplification conditions with a 58°C annealing temperature (***Figure 3.10 (ii)***). The SOE-PCR sample containing the 5% (v/v) DMSO yielded the most specific desired product with minimal streaking and significantly reduced amplification of the 600bp product. Thus, the desired product was amplified by the addition of 5% (v/v) DMSO using Phusion DNA polymerase High Fidelity buffer supplemented with 3mM $MgCl_2$ (***Figure 3.10 (iii)***).

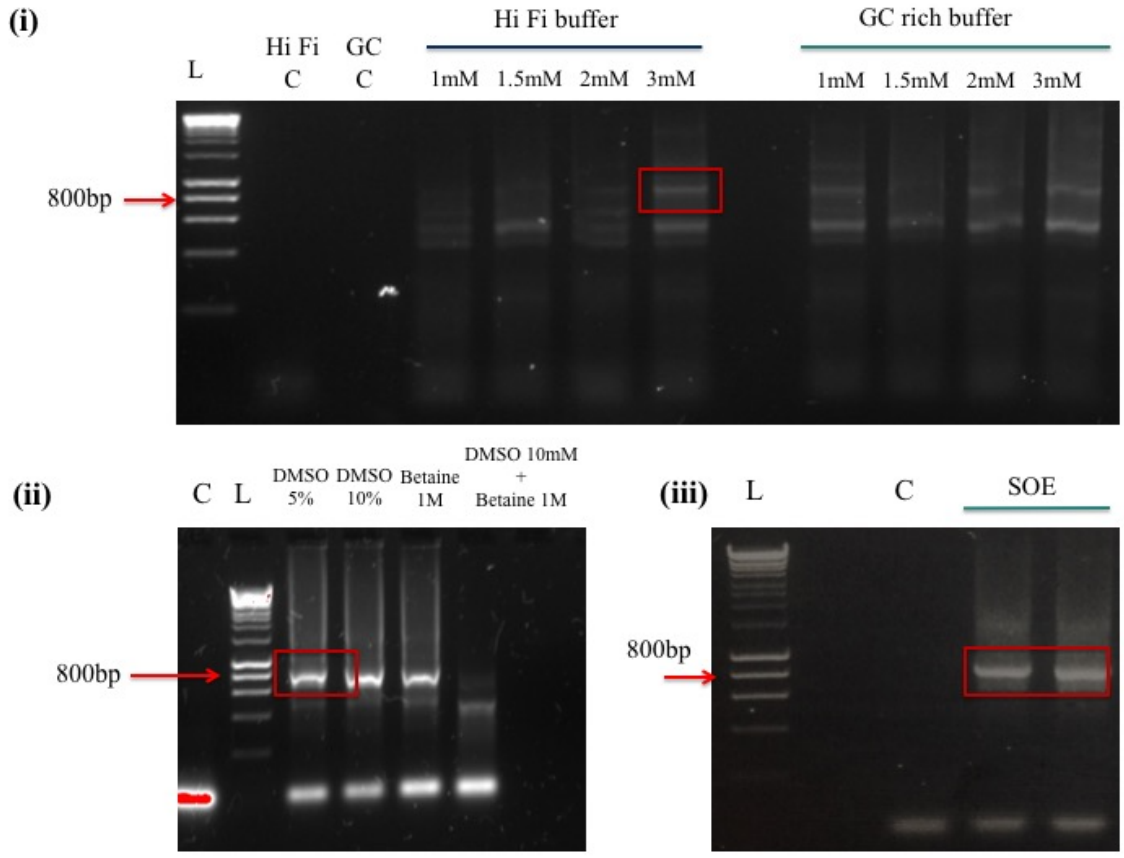

Figure 3.10 Optimisation of Phusion DNA polymerase and PCR additives for amplification of a specific SOE product

(i) *Optimisation of $MgCl_2$ concentration for the SOE product using Phusion DNA polymerase.* ***(ii)*** *Optimisation of the SOE-PCR product using a DMSO gradient (5-10% (v/v) and betaine (1M).* ***(iii)*** *Large-scale SOE amplification using optimum PCR conditions. Determined optimum conditions were used. L = 1kb Ladder (Bioline HyperLadder™); N = Control sample without DNA template; NOA = No additives in the PCR sample.*

3.2.1.7 Library construction

After large-scale amplification, the SOE product was gel-purified and ethanol-precipitated. The sample was quantified and digested using the *Sfi*I restriction enzyme. Simultaneously, the pComb3XSS vector was streaked on LB agar plates and a single colony was picked, grown and purified using a plasmid prep kit. The vector was then digested with the *Sfi*I enzyme which produced three products, undigested pComb3XSS, digested pComb3XSS and the removed stuffer fragment ***(Figure 3.11)***. The digested vector was then treated with Antarctic Phosphatase to ensure no self-ligation of the vector occurred by removal of the phosphorylated ends. The digested vector and overlap product were resolved and purified from a 0.6% (w/v) and 1% (w/v) agarose gel, respectively.

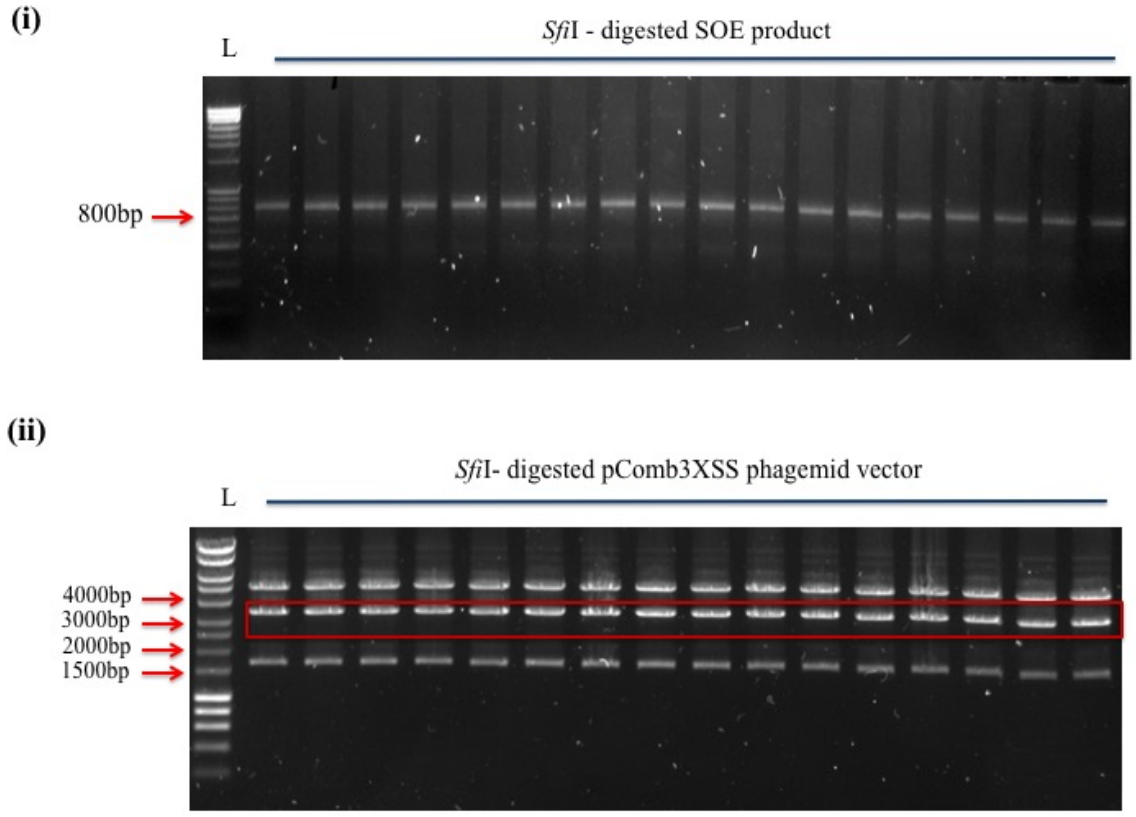

Figure 3.11 Digestion of the SOE product and pComb3XSS phagemid vector using SfiI enzyme

(i) *Analysis of the SfiI- digested overlap product.* ***(ii)*** *Analysis of SfiI- digested pComb3XSS phage display vector. L = 1kb Ladder (Bioline HyperLadder™)*

The gel-purified *Sfi*I-digested products were concentrated by ethanol-precipitation and quantified on the NanoDrop™ 1000. The purified overlap product was then successfully ligated into the pComb3XSS vector using T4 DNA ligase ***(Figure 3.12)***.

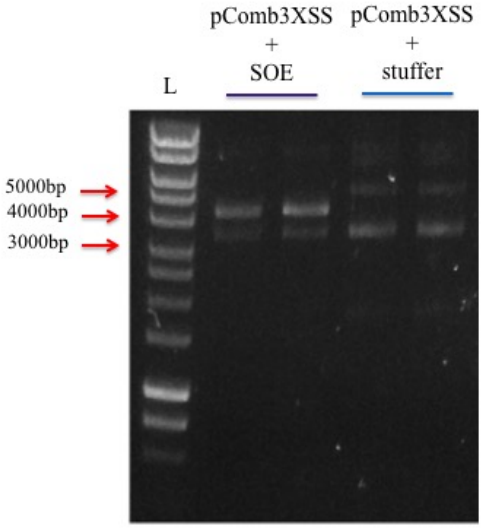

Figure 3.12 Analysis of the ligation reaction products of the SfiI-digested murine-derived SOE product, the stuffer fragment and the pComb3XSS phage display vector*. L = 1kb Ladder (Bioline HyperLadder™); The two bands in lane 1 and 2 represent pComb3XSS at ~ 3300bp and the ligated product of pComb3XSS and SOE at ~4100bp. The two bands present in lane 3 and 4 represent pComb3XSS at ~ 3300bp and the ligated product of pComb3XSS and the stuffer fragment at ~5100bp.*

3.2.1.8 Transformation of library efficiency and analysis of clone variability

The transformed murine Capan-1 scFv library size was ~10^6 cfu/mL. A colony-pick PCR was carried out on the transformed library to investigate the transformation efficiency and determine the percentage of colonies containing the 800bp insert. For this 10 colonies were randomly selected. It can be observed in ***Figure 3.13*** that all of the colonies contained the scFv insert suggesting 100% insert retention.

Genetic fingerprinting analysis was then performed on the selected colonies which allows for a rapid basic assessment of the diversity within the antibody library by fragment length polymorphism (RFLP). Digestion with the two restriction enzymes Bst*N*I and Alu*I* (***Figure 3.14)*** randomly cut the scFv gene and generate a genetic fingerprint from variations in the recognition site patterns as a result of the DNA sequence diversity within the library (Aavula *et al.,* 2011).

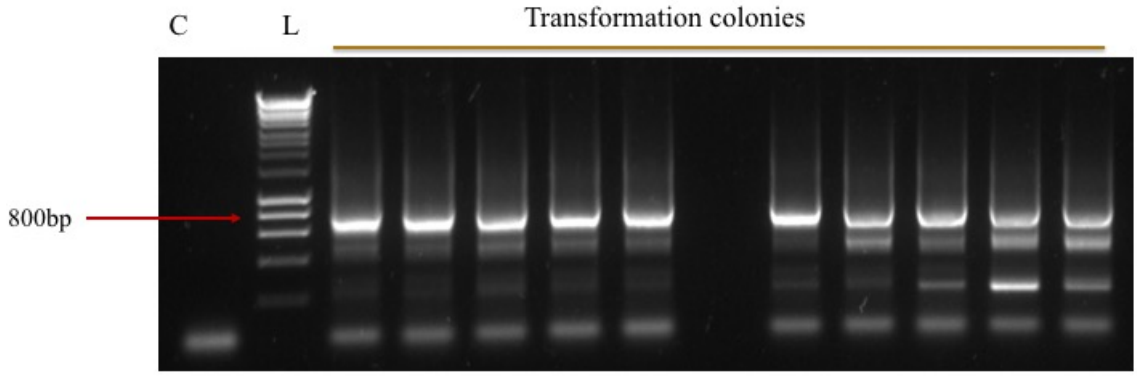

Figure 3.13 Colony-pick analysis on transformed murine Capan-1 library

Analysis of a colony-pick PCR performed on 10 randomly selected colonies to determine the transformation efficiency of the Capan-1 library into XL1-Blue electrocompetent E. coli cells. C= PCR performed without the addition of a single colony. L = 1kb Ladder (Bioline HyperLadder™).

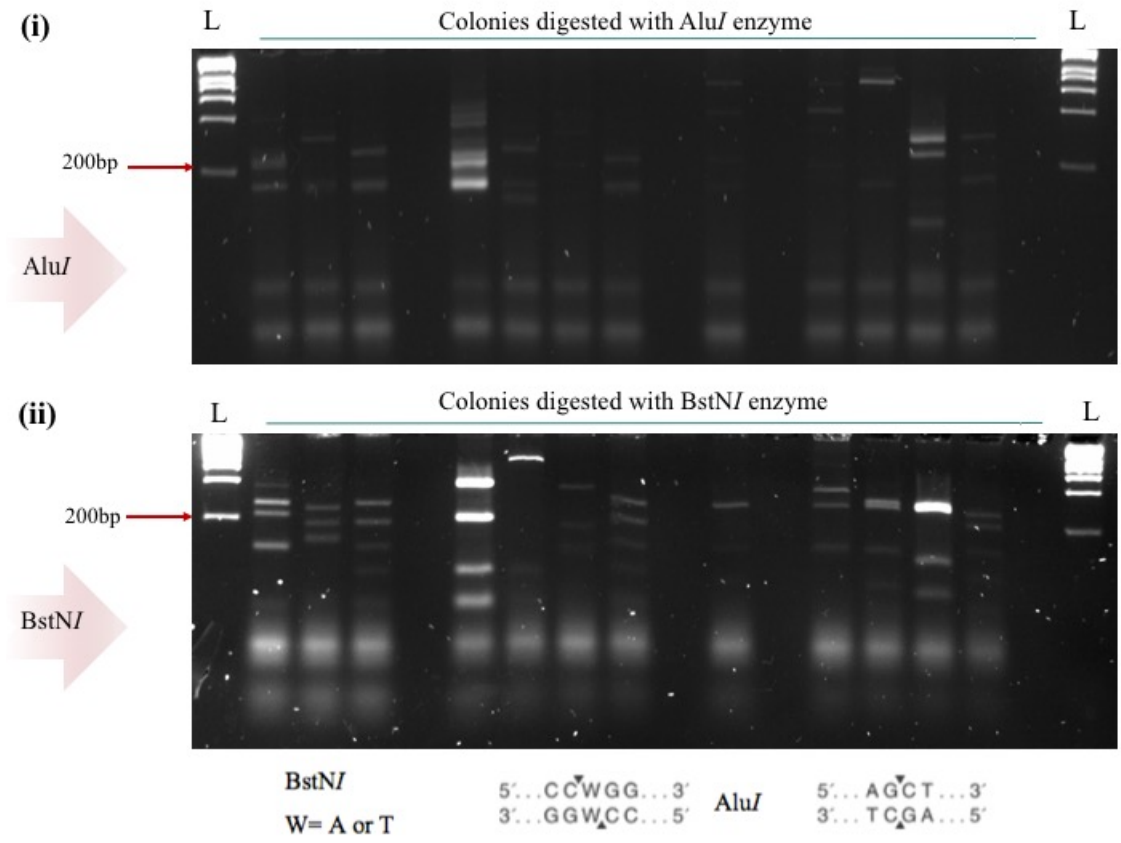

Figure 3.14 Genetic fingerprint analysis of 11 clones from transformation plates

*Purified inserts were restriction fingerprinted with **(i)** AluI and **(ii)** BstNI to investigate the diversity in the DNA sequences of the transformed library. L = 1kb Ladder (Bioline HyperLadder™)*

This concluded the work carried out on the generation of the communal biased-murine Capan-1 scFv library which was later employed in this chapter for isolation of MSLN-specific scFv and subsequently used again in *Chapter 4.*

3.2.2 Generation of a recombinant MSLN protein in an *E. coli* expression system

3.2.2.1 Optimisation of expression of MSLN protein using IPTG induction

The pPB-MSLN-N-His plasmid was transformed using a basic heat-shock protocol into BL21 (DE3) chemically competent cells. The transformation stock was spread onto LB agar plates supplemented with kanamycin and incubated O/N at 37°C. The following day a single colony was used to inoculate a 10 mL culture supplemented with kanamycin, for optimisation of recombinant MSLN protein expression conditions. In order to carry out a full optimization of the expression of the recombinant MSLN, IPTG concentration, time points post-induction, and growth temperatures of 30°C and 37°C were investigated. The overnight 10 mL culture was used to inoculate a variety of small-scale LB cultures. The growth was monitored until an OD_{600} of ~0.6 was obtained and each of the individual cultures was induced using the appropriate concentration of IPTG. One culture from each IPTG concentration was then incubated at 30°C and the other at 37°C. A 1 mL sample was then removed from each culture at 2 hr, 3 hr, 4 hr and O/N post-induction. The 1 mL culture samples were centrifuged for 15 min at 12,000*g* and the pellet resuspended in 200 µL of 1 mg/mL lysozyme and subsequently subjected to 3 freeze-thaw cycles. The lysate samples were then analysed by SDS-PAGE and WB for expression of recombinant MSLN (***Figure 3.15***). From these figures, it is apparent that there is no positive expression of MSLN at any time point regardless of IPTG concentration or incubation temperature.

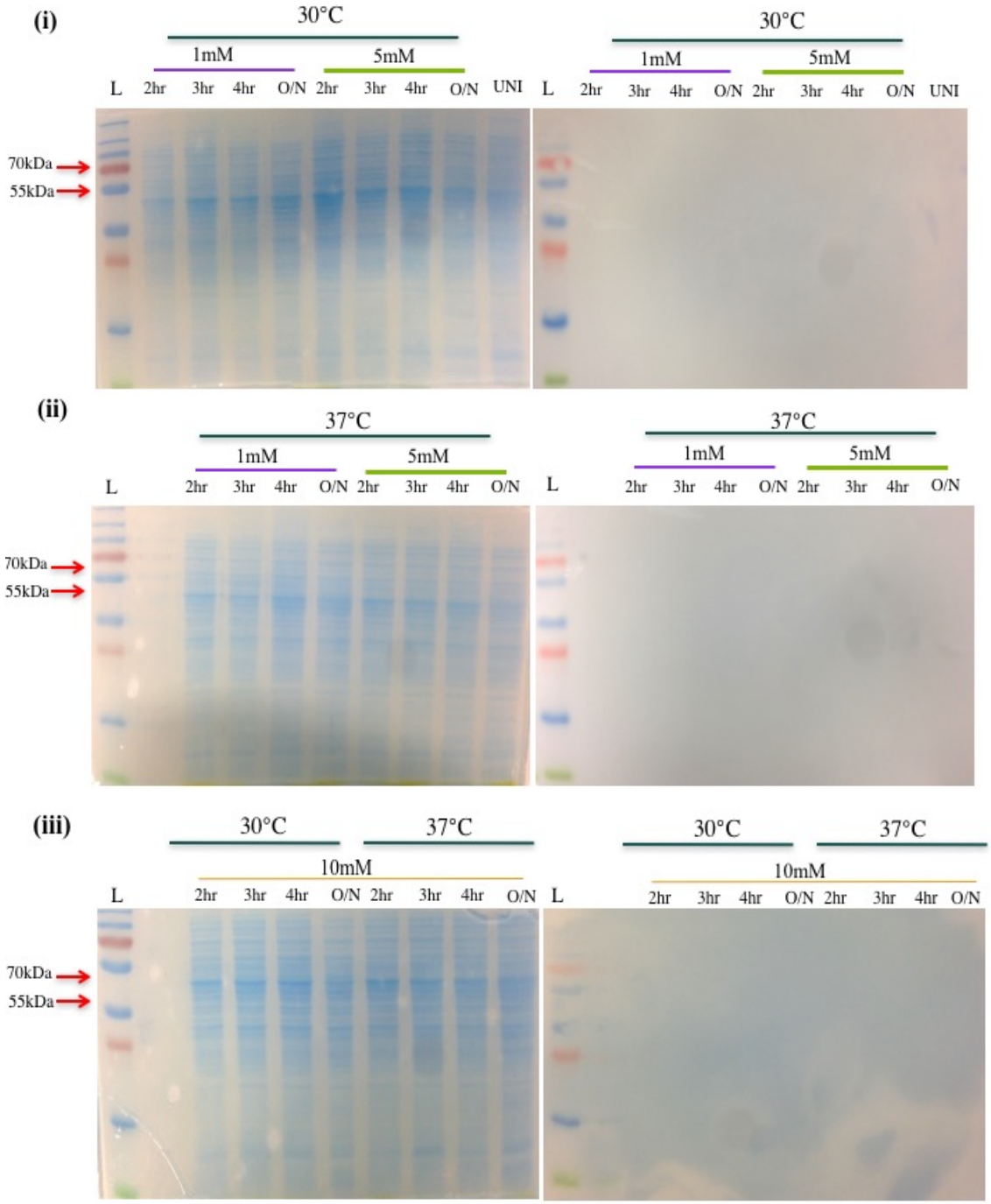

Figure 3.15 Optimisation of MSLN expression using IPTG induction.

(i) *SDS-PAGE and WB of cultures induced with 1mM and 5mM IPTG at 37°C.* ***(ii)*** *SDS-PAGE and WB of cultures induced with 1mM and 5mM IPTG at 30°C.* ***(iii)*** *SDS-PAGE and WB of cultures induced with 10mM IPTG at 30°C and 37°C. WB was probed with anti-HIS-HRP-labelled antibody. L= PageRuler™ Plus Prestained Protein Ladder (See Appendix E).*

3.2.2.2 Optimisation of MSLN expression using TB media at lower expression temperatures

Expression of recombinant proteins at lower temperatures can increase solubility of the protein, limit possible protein degradation and reduce protein aggregation. The lower temperatures reduce the speed of cell processes such as transcription and translation resulting in reduced protein aggregation. Another factor to consider when attempting expression of complex or difficult proteins is the media choice. Terrific broth (TB) is a rich media of choice for high protein yields in *E. coli*. Its enriched composition provides superior physiological conditions. It contains more tryptone and yeast extract than LB and also contains potassium phosphate and glycerol. The tryptone and yeast extract provide, amino acids and vitamins and trace elements which aid in increased cell yields. The potassium phosphate maintains the pH of medium and the glycerol provides a source of carbon and carbohydrates. To combat the lack of protein expression, lower temperatures using TB media were investigated.

Fourteen colonies were randomly selected from transformation spread plates. Each of the fourteen colonies was grown overnight in TB media. The following day each of the 14 overnight cultures was used to inoculate two small-scale cultures of TB media supplemented with kanamycin. All cultures were induced using 5mM IPTG. Half were incubated at 20°C and the remaining at 25°C O/N. The next day a 1 mL sample was removed and centrifuged at 12,000*g* (Eppendorf™ centrifuge fixed angle rotor (F-45-30-11)) for 15 min. The cells were lysed by addition of 1 mg/mL lysozyme and subjected to freeze-thaw cycles as per *Section 2.13.1.5.1*. The lysed samples were centrifuged at 11,000*g* for 20 min. The supernatant was removed, mixed with 4 X loading dye and boiled for 5 min at 95°C. The samples were analysed by SDS-PAGE and WB (***Figure 3.16***). Faint bands can be observed at the expected size of ~69kDa in two wells, one colony at each temperature. While faint, the present bands suggests the presence of the recombinant MSLN gene in the plasmid.

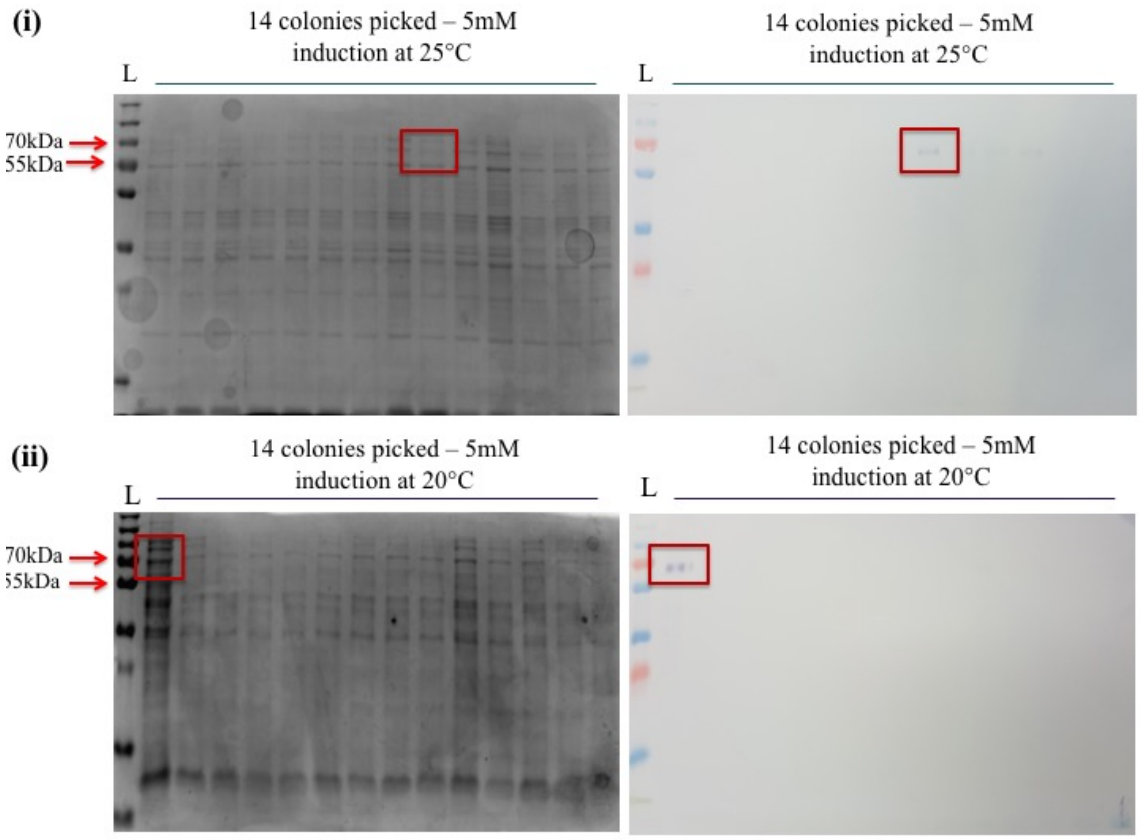

Figure 3.16 Optimisation of MSLN using TB broth as lower temperatures of 20°C and 25°C

(i) *SDS-PAGE and WB analysis of colonies expressed at 25°C .* ***(ii)*** *SDS-PAGE and WB analysis of colonies expressed at 20°C. WB analysis probed with a HRP-labelled anti-HIS antibody. L = PageRuler™ Plus Prestained Protein Ladder*

3.2.2.3 Optimisation of expression of MSLN protein using auto-induction media

The level of expression observed using IPTG induction was not sufficient for large-scale expression and purification. The effect of auto-induction media with a TB broth base on the recombinant protein expression at a variety of temperatures was then evaluated. The two MSLN-expressing colonies identified in ***Figure 3.17*** were used to inoculate two 10 mL cultures containing TB supplemented with kanamycin and grown O/N at 37°C. The following day each O/N culture was sub-cultured into four separate 10 mL cultures containing auto-induction media with a TB broth base. The cultures were grown O/N at the appropriate temperature. The following day 1 mL lysate samples were obtained, as described in the previous section, and analysed on SDS-PAGE and WB for recombinant MSLN expression.

It can be observed in ***Figure 3.17*** that limited MSLN expression has occurred. A single band is present in the lane representing the positive-MSLN expressing colony from ***Figure 3.16 (ii)*** in auto-induction media grown at 37°C. This extremely limited expression is negligible and entirely insufficient for large-scale expression and purification. MSLN is a glycoprotein and could require eukaryotic expression for correct post-translational modifications. Work was subsequently carried out to express a recombinant MSLN protein in the transfection cell line, HEK293.

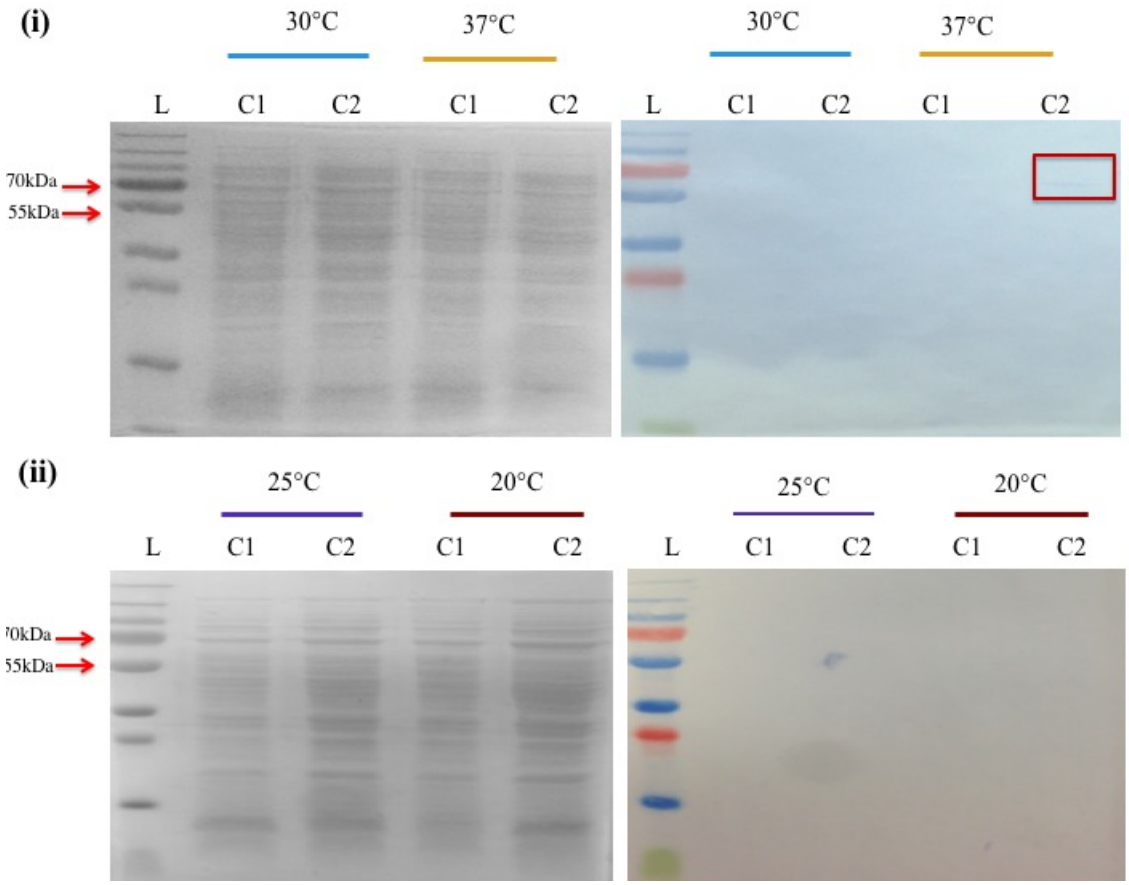

Figure 3.17 Optimisation of MSLN expression using auto-induction media with TB and broth bases at temperatures 30°C and 37°C

(i) *30°C and 37°C SDS-PAGE gel and WB.* ***(ii)*** *20°C and 25°C SDS-PAGE gel and WB WB was probed with a anti-HIS-HRP-labelled antibody. L = PageRuler™ Plus Prestained Protein Ladder. C1 = MSLN-expressing colony identified in* ***Figure 3.16(i)****; C2 = MSLN-expressing colony identified in* ***Figure 3.16(ii).***

3.2.3 Expression of a recombinant MSLN protein in mammalian HEK293 cells

3.2.3.1 Propagation of HEK293 cells

The human embryonic kidney (HEK) 293 cell line is a widely used transient expression system because of its amenability to transfection and capacity to carry out post-translational modifications and folding which produces a functional protein (Thomas and Smart., 2005) (See *Sections 2.11.1-2.11.6)*.

3.2.3.2 Isolation and linearization of vector DNA

Traditionally, two methods are used to generate recombinant adenoviruses, the first is ligation of the gene of interest into the adenoviral genome and the second involves cloning the gene of interest into a shuttle vector and transferring the gene to the genome by homologous recombination in a mammalian cell line. This does not require further tedious steps to isolate recombinant adenovirus. The pAdEasy system, as previously described, uses the homologous recombination machinery in *E. coli* whereby a recombinant adenovirus is produced by double-recombination between the pAdEasy vector and the shuttle vector. The pAdEasy-Msln-iCre-HA-Flag vector was sourced from Addgene. In its shipped form, the vector had already undergone double-recombination with the shuttle vector and contained the MSLN gene of interest. The cells containing the recombinant plasmid were grown up in SB media supplemented with kanamycin and the recombinant pAdEasy vector DNA was purified as per *Section 2.10.7*. The purified recombinant pAdEasy vector DNA was digested with *Pac*I restriction enzyme to expose its inverted terminal repeats (ITR) which contain the necessary elements for replication and packaging. The digested vector was analysed on a 0.6 % (w/v) agarose gel next to a non-digested sample for comparison (***Figure 3.18***). Digestion of the vector with the *Pac*I enzyme yielded two products, one larger product of ~30kb and a smaller fragment of ~4.5kb. The undigested sample contains a smeared band near the well and a lower band of just under ~30kb. The ladder used for size estimation only measures up to 10kb, however it can be clearly seen that there is a smaller band at ~4.5-5kb in the digested products and larger smeared bands in the undigested samples that conclusively show successful digestion by the *Pac*I enzyme. The digested vector was precipitated using ethanol and quantified on the NanoDrop™ 1000.

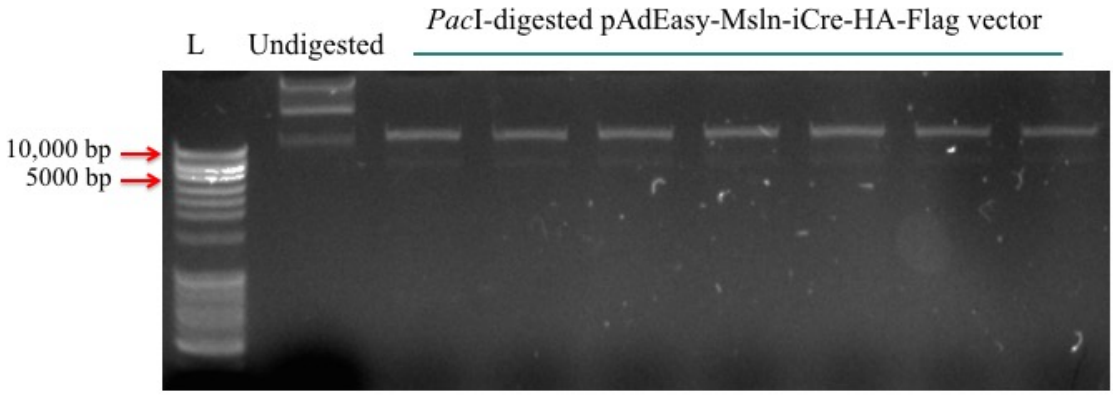

Figure 3.18 Digestion of recombinant Ad plasmid DNA with PacI

pAdEasy-Msln-iCre-HA-Flag vector linearized with PacI restriction enzyme analysed on a 0.6 % (w/v) agarose gel with uncut vector as a control. L = 1kb Ladder Bioline HyperLadder™ (See Appendix E).

3.2.3.3 Transfection of the digested pAdEasy-Msln-iCre-HA-Flag into the HEK293 cell line

The pAdEasy systems uses human adenovirus and human host cell lines. Consequently, the human MSLN protein is expressed in abundance with the correct post-translational modification and folding. The ViraPack transfection Kit, which is based on a modified version of the $CaPO_4$ method of transfection, was employed for transfection of the recombinant pAd vector into proliferated HEK293 cells. The $CaPO_4$ method of transfection works by forming a precipitate that results in DNA uptake by the cells by enhancing the adsorption of DNA to the cell membrane. The kit is an altered version of this protocol and employs a specifically modified bovine serum (MBS) in place of fetal bovine serum (FBS) during the incubation of the cells with the $CaPO_4$-DNA precipitate.

Exponentially growing HEK293 cells were inoculated at 5 x 10^5 cells /well in 5 mL CGM in a 6-well plate O/N. Five µg of linearized recombinant pAd vector was prepared as per the manufacturer's guidelines. The cells were washed twice with DPBS and 5 mL culture media containing 6 % (v/v) MBS was added to each well. While optimisation of MBS can be necessary, it is advised to begin at 6 % as this is optimal for the majority of cell lines. Once the cells and DNA were appropriately prepared, 500 µL of DNA suspension was added to each well and incubated at 37°C/5% CO_2 for three hours. At this point a notable precipitate was present in the transfected wells. The cells were once again washed

with DPBS to remove the precipitate and 5 mL of fresh CGM containing FBS was added to the plate. The cells were then incubated at 37°C/ 5% CO_2 and allowed to proliferate.

3.2.3.4 Harvesting of transfected cells and purification of MSLN protein

To identify successful transfection, recombinant MSLN expression 4 days post-transfection was analysed. Using a rubber policeman, one well of transfected cells were removed from the adherent surface. The cell suspension was centrifuged at 1,200*g* (Eppendorf™ centrifuge fixed angle rotor (F-45-30-11)) for 5 min. Then 5 mL of medium was removed, concentrated and buffered exchanged into 1 X PBS containing protease inhibitors (1 tablet per 10 mL) using a viva-spin column. The cell pellet was resuspended in 1 mL 1 X PBS and subjected to lysing by sonication (25% amplitude, 2 sec on pulse, 2 sec off pulse for 2 min). The lysed sample was centrifuged at 4,000*g* (Eppendorf™ centrifuge fixed angle rotor (F-45-30-11)) and the lysate removed for analysis of protein expression. Both fractions were analysed on SDS-PAGE and WB (***Figure 3.19***). On observation of the SDS-PAGE the media supernatant contains a specific band at the expected size of ~61kDa with a corresponding thick band present in the WB analysis probed with a rabbit anti-MSLN antibody followed by a HRP-labelled anti-rabbit secondary antibody. There is a strong band present in the pellet at ~55kDa which is significantly lower than the expected size of MSLN with a faint band at ~61kDa, indicating presence of MSLN in the supernatant which is to be expected. As such, both fractions were pooled for further purification of the desired protein.

The expressed MSLN was released from the remaining transfected cells and media supernatant by sonication (25% amplitude, 2 sec on pulse, 2 sec off pulse for 2 min) and concentrated to a yield of 10 mg/mL in 1 X PBS. The MSLN-containing fraction was subjected to size exclusion chromatography (SEC) on the ÄKTA pure system to isolate the MSLN protein (*Section 2.12.8*). Numerous peak fractions were eluted and analysed by SDS-PAGE. ***Figure 3.19*** shows the SDS-PAGE analysis of the eluted fractions of the contaminant bands with the MSLN-containing fraction. It can be observed that the SEC protocol was successful as the MSLN-containing fraction has very minimal residual contaminate bands**.** To confirm the protein eluted was MSLN, the fraction was analysed on an SDS-PAGE gel and by western blot. The western blot was probed with an anti-MSLN antibody followed by a HRP-labelled detection antibody (***Figure 3.20***). This pure recombinant protein was quantified at ~5mg/mL on the NanoDrop™ 1000.

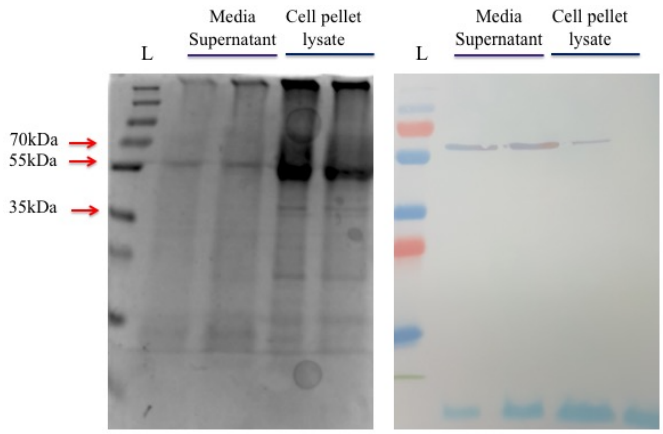

Figure 3.19 SDS PAGE and WB analysis of MSLN expression in HEK293 cells

SDS-PAGE and WB analyses of MSLN found in the cell pellet and the media supernatant of the transfected HEK293 cells. The WB was probed with a rabbit anti-MSLN antibody followed by a HRP-labelled anti-rabbit secondary antibody. L = PageRuler™ Plus Prestained Protein Ladder

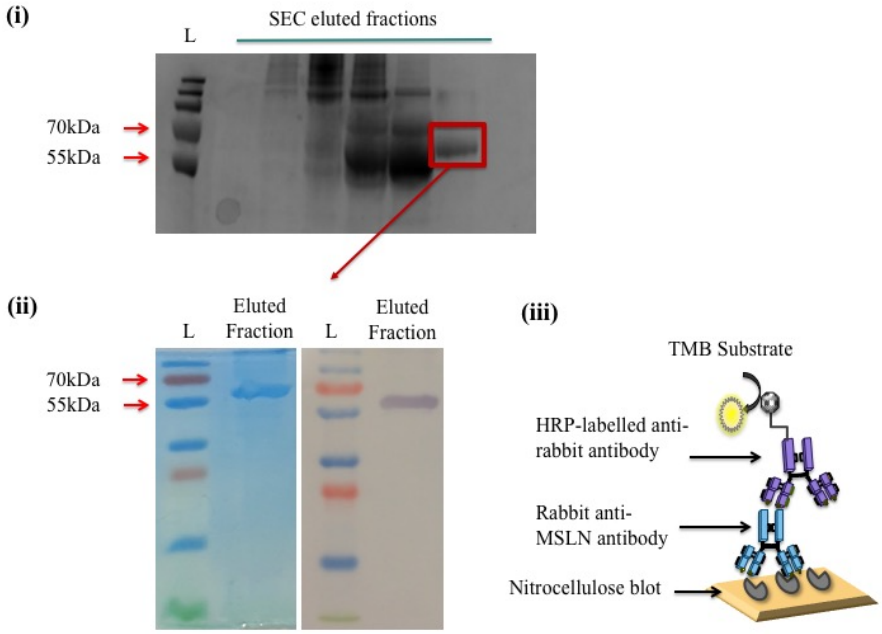

Figure 3.20 SDS-PAGE analysis of size exclusion chromatography purification of a recombinant MSLN protein

(i) *SDS-PAGE analysis of eluted fractions from size exclusion chromatography of MSLN protein from contaminant bands.* ***(ii)*** *SDS-PAGE and western blot analysis for confirmation of purified MSLN protein.* ***(iii)*** *Simplistic illustration representing the detection format of the western blot analysis. The blot was probed with a rabbit anti-MSLN antibody followed by detection using a HRP-labelled anti-rabbit antibody. L = PageRuler™ Plus Prestained Protein Ladder*

3.2.4 Antibody Library screening

3.2.4.1 Enrichment of an anti-Capan-1 phage library via biopanning

After the transformation efficiency was determined in *Section 3.2.1.8*, the expressed recombinant MSLN protein was employed to selectively amplify specific clones from the immune library by phage display panning. Four rounds of affinity selection via panning were performed on MSLN-coated immunotube™ with each selection round becoming exponentially more stringent by lowering the concentration of coated MSLN and increasing the number of wash steps. (***Table 3.1)***.

Table 3.1 *Panning conditions employed for each round of selection of the murine anti-Capan-1 scFv library against MSLN.*

Panning round	MSLN coating conc.	Number of washes
1	50 µg/ mL	3 X PBS, 3 X PBS-T (0.05% (v/v))
2	25 µg/ mL	5 X PBS, 5 X PBS-T (0.05% (v/v))
3	12.5 µg/ mL	10 X PBS, 10 X PBS-T (0.05% (v/v))
4	5 µg/ mL	15 X PBS, 15 X PBS-T (0.05% (v/v))

The precipitated input phage from each round of panning (1-4) was incorporated into a polyclonal phage ELISA to test for enrichment against the MSLN protein. Successful enrichment was demonstrated by an increase in ELISA absorbance signal after incubating the phage with the MSLN protein and detecting any bound phage with a HRP-labelled anti-M13 secondary antibody (GE Healthcare) (***Figure 3.21***). There is a noticeable reduction in absorbance after the initial round. This may be a result of non-stringent conditions in the first round, resulting in substantial non-specific binding and while this absorbance is desirable may not be representative of scFv with the desired affinity and specificity. The absorbance increases with rounds 3 and 4 indicating enrichment of anti-MSLN clones. Consequently, clones from these rounds were selected for soluble expression.

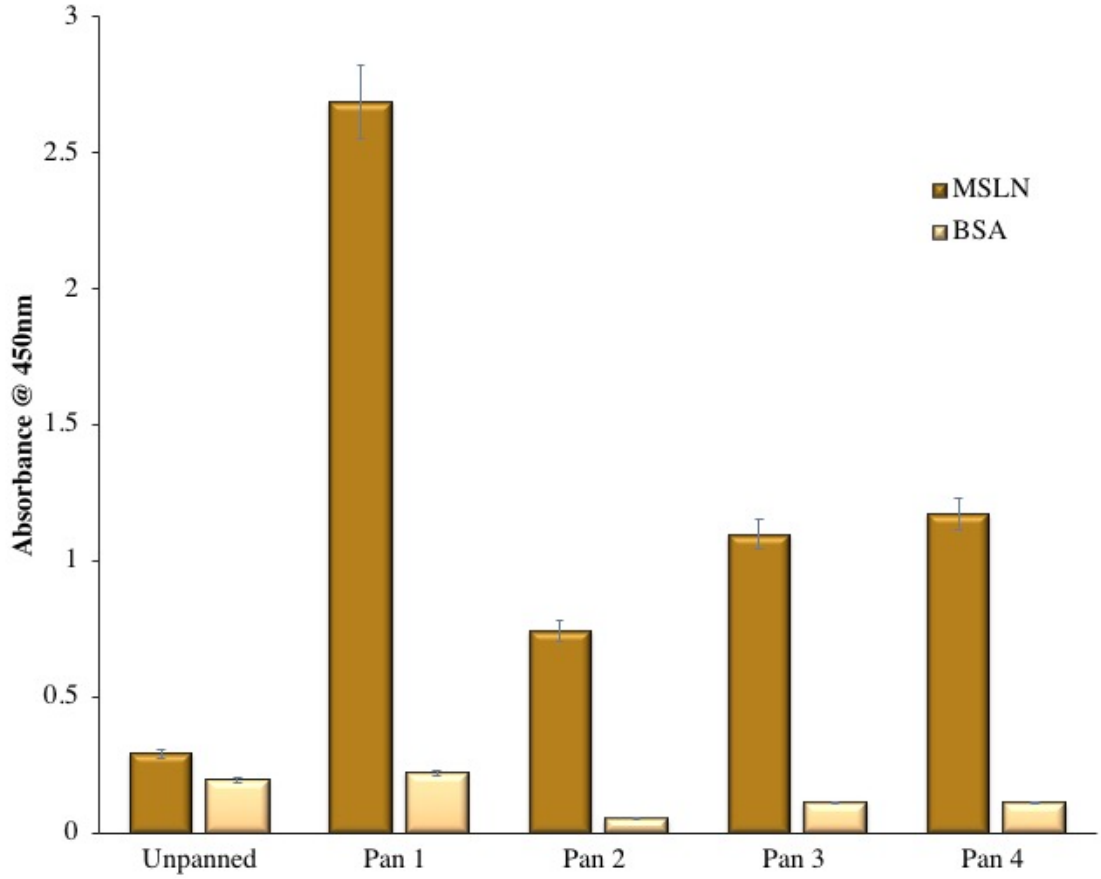

Figure 3.21 Polyclonal phage ELISA

Polyclonal phage ELISA screening for anti-MSLN scFv displayed on phage following completion of panning. Phage pools from each round were tested and a negative control was incorporated. The negative control had no phage added. The scFv-displaying phage were detected using a HRP-labelled anti-M13 secondary antibody and the absorbance was read at 450 nm using a Tecan Safire^{TM} plate reader.

3.2.4.2 Soluble expression and monoclonal analysis of single clones by ELISA

Phage pools from the third and final rounds were infected into a 'non-suppressor' strain of *E. coli,* Top10F', to express soluble antibody fragments, without the pIII protein. While in XL1-Blue *E. coli*, a suppressor transfer RNA (tRNA) binds to the TAG 'amber' codons resulting in the production of a scFv-pIII fusion protein (Barbas *et al.,* 2001). The Top10F' strain does not contain this suppressor tRNA mutation and recognises the stop codon located between the pIII protein gene and the scFv fragment. This allows for the soluble expression of the scFv without the pIII protein. Single clone analysis of 192 single colonies was performed by monoclonal ELISA (***Figure 3.22***).

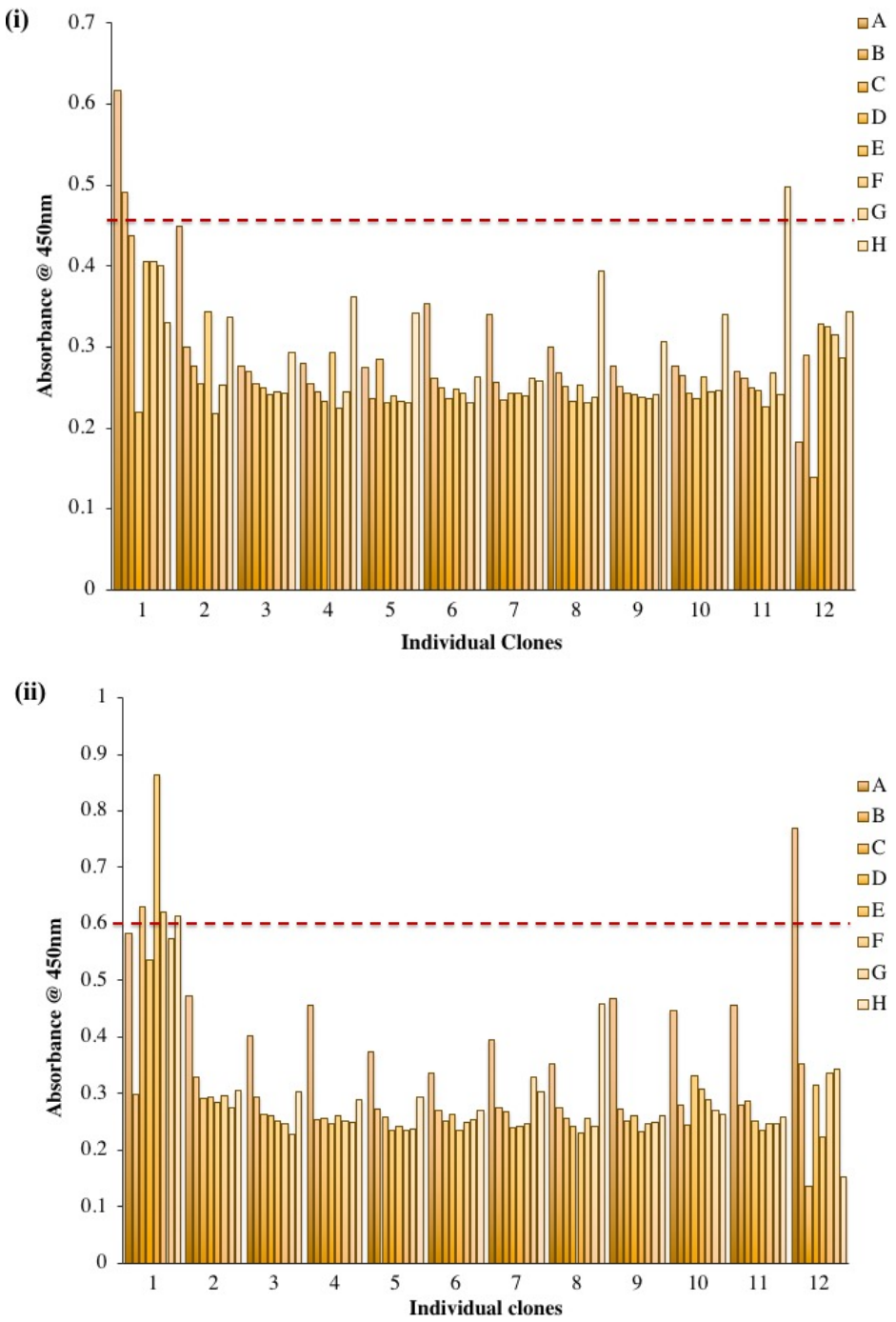

Figure 3.22 Soluble monoclonal ELISA screening for anti-MSLN scFv from 192 randomly selected clones from:

(i) *Round 3;* ***(ii)*** *Round 4. Periplasmic lysates were applied to the MSLN-coated plate and any specific scFv were detected using a HRP-labelled anti-HA antibody. The red dashed line represents the "cut-off" value (twice the background optical density).*

From the 192 clones, 7 were positive for MSLN-binding when analysed in a direct lysate titre ELISA. Unfortunately, none of the clones selected showed the required specificity for MSLN. The false-positives combined with the high background observed could be indicative of poor washing steps. Consequently a further 96 clones were selected from the final biopanning round and analysed in a monoclonal ELISA as before, with the addition of 2 wash steps with PBS and PBS-T (0.05% v/v) (***Figure 3.23***). Out of 96 clones, five were positive for MSLN binding. A decreased background with a higher cut-off value provided more confidence in the specificity of the MSLN-binding clones identified.

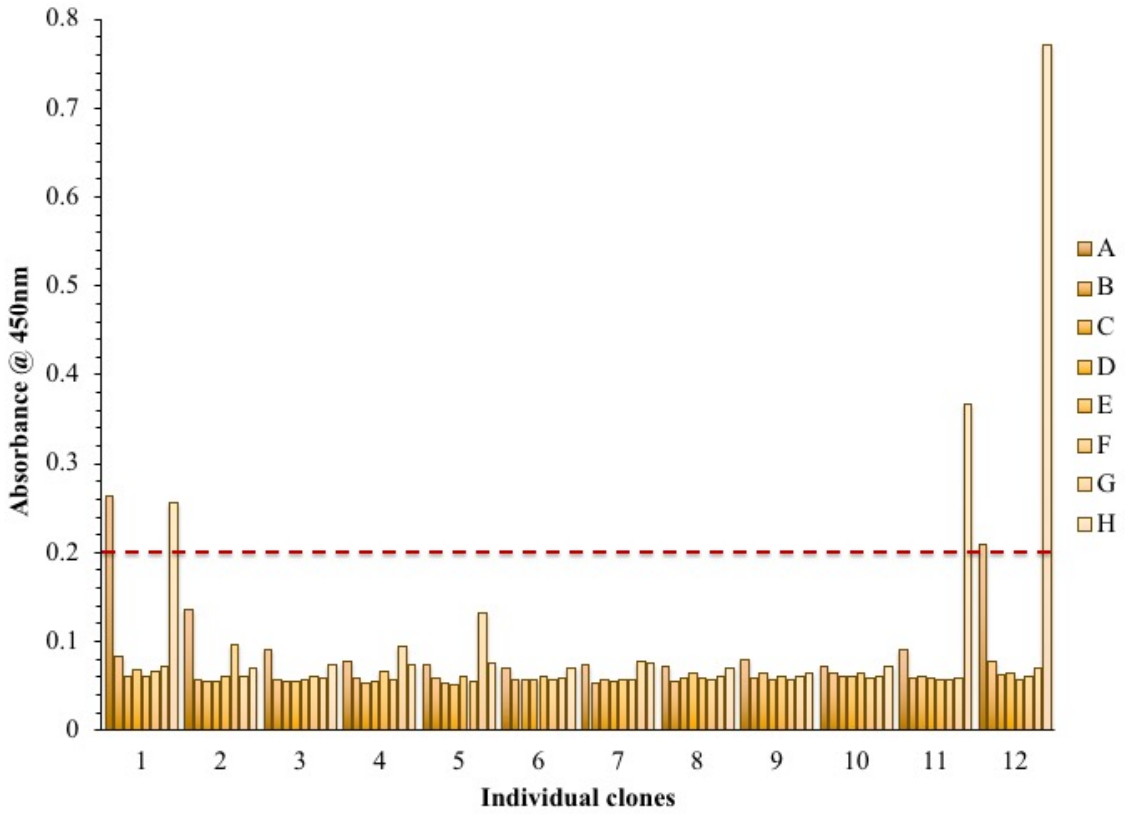

Figure 3.23 Soluble monoclonal ELISA screening for anti-MSLN scFv from 96 randomly selected clones from the final round.

Periplasmic lysates were applied to the MSLN -coated plate and any specifically-bound scFv were detected using a HRP-labelled anti-HA antibody. The red dashed line represents the "cut-off" value (3 times the background optical density).

3.2.4.3 Analysis of five clones by indirect ELISA analysis of lysate

The five clones were taken forward for a lysate titration against MSLN to confirm specificity for the antigen. Doubling dilutions (neat - 1/64) were performed of the scFv-enriched lysate and added to the MSLN-coated ELISA plate (***Figure 3.24***). The results indicated that two clones successfully bound to the MSLN protein and were selected for expression studies and characterization.

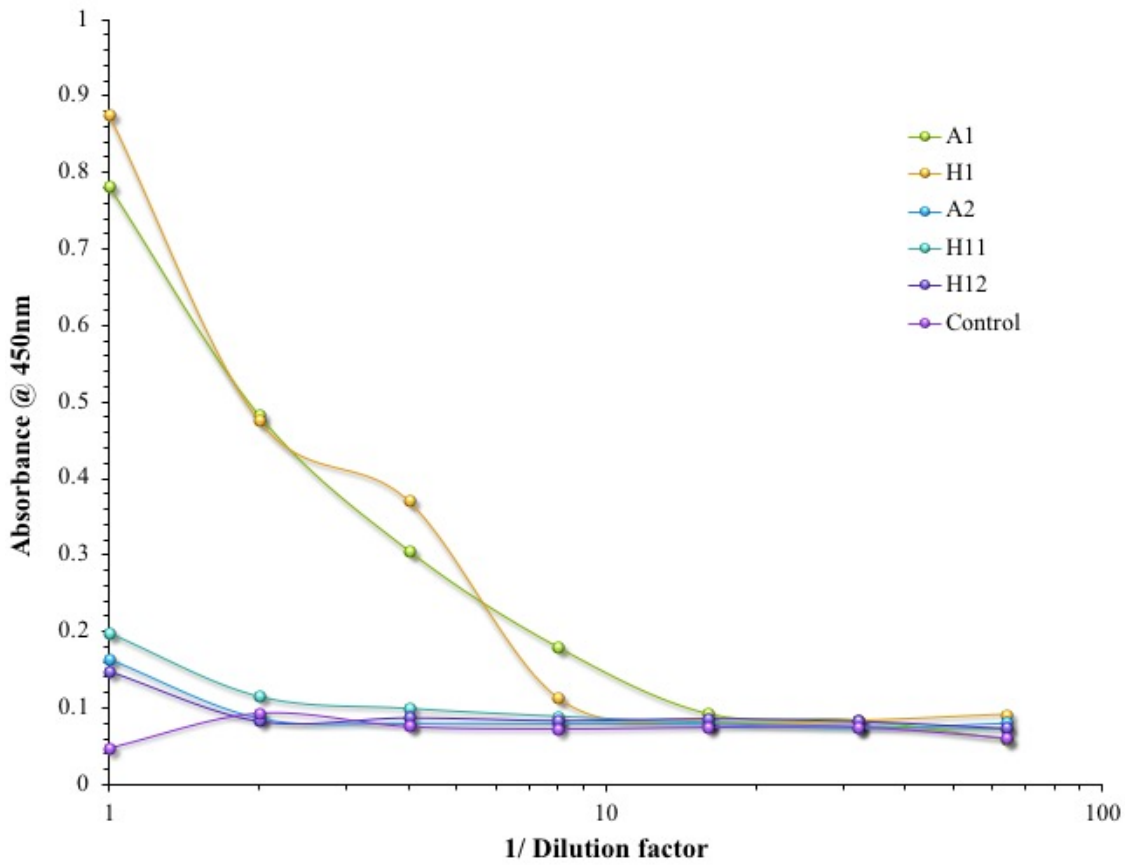

Figure 3.24 Lysate Titration of MSLN-binding scFv by indirect ELISA

The lysate was applied to a MSLN-coated ELISA plate. The bound scFv were detected using a HRP-labelled anti-HIS antibody. Detection was carried out using a HRP-labelled anti-HIS antibody as the purified MSLN recombinant protein is expressed harbouring a HA tag. Control – ELISA was performed without the addition of scFv lysate.

3.2.4.4 Optimisation of scFv expression and purification

Soluble antibody expression conditions were optimised as outlined in *Section 2.10.8.* The scFv levels within the lysates were analysed by indirect ELISA. It can be observed in ***Figure 3.25*** that the optimal expression conditions for clone A1 and H1 are 10 mM IPTG at 37°C and 5 mM IPTG at 25°C, respectively. These conditions were then used to express the scFv clones on a large-scale.

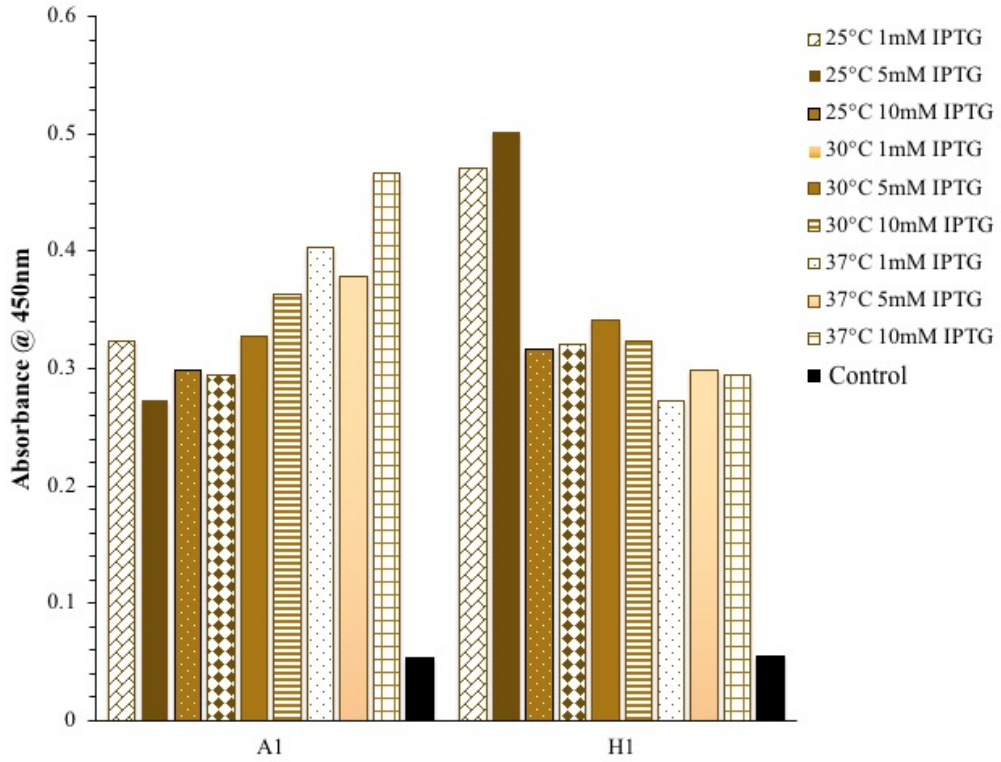

Figure 3.25 Analysis of optimal IPTG concentration and expression temperature for anti-MSLN clones A1 and H2

Expression of the scFv was induced with different IPTG concentrations (1mM – 10mM) and temperatures (25°C, 30°C and 37°C). The lysate was tested in an indirect ELISA format and bound antibody was detected using a HRP-labelled anti-HIS antibody. Control – ELISA was performed without the addition of lysate.

Large-scale expressions of the murine anti-MSLN clones A1 and H1 were performed in 1L cultures. The scFv protein was extracted from the periplasm by sonication (25% amplitude, 2 sec on pulse, 2 sec off pulse for 2 min) and the cell pellet debris collected by centrifugation at 4,000*g* (Eppendorf™ centrifuge fixed angle rotor (F-45-30-11)) for 20 min. Before addition to the nickel resin, the lysate was filtered through a 0.2 µM filter which removes any additional debris that could cause clogging within the resin and result

in poor purification. The filtered lysate was then added to the resin and was incubated on a roller for an hour to promote binding. Two wash steps were performed with increasing imidazole concentration to remove any non-specifically-bound proteins. The bound scFv protein was eluted by the addition of a high concentration of imidazole which competes with the histidine moieties for binding to the nickel resin and displaces the bound histidine-tagged protein from the resin. The eluted fractions were concentrated and analysed by SDS-PAGE and WB (***Figure 3.26***). Concentrated protein was quantified using the Nanodrop™ with resulting yields diluted to 0.5 mg/mL for homogeneity.

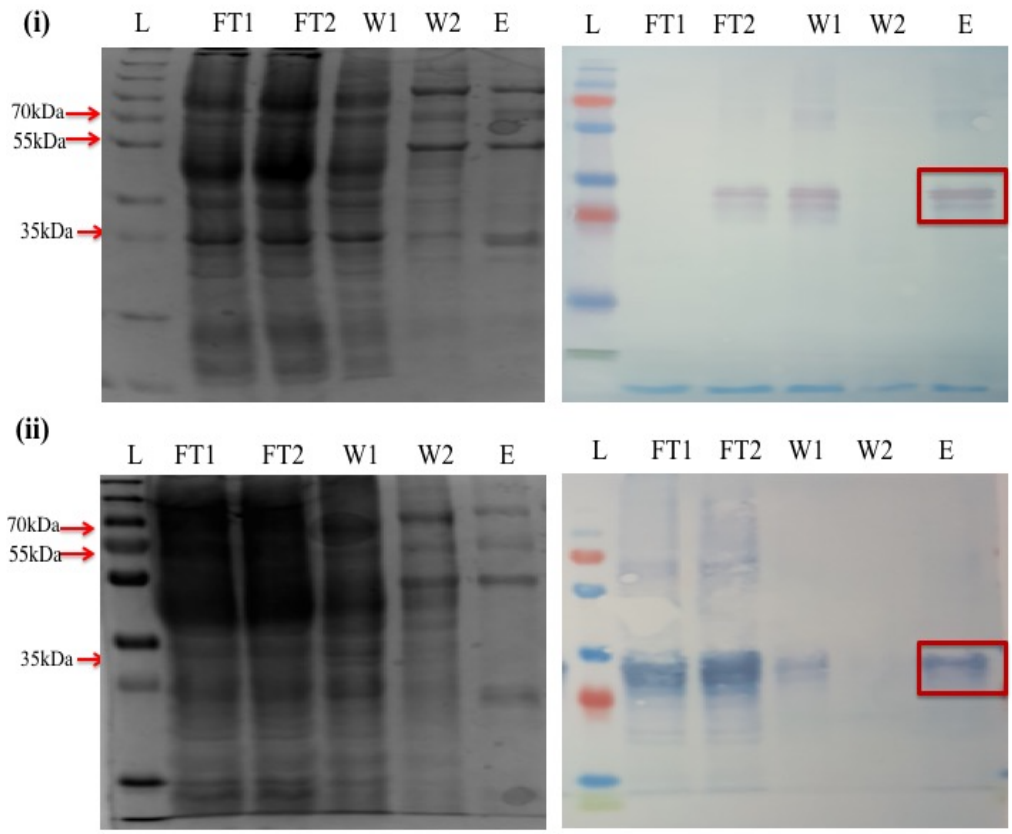

Figure 3.26 SDS PAGE and Western blot analysis of scFv A1 and H1 purification using IMAC

(i) *A1;* ***(ii)*** *H1. SDS-PAGE and WB analysis of the fractions obtained during IMAC purification. The WB was probed with a peroxidase-labelled anti-HA antibody. Both SDS and WB show the primary band at ~25kDa representing the purified scFv. The WB representing the purification of clone A1 shows an additional band just under the 55kDa marker which could be a dimerization of the scFv. L = PageRuler™ Plus Prestained Protein Ladder. FT1 = Flow through 1; FT2 = Flow through 2; W1 = Wash 1; W2 = Wash 2 E = Elution.*

3.2.4.5 Sequence analysis of the MSLN-specific recombinant antibodies

Plasmid preparations of *E. coli* Top10F' containing the pComb3XSS vector bearing the scFv clones A1 and H1 were sent to Source Bio-Sciences for sequencing. The resulting DNA sequences were translated using ExPASy translation tool into their amino acid sequence. The amino acid sequences were aligned using MultAlin software and the CDR regions identified using the Kabat scheme (***Table 3.2***). The CDR sequences between the two clones show significant variation, with limited homologous sequences, providing evidence of diversity between these clones. Both clones were taken forward for further characterization.

Table 3.2 Murine anti-MSLN scFv amino acid sequences.

The sequences were translated into amino acid sequences using ExPasy translate tool and aligned using the MultAlin alignment program.

	CDR-L1	***CDR-L2***	***CDR-L3***
A1	**RSSTGAVTASNYAN**	**TSNRAPG**	**ALWYSTHWV**
HI	**---VLQSDAKGKLD**	**VSGLANG**	**TNNFPSIFV**

	CDR-H1	***CDR-H2***	***CDR-H3***
A1	**GYAMV**	**SSSISGQSGAVRA**	**HQNYGNSLDY**
HI	**YFS-V**	**SSSTAHTRTTERNSV**	**PAYGYDNS-QY**

3.2.4.6 Analysis of anti-MSLN clones, A1 and H1 by indirect and competitive ELISA

Following purification of the two clones, their performance in competitive immunoassay was determined. Initially, the purified clones were titred against MSLN to select a suitable scFv concentration for competitive analysis (***Figure 3.27***). The suitable dilution determined was found to be 1/4 for H1 and 1/8 for A1 clone. This was calculated by taking the lysate dilution that results in an absorbance value closest to 1. To determine which clone had the greatest sensitivity to MSLN and the lowest capability, a competitive ELISA was performed. The diluted purified scFv were incubated with various concentrations of free MSLN antigen, from 0 ng/mL to 1,000 ng/mL and the assay

performed in triplicate. The A1 scFv clone exhibited some specificity for MSLN in solution while the H1 clone curve suggests this clone binds only to immobilised protein (***Figure 3.28***).

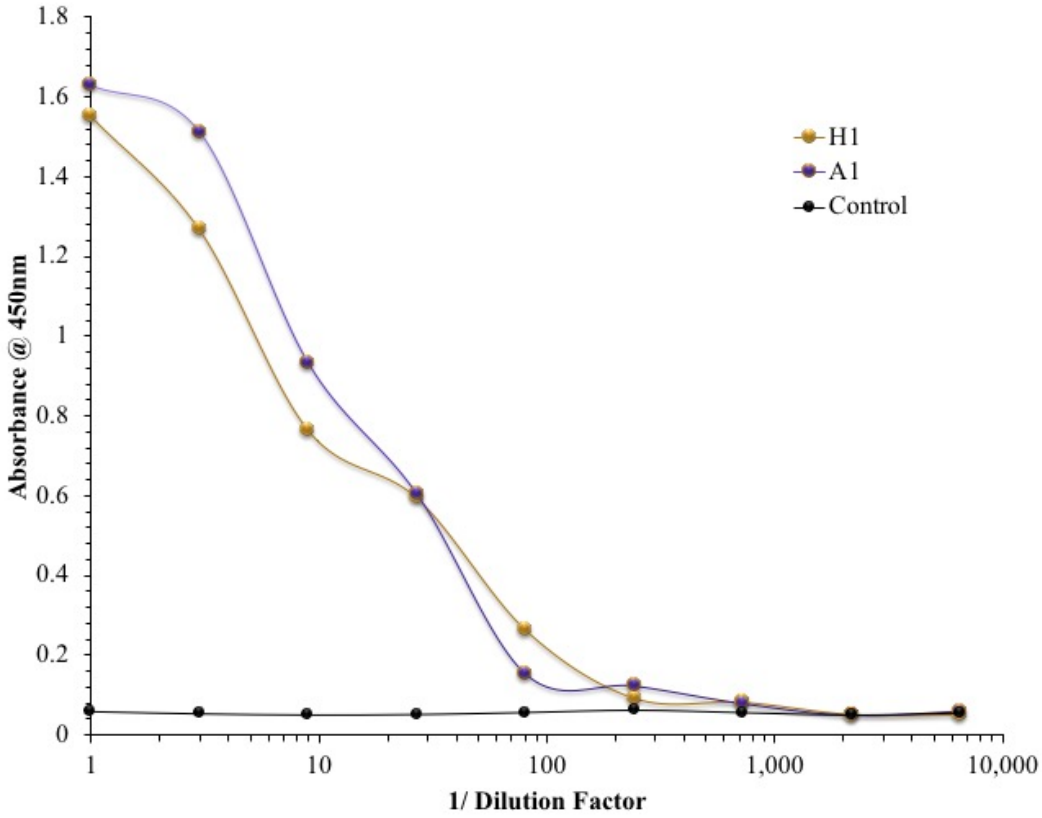

Figure 3.27 Titration of purified MSLN-specific scFv, A1 and H1 against bound MSLN.

The IMAC-purified scFv clones were applied to a MSLN-coated ELISA plate. The bound scFv were detected using a HRP-labelled anti-HIS antibody. Control – ELISA was performed without the addition of purified scFv.

It was intended that the MSLN-binding scFv be incorporated into the multi-marker panel as a tissue and serum marker. However, the poor abilities of the purified scFv to bind to MSLN in solution altered the future application of this scFv as solely tissue-based as work to improve the A1 solution binding abilities would involve extensive and time consuming additional work. As such, further work focused on determining the scFv's applicability in applications as a tissue-based marker.

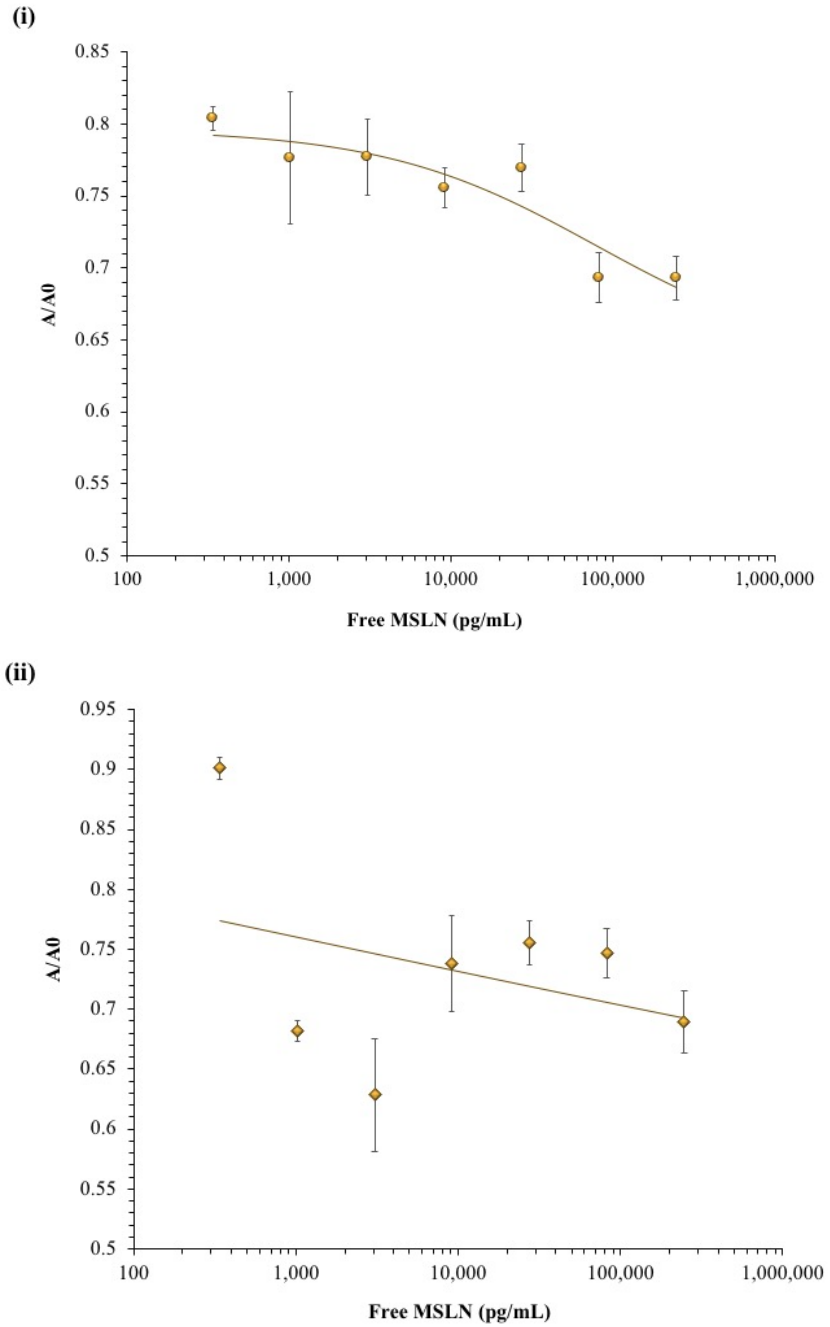

Figure 3.28 Competitive analysis of purified anti-MSLN scFv (i) A1 and (ii) H1

Each clone was incubated with decreasing concentrations of MSLN. One µg of the MSLN protein was coated on the surface of a Nunc MaxiSorp™ ELISA plate. The purified scFv (dilution extrapolated from indirect ELISA graph in ***Figure 3.27****) was incubated with free MSLN and added to the plate where competition occurs between the immobilized and free antigen. Bound antibody was detected using a HRP-labelled anti-HIS antibody. The results are shown as A/A0, where the absorbance values of the evaluated samples (A), are normalised by expressing them as a function of the blank standard(A0)*

3.2.4.7 Analysis of anti-MSLN scFv, A1 and H1 epitope recognition capabilities

It is a desirable quality of a diagnostic antibody to have the ability to recognise its target protein in both linear and conformational epitopes. A linear epitope is a continuous stretch of amino acids sufficient for binding, while a conformational epitope is composed of amino acids that are brought together by the folding of the protein. Conformational epitopes are often preferred for flow cytometry and therapeutic applications while linear are preferred for applications that required denatured samples such as western blots. Both are employed for immunohistochemistry depending on the antigen retrieval method used (Forsström *et al.,* 2015). The MSLN-binding scFv should have the ability bind to both epitope confirmations for future use as a diagnostic antibody. To investigate the MSLN-binding clones recognition abilities for both epitope forms, WB and dot blot analysis were performed. The WB requires the denaturation of the protein, consequently testing the binding of the clones to the epitope in linear form. Conversely, the dot blot protocol does not require denaturation of the protein and therefore tests the ability of the antibodies to detect the conformational epitope.

For WB analysis of both scFv, 2 µg of MSLN was prepared in 4 X loading dye, denatured at 95°C for 5 mins and loaded 10 µL/well. The protein was resolved by electrophoresis and transferred onto a nitrocellulose membrane. The blots were all blocked in 3% BSA (w/v) in PBS for 1 hour. The various dilutions of H1 and A1 anti-MSLN clones were prepared in 1% BSA (w/v) in PBS and incubated with the blots at RT for 1 hour. The dilutions, 1/50, 1/100, 1/200, 1/500 and 1/1,000, were selected as the purified antibody was quantified as 0.5 mg/mL, comparatively, commercially available primary anti-MSLN antibodies are primarily used at a 1/ 2,000 – 1/5,000 dilution at a concentration of 1 mg/mL. The blots were extensively washed to remove any non-specific binding. Bound scFv was detected by a HRP-labelled anti-HIS antibody followed by addition of TMB substrate. A negative control was performed by probing a blot with a 1/5,000 dilution of a previously characterized anti-HER2 scFv and detected as before. A positive control was performed by the addition of a rabbit anti-MSLN antibody for 1 hour and detected by a HRP-labelled anti-rabbit antibody and TMB substrate. The results of this analysis indicated successful binding of both clones down to a 1/500 dilution, however, this is very minimal. Therefore, as shown in ***Figure 3.29*** it can be concluded that both clones detect optimally down to approximately 1/ 500 dilution when the protein is presented in a denatured form.

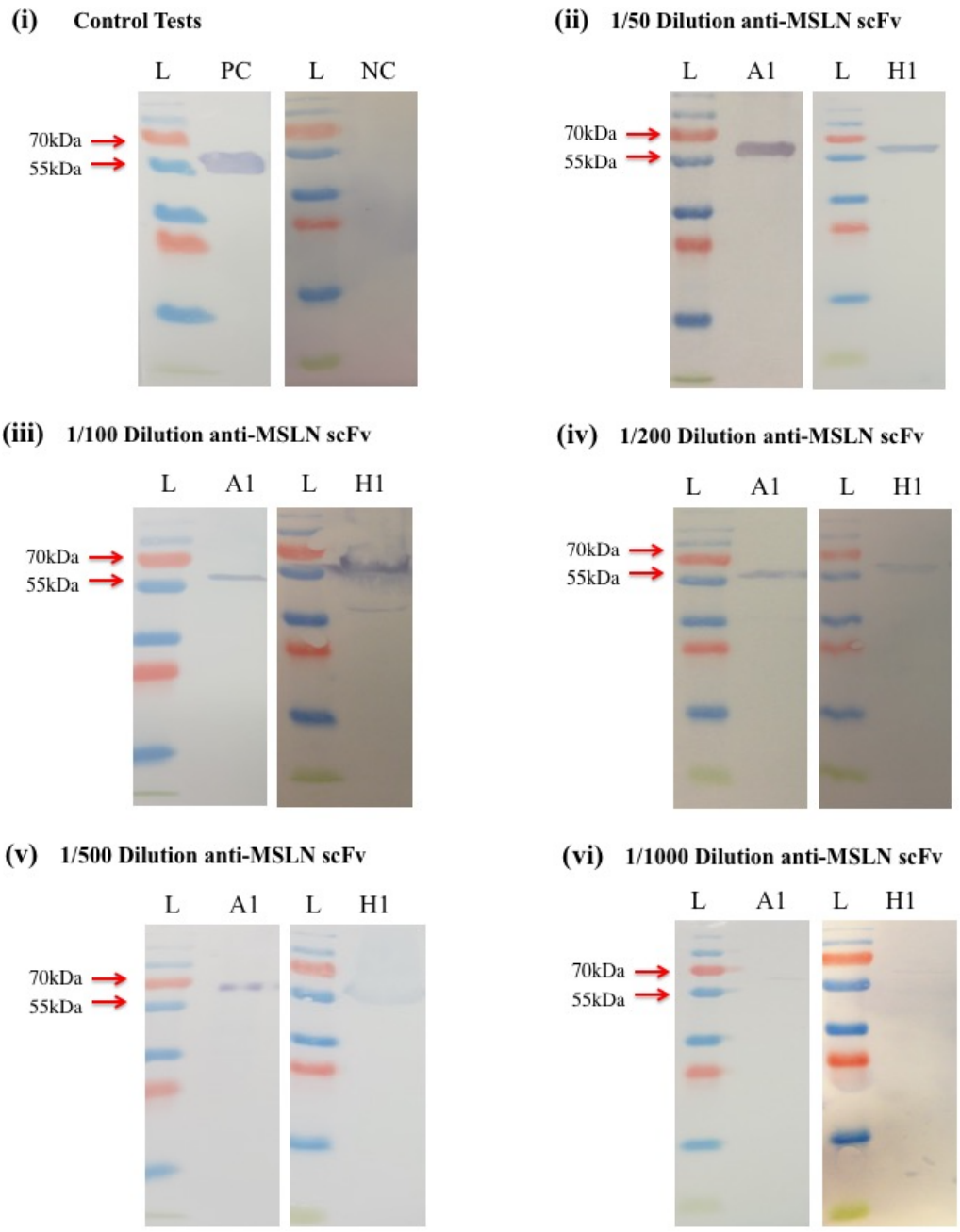

Figure 3.29 Analysis of anti-MSLN scFv H1 and A1 as primary antibodies in WB

(i) *Control tests;* ***(ii)*** *1/50;* ***(iii)****1/100;* ***(iv)****1/200;* ***(v)*** *1/500;* ***(vi)*** *1/1,000 dilution of anti-MSLN scFv.Varying dilutions of the two anti-MSLN scFv clones were used as primary antibodies to probe a western blot. The blot was prepared by transferring resolved MSLN protein from an SDS-PAGE gel. The clones were allowed to probe for 1 hour and bound scFv was detected by the addition of HRP-labelled anti-HIS antibody. A rabbit anti-MSLN antibody with a HRP-labelled anti-rabbit antibody acted as the positive control. The negative control was performed by the addition of an anti-HER2 scFv. L = PageRuler™ Plus Prestained Protein Ladder.*

As described in *Section 2.17.5,* the dot blot is a simplistic derivative of the Western blot but differs as the protein sample is not electrophoretically separated or denatured but is spotted in dots directly onto the nitrocellulose membrane. Dot blot analysis was performed here to determine the scFv ability to detect the conformational epitope of MSLN. Here 2 µg/mL of MSLN was dotted directly onto nitrocellulose paper and allowed to dry. The blots were blocked as before. Various dilutions of the scFv were prepared in 1% BSA (w/v) in PBS and were incubated with the blots for 1 hour at RT. Bound scFv were detected as before. Identical controls as used for the WB analysis were performed. This analysis showed that the 1/5,000 dilutions of the clones had the ability to detect the protein in its native form. However the optimum dilution for visual detection for both clones is a 1/200 dilution **(*Figure 2.30*)**. Combined, this analysis suggests both anti-MSLN clones possess the ability to detect linear and conformational epitopes.

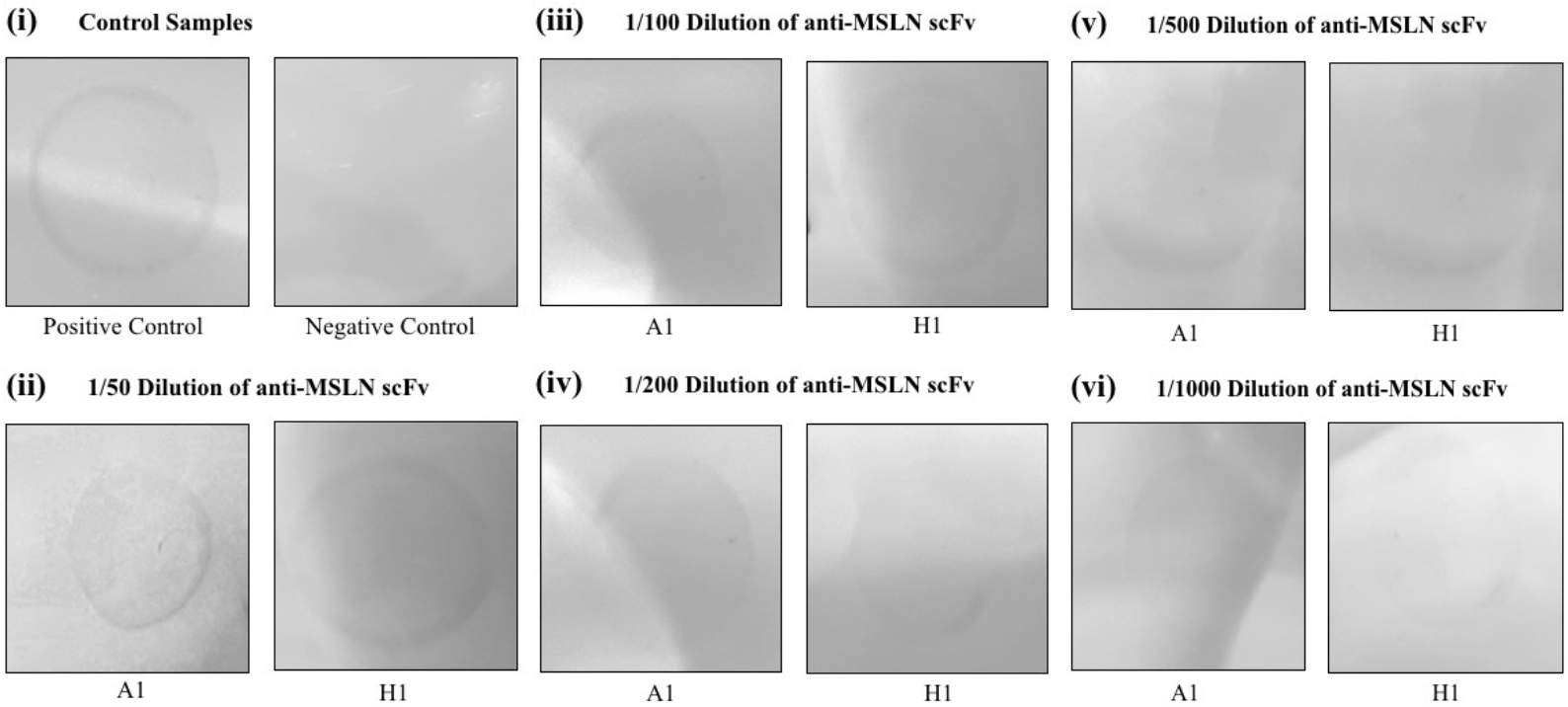

Figure 3.30 Dot blot analysis of anti-MSLN scFv H1 and A1

(i) *Control samples;* ***(ii)*** *1/50;* ***(iii)****1/100;* ***(iv)*** *1/200;* ***(v)*** *1/500;* ***(vi)*** *1/1,000 dilution of anti-MSLN scFv . Two µg/mL of MSLN was added to a nitrocellulose membrane and allowed to dry. The blot was blocked with 3% BSA (w/v) in PBS for 1 hour at RT. Varying dilutions of the anti-MSLN antibodies were prepared in 1% BSA (w/v) in PBS. Bound scFv was detected by the addition of a HRP-labelled anti-HIS antibody. A rabbit anti-MSLN antibody with a HRP-labelled anti-rabbit antibody acted as the positive control. The negative control was performed by the addition of an anti-HER2 scFv.*

3.3 Discussion and Conclusion

As previously described in-depth, current methods of PDAC diagnosis involves a plethora of scans in conjunction with the marker CA19-9, first described in 1979 and remains the only FDA-approved biomarker for PDAC diagnosis. However, the average stage of diagnosis for pancreatic cancer is stage 4 where distant metastasises have occurred and overall survival is bleak (Krška *et al.,* 2015). Much work has taken place researching methods to improve diagnosis with many researchers and clinicians recently turning to antibodies and novel PDAC markers to achieve this. In 1988, a study was performed to test the levels of five serum tumour-associated antigens and their diagnostic abilities in combination and alone on patients presenting with pancreatic disease. This work found that the panel, when used in such a combination, may be able to identify patients harbouring pancreatic cancer (Benini *et al*., 1988). Then in 1994, Kawa *et al*. compared the PDAC diagnostic abilities of CA19-9 to CA242 and found the latter was superior to CA19-9. Later, Ghazale and colleagues (2007) investigated elevated serum IgG4 levels as a means to distinguish autoimmune pancreatitis and pancreatic cancer. More recently, an anti-MUC1 antibody was successfully employed to detect PDAC in mice at early stages of PanIN lesions (Wu *et al*., 2018). Antibodies are widely used for diagnostic applications. However, the work to use antibodies for PDAC diagnosis primarily focuses on employing monoclonal antibodies for detecting changes in marker levels. Recombinant antibodies overcome issues associated with monoclonal and polyclonal antibodies as diagnostic agents (O'Kennedy *et al*., 2017). The scFv antibody, comprised of the variable heavy and light chains, is a particularly useful recombinant antibody format for a diagnostic entity as it lacks the Fc region reducing potential assay interference resulting from Fc-mediated interactions (Hearty and O'Kennedy, 2011). For optimum diagnostic performance antibodies are tested on specificity and affinity which can be optimised when isolated from combinatorial antibodies libraries (Lerner, 2016).

This chapter describes the work undertaken to generate an anti-MSLN scFv designed for incorporation into an hypothesized multi-marker diagnostic panel. The MSLN marker can provide invaluable information on pancreatic cancer progression and sensitivity to chemotherapy (Li *et al.,* 2008). Two anti-MSLN scFv were successfully isolated from a pancreatic-cancer biased murine scFv library. The isolated scFv were characterized and their abilities to detect MSLN in serum and in tissue investigated. Both scFv clones were

subjected to indirect and competitive ELISA analysis. The A1 anti-MSLN scFv showed limited specificity for the MSLN protein in solution. However, the anti-MSLN scFv H1 exhibited the ability to only bind to the MSLN when immobilised and not in solution. This is possibly attributed to the favourable orientation of bound protein. When bound to an ELISA plate or presented in a blot format the antigen is presented at a high local concentration of available epitopes. This availability allows more opportunity for scFv-antigen binding to occur. As specificity is dependent on a plethora of factors such as immunoassay format and not only the binding properties of the antibody-antigen complex, further work including cross reactivity studies could reveal potential off-target binding of the H1 clone (Tate and Ward, 2004). This issue altered the future applications of these scFv. Initially, it had been proposed that the MSLN scFv could be applicable for serum and tissue detection. The scFv inability to detect free MSLN renders them unsuitable as serum marker detectors. Consequently, further characterization was dictated by specific requirements of the scFv to detect MSLN in tissue. Consequently, it was decided to determine the capabilities of the scFv to bind to both linear and conformational epitopes on MSLN. This was investigated using WB and dot blots. Various dilutions of the two purified clones were added to the blots to detect the MSLN protein. The results obtained indicated that the purified scFv were capable of detecting the target protein in its denatured and native form at a ~1/200 - 1/500 dilutions.

The current literature shows that MSLN antibodies are often generated for therapeutic applications such as drug delivery but infrequently as diagnostic agents (Ho *et al.,* 2011). However, monoclonal primary antibodies against MSLN are available for detection such as 5BS and 2131 both employed for detection of MSLN in immunohistochemistry (Inaguma *et al.,* 2017). For direct comparison, anti-MSLN antibodies currently on the market were investigated to determine if the scFv generated herein were superior for MSLN detection. Currently, widely used primary monoclonal anti-MSLN antibodies employed for western blot analysis include, MN-1 with a working concentration of 1:1,000 at a concentration of 1 mg/mL, EPR2685(2) used at a dilution of 1:1,000-10,000 when at a concentration of 0.6 mg/mL and EPR19025-42 (0.5 mg/mL) also used at a concentration of 1:1,000. In comparison, the working concentrations of both scFv clones for western blot analysis were found to be 1:500 of 0.5 mg/mL. While similar to that suggested for the anti-MSLN antibody EPR19025-42 it is significantly different from other available antibodies requiring a higher dilution and concentration to achieve similar

results. Therefore the scFv within this work are not preferential or beneficial over current anti-MSLN primary antibodies.

However, further work could improve these scFv, in particular the A1 scFv clone which showed specificity to MSLN in solution. Often upon isolation of scFv, it is often still may be necessary to improve or alter antibody functionality, affinity, and specificity to optimise for its role. Due to time constraints, improvements were not attempted in this research. In the future, techniques such as affinity maturation, error prone PCR, which introduces random nucleotide errors throughout a gene by use of a low fidelity Taq polymerase, and site-directed mutagenesis where specific mutations of one or more of the amino acids are created, could be applied to the anti-MSLN clone A1 (McCullum *et al.,* 2010; Lin *et al.,* 2011). Additionally, chain shuffling, a method which involves the re-cloning of the gene for one of the variable domains into a repertoire of genes for the other chain could be beneficial as it has been shown to improve antibody sensitivity (Fitzgerald *et al.,* 2011). This results in a new library constructed of one domain parent gene and one random domain gene. The approach mimics somatic hypermutation rendering it more efficient in producing functional antibodies. Other methods to enhance sensitivity or specificity of an antibody include, CDR walking mutagenesis and alanine scanning (Hu *et al.,* 2015). The anti-MSLN A1 scFv could benefit from altering the functionality to improve specificity to MSLN thus rendering it more applicable for detection of MSLN in serum and tissue.

In conclusion, this chapter describes the generation of a communal murine immune library against the pancreatic cancer cell line Capan-1 cell line for the isolation of all scFv on the proposed multi-marker panel. From this library, two antibody fragments were obtained that successfully bind to the expressed recombinant MSLN protein. Upon characterisation of these scFv it was discovered that the anti-MSLN scFv H1 does not bind to the MSLN antigen in solution despite binding bound protein. Conversely, the anti-MSLN scFv A1 showed some minor binding capabilities for free and bound protein indicating potential to be applied in the future to the diagnosis of pancreatic cancer by detection of MSLN in serum and tissue.

Chapter 4

The isolation and characterisation of anti-AGR2 and anti-MUC1 antibody fragments from a synthetic human library

Chapter outline

The work described in this chapter outlines the generation of specific scFv to , Mucin 1 (MUC1) and Anterior Gradient 2 (AGR2), that make up the diagnostic panel described in *Chapter 3*. Initially, the murine anti-Capan-1 scFv library was employed for the isolation of scFv specific to MUC1 and AGR2. However, when screened, it was determined that no specific antibodies were present in this library. To avoid immunisation of additional animals and to adhere to the 'three Rs' sustainability hierarchy, the naïve synthetic human Tomlinson I and J libraries were used to screen for specific scFv. Selection of anti-AGR2 and anti-MUC1 scFv was successful, and the antibody fragments were extensively characterized. An overview of the approach is shown in (***Figure 4.1***). In order to mimic the scFv performance characteristics *in situ*, these antibodies were analysed for determination of any matrix effect in normal human serum.

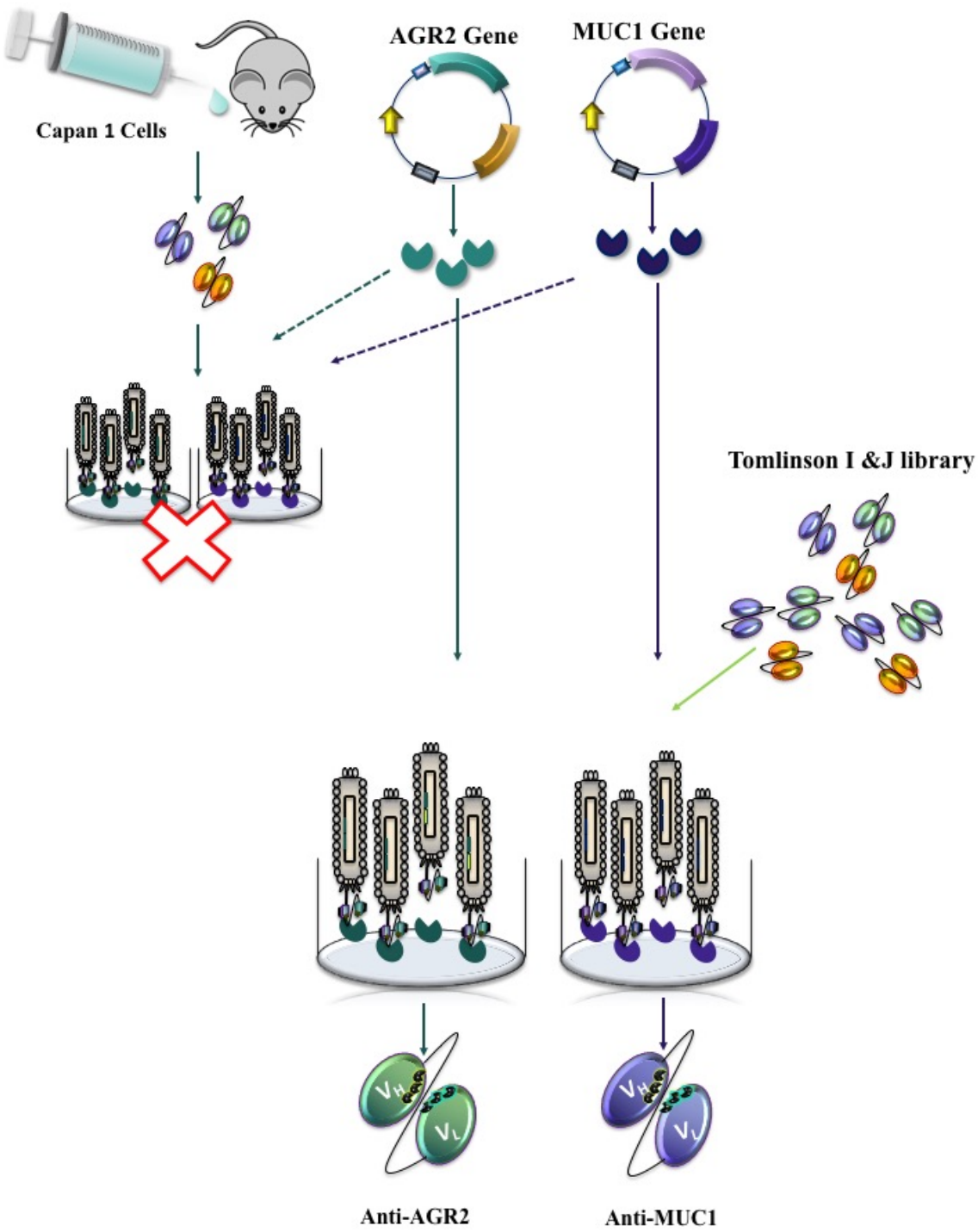

Figure 4.1 Illustration of workflow for Chapter 4

This diagram illustrates the work carried out within this chapter. Using the expressed and purified AGR2 and MUC1 proteins, attempts to isolate specific scFv from the communal anti-Capan-1 library were unsuccessful. Consequently, the naïve human synthetic Tomlinson I and J libraries were employed for biopanning from which specific scFv against AGR2 and MUC1 were obtained and characterised.

4.1 Introduction

There are four types of antibody libraries, immune, naïve, semisynthetic and synthetic. Immune libraries are created in an animal host that is immunised with a target protein to elicit a 'biased' immune response. They are widely used in research and within the pharmaceutical industry for isolation of protein-specific antibodies (Dantas-Barbosa *et al.,* 2012). A naïve human library is constructed from unimmunized human rearranged, synthetic or shuffled V genes. Semi-synthetic libraries are composed of an antibody framework with a genetically randomized CDR, whereas synthetic libraries are composed of a specific framework with diversity accomplished by the insertion of random codons at specific sites within the CDRs (Weber *et al.,* 2014; Nilvebrant and Sidhu, 2018). Synthetic libraries are often labelled "naïve" as they are unbiased and antigen independent. These libraries are constructed artificially by *in vitro* assembly making higher levels of diversity achievable. The disadvantage of these libraries is the lack of immune-repertoire bias when selecting for a target-specific antibody. In order to successfully select antibodies with optimum specificity and affinity, library size and diversity are crucial variables. Larger library size and diversity (extensive paratopes to a multitude of epitopes) greatly improves the chances of finding specific antibodies (Puri *et al.,* 2013; Schwimmer *et al.,* 2013). Synthetic libraries offer improved diversity with repertoires of up to 10^{14} clones reported (Schwimmer *et al.,* 2013; Burkovitz and Ofran, 2016). The variability outside of the CDR region is very limited, whereas, variability within the CDR is achieved by combining random nucleotides. The disadvantage with this approach is the introduction of a small number of unnatural sequences, but advantageously results in increased stability, solubility and expression levels due to the fewer framework variations (Bai *et al.,* 2015). Often synthetic antibodies rely predominantly or wholly on CDRH3 for antigen binding and recognition which reduces the complexity of the interaction with the cognate antigen (Burkovitz and Ofran, 2016).

The naïve, synthetic human libraries, Tomlinson I and J (distributed by the MRC HGMP Resource Centre) were utilised within this chapter for the selection of anti-AGR2 and anti-MUC1 scFv. This was performed, as attempts to isolate specific-antibody fragments from a biased-murine library were unsuccessful. The Tomlinson I and J libraries are human single-fold scFv synthetic libraries with library sizes of 1.47 x 10^8 with a 96% insert and 1.37 x10^8 with 88% insert, respectively (Eteshola, 2011). The libraries are

constructed using one framework for V_H and V_L domains with diversity found in the antigen binding sites. The framework structure employed is the most common in the human antibody repertoire, V_H (V3-23/DP-47 and JH4b) and Vκ (O12/O2/DPK9 and Jκ1) (Kaku *et al.,* 2012). Both libraries are constructed in the pIT2 phagemid vector. Diversified side chains are found in the following 18 residues, H50, H52, H52a, H53, H55, H56, H58, H95, H96, H97, H98, L50, L53, L91, L92, L93, L94 and L96 (***Figure 4.2***). These libraries have been designed to include a short CDR3 region that retains the ability to form an antigen binding site. It was postulated that the shorter CDR3 could provide space to allow further interaction of the CDR1 and CDR2 with the antigen which can increase affinity (Rosner *et al.,* 2001). The libraries have been pre-screened for binding with Protein A and L resulting in the identification of a high percentage of functional specific clones (Ossysek *et al.,* 2015).

For the purposes of isolation, characterisation and immunoassay development for the Tomlinson library-derived scFv, the target proteins were required. MUC1- and AGR2-containing plasmids were sourced for expression of the recombinant proteins in *E. coli* expression systems. The pPB-MUC1-N-His plasmid was purchased from NBS Biologicals Ltd. and transformed into BL21 (DE3) *E. coli* cells for protein expression (***Figure 4.3***). The HIS-tag allowed the recombinant MUC1 protein to be purified via IMAC and a further polishing purification step using SEC was carried out. This recombinant MUC1 protein was used for isolation and characterization of an anti-MUC1 scFv.

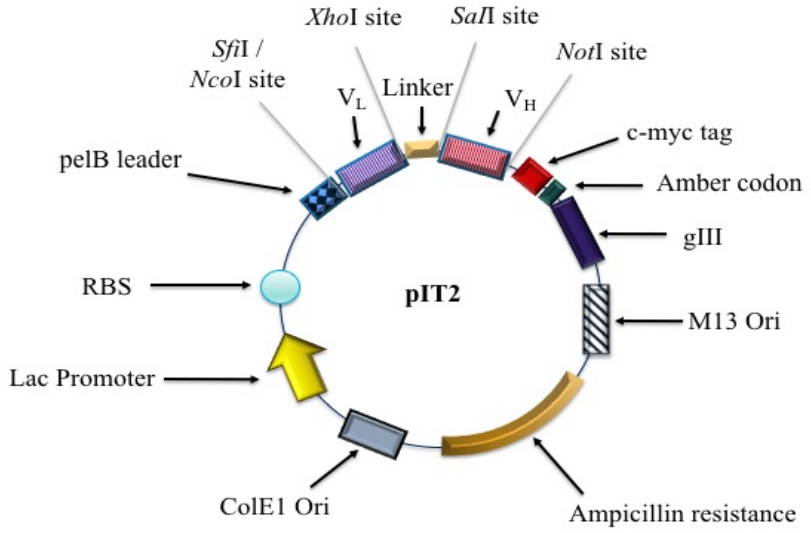

Figure 4.2 Map of the pIT2 phagemid vector

Map of pIT2 phagemid vector containing a scFv insert. The vector includes, a ribosome binding site (RBS), pelB leader peptide sequence, V_H and V_L genes, a $(Gly_4Ser)_3$ linker, ampicillin resistance gene, c-myc tag and an amber stop codon to allow for soluble expression of the scFv gene without the PIII fusion protein. Full map of pIT2 vector can be found in Appendix C.

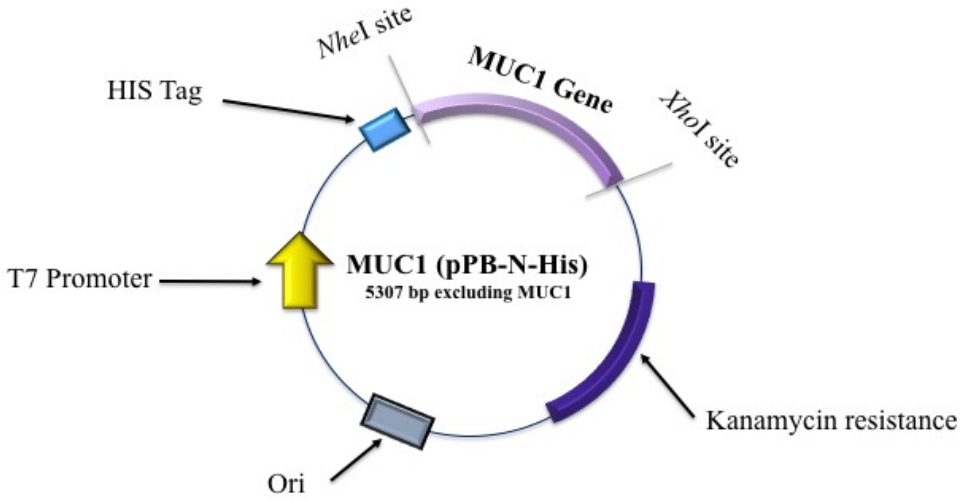

Figure 4.3 Map of MUC1 Protein Vector (Human) (pPB-N-His)

This map of the vector pPB-MUC1-N-His illustrates the recombinant MUC1 protein gene with the N-terminal polyhistidine-tag for identification and protein purification, and the kanamycin antibiotic resistance gene. Full map of pPB-N-His vector can be found in Appendix C.

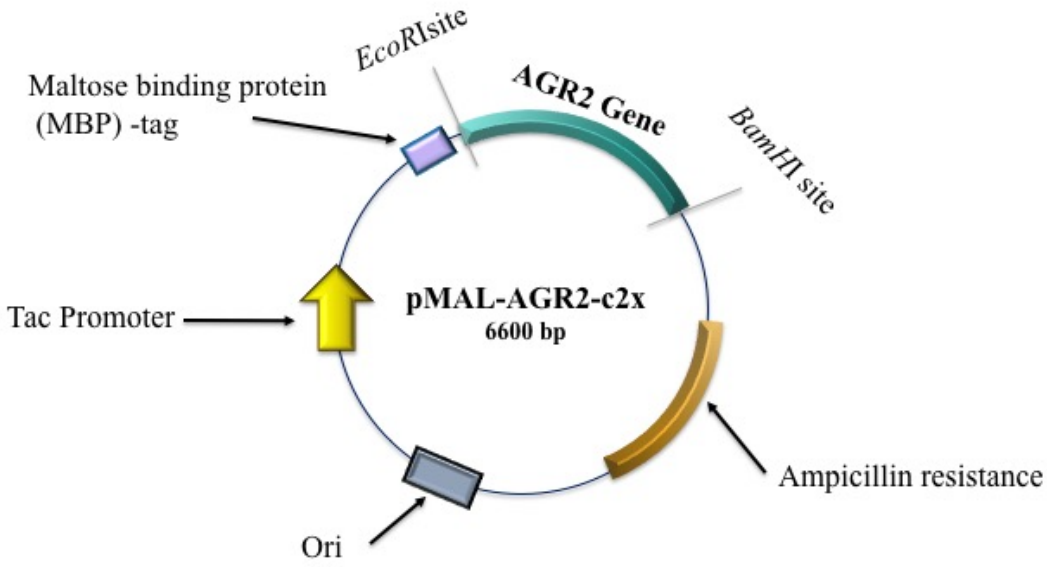

Figure 4.4 Map of pMAL-AGR2-c2x vector

This map illustrates the basic components of the pMAL-AGR2-c2x vector including the recombinant AGR2 gene, MBP fusion partner and the ampicillin antibiotic resistance gene. Full map of pMAL-c2x vector can be found in Appendix C.

To express the recombinant AGR2 protein, the plasmid pMAL-AGR2 was purchased from Addgene (***Figure 4.4***). Within the pMAL vector, the AGR2 gene is inserted downstream of the *malE* gene of *E. coli* which encodes for the Maltose Binding Protein (MBP). Therefore, the AGR2 protein was expressed as a fusion with MBP. This fusion partnership aids in the solubility of AGR2 and allows for one-step purification of the fusion protein by exploiting MBP's affinity for amylose. However, to use the recombinant AGR2 as a target for antibody selection, it is necessary that MBP be cleaved from the AGR2 prior to use (Krisna *et al.,* 2015). This is performed using the protease Factor Xa. The pMAL vector contains a sequence coding for the recognition site of the Factor Xa protease allowing the MBP to be cleaved from the protein of interest after purification (Nagai & Thøgersen, 1984) (***Figure 4.5***). Once cleaved, the AGR2 protein was isolated by SEC and the purified protein was employed in panning for identification of AGR2-binding antibody fragments.

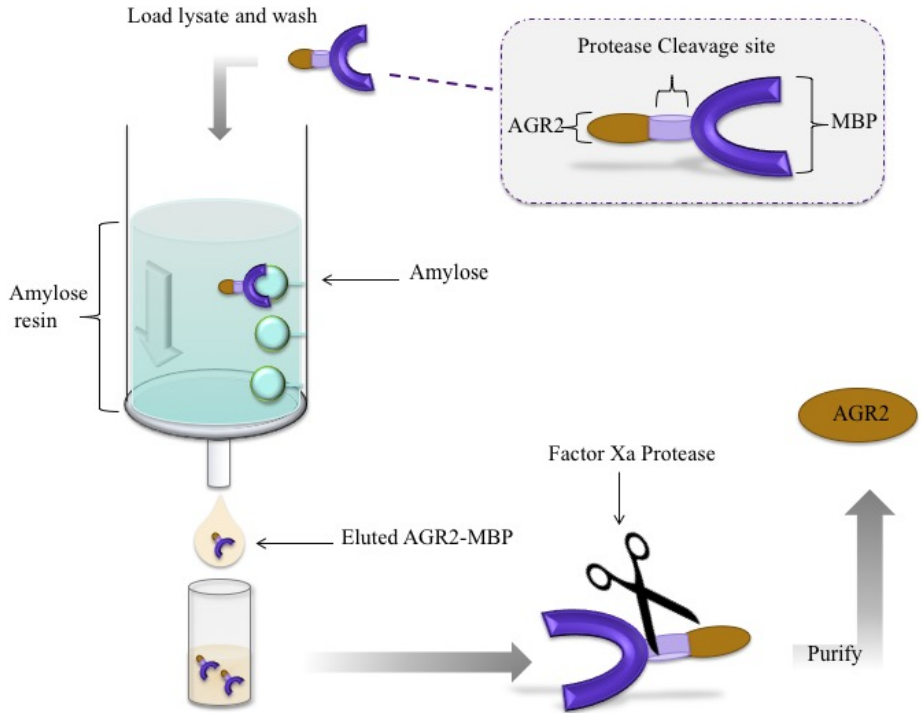

Figure 4.5 Diagrammatic representation of affinity chromatographic purification of the fusion protein AGR2-MBP by amylose resin and cleavage by Factor Xa

Lysate containing the AGR2-MBP fusion protein was applied to the amylose resin which bound to the MBP on the fusion protein. By the addition of 10 mM maltose, the fusion MBP-AGR2 protein was competitively eluted from the column. Using Factor Xa, the MBP expression partner was removed from the desired AGR2 protein and a further purification step using SEC was applied to isolate the recombinant AGR2 protein.

As previously discussed in *Chapter 3,* each marker selected for incorporation into the diagnostic scFv panel provides invaluable information regarding tumour characteristics and further therapeutic routes. MUC1 overexpression is evident during the earlier developmental stages of PDAC (Herreros-Villanueva *et al.,* 2013). It is thought to play a role in maintaining the lumina of ductal epithelial cells, while in cancer its role is thought to aid in the vascular spread of carcinoma cells (Levi *et al.,* 2004). MUC1 consists of a N-terminal extracellular domain and a C-terminal intracellular domain. The MUC1 C-terminal acts as an adaptor protein, which influences signal transduction pathways, resulting in deregulation of apoptosis and cell proliferation (Nath *et al.,* 2013). Knock-down of MUC1 expression decreases growth and metastatic potential of pancreatic cancer cells providing evidence that mucins are essential in PDAC progression (Rachagani *et al.,* 2012). MUC1 is considered a very valuable marker for the diagnosis of PDAC. It is

overexpressed in 90% of pancreatic cancers and its expression is indicative of reduced survival (Balmaña *et al.,* 2018; Doiron and DeFronzo, 2018). A study carried out by Park and colleagues (2015) tested the hypothesis that a MUC1 antibody conjugated to a fluorophore could be used to visualize pancreatic cancer. This theory was shown to be successful and could potentially improve PDAC diagnosis. Another study analysed the detection capabilities of an anti-MUC1 antibody conjugated to a fluorophore in PDAC mouse models. The results showed that the antibody targets early PanIN lesions prior to development of adenocarcinoma (Wu *et al.,* 2018). The results of this study highlight the promising potential of MUC1 as an early PDAC diagnostic marker.

AGR2, a 19kDa protein, is a member of the disulphide isomerase family of endoplasmic reticulum-resident proteins (Brychtova *et al.,* 2011). It encodes for a thioredoxin located in the endoplasmic reticulum and is thought to be involved in the folding and assembly of proteins (Wodziak *et al,* 2016). It is a pro-oncogenic, metastasis-associated protein, known to contribute to cell survival and tumour cell growth. It is up-regulated in various cancers, including pancreatic cancer. While unclear, it is thought to have conserved roles in cancer development and tissue regeneration, proliferation and migration (Xue *et al.,* 2018). AGR2 also confers a level of chemo-resistance (Liu *et al.,* 2018). A study previously performed, induced AGR2 expression in all sporadic and familial PanIN PDAC, CTCs and metastases. Analytical methods such as flow cytometry and immunofluorescent staining indicated that AGR2 localised to the endoplasmic reticulum and the outside of the tumour cells. It was noted that AGR2 induction resulted in the regulation of endoplasmic reticulum chaperones and lysosomal proteases. AGR2 expression levels were proportional to the level of PDAC invasiveness and high expression levels indicate poor overall survival (Dumartin *et al.,* 2011). AGR2 is a potentially exploitable biomarker as it is highly expressed in the earliest developmental stages of precancerous pancreatic lesions PanIN lesions (Dumartin *et al.,* 2017; Ferrerira *et al.,* 2017). This characteristic renders AGR2 useful as a diagnostic marker, with the potential ability to identify early stages of lesions prior to metastatic development. Additionally, in later stages, the degree of AGR2 expression is proportional to the invasiveness of pancreatic cancer cells (Tian *et al.,* 2017). Due to the diagnostic and prognostic abilities of the markers, AGR2 and MUC1, they were selected for incorporation into the multi-marker diagnostic panel.

4.2 Results

4.2.1 Generation of a recombinant MUC1 protein

4.2.1.1 Optimisation of expression of MUC1 protein using auto-induction media

The pPB-N-His vector, containing the recombinant human MUC1 gene, was purchased from NBS Biologicals Ltd. The vector was transformed into BL21 (DE3) cells using a basic heat-shock protocol outlined in *Section 2.13.1.* The transformation was plated onto LB agar plates containing 60 μg/mL kanamycin. Random single colonies were selected for optimisation of recombinant MUC1 expression. A 10 mL culture, containing a single colony, was grown overnight and sub-cultured into auto-induction media the following day.

Auto-induction media takes advantage of the bacteria's use of carbon and energy sources. Glucose present in the growth media prevents the uptake of lactose, which is also present in the media. Once the glucose is depleted, lactose is taken up in small amounts and converted to the natural lac inducer allolactose, resulting in the induction of expression of the recombinant protein (Fox and Blommel, 2009). Small-scale expression studies such as optimisation of temperature (30°C and 37°C) and auto-induction broth base optimisation (TB and LB) were carried out. These optimisations yielded dense protein bands on an SDS-PAGE at the expected MUC1 size of 29.4kDa, under the conditions of 37°C with both LB and TB auto-induction media (***Figure 4.6***). Further expression studies were not required and the recombinant MUC1 protein was expressed large-scale (1L) using TB-based auto-induction media at a temperature of 37°C.

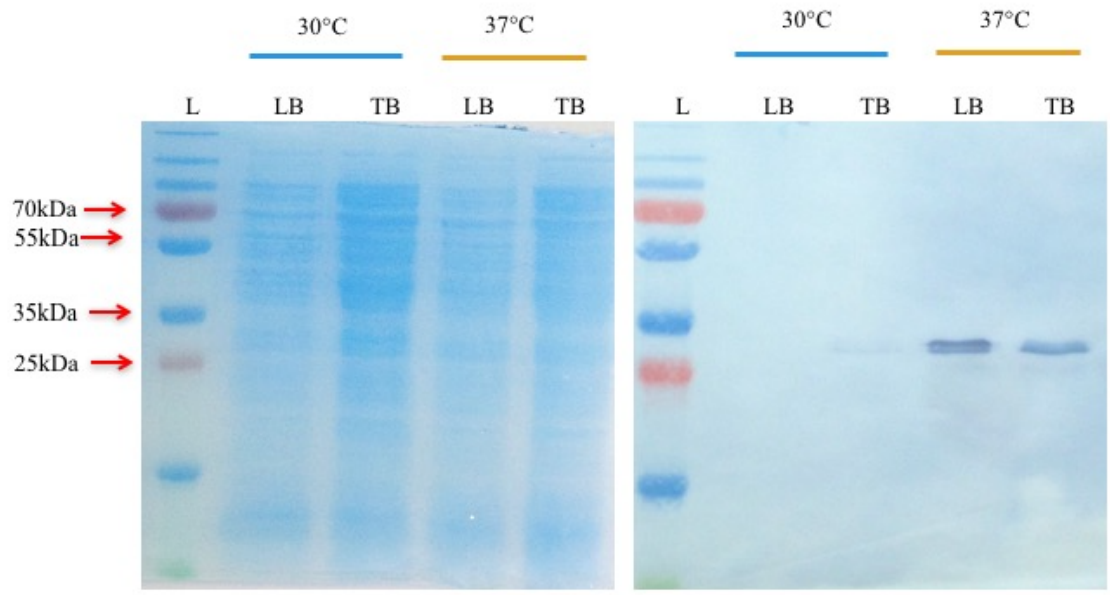

Figure 4.6 Optimisation of MUC1 expression using auto-induction media with various broth bases at temperatures 30°C and 37°C

The western-blot was probed with a HRP-labelled anti-His antibody. L = PageRuler™ Plus Prestained Protein Ladder; LB = Luria Broth; TB= Terrific Broth.

4.2.1.2 Purification of the expressed recombinant MUC1 protein

A 10 mL culture was grown overnight and subsequently used to inoculate 5 x 200 mL TB-auto-induction media cultures. These cultures were grown O/N in a shaker incubator at 37°C. The 1L culture was spun down at 4,000*g* (Eppendorf™ centrifuge fixed angle rotor (F-45-30-11)) for 20 min. The pellet was resuspended in lysis buffer (50mM NaH_2PO_4, 300mM NaCl, 10mM imidazole, pH 8) and sonicated as per *Section 2.13.1.7.1.* The sample was then re-centrifuged at 11,000*g* (Eppendorf™ centrifuge fixed angle rotor (F-45-30-11)) for 30 min the supernatant was collected and filtered through a 0.2µm filter. The IMAC column was equilibrated (50 mM NaH_2PO_4, 100 mM NaCl, pH 8) and kept at 4°C for the duration of the purification to reduce protease activity. The lysate was applied to the column and allowed to flow through twice followed by two wash steps of increasing imidazole concentration (1 X PBS, 150 mM NaCl, 20 mM/30 mM imidazole, pH 8) to remove any non-specific proteins bound to the column. The recombinant MUC1 protein was then eluted from the column in 4 x 2mL fractions upon the addition of elution buffer (1 X PBS, 150 mM NaCl, 300 mM imidazole, pH 8).

The purification was analysed by SDS-PAGE and WB. It can be seen in ***Figure 4.7,*** that the purification of the recombinant MUC1 protein was successful with dense bands present at the expected size of MUC1 (29.4kDa) in the filtered lysate, both 'flow-through' samples and in the initial wash step. The second wash step shows the removal of contaminant bands without any loss of the MUC1 protein. A double band or duplet band can be seen in the eluted fractions of the MUC1 protein. Minor protein degradation during the purification process, more specifically at elution, is the most likely cause (Fu *et al.,* 2010). Additionally, there is a band present on the WB double the expected size of MUC1, possibly a dimer of the protein (Platonova *et al.,* 2014).

The eluted fractions 2-4 were pooled, concentrated and buffer exchanged against 1 X PBS using a 10kDa molecular weight cut-off Vivaspin 6 column. The concentration of eluted MUC1 protein was determined using the NanoDrop^{TM} 1000 and the yield obtained was 0.93mg/mL. As the eluted fractions contained a significant amount of contaminant bands, a further polishing purification step was required. This was carried out on the ÄKTA Pure system by size exclusion chromatography (SEC). This is a necessity, as the presence of significant contaminant bands present pose the risk of isolating non-specific scFv antibodies during phage display and biopanning. The protein was eluted from the column by peak fractionation, meaning only fractions containing protein were collected and analysed. The peak that contained the eluted MUC1 protein was analysed on SDS and WB and showed significant reduction in the presence of any contaminant bands.

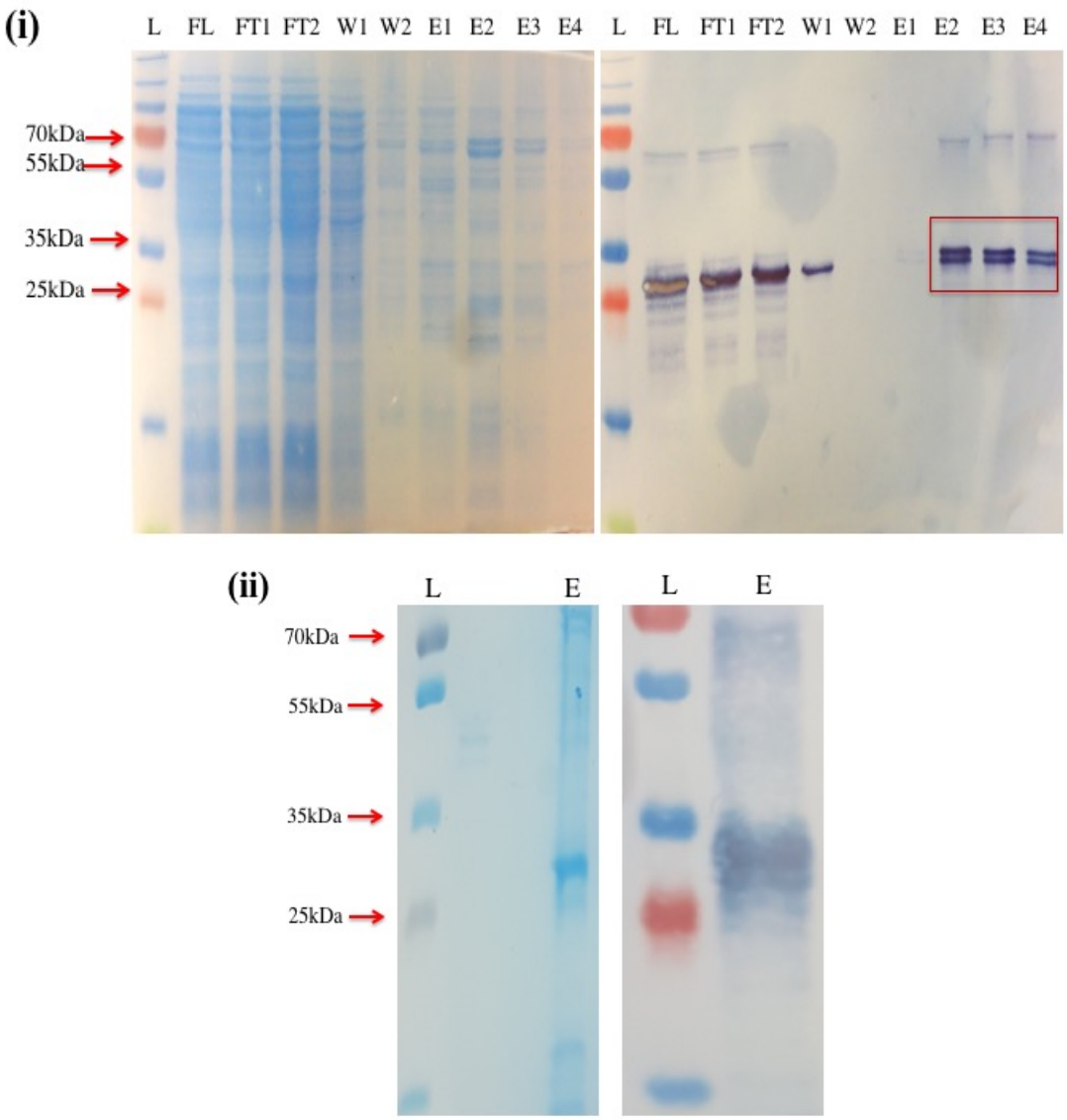

Figure 4.7 Purification of a MUC1 recombinant protein

(i) *Analysis of MUC1 purification using IMAC on SDS-PAGE gel and Western blot. Blot was probed with an anti-MUC1 antibody followed by a HRP-labelled anti-mouse IgG antibody. L = PageRuler™ Plus Prestained Protein Ladder; FL = Filtered Lysate; FT1 = Flow-through 1; FT2 = Flow-through 2; W1 = Wash 1; W2 = Wash 2; E1 = Elution 1; E2 = Elution 2; E3 = Elution 3; E4 = Elution 4* ***(ii)*** *Analysis of SEC purified MUC1 on the ÄKTA pure system. Blot was probed with an anti-MUC1 antibody followed by a HRP-labelled anti-mouse IgG antibody. L = PageRuler™ Plus Prestained Protein Ladder; E= Elution from SEC column.*

4.2.2 Screening of a Capan-1 murine immune library against MUC1

4.2.2.1 Antibody library screening against a recombinant MUC1 protein

The anti-Capan-1 immune library was initially screened for identification of MUC1-binding antibody fragments. This was performed as per *Section 2.16* and the conditions undertaken are laid out in ***Table 4.1.***

Table 4.1 *Panning conditions employed for each round of selection of the murine anti-Capan-1 scFv library against the MUC1 protein.*

Panning round	MUC1 coating conc.	Number of washes
1	50 µg/ mL	3 X PBS, 3 X PBS-T (0.05% (v/v))
2	25 µg/ mL	5 X PBS, 5 X PBS-T (0.05% (v/v))
3	12.5 µg/ mL	10 X PBS, 10 X PBS-T (0.05% (v/v))
4	5 µg/ mL	15 X PBS, 15 X PBS-T (0.05% (v/v))

The precipitated input phage from each round of panning (1-4) was incorporated into a polyclonal phage ELISA to test for enrichment against the MUC1 protein. Successful enrichment was demonstrated by an increase in absorbance signal after incubating phage with the MUC1 protein and detecting bound phage with a HRP-labelled anti-M13 secondary antibody (GE Healthcare) (***Figure 4.8***). There is a notable reduction in absorbance after round 2, which may indicate that the panning conditions became too stringent, hindering the enrichment of all the clones in the library and resulting in loss of diversity. Despite the reduction in signal, colonies were brought forward from rounds 2 and 3 for further analysis.

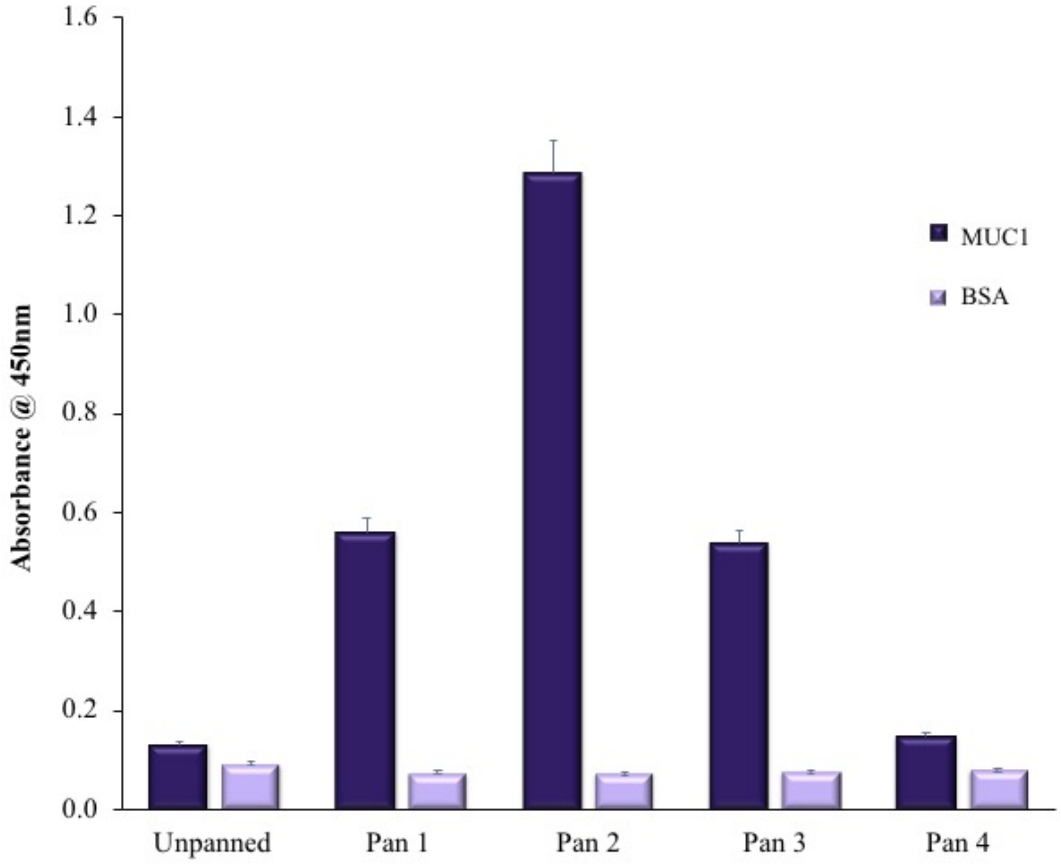

Figure 4.8 Polyclonal phage ELISA screening for anti-MUC1 scFv displayed on enriched phage pools

Phage pools from each round were diluted 1/3 in 1% (w/v) BSA in PBS-T and 100 µL per well was applied on a MUC1-coated ELISA plate. The scFv-displaying phage were detected using a HRP-labelled anti-M13 secondary antibody and, following the addition of TMB, the absorbance was read at 450nm using a Tecan Safire™ plate reader.

4.2.2.2 Soluble expression and monoclonal analysis of single clones by ELISA

Soluble expression of the antibody fragments was achieved by transforming phage from rounds 2 and 3 into the non-suppressor strain of *E. coli* Top10F'. While in XL1-Blue *E. coli*, a suppressor transfer RNA (tRNA) binds to the TAG 'amber' codons resulting in the production of a scFv-pIII fusion protein (Barbas *et al.,* 2001). The Top10F' strain does not contain this suppressor tRNA mutation and recognises the stop codon located between the pIII protein gene and the scFv fragment. This allows for the soluble expression of the scFv without the pIII protein. Single colonies (192) from rounds 2 and 3 were analysed for MUC1-specific binding by monoclonal ELISA (*Section 2.16.7*) (***Figure 4.9***).

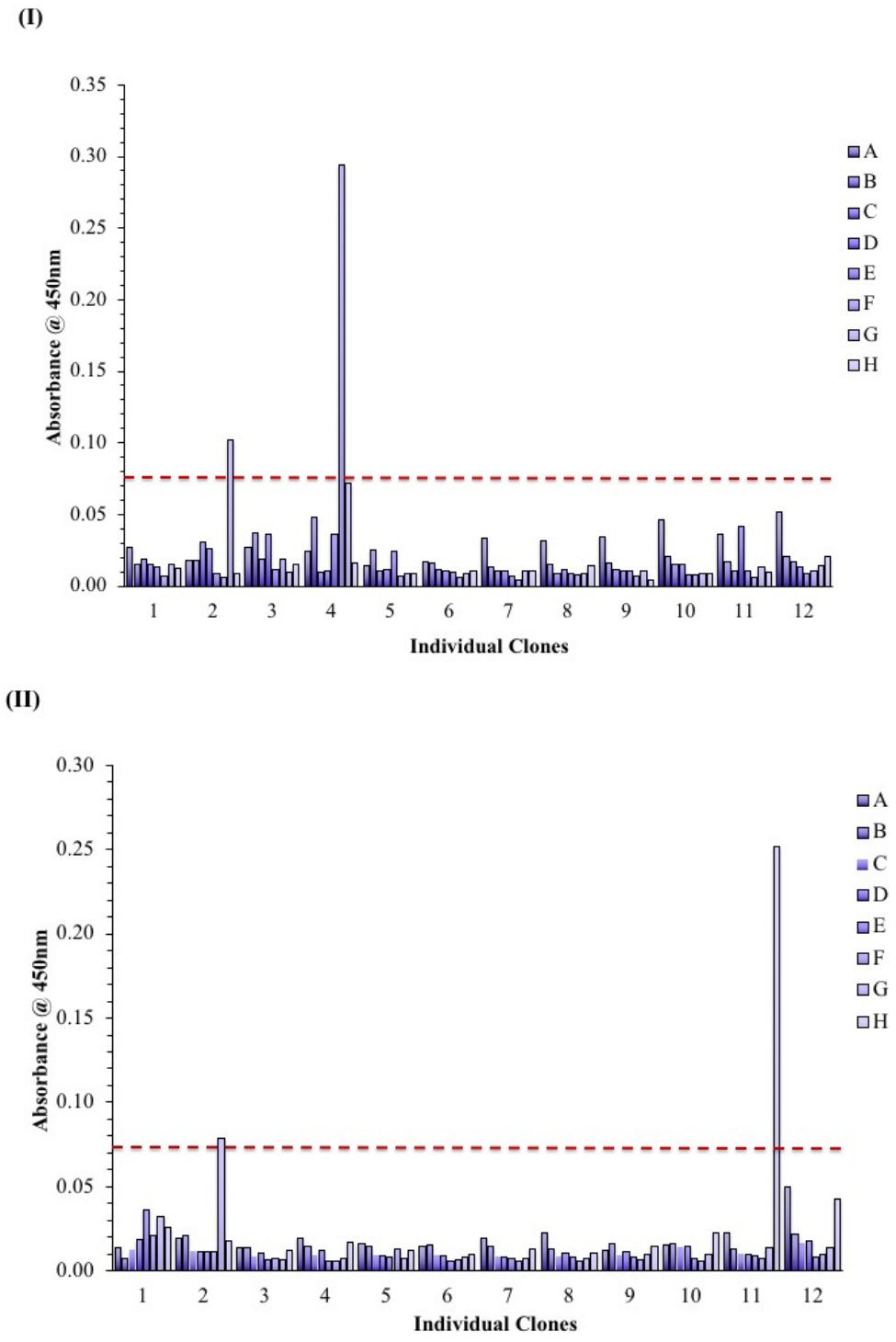

Figure 4.9 Soluble monoclonal ELISA screening for anti-MUC1 scFv from 192 randomly selected clones from (i) *Round 2;* ***(ii)*** *Round 3. Periplasmic lysates of the clones were applied to the MUC1-coated plates and any specific scFv were detected using a HRP-labelled anti-HA antibody. The red dashed line represents the "cut-off" value (x 3 the background optical density).*

Three positive clones, with optical density readings above the set 'cut-off' point, were selected. These were analysed by indirect ELISA, but showed no specificity for the MUC1 protein. Due to the combined low absorbance observed in the monoclonal ELISA and the lack of specificity of the positive clones for the MUC1 protein, it was concluded that the library did not contain MUC1-specific antibody fragments. This could be attributed to issues encountered during the construction of the immune scFv library (data shown in *Chapter 3*). Numerous optimisations steps were required for generating the overlap product through PCR. As it was not highly efficient it is possible sequence frameshifts occurred resulting in a library of poor quality (Koohapitagtam *et al.,* 2010). Furthermore, the immune library was created and analysed using a cell line meaning the immune bias towards MUC1 may not have been sufficient for selection of highly specific anti-MUC1 scFv. An alternative route to obtain scFv that bind to MUC1 was taken by employing the synthetic human Tomlinson libraries, addressed later within this chapter.

4.2.3 Generation of a recombinant AGR2 protein

4.2.3.1 Optimisation of expression of AGR2-MBP from the pMAL-AGR2 plasmid

The pMAL-AGR2 plasmid was supplied as a bacterial stab in BL21 (DE3) cells (See *Section 2.9*). The plasmid-containing bacteria were streaked onto LB agar plates supplemented with 100 μg/mL carbenicillin. An overnight culture, containing a single colony from the streak plates was grown and sub-cultured the following day for expression studies of the AGR2-MBP fusion protein. The expression of recombinant proteins using *E. coli* is widely used, with many protocols using IPTG as an induction method. This involves numerous optimization steps including IPTG concentration and optimum expression time post-induction. Auto-induction media removes the need to monitor or optimize induction times and concentrations. Initially, small-scale expression using auto-induction media was carried out using LB and TB bases at three different temperatures 25°C, 30°C and 37°C.

One mL was removed from each culture, lysed by the addition of 1 mg/mL lysozyme and subjected to 3 free-thaw cycles. The samples were centrifuged at 12,000*g* (Eppendorf™ centrifuge fixed angle rotor (F-45-30-11)) for 15 min and the supernatant removed, mixed with 4 X loading dye and boiled to denature the protein. The samples were then analysed by SDS-PAGE and WB. The WB was probed with an anti-MBP-HRP-labelled

antibody. The predicted sizes of MBP and AGR2 are 42.5kDa and 19kDa, respectively, with a combined weight of 61.5kDa. In the SDS, bands were observed at ~61 kDa. The largest protein bands were observed when using TB-based auto-induction media at 37°C, indicating that the optimum expression of the AGR2-MBP protein was achieved under these conditions. Additionally, a second lower band was observed at ~42kDa, consistent with the size of MBP (***Figure 4.10***). AGR2-MBP was expressed large-scale (1L culture) and purified by affinity chromatography.

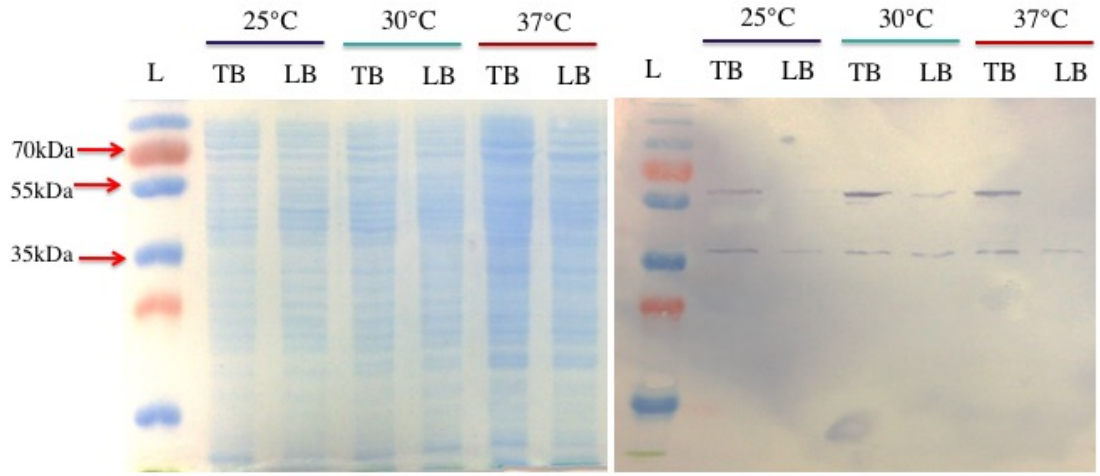

Figure 4.10 Optimisation of AGR2-MBP expression from the pMal-AGR2 plasmid using auto-induction media with various broth bases at a variety of temperatures.
(i) *SDS-PAGE gel analysis;* ***(ii)*** *Western blot probed with an anti-MBP-HRP-labelled antibody. L = PageRuler™ Plus Prestained Protein Ladder; TB = Terrific Broth; LB = Luria Broth.*

4.2.3.2 Purification of the AGR2-MBP fusion protein using amylose resin

MBP, as a fusion protein, not only acts a solubility enhancer but as a tag that allows purification using amylose resin. This resin exploits the affinity of MBP for α-(1–4) maltodextrin (Duong-Ly and Gabelli, 2015). The 1L culture was centrifuged at 4,000*g* (Eppendorf™ centrifuge fixed angle rotor (F-45-30-11)) for 20 min and the supernatant discarded. The pellet was then resuspended in ice-cold column buffer (20 mM Tri-HCl, 200 mM NaCl, 1 mM EDTA) and sonicated (25% amplitude, 2 sec on pulse, 2 sec off pulse for 2 min). The lysed sample was centrifuged (11,000*g* (Eppendorf™ centrifuge fixed angle rotor (F-45-30-11)) for 30 min) and the supernatant was collected, filtered through a 0.2 µM filter and diluted 1:6 with ice-cold column buffer. The lysate was passed

through the column twice, followed by two wash steps to remove any non-specifically bound proteins. The AGR2-MBP fusion protein was then eluted in four fractions by the addition of 10 mM maltose in column buffer.

The purification was analysed on SDS-PAGE and WB. The WB was probed using a HRP-labelled anti-MBP antibody. It can be observed in ***Figure 4.11***, that the purification of AGR2-MBP was successful. The eluted fractions show bands at the expected size of 61.5kDa with very minor impurities present. The eluted protein was then buffer exchanged into 1 X PBS and concentrated to 1 mL volume, in a 30kDa MW cut-off Vivaspin column. The concentrated protein yield of 7.46 mg/mL was determined using the NanoDrop ™ 1000.

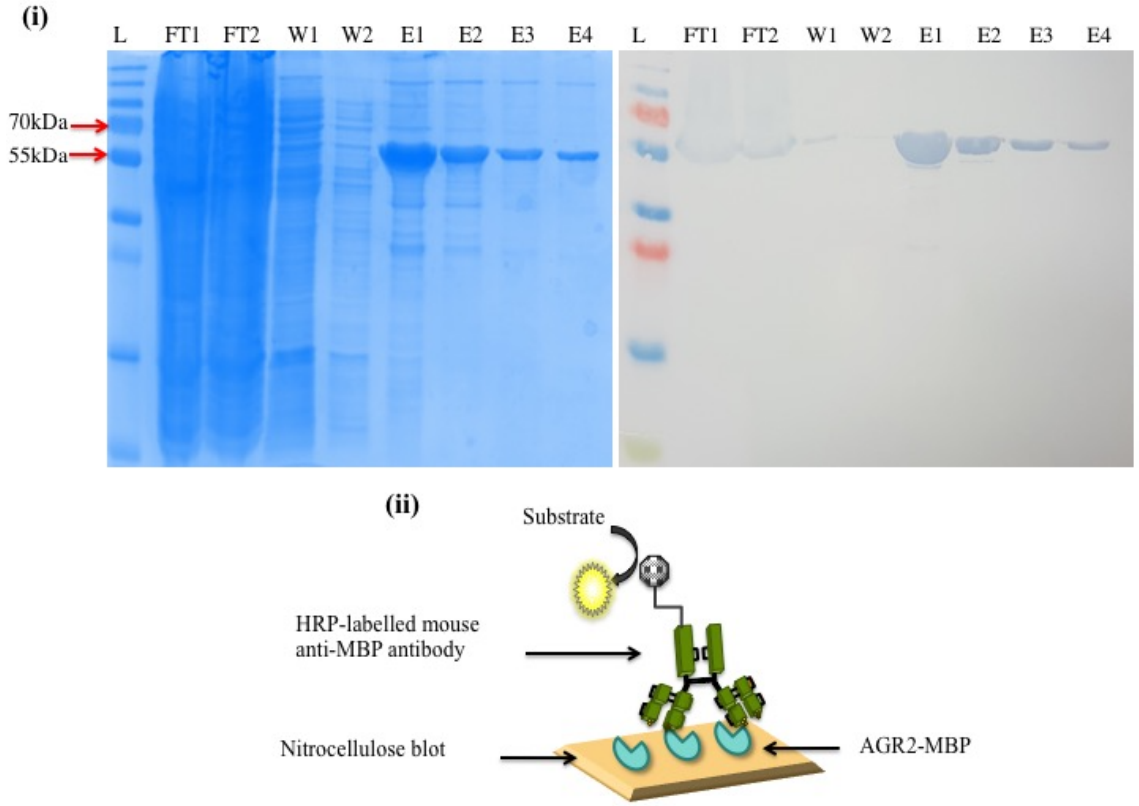

Figure 4.11 Purification of AGR2-MBP fusion protein using amylose resin

(i) *SDS-PAGE and Western blot analysis of the purification of the fusion protein AGR2-MBP.* ***(ii)*** *The western blot was probed with an anti-MBP HRP-labelled antibody and a simplistic schematic of the detection format is shown below the blot. L = PageRuler™ Plus Prestained Protein Ladder; FT1 = Flow-through 1; FT2 = Flow-through 2; W1 = Wash 1; W2 = Wash 2; E1 = Elution 1; E2 = Elution 2; E3 = Elution 3; E4 = Elution 4.*

4.2.3.3 Cleavage of AGR2 from MBP

Factor Xa protease was used to cleave MBP from AGR2. The cleavage is carried out at ratio of 1 µg Factor Xa to 50 µg of fusion protein and incubated O/N at RT. The following day the reaction was stopped by the addition of 2 µM dansyl-Glu-Gly-Arg Chloromethyl Ketone (Merck Millipore) which irreversibly inactivates Factor Xa. The cleaved sample and a non-cleaved control sample were prepared and analysed on SDS-PAGE and WB.

For confirmation, two WB analyses were performed. The first was probed with an anti-MBP-HRP labelled antibody. It can be observed in ***Figure 4.12 (i)*** that in the non-cleaved sample there are two bands, one at ~61kDa (AGR2-MBP) and another at ~42kDa (MBP). Comparatively, in the cleaved sample, the 42kDa band has become significantly thicker indicating an increase in uncoupled MBP. Coupled with the presence of a lower band at ~19kDa in the SDS-PAGE gel which is the expected size of AGR2 alone, it can be assumed that the cleavage was successful. For confirmation, a second blot was carried out and probed with a mouse monoclonal anti-AGR2 antibody, followed by an anti-mouse-HRP-labelled antibody for detection (***Figure 4.12 (ii)***). In the non-cleaved sample there is one band at the expected size (~61kDa) of the fusion AGR2-MBP protein. In the cleaved sample there are two bands present, one at ~61kDa, representing the remainder of the non-cleaved fusion protein, and the other at 19kDa, the expected size of AGR2. The combined results showed the successful cleavage of AGR2 from MBP fusion partner (***Figure 4.12***).

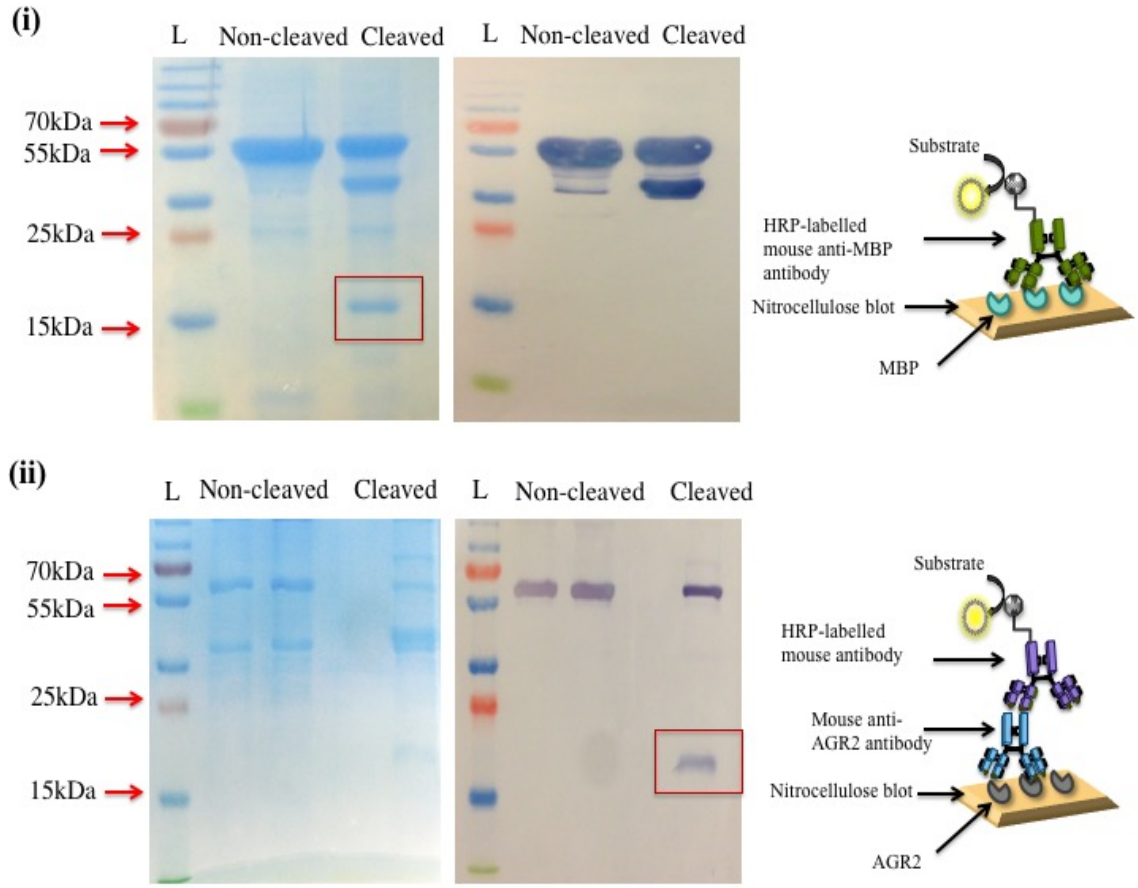

Figure 4.12 Cleavage of MBP from AGR2

(i) *SDS-PAGE gel and WB analysis of AGR2-MBP cleaved by Factor Xa. WB was probed using a HRP-labelled anti-MBP antibody.* ***(ii)*** *SDS-PAGE gel and WB analysis of AGR2-MBP cleaved by Factor Xa. WB was probed with an anti-AGR2 antibody and subsequently a HRP-labelled anti-mouse antibody. L = PageRuler™ Plus Prestained Protein Ladder.*

4.2.3.4 Purification of AGR2 protein after cleavage from MBP tag

For removal of Factor Xa, MBP and any residual fusion protein, the ÄKTA pure system was employed to separate the proteins using SEC. A Superdex 75 10/300 GL column was equilibrated in 1 X PBS pH 7.4 and 500 µL of purified protein (7.45 mg/mL) was applied to the column at a flow rate of 0.5 mL/min. The protein was eluted in two column volumes at the same flow rate. Any protein peaks detected during elution were dispensed into individual fractions. The putative AGR2-containing fraction was analysed via SDS-PAGE gel and WB and was found to contain minimal contaminant bands (***Figure 4.13***).

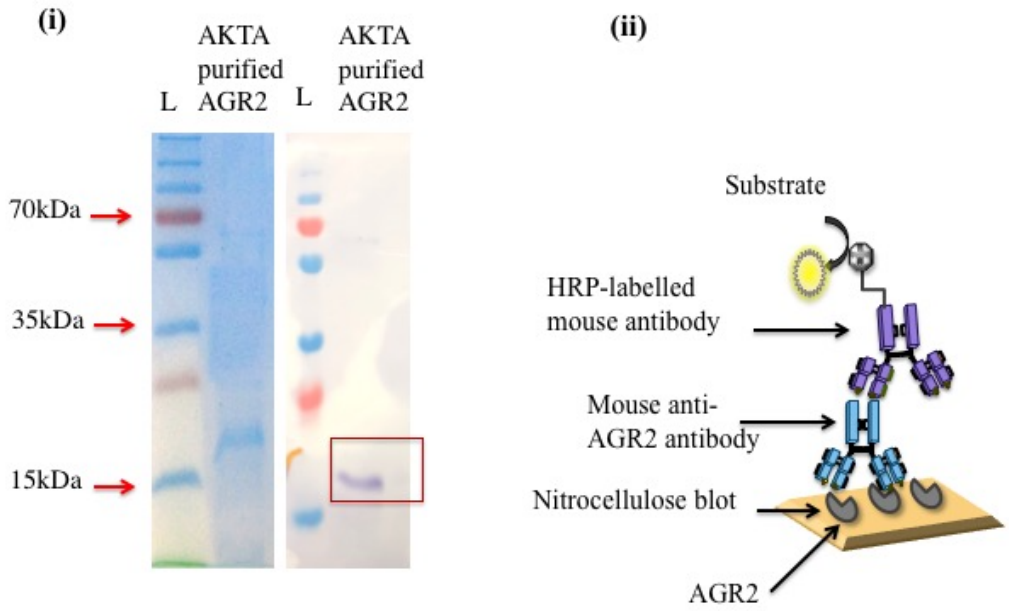

Figure 4.13 Purification of AGR2 by size exclusion chromatography

(i) *Eluted fraction containing AGR2 was analysed on SDS-PAGE and western blot.* ***(ii)*** *Western blot analysis was probed with an anti-AGR2 antibody and a secondary HRP-labelled anti-mouse antibody. L = PageRuler™ Plus Prestained Protein Ladder.*

4.2.4 Screening of a Capan-1 murine immune library against AGR2

4.2.4.1 Antibody library screening against a recombinant AGR2 protein

The purified AGR2 protein was used for affinity selection, to isolate any AGR2-specific scFv from the murine Capan-1 library. Four rounds of panning were carried out using the conditions set out in ***Table 4.2***, below. In regards to the panning process for selection of anti-AGR2 scFv, an additional step was added to ensure that enrichment of anti-MBP scFv did not occur. While the SEC protocol successfully isolated the cleaved AGR2 protein, the presence of any residual fusion-protein or cleaved MBP could result in the isolation of anti-MBP scFv. Consequently, a depletion step using immobilised MBP was added to this protocol. The precipitated phage was initially incubated in an immunotube with MBP, coated at the same concentration as the target antigen. The phage pool was allowed to bind for 1 hour, rolling at RT. Any MBP-specific phage would bind to the immunotube, the remaining phage in solution were subsequently removed gently to ensure any bound phage were not dislodged. The MBP-depleted phage pool was then incubated in the AGR2-coated immunotube and the protocol resumed as per *Section 2.16.*

Table 4.2 *Panning conditions employed for each round of selection of the murine anti-Capan-1 scFv library against a recombinant AGR2 protein*

Panning round	AGR2 coating conc.	Number of washes
1	50 µg/ mL	3 X PBS, 3 X PBS-T (0.05% (v/v))
2	25 µg/ mL	5 X PBS, 5 X PBS-T (0.05% (v/v))
3	12.5 µg/ mL	10 X PBS, 10 X PBS-T (0.05% (v/v))
4	5 µg/ mL	15 X PBS, 15 X PBS-T (0.05% (v/v))

Due to the issues encountered with false-positive clones during soluble expression of the MUC1-specific clones, a colony-pick PCR was performed on clones from the final round output, prior to polyclonal phage pool analysis. This was to determine the enrichment of colonies containing the full scFv product. The result showed only 6.25% insert retention when 16 colonies were tested (***Figure 4.14***). On completion of the affinity selection, retention of phage containing the scFv insert provides confidence in the efficiency of the technique (Kushwaha *et al.,* 2014). Contamination of scFv-free phage which results in a failure to enrich scFv containing phage is a huge hindrance of phage display. It occurs as a result of incomplete restriction and/or ligation of the scFv into the phagemid vector and low efficacy during the generation of recombinant phage by the addition of helper phage. The smaller size of the insert-free vector advantageously outgrows insert-containing phage (Tur *et al.,* 2001). As such, the phage pools were not taken forward for analysis in a polyclonal phage ELISA.

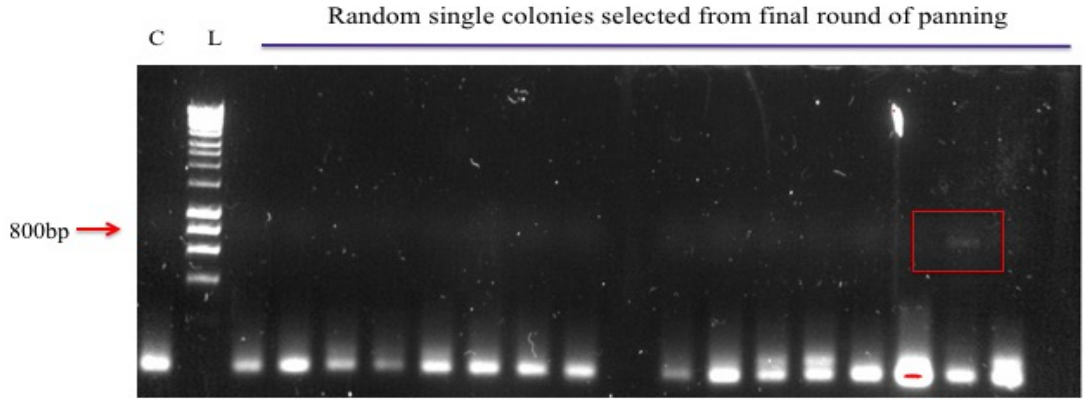

Figure 4.14 Colony-pick PCR analysis of final round output clones

Analysis of randomly selected colonies from the final round output titre plates of phage display panning of the murine-derived Capan-1 scFv library. C = Control lane, PCR reaction without a colony; L = 1kb Ladder (Bioline HyperLadder).

4.2.5 Antibody screening of the Tomlinson I and J library for AGR2- and MUC1 - specific scFv

Due to the inability to isolate anti-MUC1 or anti-AGR2 specific scFv from the murine library, it was decided to screen the synthetic, human, naïve Tomlinson I & J libraries for potential antibodies, by biopanning. The conditions undertaken for both panning protocols are outlined in the table below.

Table 4.3 *Panning conditions employed for each round of selection of the human Tomlinson library.*

Panning round	Antigen coating conc.	Number of washes
1	50 µg/ mL	5 X PBS, 5 X PBS-T (0.05% (v/v))
2	20 µg/ mL	10 X PBS, 10 X PBS-T (0.05% (v/v))
3	5 µg/ mL	15 X PBS, 15 X PBS-T (0.05% (v/v))

Randomly selected colonies from the final output of both the MUC1 and AGR2 panning protocols were subjected to a colony-pick PCR and visualised on a 1.5% (w/v) agarose gel. Both panning regimes retained the 800bp scFv product with the colony picks showing 100% insert retention (***Figure 4.15***). Input phage pools from each panning round were taken forward for incorporation into a polyclonal phage ELISA (***Figure 4.16***).

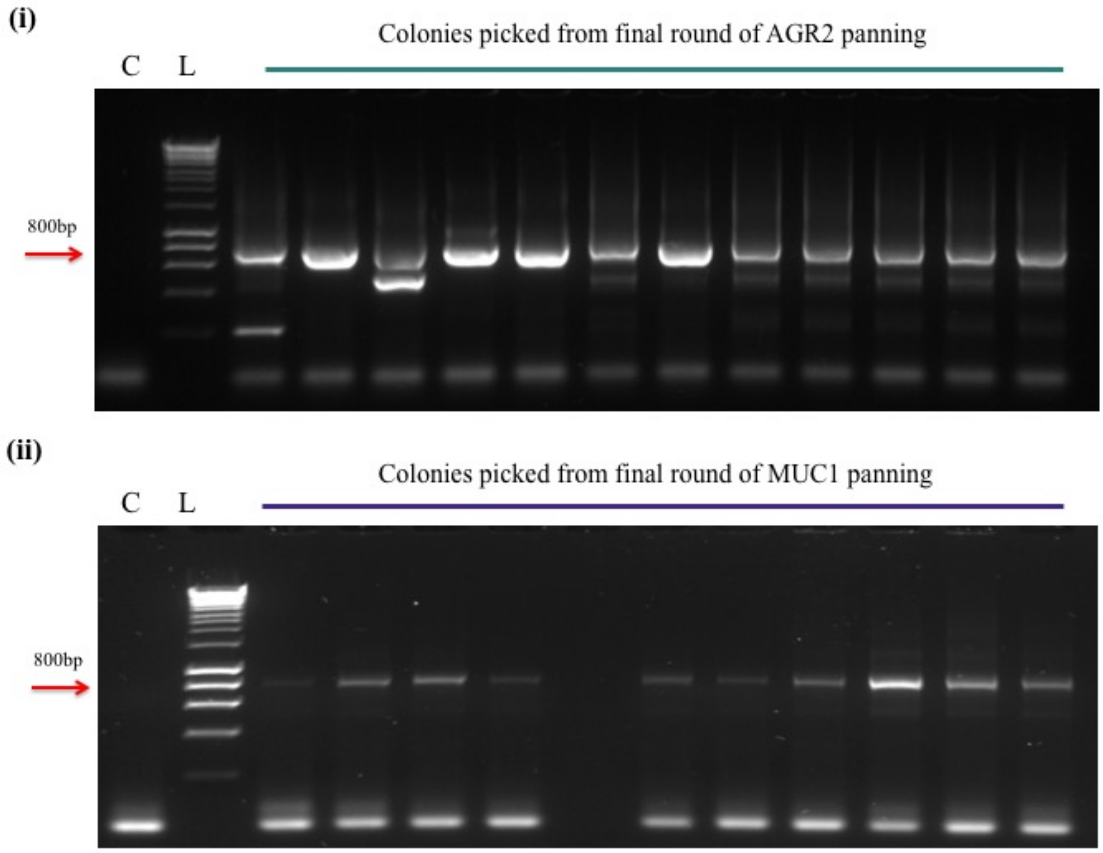

Figure 4.15 Analysis of randomly selected colonies from the output titre plates from the final round of Tomlinson library panning

(i) *Colonies selected from final round of AGR2 panning process.* ***(ii)*** *Colonies picked from final round of the MUC1 panning process and amplified by PCR using scFv specific primers. C = Control lane, PCR reaction without a colony; L = 1kb Ladder (Bioline HyperLadder).*

Successful enrichment against the AGR2 and MUC1 proteins was confirmed by an increase in absorbance signal after incubating precipitated phage pools with the target protein and detecting the bound phage with a HRP-labelled anti-M13 secondary antibody (GE Healthcare). This absorbance increase indicates the presence of antigen-specific scFv-displaying phage in the library (***Figure 4.16***). Phage pools from the final rounds of biopanning were taken forward for further analysis.

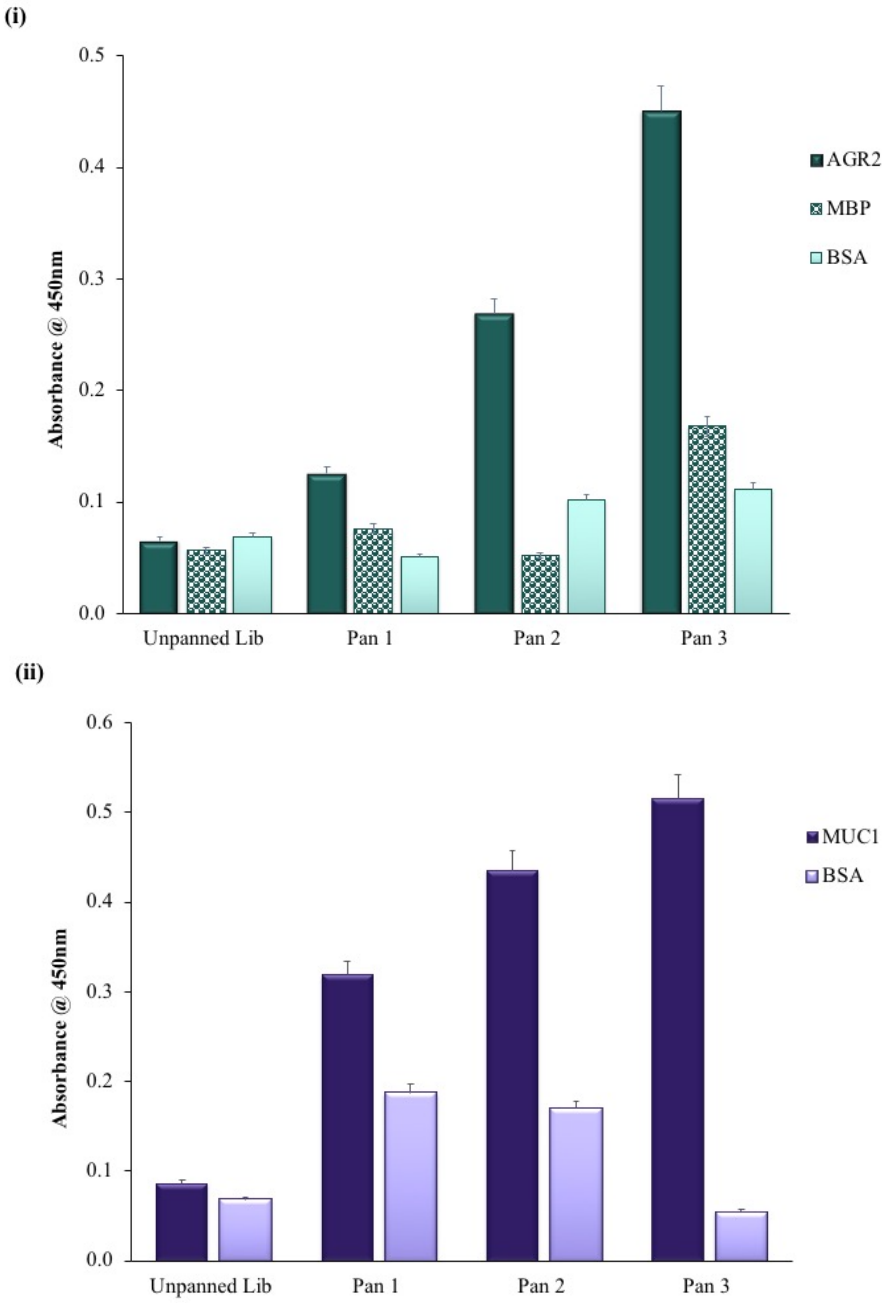

Figure 4.16 Polyclonal phage ELISA

(i) *Polyclonal phage screening for anti-AGR2 scFv displayed on phage following completion of panning.* ***(ii)*** *Polyclonal phage ELISA screening for anti-MUC1 scFv displayed on phage following completion of panning. Phage pools from each round were diluted 1/3 in 1% (w/v) BSA in PBS-T and were added to antigen-coated ELISA plates (1 µg/ mL). The scFv-displaying-phage were detected using a HRP-labelled anti-M13 secondary antibody and the absorbance was read at 450 nm using a Tecan Safire™ plate reader.*

4.2.5.1 Soluble expression and monoclonal analysis of single clones by ELISA

The selected phage pools were infected into Top10F' for soluble expression of the scFv. Ninety-six single colonies were selected from each infected phage pool and were solubly expressed. The periplasmic lysate was applied to the monoclonal ELISA to identify antigen-specific scFv. The results shown in the following figures indicate the presence of scFv clones positive for AGR2 and MUC1-binding which were taken forward for further study (***Figure 4.17*** and ***4.18***).

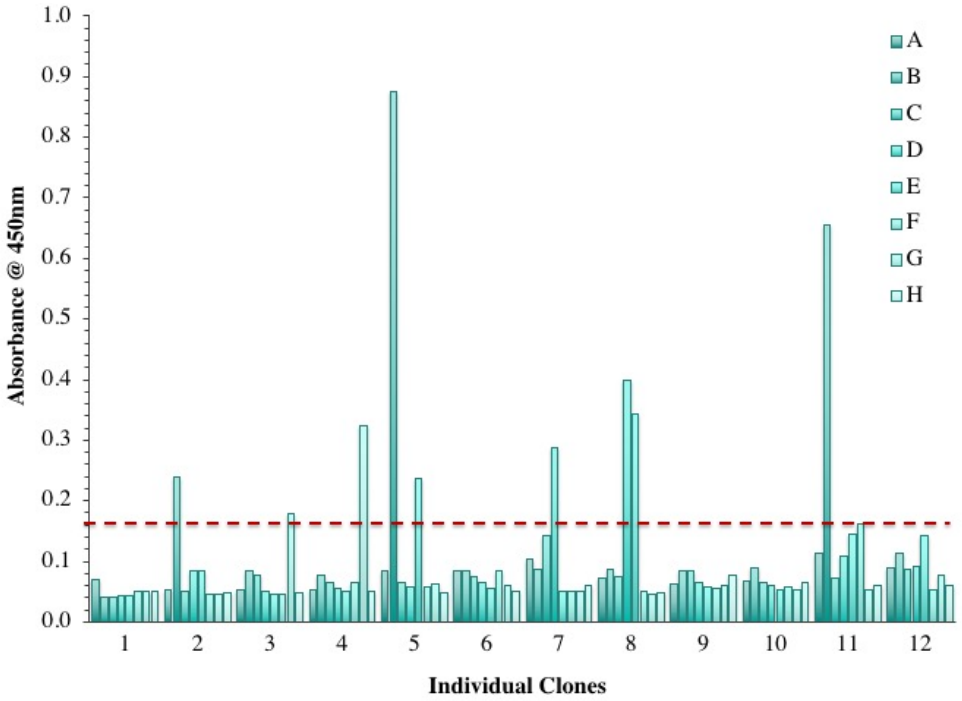

Figure 4.17 Monoclonal ELISA to select for specific scFv against AGR2

Soluble monoclonal ELISA screening for anti-AGR2 scFv from 96 randomly selected clones from the final round of panning Periplasmic lysates were applied to the AGR2-coated plate (1 µg/mL) and any specific scFv were detected using a HRP-labelled anti-c-myc antibody. The red dashed line represents the "cut-off" value (x 3 the background optical density).

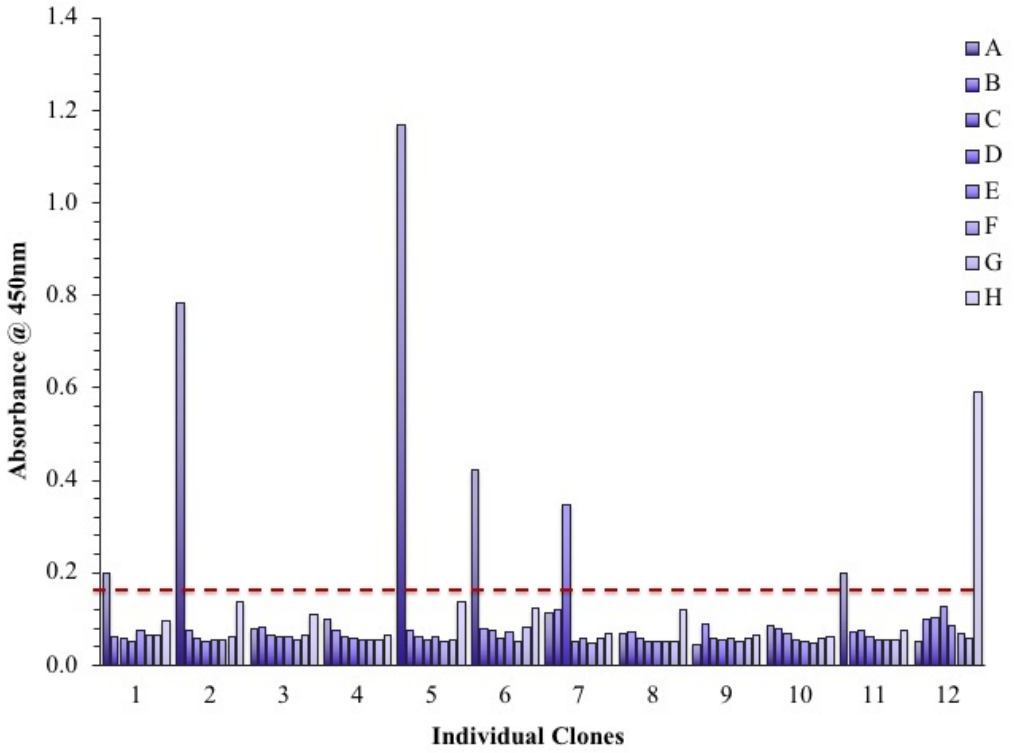

Figure 4.18 Monoclonal ELISA to select for specific scFv against MUC1

Soluble monoclonal ELISA screening for anti-MUC1 scFv from 96 randomly selected clones from panning round 3. Periplasmic lysates were applied to the MUC1-coated plate (1 μg/mL) and any specific scFv were detected using a HRP-labelled anti-c-myc antibody. The red dashed line represents the "cut-off" value (x 3 the background optical density).

4.2.5.2 Analysis of positive clones by indirect ELISA

Positive clones, selected by observed absorbance above the determined "cut-off" value, from each library were taken forward for characterisation studies. Cultures of 10 mL SB, supplemented with carbenicillin, were inoculated with the selected clones and grown O/N at 37°C. The following day, these were sub-cultured into fresh media, induced with 1 mM IPTG and grown O/N at 30°C. One mL samples of the cultures were taken and pelleted by centrifugation at 4,000*g* (Eppendorf™ centrifuge fixed angle rotor (F-45-30-11)) for 20 min. The bacterial cell pellets were lysed by resuspension in 1 mg/mL lysozyme, followed by freeze-thaw cycles outlined in *Section 2.16.7*. The clarified lysate was analysed by ELISA through the addition of the scFv-enriched lysate, in doubling dilutions, to the antigen-coated plate (1 μg/mL target protein) (***Figure 4.19***).

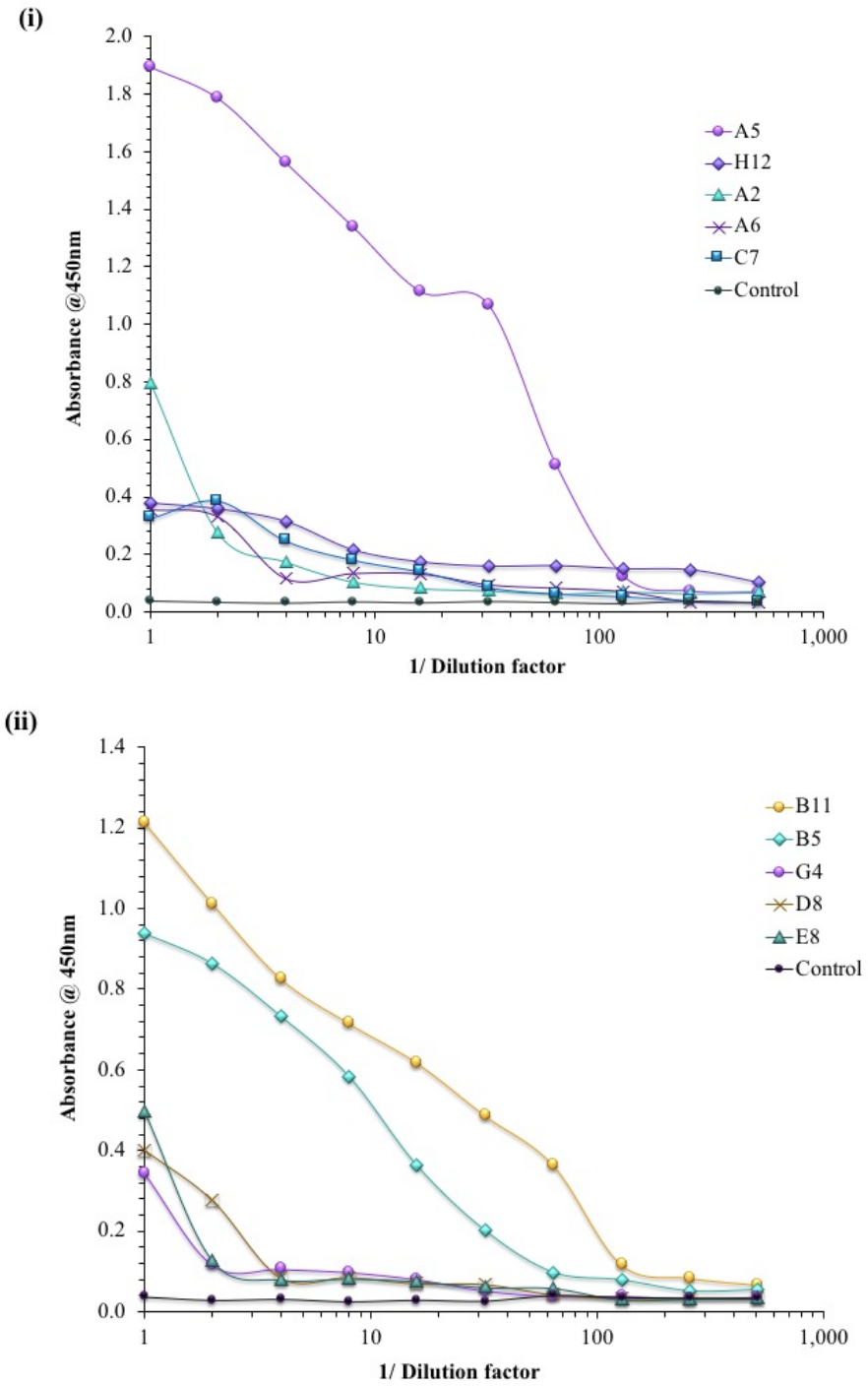

Figure 4.19 Titration of scFv lysate by ELISA against purified recombinant protein

(i) *Titration of MUC1 binding scFv clones against expressed MUC1 recombinant protein.* ***(ii)*** *Titration of AGR2 binding scFv clones against AGR2 recombinant protein. The lysate was applied to an antigen-coated ELISA plate. The bound scFv were detected using a HRP-labelled anti-c-myc antibody. Control – ELISA performed without the addition of scFv lysate.*

The anti-AGR2 clones, B11 and B5 indicated expression of functional scFv that titre against the recombinant AGR2 protein. Additionally, the A5 clone that positively binds to MUC1 expresses a functional scFv that titres against MUC1.The remaining scFv were not taken forward for further analysis due to poor expression/specific binding levels exhibited.

4.2.5.2.1 Initial competitive analysis of clones

To analyse all clones capacity to bind to the appropriate antigen in solution, preliminary competitive assays were performed by incubating the scFv-enriched lysate with free antigen and adding the mixture to a pre-coated microplate. The anti-AGR2 and anti-MUC1 scFv abilities to bind to the appropriate antigen in solution relative to the immobilised antigen coated onto the surface were determined by analysing the scFv without addition free antigen. Each assay was performed in triplicate and the standard deviations were calculated and are indicated by error bars. All three clones exhibited specificity for the cognate antigens in solution (***Figure 4.20***).

4.2.5.3 Optimisation of scFv expression and subsequent purification using IMAC

Optimisation of expression was carried out as outlined in *Section 2.10.8*. Temperature variation was investigated as a reduction in the protein production rate can provide recombinant proteins with the necessary time to fold correctly. Lowering the temperature is the most common method to reduce protein production. This decreases aggregation found frequently at higher temperatures. It has also been found that conformational quality and functionality of recombinant proteins is increased at lower temperatures (Rosano and Ceccarelli, 2014). The use of IPTG can significantly increase protein yields, as varying the concentration results in regulation of protein expression. With many proteins, slow induction is a requirement for good conformation and functionality. This is achieved by using lower IPTG concentrations, while with other proteins a high yield is necessary, which would require increased concentrations of IPTG (Sadeghi *et al.,* 2011). While a high yield is desired, it is also important that the protein be correctly folded, therefore, IPTG concentrations over various temperatures was investigated.

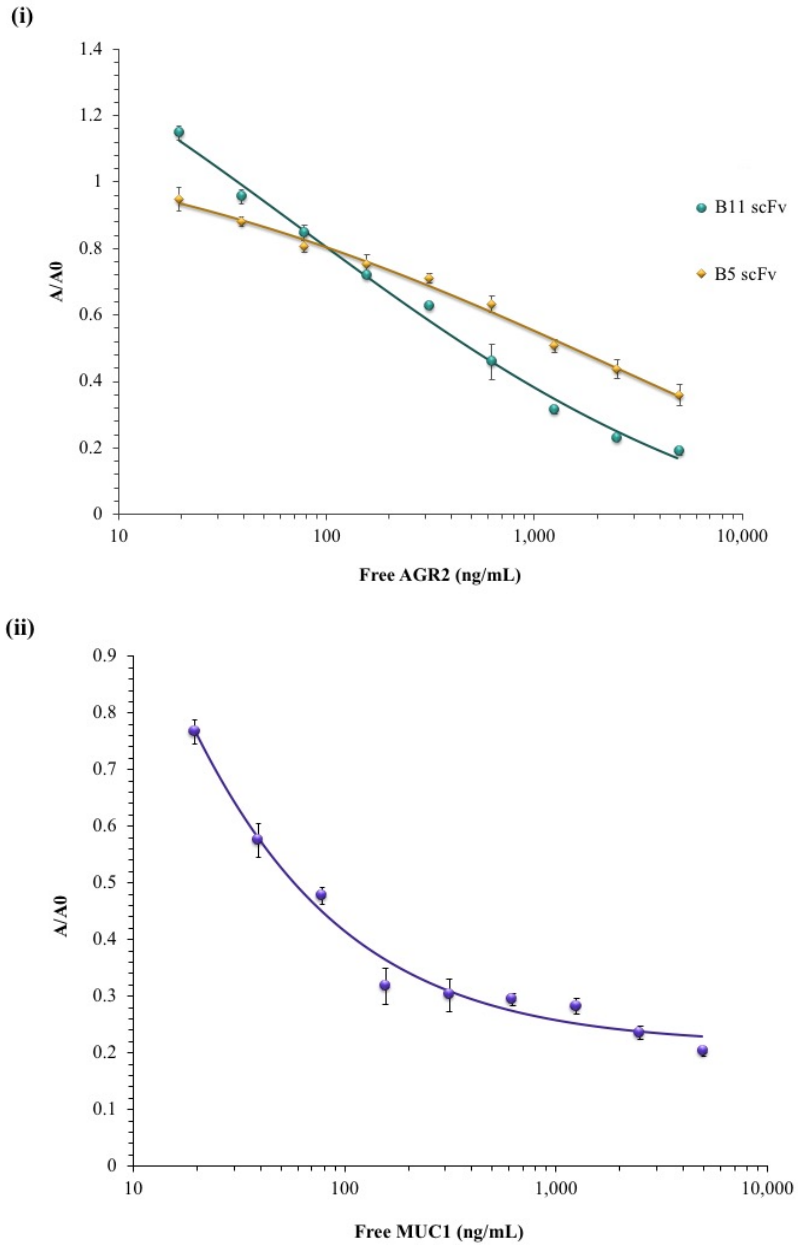

Figure 4.20 Competitive ELISA analysis of anti-MUC1 and anti-AGR2 clones

(i) Competitive analysis of AGR2-specific B11 clone and B5 clone was performed. Two µg/mL AGR2 was coated on the surface of a Nunc MaxiSorp™ ELISA plate. (ii) Competitive analysis of MUC1-specific A5 was performed. Two µg/mL MUC1 was coated on the surface of a Nunc MaxiSorp™ ELISA plate. The scFv-enriched lysate was incubated with free antigen and added to the plate where competition occurs between the immobilized and free antigen. Bound antibody was detected using a HRP-labelled anti-c-myc antibody. The results are shown as A/A0, where the absorbance values of the evaluated samples (A), are normalised by expressing them as a function of the blank standard (A0).

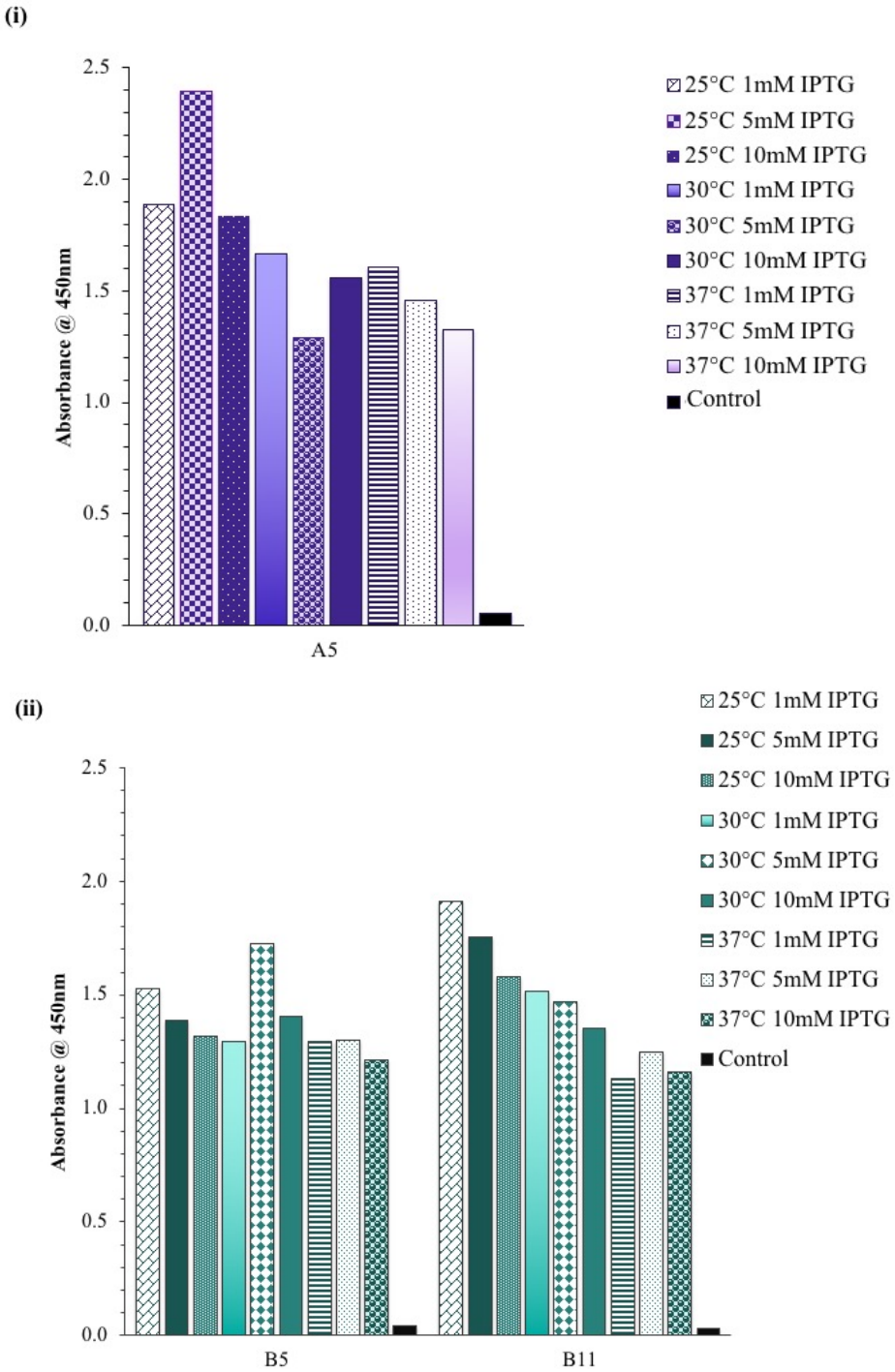

Figure 4.21 Optimisation of expression of the scFv clones

(i) *Analysis of optimal IPTG concentration and expression temperature for anti-MUC1 clone A5.* ***(ii)*** *Analysis of optimal IPTG concentration and expression temperature for anti-AGR2 clones, B5 and B11. The scFv were induced with different IPTG concentrations (1mM – 10mM) and incubated at a range of temperatures (25°C, 30°C and 37°C). The lysate was tested in indirect ELISA format and bound antibody was detected by the addition of a HRP-labelled anti-c-myc antibody. Control – ELISA performed without the addition of lysate.*

The optimum expression conditions for the anti-MUC1 clone, A5, were identified as induction with 5 mM IPTG at 25°C. In relation to the anti-AGR2 clones B11 and B5, the optimum expression conditions were observed as 1 mM IPTG at 25°C and 5 mM IPTG at 30°C, respectively (***Figure 4.21***).

All clones were expressed large-scale, as outlined in *Section 2.13.2,* and purified as described in *Section 2.13.5*. The fractions containing the IMAC-purified scFv were analysed by SDS-PAGE and WB (***Figure 4.22***). All blots were probed with a HRP-labelled anti-His antibody. A dense band at the expected size of the scFv, ~25kDa, can be observed in the eluted fractions of all three purifications. This indicates successful scFv purification. The scFv-containing eluents were buffer exchanged into 1 X PBS, concentrated and quantified on the Nanodrop™ 1000. All yields were diluted to 1 mg/mL for homogeneity.

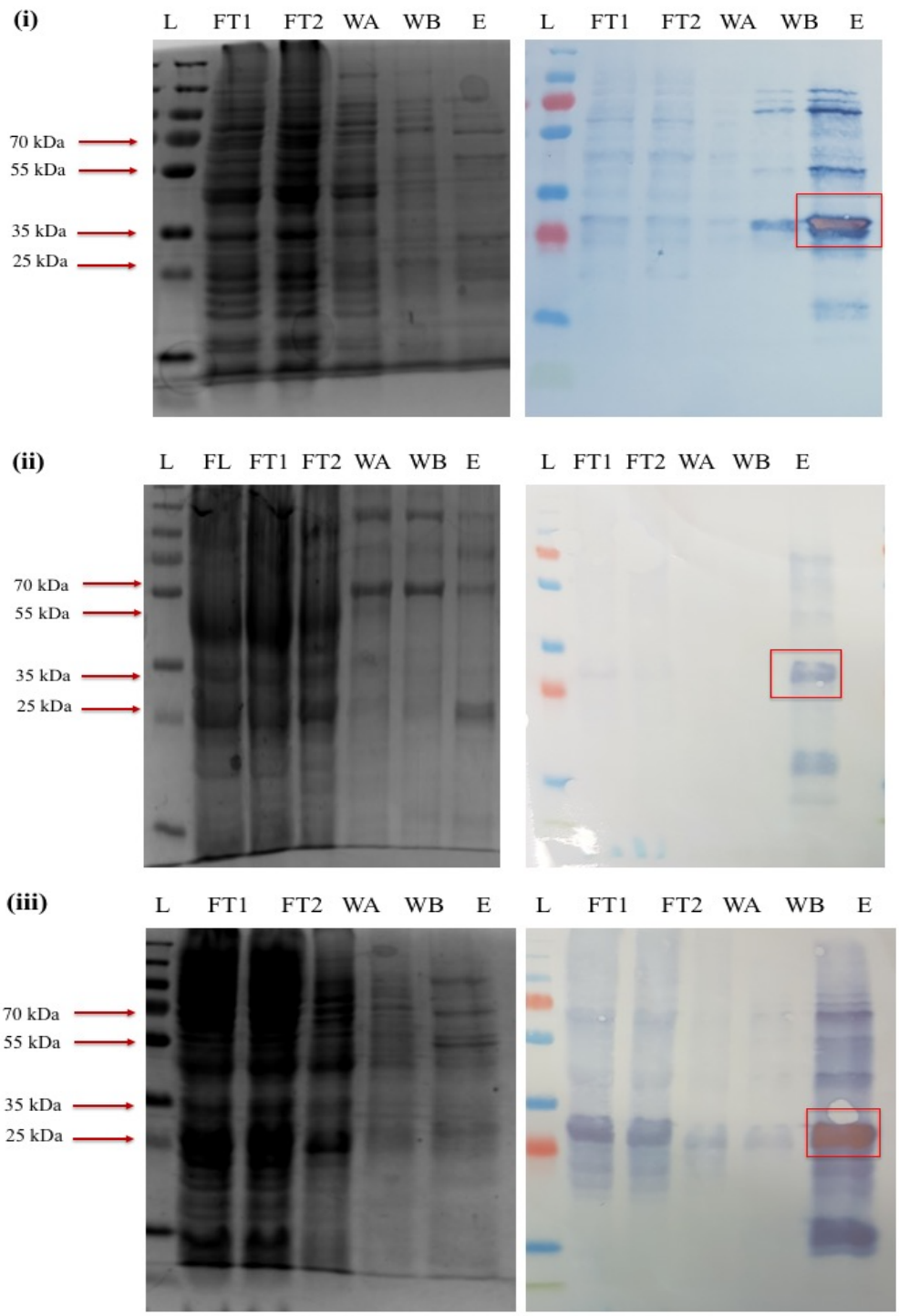

Figure 4.22 SDS-PAGE and western blot analysis of IMAC purified scFv

(i) *A5, anti-MUC1 clone* ***(ii)*** *B5, anti-AGR2 clone* ***(iii)*** *B11, anti-AGR2 clone. WBs were probed with an anti-His HRP-labelled antibody. L = PageRuler™ Plus Prestained Protein Ladder; FT1 = Flow-through 1; FT2 = Flow-through 2; WA = Wash A; WB = Wash B; E = Elution.*

4.2.5.4 Sequencing analysis of the anti-AGR2 clones B5 and B11 and the anti-MUC1 clone A5

Plasmid preparations of *E. coli* Top10F',containing pIT2 housing the three clones of interest, were sent to Source Bio-Sciences for sequencing. The resulting amino acid sequences were aligned and the CDRs of the clones identified. The Tomlinson I & J library have diversified side chains at 18 positions in the CDR regions. Within the Tomlinson I library, the varied amino acid positions may contain Cys, Asp, Asn, Thr, Ser, Tyr, Gly or Ala. In the Tomlinson J library any amino acid is possible at the varied positions. The diversity exists in residues H50, H52, H52a, H53, H55, H56, H58, H95, H96, H97, H98, L50, L53, L91, L92, L93, L94 and L96. The CDR regions of the three clones were identified and detailed in ***Table 4.4***. Here, the amino acids are highlighted in yellow to indicate the 18 diversity-housing residues. The majority of the sequences for the three clones are identical, however, this is expected when isolating clones from the Tomlinson libraries which are based on a single human V_H and V_L framework. This is evident by the identical CDR-H1 and CDR-L1 sequences, as neither of these CDRs house any of the diversified residues. Variations in all 18 residues confirms these are three different clones.

Table 4.4 Sequencing analysis of the three clones, A5 , B11 and B5.

The gene sequences were translated into amino acid sequences using the ExPasy Translate tool and aligned using MultAlin alignment program. The aligned sequences were analysed and the complementarity determining regions (CDR) were identified. The diverse amino acids are highlighted in yellow.

	CDR-H1	CDR-H2	CDR-H3
A5	GFTFSSYA	LEWV-SITSTGGRTS	AKLPRAFDY
B5	GFTFSSYA	LEWV-GISAAGSATG	AKASNSFDY
B11	GFTFSSYA	LEWVSGISSTGSYTN	AKSYDYFDY

	CDR-L1	CDR-L2	CDR-L3
A5	SISSYL	AASS	QQSYSTPNT
B5	SISSYL	SASD	QQYANDPST
B11	SISSYL	DASS	QQSYSCPAT

4.2.5.5 Optimisation of an ELISA for the detection of MUC1 and AGR2 using purified scFv

Following purification of the scFv, their use in a competitive immunoassay for the detection of AGR2 and MUC1 was investigated. To maximise assay performance, numerous parameters were optimised. The coating concentration of the antigen and concentration of antibody used was explored in a checkerboard ELISA. Upon determination of these parameters, intra-/inter-day assays were performed to establish the reproducibility of the assay. A second set of intra-/inter-day assays were then performed in normal human serum to establish the variance of the assay within physiological conditions. Precision testing on the extrapolated limit of detection (LOD) for each scFv was subsequently performed. Initially, a titration was performed using the purified scFv antibodies against the cognate antigen and irrelevant proteins to ensure the scFv were specific for the target antigens (***Figure 4.23***).

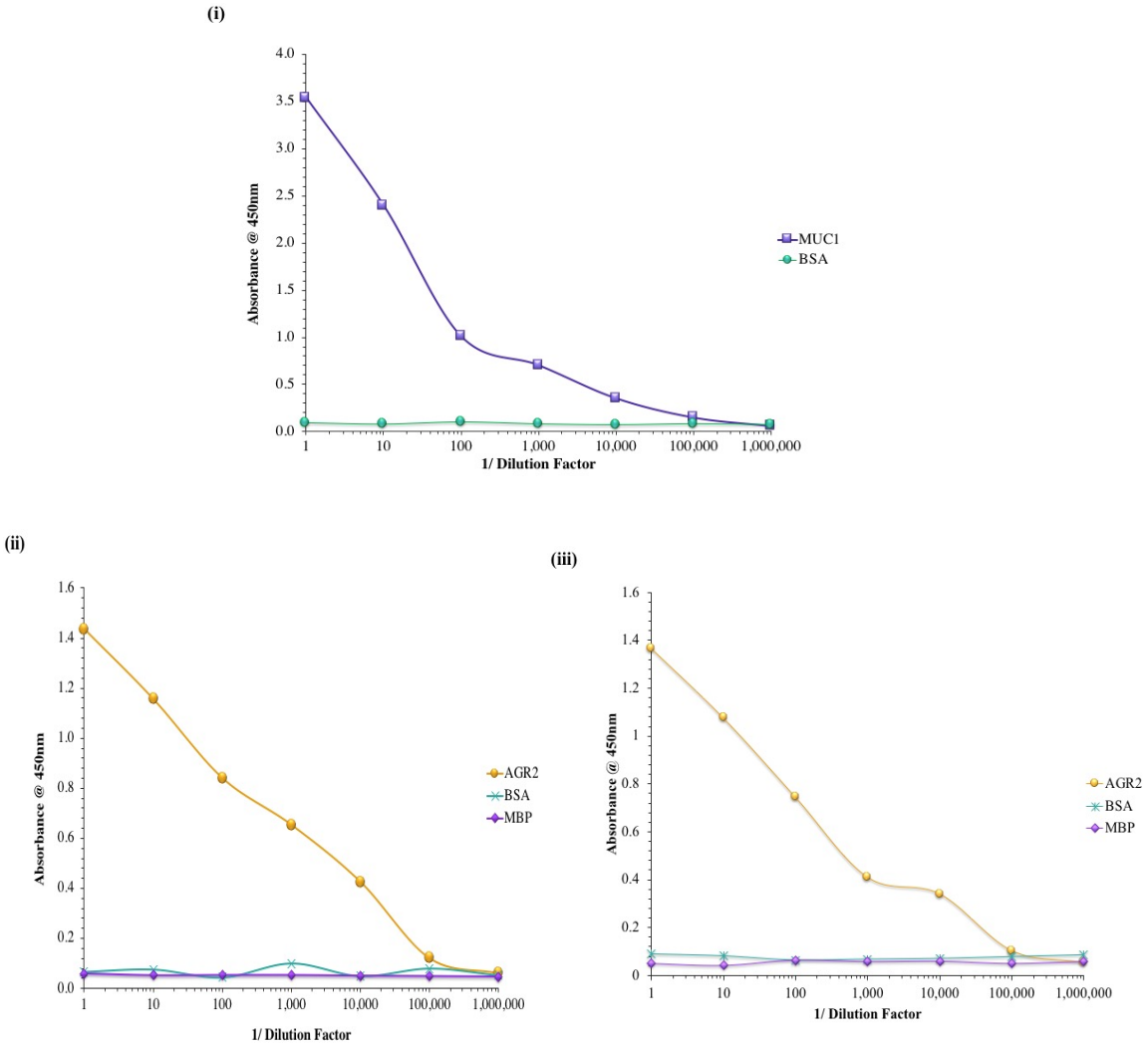

Figure 4.23 Titration of purified scFv by ELISA against purified recombinant protein ***(i)*** *Titration of MUC1 binding scFv A5 against expressed MUC1 recombinant protein.* ***(ii)*** *Titration of AGR2 binding scFv B11 against AGR2 recombinant protein.* ***(iii)*** *Titration of AGR2 binding scFv B5 against AGR2 recombinant protein The purified scFv was applied to an antigen-coated ELISA plate (1 µg/mL). The bound scFv were detected using a HRP-labelled anti-c-myc antibody. Controls – ELISA performed on wells coated with BSA and/or MBP protein at a concentration of 1 µg/mL.*

4.2.5.5.1 Checkerboard ELISA for the determination of the optimum antibody dilution and coating concentration

To determine the combination of antigen concentration and antibody dilution which would provide the best assay sensitivity, a checkerboard ELISA was performed. Three Nunc MaxiSorp™ ELISA plates were coated with various concentrations of the appropriate antigen (10 µg/mL – 0 µg/mL), in 1 X PBS. The results indicated that for the MUC1-specific scFv, A5, the optimum conditions were a coating concentration of 9 µg/mL and an antibody dilution of 1/20. These gave the highest absorbance using the most economical antigen and antibody concentrations (***Figure 4.24***). In relation to the two AGR2 scFv, B5 and B11, the optimal concentrations were, 5 µg/mL antigen coating and 1/80 antibody dilution (***Figure 4.25***).

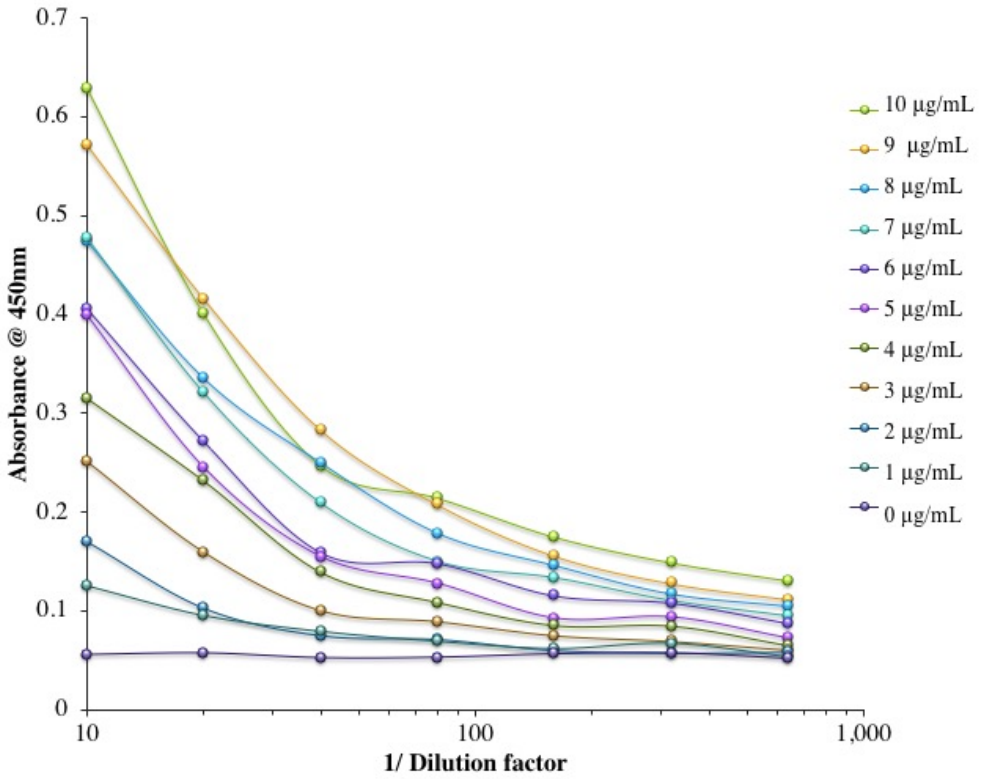

Figure 4.24 Checkerboard ELISA for the determination of the optimal MUC1 coating concentration and scFv dilution for use in a competitive ELISA

Antigen concentrations of 10 µg/mL to 0 µg/mL were used in an indirect ELISA with varying dilutions of antibody ranging from 1/10 to 1/1,640. Bound antibody was detected using a HRP-labelled anti-c-myc antibody.

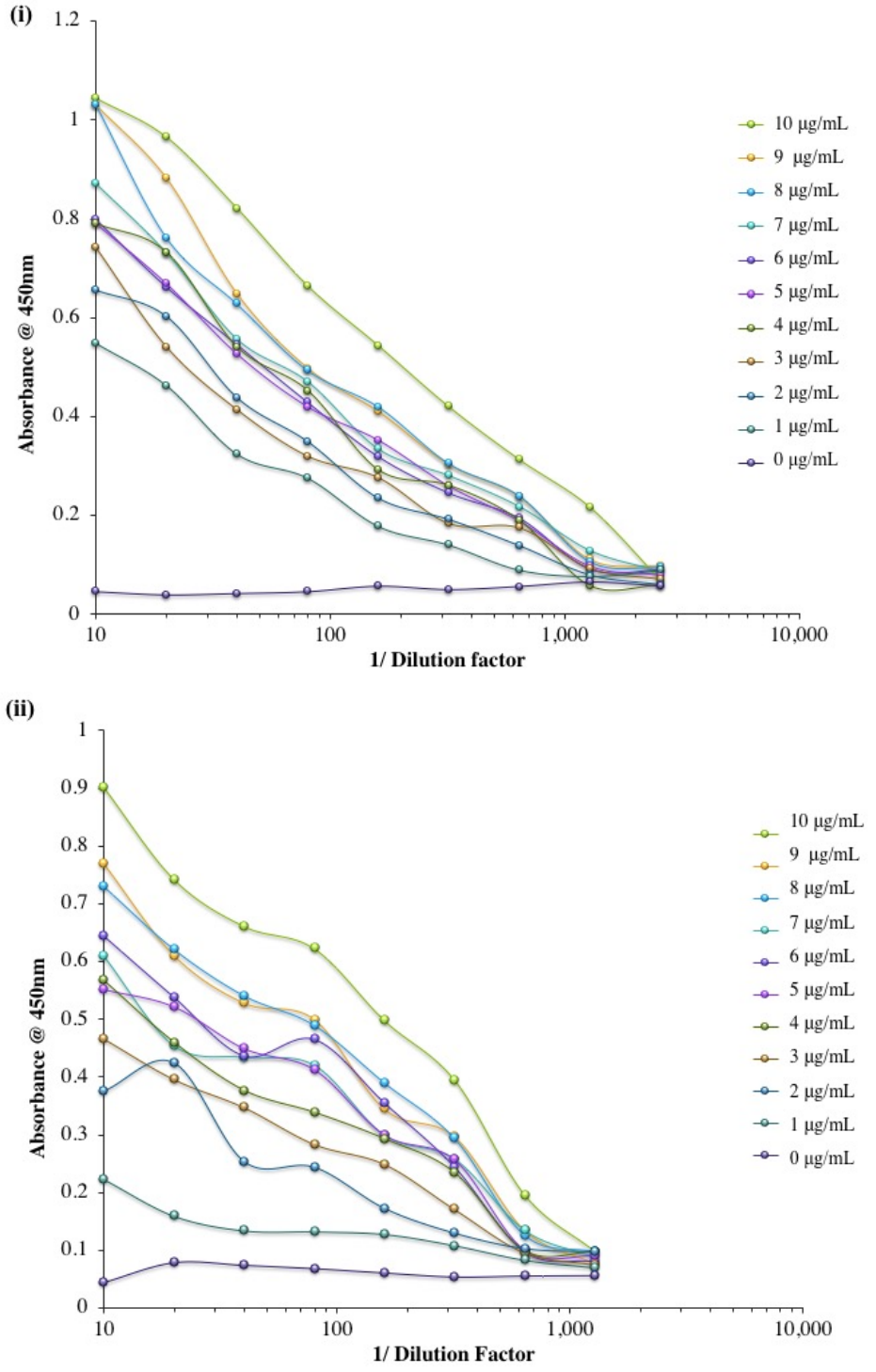

Figure 4.25 Checkerboard ELISA for the determination of the optimal AGR2 coating concentration and antibody dilution for use in a competitive ELISA

Checkerboard analysis of ***(i)*** *AGR2-specific B11 scFv and* ***(ii)*** *AGR2-specific B5 scFv. Antigen concentrations of 10 µg/mL to 0 µg/mL were used in an indirect ELISA with varying dilutions of antibody ranging from 1/10 to 1/1,640. Bound antibody was detected using a HRP-labelled anti-c-myc antibody.*

4.2.5.5.2 Intra-/Inter-assay variability studies for the competitive ELISA analysis of each scFv in PBS

Using the parameters previously optimised, a competitive assay was initially carried out in PBS. A microtitre plate was coated in the appropriate concentrations of MUC1/AGR2, as identified in the checkerboard ELISA in *Section 4.2.2.,* and blocked in 3% (w/v) BSA in 1 X PBS. AGR2 and MUC1 standards were prepared as required and mixed with the appropriate antibody dilution. The final concentrations of AGR2 ranged from 10 µg/mL - 1.024 pg/mL for scFv B11 and 20 µg/mL – 339 pg/mL for scFv B5. In relation to the anti-MUC1 scFv, A5, the final concentration of MUC1 ranged from 18 µg/mL – 304 pg/mL. The scFv at their optimal dilutions were added to the plates, incubated, washed, and bound scFv were detected by the addition of a HRP-labelled anti-c-myc antibody. Calibration curves were created using BiaEvaluation^{TM} software, using a four parameter equation fitted to the data. The four parameter curve follows a sigmoidal 'S' shape and is used for characterizing immunoassays as they are only linear across a specific range of concentrations (Pang and Cowen, 2017).

Intra-assay studies were performed to measure the accuracy of the immunoassay (Bastarache *et al.,* 2011). Such studies require the assay to be performed three times within the same day. The results obtained for the intra-assay studies for the three scFv, B11 , B5 and A5 are shown in ***Tables 4.5, 4.6*** and ***4.7,*** respectively. The coefficients of variation (CV) were determined in order to assess the reproducibility. As standard deviation increase/decreases proportional to the mean the CV represents a standardization of the SD which allows for comparison of variability within the working range of the assay (Reed *et al.,* 2002). Here the percentage CV was calculated by dividing the standard deviation by the means values multiplied by 100. With regards to the anti-AGR2 scFv, CVs ranged from 1.76-10.5% for scFv B11 with an average of 4.7% and 1.2-4.8% for scFv B5 with an average of 3.1%. The anti-MUC1 scFv, A5, was determined to have a CV of 1.2-7.1% with a 3.2% average. All averages are below the recommended 20% CV for intra-assay evaluation, indicating sufficiently high levels of precision (Findlay *et al.,* 2000; Thomsson *et al.,* 2014). Inter-day assays were carried out determine the precision of repeated measurements that could be effected by variations such as days and reagents and the reproducibility of the assay (Chesher, 2008; Bastarache *et al.,* 2011; Andreasson *et al.,* 2015). This study is carried out three times over three days. The results are shown in ***Tables 4.5, 4.6*** and ***4.7***. The highest CV was calculated at 14% with the averages

ranging from 4 – 7.5%, this complies with recommendations that inter-assay CV percentage should be below 15-20% (Findlay *et al.,* 2000; Thomsson *et al.,* 2014). The percentage accuracies of the curves (***Tables 4.5, 4.6*** and ***4.7***) are within acceptable variance ranges, with any inaccuracies primarily falling outside of the linear ranges of the curves. This shows that these curves provide an accurate representation of the sigmoidal relationship between the measured response and the logarithm of concentration observed for the immunoassay. Furthermore, to determine if the theoretical values and measured values were in agreement, the % accuracy was calculated by expressing the measured concentration as a percentage of the back-calculated concentration.

The calibration curves of the inter-day assay were generated using a 4-parameter equation in BiaEvaluation^{TM}(***Figure 4.26 and 4.27***). It can be observed that the dynamic range analysed was not appropriately extensive when analysing the anti-MUC1 scFv, consequently, a larger MUC1 concentration range was investigated in the inter-day and intra-day assays, that were performed in normal human serum.

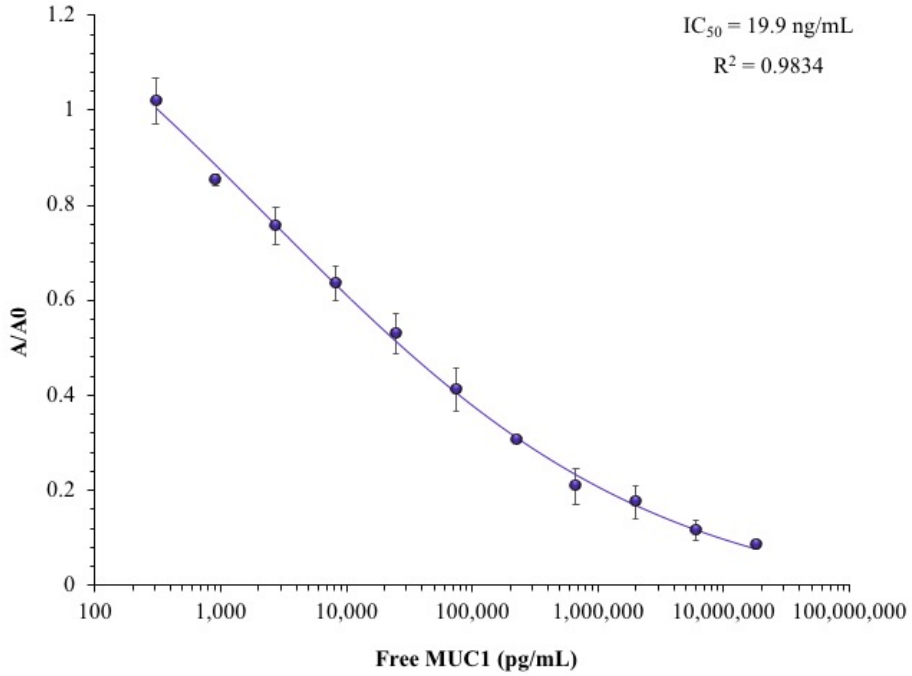

Figure 4.26 Inter-day assay calibration curve of anti-MUC1 scFv A5 in PBS

The calibration curve was constructed using a 4-parameter equation in BiaEvaluation^{TM}. The inter-day assay means and CV are tabulated in ***Table 4.5.*** *Each point on the curve is the mean of 3 replicate measurements analysed over 3 days. The absorbance of the evaluated samples was normalised by expressing the absorbance as a function of the blank standard (A/A0).*

Table 4.5 Intra – and inter-day assay CV and percentage accuracies for the anti-MUC1 scFv A5 in PBS.

Coefficient of variation (CV) was calculated by % CV=(S.D/Mean) x 100 (Jelliffe et al., 2015). The standard deviation (S.D) for intra-day analysis was calculated from 3 replicate analyses within a single assay, whereas the S.D for inter-day analyses was calculated from 3 replicates over 3 assays on 3 separate days. Table cells that contain a "-" indicate that no value could be extrapolated as the data point did not fit the calibration curve.

	Intra-day			***Inter-day***		
MUC1 Conc. (pg/mL)	**CV (%)**	**Back Calculated Conc. (pg/mL)**	**Accuracies (%)**	**CV (%)**	**Back Calculated Conc. (pg/mL)**	**Accuracies (%)**
18,000,000	3.1	-	-	2.9	14,449,300	80
6,000,000	3.4	5,659,710	94	11.1	6,338,800	106
2,000,000	7.1	1,877,383	94	3.2	1,791,920	90
666,667	2.4	786,098	118	3.3	779,267	116
222,222	1.3	159,827	72	5.9	234,771	106
74,074	3.7	78,807	106	5.2	70,114	95
24,691	2.8	22,122	90	5.3	20,940	85
8,230	2.6	8,374	102	2.7	8,231	100
2,743	1.2	3,611	132	1	2,327	85
914	4.3	1,028	112	3.6	1,139	125
304	2.3	-	-	3.1	-	-

Table 4.6 Intra – and inter-day assay CV and percentage accuracies for the anti-AGR2 scFv B11 in PBS.

Coefficient of variation (CV) was calculated by % CV=(S.D/Mean) x 100. The standard deviation (S.D) for intra-day analysis was calculated from 3 replicate analyses within a single assay, whereas the S.D for inter-day analyses was calculated from 3 replicates over 3 assays on 3 separate days. Table cells that contain a "-" indicate that no value could be extrapolated as the data point did not fit the calibration curve.

	Intra-day			***Inter-day***		
AGR2 Conc. (pg/mL)	**CV (%)**	**Back Calculated Conc. (pg/mL)**	**Accuracies (%)**	**CV (%)**	**Back Calculated Conc. (pg/mL)**	**Accuracies (%)**
10,000,000	7.1	7,855,150	79	1.6	-	-
2,000,000	10.5	1,845,360	92	2.1	2,167,600	108
400,000	3.9	569,379	142	3.4	550,610	137
80,000	6.9	53,499	67	14	45,546	57
16,000	4.12	12,568	79	2.5	11,597	72
3,200	2.32	3,621	113	3.4	3,074	96
640	6.14	595	93	3.2	683	106
128	1.76	139	109	2.1	93	73
25.6	1.99	27.2	105	1.6	22.4	88
5.12	4.32	4.7	92	4.1	4.2	78
1.024	3.1	1.3	126	7.8	1.8	176

Table 4.7 Intra – and inter-day assay CV and percentage accuracies for the anti-AGR2 scFv B5 in PBS.

Coefficient of variation (CV) was calculated by % CV=(S.D/Mean) x 100. The standard deviation (S.D) for intra-day analysis was calculated from 3 replicate analyses within a single assay, whereas the S.D for inter-day analyses was calculated from 3 replicates over 3 assays on 3 separate days. Table cells that contain a "-" indicate that no value could be extrapolated as the data point did not fit the calibration curve.

	Intra-day			***Inter-day***		
AGR2 Conc. (pg/mL)	**CV (%)**	**Back Calculated Conc. (pg/mL)**	**Accuracies (%)**	**CV (%)**	**Back Calculated Conc. (pg/mL)**	**Accuracies (%)**
20,000,000	1.2	13,615,600	68	1.4	9,792,670	49
6,666,667	4.6	-	-	3	5,973,060	90
2,222,222	1.3	1,598,270	72	4.1	3,089,750	140
740,740	1.9	873,443	118	1.2	949,520	128
246,914	2.6	287,614	116	1.4	277,586	124
82,305	3.7	87,037	105	2.9	91,862	111
27,435	4.1	28,145	102	7.8	28,984	105
9,145	3.5	8,949	98	3.5	8,656	95
3,048	3.5	3,012	99	4.6	3,048	100
1,016	4.8	1,267	123	2.6	1,337	131
339	2.9	-	-	4.9	-	-

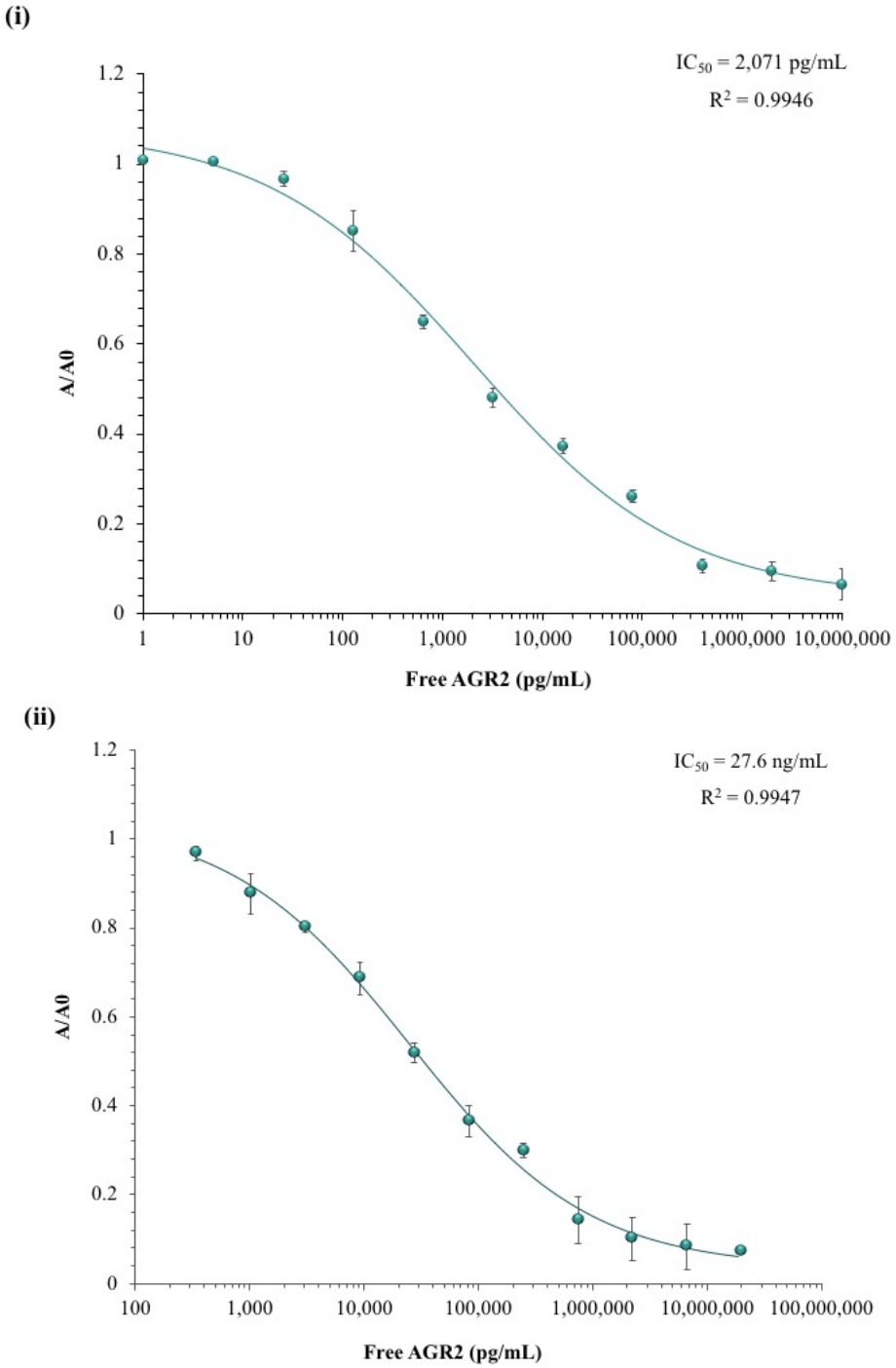

Figure 4.27 Inter-day assay calibration curve of scFv (i) B11 and (ii) B5 in PBS

The calibration curve was constructed using a 4-parameter equation in BiaEvaluation™. The inter-day assay means and CV are tabulated in ***Tables 4.6*** and ***4.7.*** *Each point on the curve is the mean of 3 replicate measurements analysed over 3 days. The absorbance of the evaluated samples was normalised by expressing the absorbance as a function of the blank standard (A/A0).*

4.2.5.5.3 Intra-/Inter-assay variability studies of the competitive ELISA of each scFv in normal human serum

To explore the feasibility of the generated scFv for detection of the appropriate antigen in clinical samples, human serum samples were spiked with AGR2 and MUC1 recombinant proteins. Investigation of assay performed in the appropriate biological matrix is essential to uncover any possible matrix effects. This occurs when components within the matrix interfere with the antibodies ability to bind to the cognate antigen (Rosenberg-Hasson *et al.,* 2014). Complex matrices such as human serum can contain high levels of endogenous biomarkers and common proteins such as albumin which can contribute to this matrix interference (Dupin *et al.,* 2016). Using the parameters already optimised, the inter- and intra-day assays were repeated to analyse immunoassay accuracy in physiological conditions and compared to those determined in PBS. This work was performed herein using normal human serum, as per *Section 2.17.3.1.*

To assess a more appropriate linear range, the protein concentration was increased to 18 µg /mL – 1.8 pg/mL for the anti-MUC1 scFv A5 and to 20 µg/mL – 203 pg/mL for the anti-AGR2 scFv B5. Protein standards and the antibody dilution were prepared in normal human serum. The remainder of the assay was performed as in previous inter-day and intra-day assay analysis (*Section 4.2.5.5.4)*. Calibration curves were created using BiaEvaluation™ software (***Figure 4.28*** and ***4.29***). The coefficients of variation (CV), tabulated in ***Table 4.8, 4.9*** and ***4.10***, were determined to assess the precision of the assay. The highest values noted were, 13.5% and 18%, 15.4% and 11.2%, and 13.1% and 12.5%, for the intra-day and inter-day assays for B11, B5 and A5, respectively. The average intra-day %CV increased from 3.1, 4.7 and 3.1% in PBS to 7.3, 7.2 and 5.4% in normal human serum for scFv A5, B11 and B5, respectively. Very similar results can be observed when comparing the inter-day %CVs in PBS of 4.3, 4.2 and 3.4% to those calculated in serum, 6.7, 7.6 and 5.6%.

To assess potential matrix interference, normal human serum spiked with standards of recombinant proteins AGR2 and MUC1 were compared to standards spiked in PBS. The recoveries in PBS, outlined in ***Tables, 4.5, 4.6*** and ***4.7***, were estimated from the calibration curve for each standard. Using this method the mean percentage recovery for the inter-day assay was calculated to be , 98.8, 99.1 and 107% for scFv A5, B11 and B5, respectively. These results indicate less than a 10% deviation from the actual

concentrations. The recoveries when the samples are analysed in normal human serum , observed in ***Tables 4.8, 4.9*** and ***4. 10,*** were calculated from the calibration curves wand found to be 102, 104 and 101.3% for scFv A5, B11 and B5, respectively. All average recoveries fell between the acceptable recovery limits of 80-120% with negligible differences in recovery percentages observed between the assay performed in PBS and normal human serum. From this it was concluded no matrix interference was occurring within the assay (Ong *et al.,* 2013).

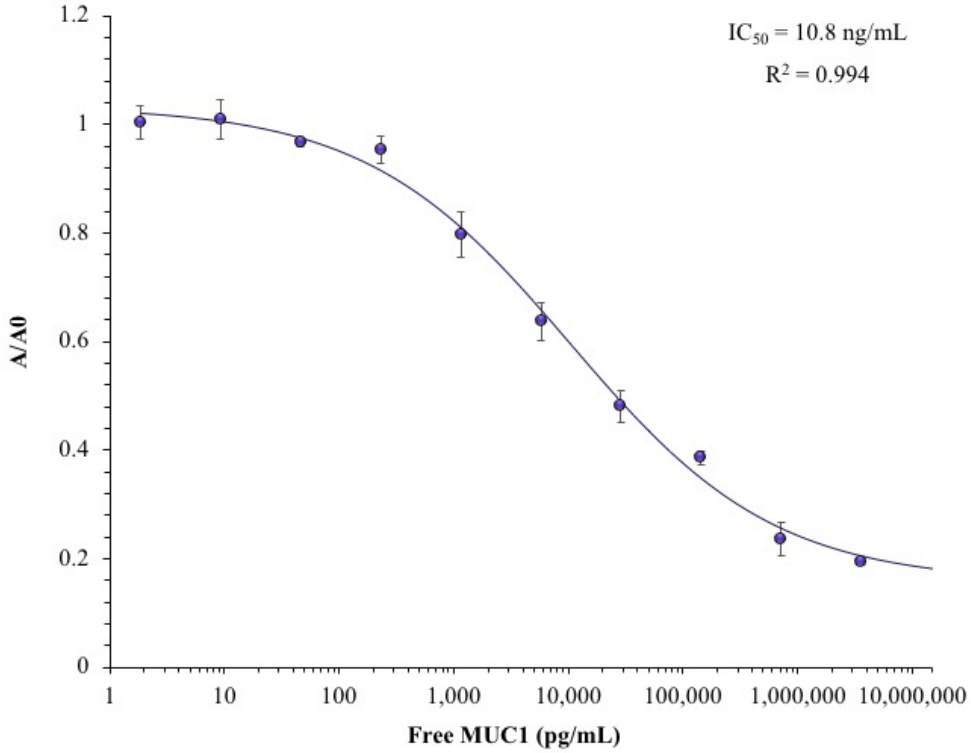

Figure 4.28 Inter-day assay calibration curve for anti-MUC1 scFv A5 in normal human serum

The calibration curve of clone A5 scFv in human serum was constructed using a 4-parameter equation in BiaEvaluation™. The inter-day assay means and CV are shown in ***Tables 4.8.*** *Each point on the curve is the mean of 3 replicate measurements analysed over 3 days. The absorbance of the evaluated samples was normalised by expressing the absorbance as a function of the blank standard (A/A0).*

Table 4.8 Intra – and inter-day assay CV and percentage accuracies for the anti-MUC1 scFv A5 in normal human serum.

Coefficient of variation (CV) was calculated by % CV=(S.D/Mean) x 100. The standard deviation (S.D) for intra-day analysis was calculated from 3 replicates analysis within a single assay, whereas the S.D for inter-day analyses was calculated from 3 replicates over 3 assays on 3 separate days.

	Intra-day			***Inter-day***		
MUC1 Conc. (pg/mL)	**CV (%)**	**Back Calculated Conc. (pg/mL)**	**Accuracies (%)**	**CV (%)**	**Back Calculated Conc. (pg/mL)**	**Accuracies (%)**
18,000,000	7.2	14,139,300	79	8.5	12,037,300	67
3,600,000	10.3	3,901,670	108	1.5	4,383,260	121
720,000	11.2	870,630	121	10.5	866,870	120
144,000	7.1	96,299	67	11.2	108,853	76
28,800	13.1	28,800	100	12.5	31,213	108
5,760	5.3	7,333	129	10.9	6,766	117
1,152	5.5	1,063	92	2.4	1,053	91
230	4.5	112	49	5.6	195	85
46	7.5	55	119	5.1	56.6	123
9	5.1	7.8	87	4.8	8.5	94
1.8	4.2	1.9	83	1.4	2.2	122

Table 4.9 Intra – and inter-day assay CV and percentage accuracies for the anti-AGR2 scFv B11 in normal human serum.

Coefficient of variation (CV) was calculated by % CV=(S.D/Mean) x 100. The standard deviation (S.D) for intra-day analysis was calculated from 3 replicates analysis within a single assay , whereas the S.D for inter-day analyses was calculated from 3 replicates over 3 assays on 3 separate days. Table cells that contain a "-" indicate that no value could be extrapolated as the data point did not fit the calibration curve.

	Intra-day			***Inter-day***		
AGR2 Conc. (pg/mL)	**CV (%)**	**Back Calculated Conc. (pg/mL)**	**Accuracies (%)**	**CV (%)**	**Back Calculated Conc. (pg/mL)**	**Accuracies (%)**
10,000,000	13.5	6,170,340	62	5.5	-	-
2,000,000	11.3	3,241,310	162	18	3,147,800	157
400,000	5.3	469,220	117	1.5	482,586	121
80,000	5.8	89,628	112	3.6	85,546	106
16,000	5.2	14,872	93	2.2	13,596	85
3,200	11.5	3,201	100	15.8	3,073	96
640	8.6	657	103	14	683	106
128	4.1	117	91	5.1	104	81
25.6	2.3	21.7	85	3.6	20.2	79
5.12	3.1	4.6	90	6.3	5.3	104
1.024	9.2	-	-	7.3	-	-

Table 4.10 Intra – and inter-day assay CV and percentage accuracies for the anti-AGR2 scFv B5 in normal human serum.

Coefficient of variation (CV) was calculated by % CV=(S.D/Mean) x 100. The standard deviation (S.D) for intra-day analysis was calculated from 3 replicates analysis within a single assay, whereas the S.D for inter-day analyses was calculated from 3 replicates over 3 assays on 3 separate days. Table cells that contain a "-" indicate that no value could be extrapolated as the data point did not fit the calibration curve.

	Intra-day			***Inter-day***		
AGR2 Conc. (pg/mL)	**CV (%)**	**Back Calculated Conc. (pg/mL)**	**Accuracies (%)**	**CV (%)**	**Back Calculated Conc. (pg/mL)**	**Accuracies (%)**
20,000,000	12.9	-	-	6.4	-	-
4,000,000	3.9	-	-	7.6	-	-
1,333,333	15.4	1,299,993	98	5.2	1,235,494	93
444,444	1.2	478,812	107	8.2	418,807	94
148,148	2.7	137,082	93	3.8	126,952	86
49,383	2.6	50,753	103	11.2	53,654	109
16,461	5.7	16,994	103	3.2	19,065	115
5,487	2.3	5,082	93	3.5	5,701	103
1,829	4.1	2,026	111	4.4	1,979	108
610	5.8	528	87	3.2	554	91
203	2.7	181	98	4.5	229	113

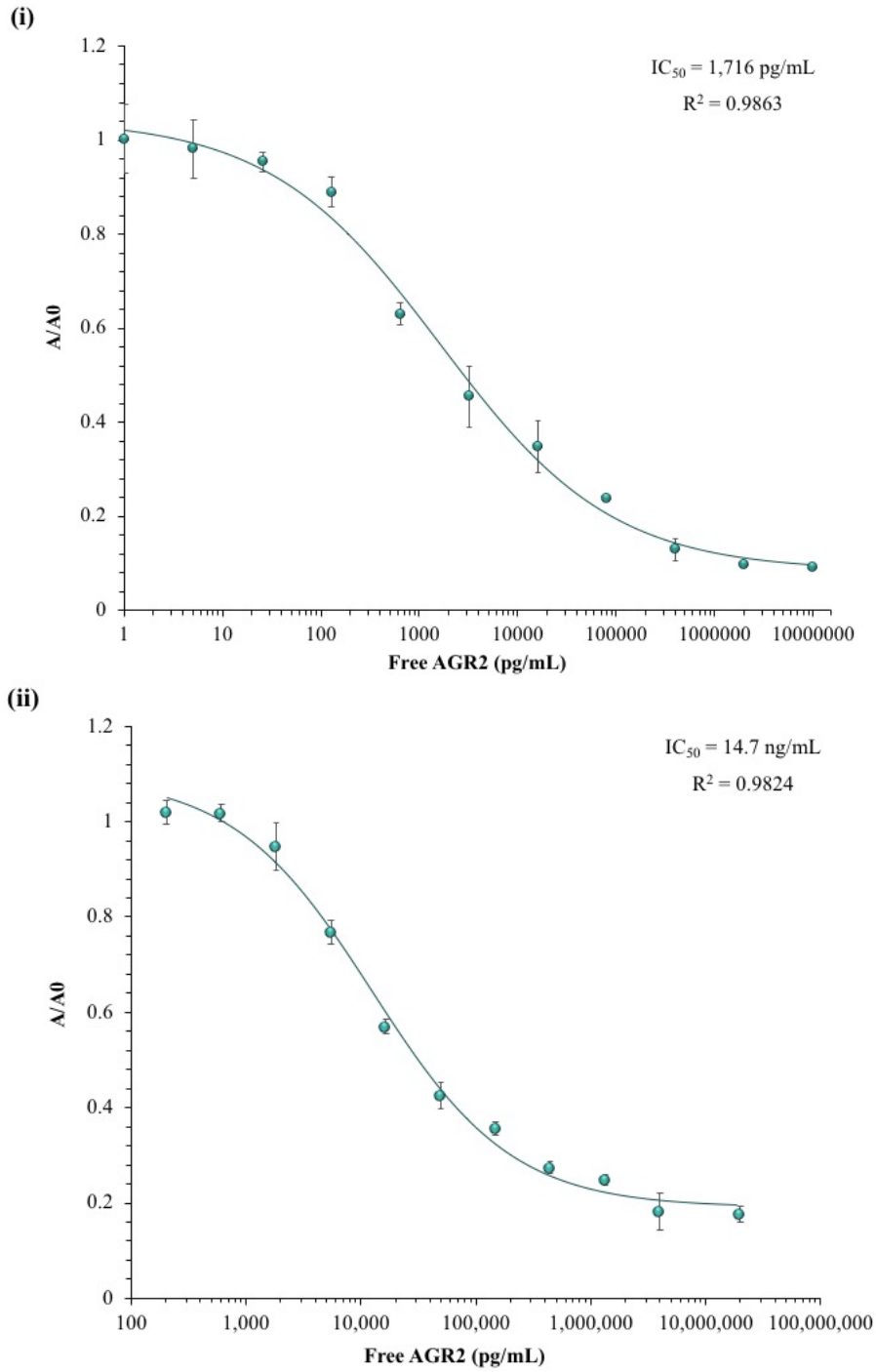

Figure 4.29 Inter-day assay calibration curve for scFv (i) B11 and (ii) B5 in normal human serum

The calibration curve of B11 ***(i)*** *and B5* ***(ii)*** *scFv in human serum was constructed using a 4-parameter equation in BiaEvaluation™. The inter-day assay means and CV are shown in* ***Tables 4.9*** and ***4.10.*** *Each point on the curve is the mean of 3 replicate measurements analysed over 3 days. The absorbance of the evaluated samples was normalised by expressing the absorbance as a function of the blank standard (A/A0).*

4.2.5.5.4 Determination of analytical limits

The limit of detection (LOD) is defined by Armbruster *et al* (1994), as the smallest concentration of analyte that produces a signal likely to be reliably distinguished from the limit of the blank (LOB). The LOD values of each antibody were calculated by selecting the mean normalised absorbance minus three standard deviations of the blank standard. When calculated extrapolated from the calibration curves the LOD values were determined as 40 pg/mL, 1 ng/mL and 20 pg/mL for B11, B5 and A5, respectively.

In order to experimentally confirm the LOD, precision assays were performed which provide accurate verification of the LOD using a smaller range of analyte concentrations. This experiment confirms the lowest concentration of analyte that can be reliably detected with a 95% certainty above the blank standard. The precision assay was performed by analysing 20 positive samples of, the previously verified LOD concentration, in conjunction with 20 samples fortified with twice the concentration of AGR2 as the LOD and 20 blank standards. From the calibration curve in normal human serum it was determined that the LOD for the anti-AGR2 scFv, B5, was ~1 ng/mL. Twenty replicates of 1 ng/mL AGR2, 2 ng/mL AGR2 and negative blank samples were assayed in a competitive format to investigate the functional detection limit of the scFv. In ***Figure 4.30*** it can be observed that 1 ng/mL AGR2 could be reliably distinguished from the blank replicates in 100% of samples, indicating that the actual LOD may potentially be lower than the previously calculated 1 ng/mL. Hence, further analysis of numerous lower concentrations could determine the functional detection limit. However, the successful generation of the other anti-AGR2 scFv, B11, which has a confirmed LOD of 40 pg/mL, as can be observed in ***Figure 4.31,*** renders further analysis of the B5 clone LOD redundant. ***Figure 4.32*** verifies the experimental LOD of the anti-MUC1 specific scFv, A5, as 20 pg/mL as it can be observed that 19/20 of the samples containing 20 pg/mL were reliably distinguished from the blank standard.

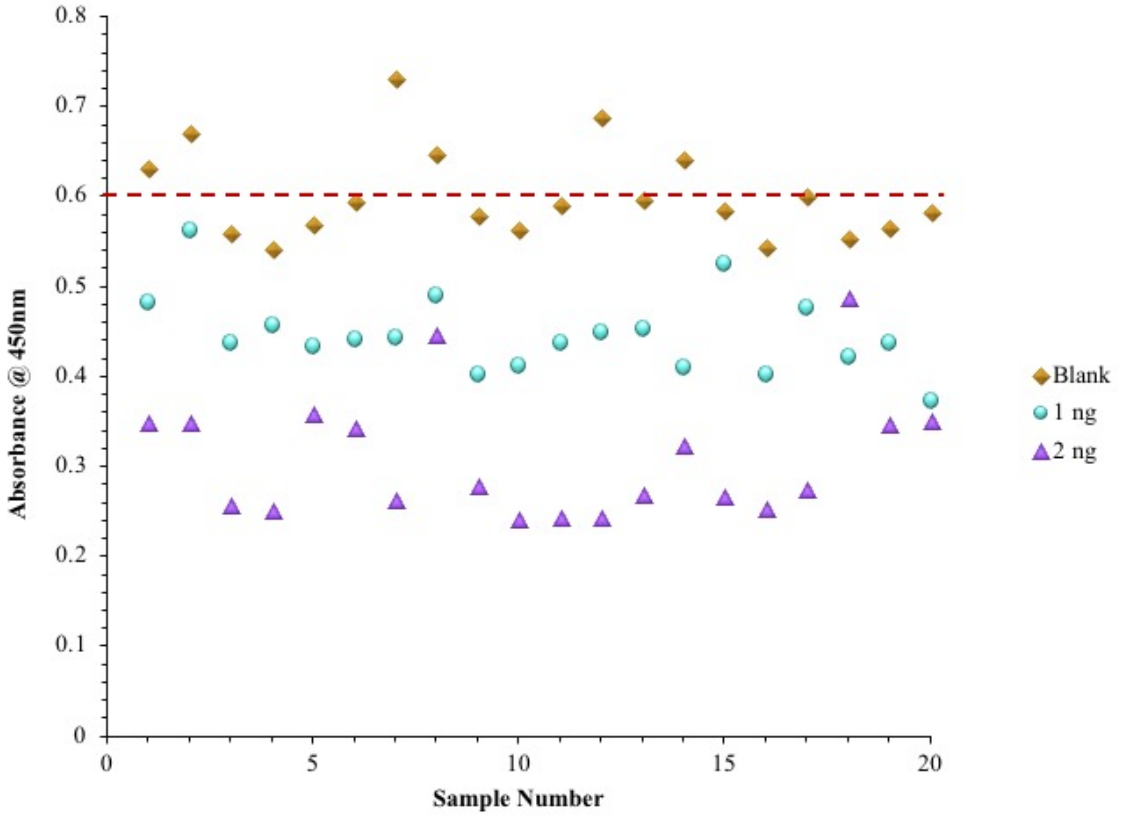

Figure 4.30 Precision assay for experimental verification of the B5 scFv LOD

The functional LOD is determined using 20 replicates of the blank standard, 20 replicates of 1 ng/mL AGR2 and 20 replicates of 2 ng/mL AGR2 in a competitive ELISA format with 1 µg/mL AGR2 coated on the immunosorbent plate. HRP-labelled anti-c-myc antibody was used to detect bound scFv. The dashed line indicates 95% compliance. This denotes the ability of the scFv to detect 95% of the samples as positive for AGR2 when compared to the blank standard. The dashed line was determined by the mean of the blank standards.

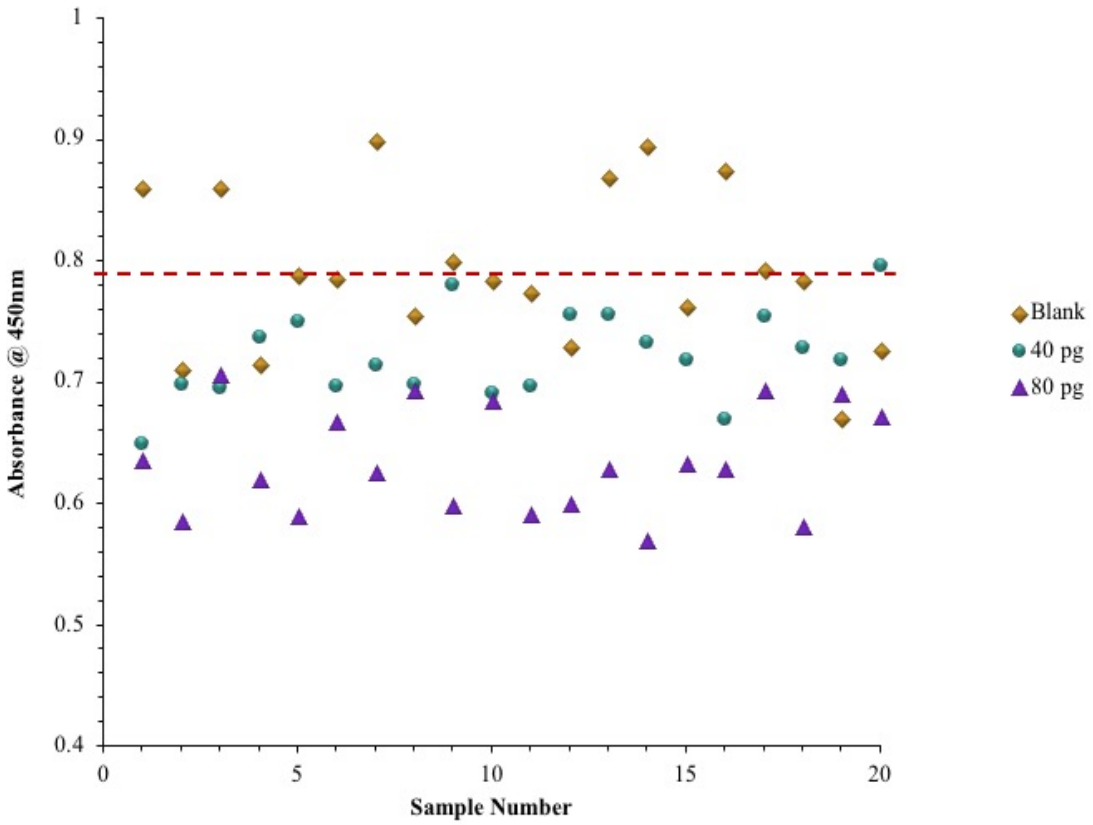

Figure 4.31 Precision assay for experimental verification of the B11 scFv LOD

The functional LOD is determined using 20 replicates of the blank standard, 20 replicates of 40 pg/mL AGR2 and 20 replicates of 80 pg/mL AGR2 in a competitive ELISA format with 1 μg/mL AGR2 coated on the immunosorbent plate. HRP-labelled anti-c-myc antibody was used to detect bound scFv. The dashed line indicates 95% compliance. This denotes the ability of the scFv to detect 95% of the samples as positive for AGR2 when compared to the blank standard. The dashed line is determined by the mean of the blank standards.

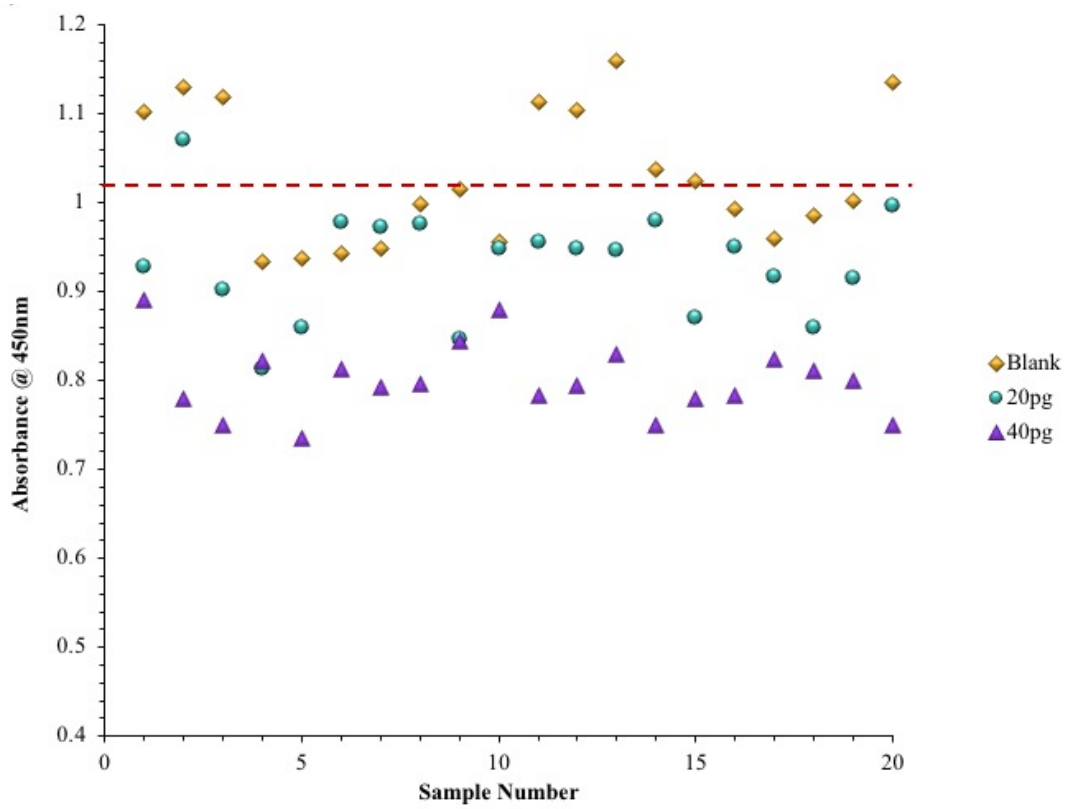

Figure 4.32 Precision assay for experimental verification of the A5 scFv LOD

The functional LOD is determined using 20 replicates of the blank standard, 20 replicates of 20 pg/mL MUC1 and 20 replicates of 40 pg/mL MUC1 in a competitive ELISA format with 1 μg/mL MUC1 coated on the immunosorbent plate. HRP-labelled anti-c-myc antibody was used to detect bound scFv. The dashed line indicates 95% compliance. This denotes the ability of the scFv to detect 95% of the samples as positive for MUC1 when compared to the blank standard. The dashed line is determined by the mean of the blank standards.

4.3 Discussion and Conclusion

Recombinant antibodies (rAb) have proven intensely beneficial as diagnostic agents as they can be produced against almost any target antigen (Groff *et al.,* 2015). RAbs are commonly developed by exploiting a hosts immune system to respond to the target antigen through immunizations. By this method diversity is achieved by the immune system, however, in synthetic libraries, such diversity is artificially created. Synthetic libraries can achieve greater diversity and it was shown that antibodies with high specificity and affinity against any target antigen can be isolated from these libraries (Robin *et al.,* 2014). Advantageously, these synthetic libraries eliminate the need for animals for the production of rAbs (Barbas and Wagner, 1995). Furthermore, as the resulting antibodies are based on human antibody genes, they have potential applications as therapeutic antibodies that shouldn't exhibit issues noted with non-human antibody reactions such as the HAMA reaction (Gretts *et al.,* 2010). Research in recent years has shown an increase in the emergence of these synthetic libraries. For example, in 2005 a human synthetic antibody phage display library was designed and constructed that boasted 3 billion individual antibody clones (Silacci *et al.,* 2005). In 2009, a synthetic human scFv library was created with six diversified CDRs which produced a final library diversity of 7.6×10^9 and Säll *et al.* (2016) designed two human synthetic scFv libraries and isolated 466 specific scFv against a diverse panel of 114 antigens using phage display (Yang *et al.,* 2009). The human synthetic Tomlinson I and J library , previously described in-depth, is a naïve human synthetic scFv library that was employed herein as a means to resolve issues encountered during attempts to select specific scFv from an immune murine library.

The aim of this chapter was to express, purify and employ the recombinant proteins, AGR2 and MUC1, for use in the isolation and characterization of specific scFv destined for inclusion into a multi-marker diagnostic panel. For scFv selection through panning and phage display, the recombinant MUC1 and AGR2 proteins were successfully expressed and biopanning, using the communal anti-Capan 1 murine library, described in *Chapter 3,* was performed. Unfortunately, no scFv were obtained. In pursuit of specific scFv with affinity for the recombinant proteins, the synthetic human naïve Tomlinson I

& J libraries were employed. These libraries completely circumvents the need for any additional animal use. Furthermore, the resulting scFv are constructed on a human-framework. While these antibodies are intended for diagnostic applications, each scFv here does have potential in therapeutics. Consequently, the resulting human-derived scFv are hugely beneficial, as they will not initiate an immune reaction if administered as a therapeutic (Harding *et al.,* 2010). Previous work has shown success in isolating specific scFv from the Tomlinson libraries against a variety of targets. An anti-CD133 scFv was developed from the scFv Tomlinson I and J libraries which, after testing in a competitive and indirect ELISA, exhibited specificity for CD133 and indicated that the developed scFv and commercial monoclonal anti-CD133 could compete with each other in binding with the recombinant CD133 antigen (Xia *et al.,* 2013). Another study in 2014 identified numerous antibodies from the Tomlinson libraries for the rapid diagnosis of norovirus. The resulting antibody fragments were characterized using SPR which showed nanomolar affinities (Huang *et al.,* 2014). Additionally, the Tomlinson libraries have been employed to develop a plethora of scFv against a variety of targets such as human fibrin clots and *Cryptosporidium parvum* (Han *et al.,* 2004; Boulter-Bitzer *et al.,* 2009).

In the research described in this chapter, scFv specific for AGR2 and MUC1 proteins were isolated from the human naïve synthetic Tomlinson I and J libraries. According to the literature, various anti-MUC1 recombinant antibodies have been previously developed in hosts such as camels, to target different diseases for such as breast and colon cancers (Rahbarizadeh *et al.,* 2005; Thie *et al.,* 2011). In 1997, an anti-MUC1 scFv of the murine anti-MUC1 monoclonal antibody C595 was produced for detection of MUC1 protein on the surface of human bladder and breast carcinoma tissues (Denton *et al.,* 1997). Later, murine anti-MUC1 scFv were isolated to target breast and prostate cancers with affinities ranging between 1.7×10^8 and 8.2×10^8 M^{-1}, which falls between the satisfactory scFv binding affinities for targeting antigens on solid tumours (Albrecht *et al.,* 2007). In another study, an anti-MUC1 scFv was generated from the variable domains of the humanised mAb huHMFG1, however, this antibody exhibited poor stability and solubility and the affinities of the scFv could not be accurately determined in ELISA, however the SPR results analysis gave low affinity values (Krauss *et al.,* 2004). Comparably, while kinetic analysis was not performed by SPR, the functional limit of detection (LOD) for the anti-MUC1 scFv generated herein, was calculated and

experimentally confirmed as 20 pg/mL. According to the current literature, anti-MUC1 scFv are primarily created for targeting breast cancers and are often humanized and therefore are not fully human. Humanized antibody generation begins with animal immunizations with the target protein and specific antibodies are identified. Portions of the initial antibody that are host-derived are grafted onto a human antibody sequence becoming 80-95% human (Mallbris *et al.,* 2016). While many approved mAbs are humanized, the process is technically demanding. Due to the advent of synthetic immune human libraries, it is now possible to select for fully human antibodies against an almost infinite number of antigens with ease(Chames *et al.,* 2010). In 1998, a study successfully isolated an anti-MUC1 scFv from a human naïve library and illustrated its potential in immunohistochemistry (Henderikx *et al.,* 1998). However, from the literature, it is evident that the anti-MUC1 scFv developed herein is the first fully human anti-MUC1 scFv isolated from a synthetic immune library developed for use against PDAC.

The field of available anti-AGR2 antibodies is dominated by mAbs. In 2010, a study carried out by Wu and colleagues prepared a mouse monoclonal against AGR2 known as clone 18A4 which binds to AGR2 in WB, immunostaining and immunoprecipitation. This mAb underwent humanization from which Fab and scFv fragments are available. Furthermore, a humanized mAb against AGR2, Agtuzumab has shown potential as a therapeutic agent by blocking the role of AGR2 in cell migration and proliferation assays (Li *et al.,* 2013). Most recently, Qudsia and others, constructed a novel scFv display library in which Agtuzumab scFv is displayed on the surface of HEK-293T cells. It would appear, the recombinant antibodies that are available are produced with the intended use for therapeutic applications (Guo *et al.,* 2016). Therefore, a significant niche exists for the development of anti-AGR2 scFv for PDAC diagnosis for which the scFv generated within this work is extremely applicable due to its low functional limit of detection of 40 pg/mL.

Upon evaluation of the performance of the scFv generated within this work in comparison with the information available about antibodies of the same target specificity, both have demonstrated strong specify for their cognate antigen down to picogram concentrations with properties rendering them highly applicable both diagnostically and therapeutically.

They appear to exceed many previously generated antibodies in terms of the performance studies undertaken. Further extensive characterisation of the kinetics of the anti-MUC1 and anti-AGR2 scFv generated needs to be carried out by surface plasmon resonance SPR which measures biomolecule binding and kinetics such as antigen-antibody interactions, shown in ***Figure 4.33***. Kinetic characterisation is required to determine the association and dissociation rates constants of these antibodies-antigen affinity interactions so that they can be effectively incorporated into the diagnostic panel for improved PDAC diagnosis (Leonard *et al.,* 2017). Furthermore, in order to be characterised as diagnostic antibodies, they must be tested initially in dot blot and western blot analysis to ensure they bind to their cognate antigen linear and conformational epitopes. This will also provide the working concentration of these scFv which can then be applied in immunohistochemistry analysis on pancreatic tumor cohorts. To determine the scFv efficiency in testing their cognate antigens in serum, a lateral flow could be employed whereby the scFv are immobilised onto a lateral flow device for detection of AGR2 and MUC1. Moreover, as previously mentioned both the MUC1 and AGR2 proteins are involved in the progression and cell proliferation of pancreatic cancer cells thus both have potential as therapeutic targets. Consequently, either scFv could potentially be reformatted into a bispecific antibody that can be employed as a potent chemotherapeutic. This bispecific antibody, known as bispecific T-cell engager (BiTE) is described in detail in *Chapter 5.*

In summation, two recombinant proteins were sufficiently expressed, purified and used for the successful isolation of three specific human antibodies from the Tomlinson I & J library. An immunoassay was developed and validated for each scFv, both in PBS and in normal human serum, with each showing excellent precision, exemplified by CV values well under 20%. The LODs identified for anti-AGR2 scFv B11 and anti-MUC1 scFv A5 were 40 pg/mL and 20 pg/mL, respectively, suggesting that they are ideal candidates for incorporation into the proposed diagnostic panel. Furthermore, as the scFv described are human-derived they are ideally suited as possible therapeutic agents. Future work to evaluate their applicability in the targeted treatment of PDAC could prove very promising.

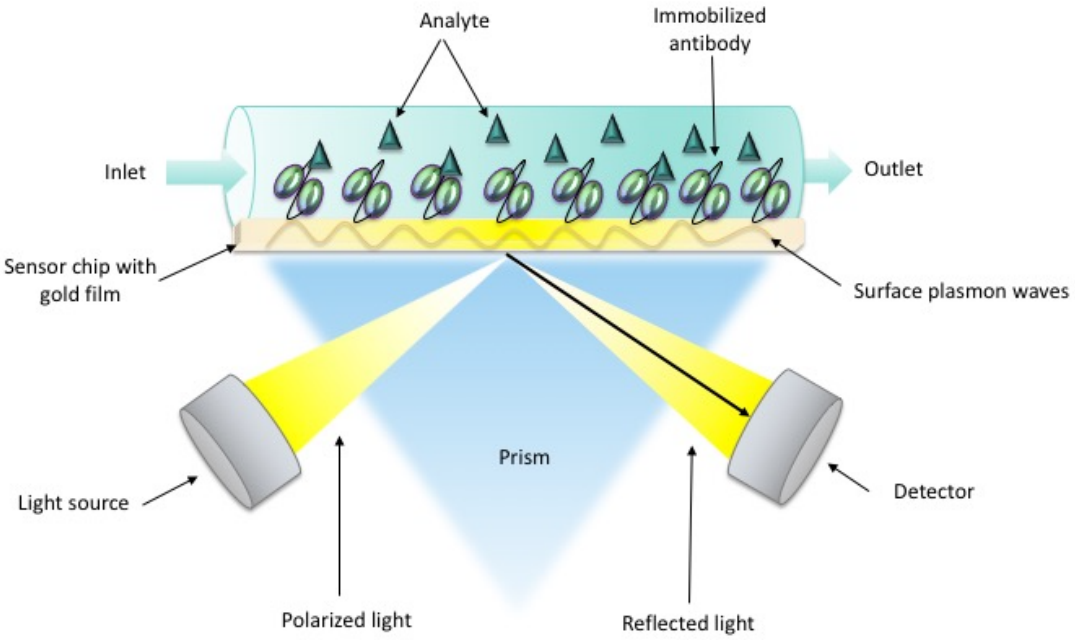

Figure 4.33 Illustration of surface plasmon resonance (SPR)

The antibody is functionalised to the metal surface of the sensor chip. The antigen is then flowed across the system. When an affinity interaction occurs between the antibody and the antigen a shift in the surface refractive index alters, changing the angle of incident light resulting in a surface plasmon. This is measure in resonance units (RU) and is plotted in a sensorgram indicating the binding kinetics of the antibody to the target antigen (Lago et al., 2018).

Chapter 5

The isolation of an avian anti-CD3ε scFv and the generation of a bispecific T-cell engager (BiTE).

Chapter Outline

The focus of the research described in this chapter is the generation of an anti-CD3ε scFv for incorporation into a bispecific antibody, known as a bispecific T-cell engager (BiTE). Initial work undertaken attempted to isolate CD3ε -specific antibody fragments from a murine anti-Jurkat scFv library. This yielded a poor phage library size, hindering the selection of high quality CD3ε -specific scFv. Subsequently, an avian anti-Jurkat library of an appropriate size was screened and an anti-CD3ε scFv was successfully isolated. The resulting antibody was extensively characterized in conjunction with an anti-HER2 scFv, previously generated within the ABG group (data not shown). The antibody fragments were then manipulated to produce a 'BiTE' construct using a 'proof-of-concept' strategy which involved PCR and cloning techniques. Initial attempts produced a BiTE antibody with limited binding capabilities. Consequently, the protocol was modified to overcome this issue. Thereafter, the BiTE was successfully expressed, purified and preliminary binding analysis indicated functional dual binding. An overview of the approach is shown (***Figure 5.1***).

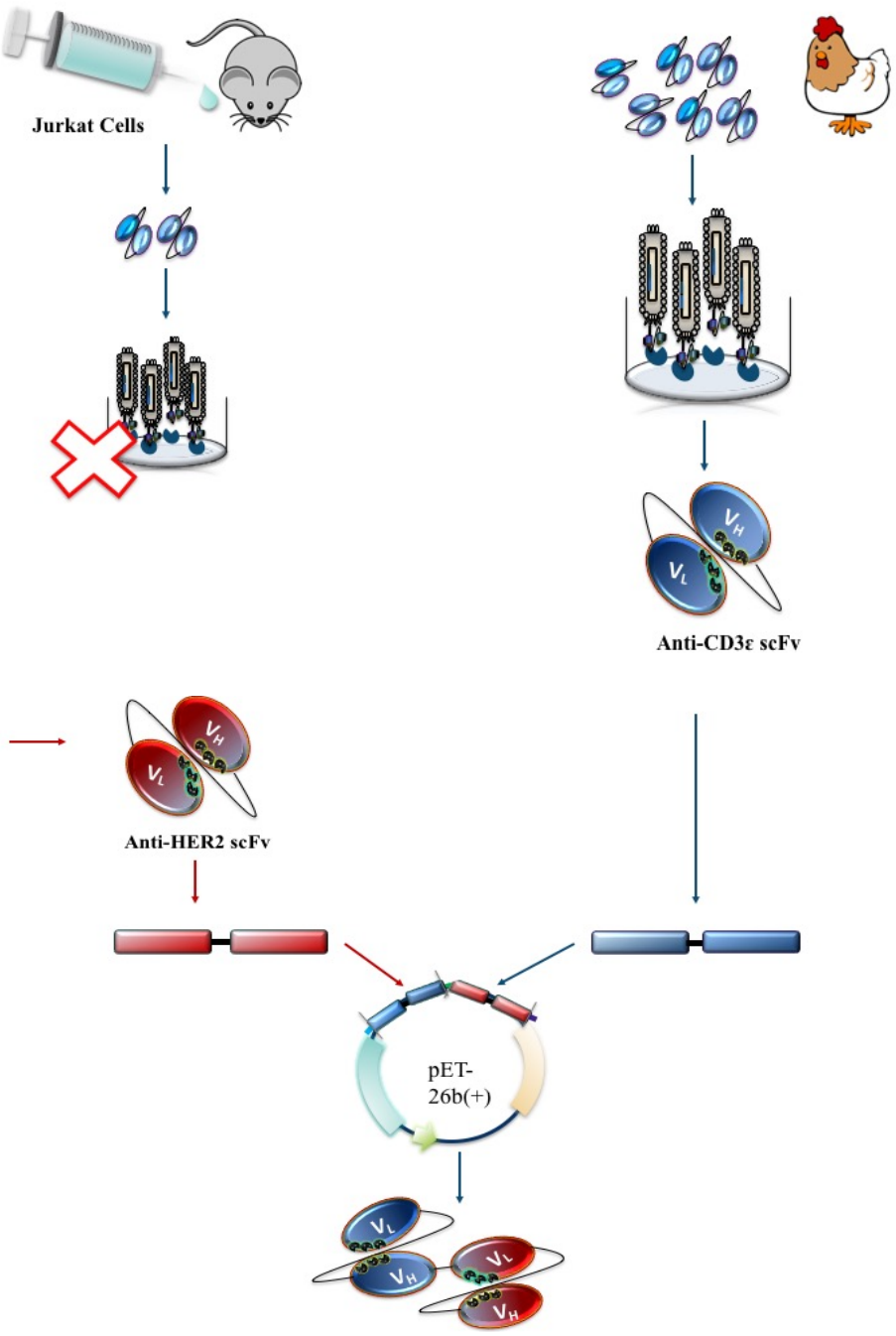

Figure 5.1 Illustration of workflow for Chapter 5

This diagram illustrates the research described within this chapter. Attempts to isolate an anti-CD3ε scFv from a murine anti-Jurkat library were unsuccessful. To resolve this, an avian anti-Jurkat library was screened, and an anti-CD3ε scFv successfully isolated. By combining a previously generated and characterised anti-HER2 scFv with the anti-CD3ε scFv, a bispecific T-cell engager was created and the binding capabilities evaluated.

5.1 Introduction

Due to the aggressive nature of pancreatic cancer, the development of novel targeted therapeutic options is imperative. The current methods of treatment, which involve the gold standard chemotherapy, gemcitabine, have limited success in increasing overall survival (Michl *et al.,* 2013; Buchsbaum *et al.,* 2014; Saif, 2014; Spadi *et al.,* 2016). It is evident that alternative treatments options must be explored. One such method, described herein, involves the exploitation of antibody applications and immune system mechanisms. More specifically, this strategy employs cytotoxic T-cells, potent killer-cells of the immune system, to directly target pancreatic tumour cells. T-cells have beneficial qualities for cancer therapeutics as they are abundant, infiltrate tumours, proliferate once activated and have the capability to kill more than once (Chames *et al.,* 2009; Dahlén *et al.,* 2018). A bispecific T-cell engager is an immunotherapeutic molecule for cancer treatment that is specific for both CD3 (a component of the TCR-CD3 complex) found on T-cells and a given tumour associated antigen (TAA) on tumour cells (Sedykh *et al.,* 2018).

The T-cell receptor (TCR) is an antigen-receptor composed of 6 polypeptides located on the surface of T-cells (***Figure 5.2***) (Alcover *et al.,* 2018). It is involved in the recognition of antigen fragments that are presented by major histocompatibility complex (MHC) molecules. This activates the T-cell and results in a cascaded immune response to the antigen presented. The TCR is associated with CD3 on the T-cell surface. CD3 is responsible for transmitting an intracellular signal when the TCR binds the MHC complex (Van der Merwe and Dushek, 2011; Ngoenkam *et al.,* 2017). The CD3 complex is composed of CD3 epsilon, gamma delta and zeta. CD3 epsilon (CD3ε) is a non-glycosylated 20kDa polypeptide chain which plays a vital role in T-cell development (Birnbaum *et al.,* 2014). Normally, a T-cell requires an antigen and secondary stimuli to become activated. When activated, they induce cell-mediated immune mechanisms by cytotoxic T-cell (CD8), an increase in antibody responses by T-helper cells (CD4) and increased antibody production by B cells. T-cells come into contact with antigen presenting cells (APC) displaying the MHC protein and specific antigen (Cochran *et al.,* 2000). Simultaneously, a variety of co-stimulatory and co-inhibitory receptors then direct T-cell function, for example, CD28 which binds to the ligand B7 on T-cells, provides

essential co-stimulatory signals for T-cell growth and survival (Chen and Flies, 2014). BiTEs, however, negate these processes and can activate T-cells through the CD3 complex without MHC antigen presentation, T-cell receptor specificity or co-stimulation (Horn *et al.,* 2017).

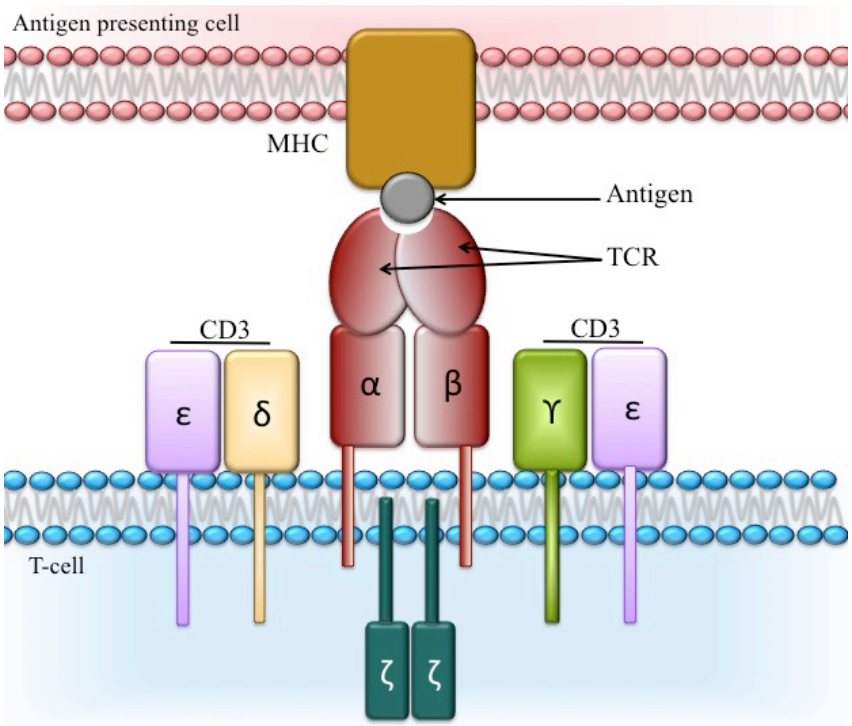

Figure 5.2 Illustration of the TCR-CD3 complex

The TCR is composed of two polypeptide chains, α and β, which are covalently linked by disulphide bonds. These chains contain an amino terminus, a constant region, variable and carboxy regions. The cytoplasmic tail of the α and β polypeptides are involved in signal transduction pathways. The entire TCR complex is composed of the α β chain, ζ proteins and CD3 complex. The CD3 complex contains ε, γ, and δ polypeptide chains (after Gascoigne, 2008 and Alcover et al., 2018).

The dual-binding specificity allows the BiTE to link a T-cell with the tumour cell, resulting in the formation of an immunological synapse. This releases perforins and granzymes from the T-cell which enter the tumour cell and cause cell apoptosis (Byrne *et al.,* 2013; Yuraszeck *et al.,* 2017). In order to successfully elicit the immunological synapse, the BiTE must simultaneously bind the T-cell and the TAA on the tumour cell. Previously, Brischwein and colleagues demonstrated that the activation of the T-cell is entirely dependent on target-cell binding, with single sided binding found to be

insufficient (Brischwein *et al.,* 2007). Further data has indicated that BiTEs preferentially activate memory T-cells (Smits and Sentman, 2016). T-cells employ two methods to induce target cell death. The first involves stimulation of death receptors on target tumour cells and the second, a granule-mediated pathway, is accomplished by the formation of a cytolytic synapse. After the formation of the cytolytic synapse, T-cells exocytose granzymes and perforin which form pores in the tumour cells and initiate apoptosis (Ross *et al.,* 2017). BiTEs are useful therapeutic agents for pancreatic cancer as the 'normal' T-cell anti-tumour response is often insufficient. Some cancer cells, such as cancer stem cells which can cause metastasis and have the ability to self-renew, have ability to evade T-cell mechanisms (Stieglmaier *et al.,* 2015; Zhao, 2016; Gnanamony and Gondi, 2017).

BiTEs currently in clinical trials include, Blinatumomab which targets CD19+ malignancies, MT-110, an anti-EpCAM BiTE for solid malignancies, MT-111 (against CEA), which is currently in trials for treating colon cancer, and AMG112, a possible treatment for prostate cancer (Huehls *et al.,* 2014; Krishnamurthy and Jimeno, 2018). The BiTE MT110, specific for EpCAM/CD3, has shown promising results for use in the elimination of primary pancreatic cancer stem cells (Cioffi *et al.,* 2012). Furthermore, the MG1122 BiTE, which binds to MSLN, has provided encouraging results, with data suggesting it effectively results in tumour cell death (Park *et al.,* 2018). These examples are of particular therapeutic importance as they illustrate the beneficial effects of a BiTE in targeting PDAC. Due to the success of MT110 and blinatumomab (CD19 x CD3ε antibody) the anti-CD3 scFv described herein was also generated against CD3ε. (Brischwein *et al.,* 2006; Riethmüller, 2012; Osada *et al.,* 2015).

5.1.1 Bispecific T-cell engager (BiTE) generation

This section introduces a 'proof-of-concept' strategy for the generation of a BiTE. This approach offers a flexible, therapeutic option where any TAA- specific scFv can be cloned into the vector construct designed, to create a BiTE against the desired antigen. It is a widely applicable approach as this flexibility means it is not disease-limited. For the purpose of this research, a previously generated anti-HER2 scFv was employed as the TAA arm of the BiTE (***Figure 5.3***). While Human Epidermal Growth Factor 2 (HER2) overexpression has been reported in nearly 45% of PDAC cases, very little evidence exists regarding its use an appropriate marker for pancreatic cancer therapy (Harder *et al.,* 2012).

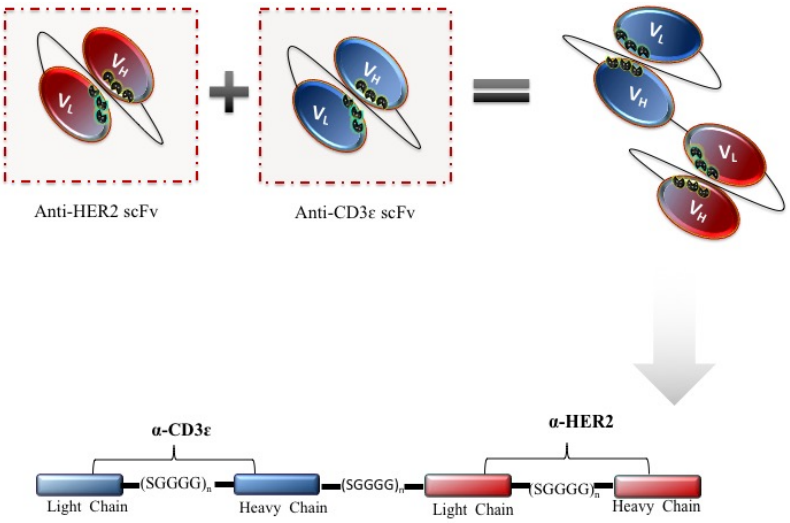

Figure 5.3 Diagrammatic representation of BiTE formation

A schematic of the proposed BiTE cloning construct, composed of an anti-HER2 scFv and anti-CD3ε scFv, linked by a flexible glycine/serine linker.

As previously described in *Chapter 1,* there are a plethora of bispecific antibody formats that are generated using a variety of approaches from chemical conjugation to hybrid-hybridomas. However, these are plagued with issues such as batch-to-batch variation and non-functional by-products (Byrne *et al.,* 2013). To alleviate these issues, recombinant techniques were embraced (Brinkmann and Kontermann, 2017). The most common recombinant strategy for developing bispecific antibodies (bsAb) is through the fusion of two scFv, known as a tandem scFv (Zhang *et al.,* 2017). BiTEs are often constructed using DNA-shuffling and ligation techniques, where the 'tandem' BiTE gene is recombinantly constructed and ligated into the expression vector (Wiemik *et al.,* 2013). Previous research performed by Zou and colleagues (2015), demonstrated construction of a BiTE with an additional hIgG1 Fc region. Whereby, they synthesized both scFv genes with cloning sites and ligated them separately into the expression vector. The construct cloning technique described herein, is based from this research described by Zou and colleagues (2015). The concept behind the devised cloning strategy involves specifically designed primers that incorporate desired restriction sites into an avian-derived scFv. These sites allow for enzymatic digestion and directional cloning of the scFv into the pET-26b(+) expression vector (***Figure 5.4***). The concept provides complete design flexibility as the anti-TAA scFv gene can be removed by these restriction sites and replaced by an scFv specific to a different target antigen of interest. The following sections describe the evaluation of this bispecific antibody construction approach.

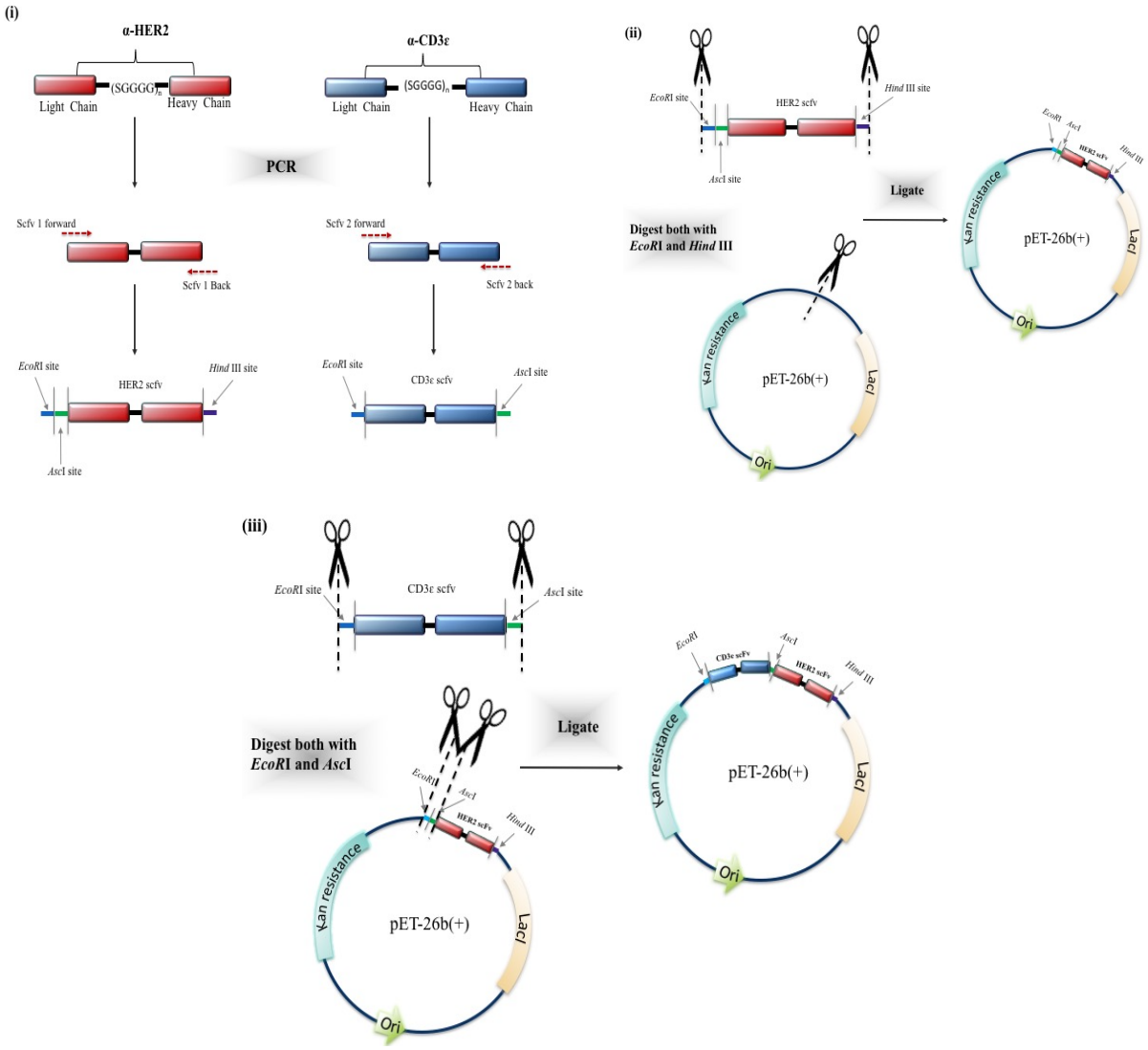

Figure 5.4 Strategy for the creation of a Bispecific T-cell Engager (BiTE)

(i) *Primers were designed to amplify the two scFv of interest and incorporate the requisite digestion sites* ***(ii)*** *The anti-HER2 scFv and the pET-26b(+) expression vector were digested using EcoRI and HindIII and the scFv ligated into the pET-26b(+) vector.* ***(iii)*** *The anti-CD3ε scFv and the pET-26b(+)vector, containing the anti-HER2 scFv, were digested with EcoRI and AscI restriction enzymes. The AscI site lies within the anti-HER2 scFv gene sequence to ensure directional cloning of the anti-CD3ε scFv. The anti-CD3ε scFv was ligated into the pET-26b(+)vector containing anti-HER2 scFv. Full map of the pET-26b(+) vector can be found in Appendix C.*

5.2 Results

5.2.1 Generation of anti-CD3ε scFv fragments

5.2.1.1 Propagation of Jurkat E6.1 clone cell line

The Jurkat E6.1 clone line (ATCC® TIB-152™) is a T-lymphocyte cell line, established from the peripheral blood of a 14-year-old boy (Mezencev and McDonald, 2011). It was selected for the immunization of three BALB/c mice as it expresses the CD3ε antigen. This cell line was propagated and maintained as described in *Sections 2.14.1.1 – 2.14.1.3.*

5.2.1.2 Immunisation of BALB/c mice with Jurkat E6.1 clone cell line

Three BALB/c mice were immunised subcutaneously with equal parts of a suspension composed of Jurkat E6.1 clone cells and Freund's complete adjuvant. Each mouse received 1 x 10^6 viable cells in sterile 1 X PBS. An initial immunisation was carried out, followed by 5 subsequent boosts mixed with Freund's incomplete adjuvant. All boosts contained the same number of viable cells as the initial immunisation. Each boost was administered 14 days apart. After four boosts, an antibody serum titre determination was performed by ELISA, against a commercially sourced human CD3ε protein (Antibodies-online GmbH).

5.2.1.3 Murine serum antibody titre determination

An ELISA was performed on a Nunc MaxiSorp™ 96-well plate coated with 1 µg /mL CD3ε and probed using varying dilutions of serum (1/100-1/200,000 in 1% (w/v) BSA in 1 X PBS). A sufficiently high immune response of over 1/200,000 was observed, indicating a high level of specific mRNA, ideal for the generation of a recombinant anti-Jurkat antibody library (***Figure 5.5***). The three mice were sacrificed and the B-cells were harvested from the spleens.

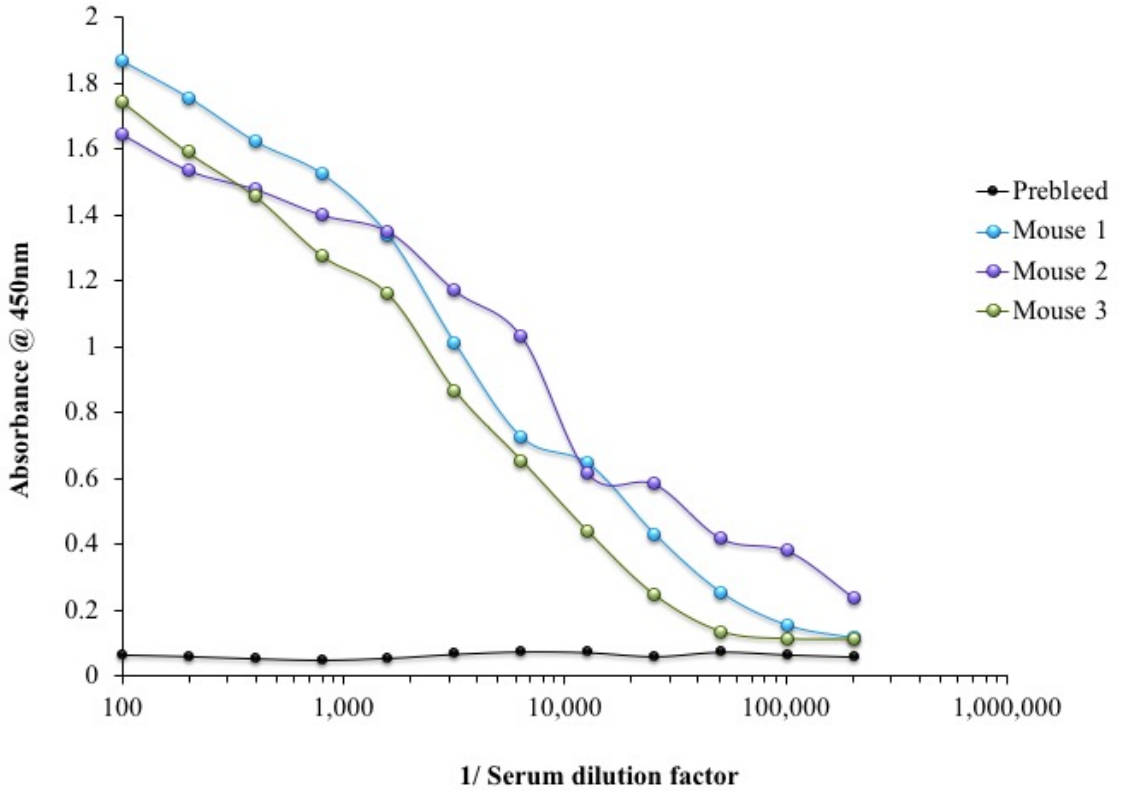

Figure 5.5 Titration of serum antibodies, obtained from mice immunised with Jurkat E6.1 clone cells after 4 boosts, determined by ELISA against CD3ε protein

Titration of serum antibodies obtained from 3 mice immunised with the Jurkat E6.1 clone cells after 4 boosts, against the protein CD3ε, as determined by ELISA. A pre-bleed was taken from the mice prior to immunisation. This was used as a control to compare the immune response after exposure. The bound antibodies were detected using a HRP-labelled goat anti-mouse IgG antibody. There was a significant response to CD3ε in the sera from all three mice.

5.2.1.4 Isolation of RNA from spleen B-cells and cDNA synthesis

The spleens were removed from the three mice and homogenised in TriZol. Total RNA was carefully extracted from the homogenized spleen samples and then quantified using the Nanodrop™ ND-1000. First-strand cDNA synthesis was performed by reverse transcription. This cDNA template was then used to amplify the variable light (λ and κ chains) and heavy chain genes.

5.2.1.5 Primer optimisation for the murine variable heavy and light chain genes

A standard PCR protocol using My*Taq*™ Red Mix 2X DNA polymerase was used for the optimisation of the variable heavy (V_H) and light region (V_κ) primers. The optimisation of the forward primers for the amplification of the V_κ and V_H chain genes was successful, resulting in substantial amplification. The primers were mixed in the volumes advised by Barbas *et al.,* (2001) and were subsequently employed for large-scale amplification of the V_κ and V_H chain genes (***Figure 5.6***).

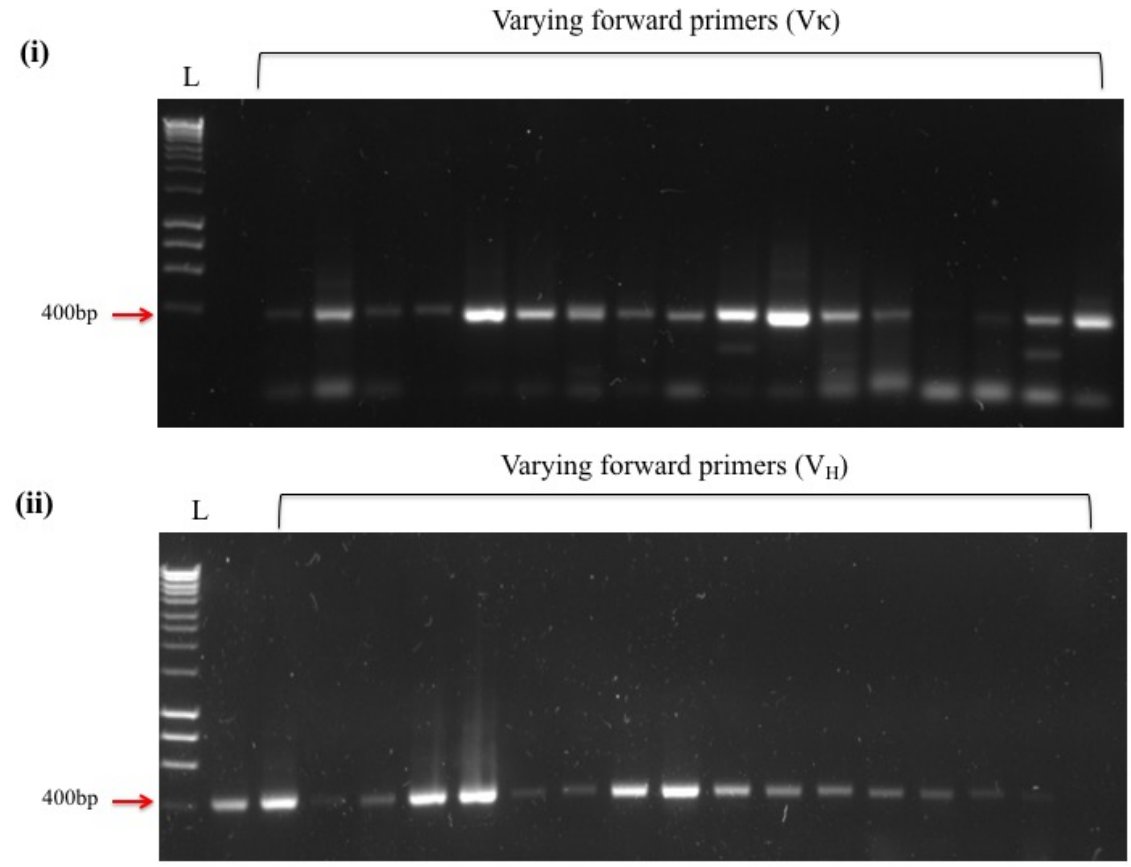

Figure 5.6 Optimisation of primer combinations

(i) *Optimisation of primer combinations to amplify murine V_κ from synthesised cDNA derived from the Jurkat E6.1 clone cell-immunised mice. Amplification was performed using MyTaq™ Red Mix 2X and the manufacturer's recommended PCR conditions.* ***(ii)*** *Optimisation of primer combinations to amplify murine V_H. The same conditions as those used for the amplification of V_κ were followed. L = 1kb Ladder (Bioline HyperLadder™).*

5.2.1.6. PCR optimisation for the murine V_H, Vκ and Vλ generation

A standard protocol was used for the amplification of the variable chain genes from the reverse transcribed cDNA (Barbas *et al.,* 2001). All regions amplified successfully, with no subsequent optimisation required (***Figure 5.7***). The variable fragments were gel-purified and linked by splice by overlap extension PCR (SOE-PCR).

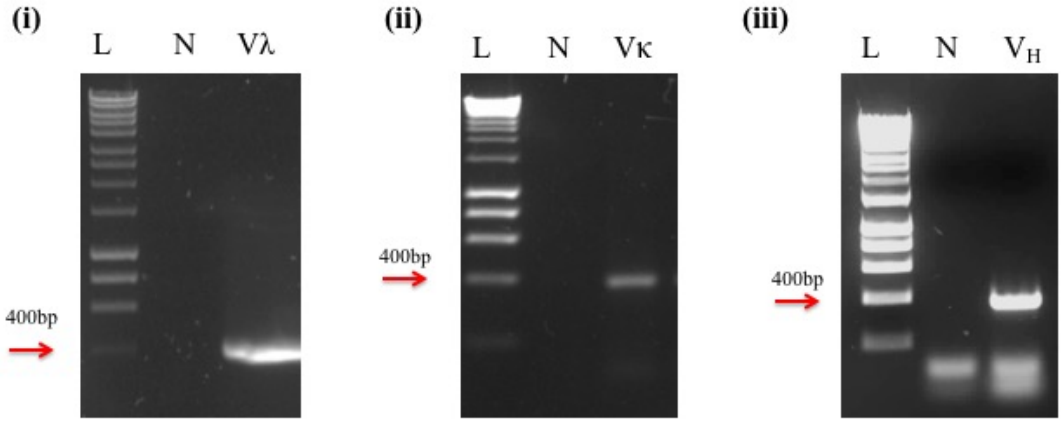

Figure 5.7 Amplification of murine variable regions

The variable ***(i)*** *Vλ,* ***(ii)*** *Vκ and* ***(iii)*** *V_H regions were amplified from synthesised cDNA. Amplification was performed using MyTaq™ Red Mix 2X using the manufacturer's recommended PCR conditions. L = 1kb Ladder (Bioline HyperLadder™). N = Control lane (This is a sample containing all the components of the PCR without the cDNA template).*

5.2.1.7. Splice by overlap extension (SOE) –PCR of the V_H and V_L chains

The gel-purified variable light and heavy chains were overlapped using SOE-PCR to generate the full-length scFv product. The cyclic extension time and final extension step time were doubled to favour the overlap of the variable chains (Lorenz, 2012). The SOE-PCR was performed under the standard conditions for My*Taq*™ Red Mix 2X polymerase, as outlined in *Section 2.12.2.6,* using equal concentrations of the purified variable domains as the DNA template. This yielded a successful variable domain overlap with a dense band present at the expected 800bp size. This PCR was performed large-scale (***Figure 5.8***).

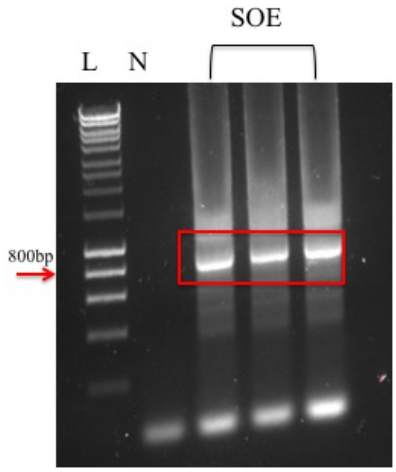

Figure 5.8 Splice by Overlap Extension-PCR of the amplified V_H and V_L fragments. *Successful amplification was observed at the expected 800bp band. L = 1kb Ladder (Bioline HyperLadder™); N = Control lane without DNA template; SOE = SOE-PCR amplification.*

5.2.1.8 Library construction

The SOE-PCR product was gel-purified, ethanol-precipitated, and subsequently digested using the *Sfi*I restriction enzyme. Concurrently, the pComb3XSS vector was grown and purified. The pComb3XSS vector was digested using *Sfi*I restriction enzyme to produce two products, the digested pComb3XSS and the excised Stuffer fragment (***Figure 5.9***). The digested vector was treated with Antarctic phosphatase to dephosphorylate the digested ends, ensuring the vector does not re-ligate. The digested vector and SOE-product were resolved on and purified from, 0.6% (w/v) and 1.5% (w/v) agarose gels, respectively.

The gel-purified *Sfi*I-digested products were concentrated by ethanol-precipitation and quantified on the NanoDrop™ 1000. The purified SOE product was ligated into the pComb3XSS vector using T4 DNA ligase. The ligated product was ethanol-precipitated, resuspended in MGH_2O and transformed into XL1-Blue electrocompetent *E. coli* cells using a Gene Pulser ™, as described in *Section 2.13.2.1* .

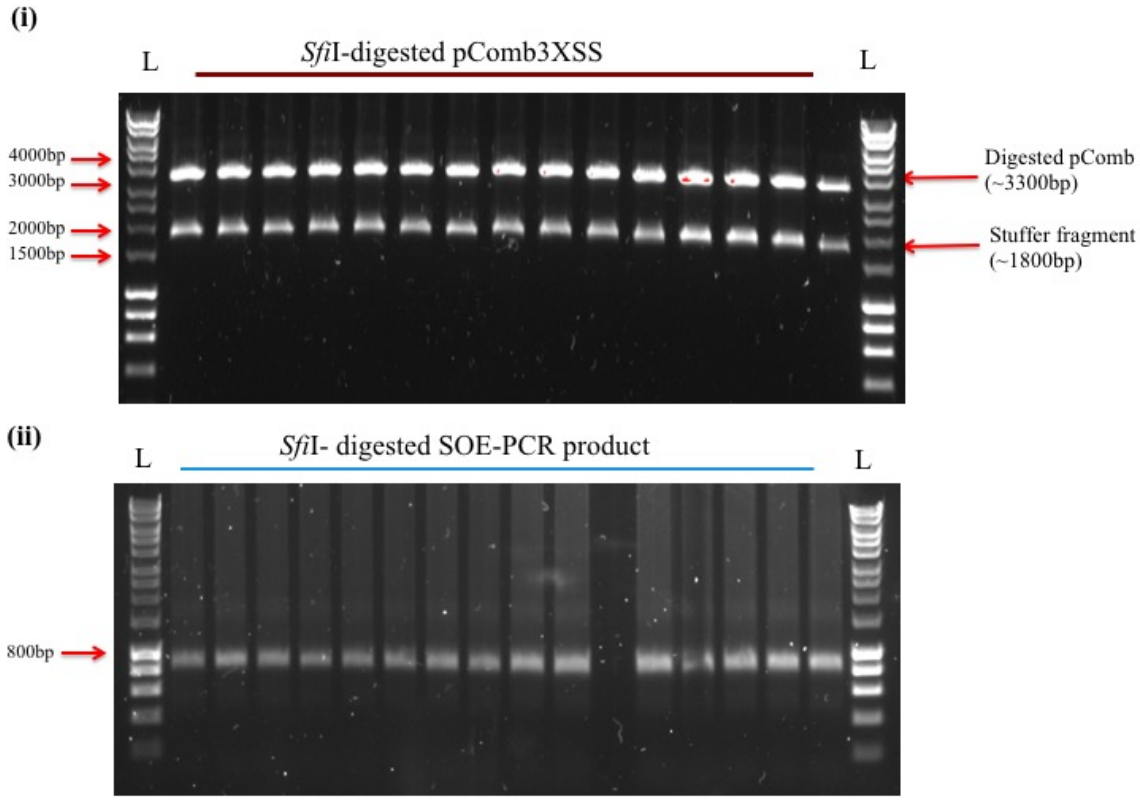

Figure 5.9 Digestion of the SOE product and pComb3XSS phagemid vector using SfiI enzyme

Qualitative analysis of ***(i)*** *SfiI- digested pComb3XSS phage display vector and* ***(ii)*** *SfiI-digested overlap product via agarose gel electrophoresis. L = 1kb Ladder (BiolineHyperLadder™)*

5.2.1.9 Library enrichment via panning against a CD3ε protein

Following vector transformation, the calculated library size of the murine anti-Jurkat scFv library produced was ~10^5 cfu/mL. It is advised that the library size should be greater than 10^6 cfu/mL for successful isolation of specific scFv, with library sizes of 10^7- 10^8 considered reasonable (Barbas *et al.,* 2001; Bazan *et al.,* 2012). An immune librarys' ability to yield high-affinity antibodies depends on the size of the immune library and the quality of the initial cloning step (Weber *et al.,* 2014). Simply put, the probability of isolating high-affinity scFv increases with library size (Ponsel *et al.,* 2011; Fantini *et al.,* 2017). It is possible that the limited diversity of the immune library was a result of inefficient variable gene assembly. In mice, the heavy chain is composed of one of several hundred V_H genes combined with one of ~ thirty D segments and one of six J segments (Barbas *et al.,* 2001). Consequently, to generate and capture a good representation of the murine antibody repertoire, a vast amount of primers and optimization steps are required.

Ideally, 166 separate primer sets are employed, however, to limit the unfeasible work-load, the reverse primers were combined in a 'master-mix' and further optimisations to improve amplifications by individual forward primers were not explored (Barbas *et al.,* 2001). This could have resulted in the loss of diversity of the immune repertoire as a result of certain primer combinations amplifying more efficiently. This, in turn, leads to a biased pool of these abundant genes over potential beneficial and conserved genes. To avoid a second immunisation regime, a previously generated avian anti-Jurkat library (data not shown) with a calculated library size ~10^7 cfu/mL was employed for selection of anti-CD3ε antibody fragments.

5.2.1.10 Selection of CD3ε-specific phage-scFv particles by panning

Four rounds of affinity selection via biopanning were performed on CD3ε-coated immunotubes. To ensure enrichment of the CD3ε-specific library, the stringency of each round was altered by increasing the number of wash steps and decreasing the concentration of coated CD3ε. These conditions are outlined in ***Table 5.1.***

Table 5.1 *Panning conditions employed for each round of selection of the avian anti-Jurkat scFv library against the CD3ε protein.*

Panning round	CD3ε coating conc.	Number of washes
1	50 µg/ mL	3 X PBS, 3 X PBS-T (0.05% (v/v))
2	25 µg/ mL	5 X PBS, 5 X PBS-T (0.05% (v/v))
3	12.5 µg/ mL	10 X PBS, 10 X PBS-T (0.05% (v/v))
4	5 µg/ mL	15 X PBS, 15 X PBS-T (0.05% (v/v))

Precipitated input phage from each round of panning (1-4) were incorporated into a polyclonal phage ELISA, to test for enrichment against the CD3ε protein. Successful enrichment against the CD3ε protein was demonstrated by an increase in absorbance signal after incubating phage with the protein of interest and detecting the bound phage with a HRP-labelled anti-M13 secondary antibody (GE Healthcare). This can be observed in ***Figure 5.10.*** However, there is a reduction in absorbance after round 3, which may indicate that the panning conditions became too stringent, hindering the enrichment of the clones in the library and resulting in loss of diversity. As the absorbance increases again in round 4, phage from this, and round 2, were selected for soluble expression.

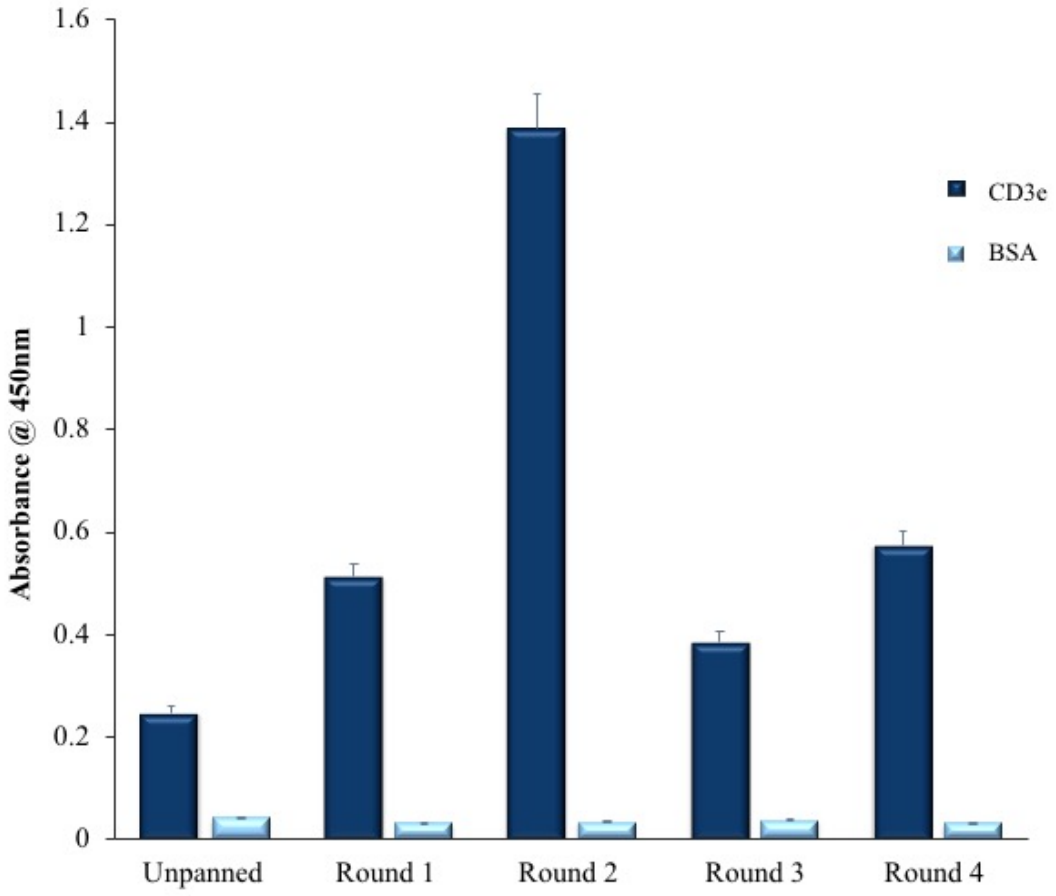

Figure 5.10 Polyclonal phage ELISA screening for anti-CD3ε scFv displayed on enriched phage pools

Phage pools from each round were diluted 1/3 in 1% (w/v) BSA in PBS-T and 100 µL per well was applied on a CD3ε-coated ELISA plate. The scFv-displaying phage were detected using a HRP-labelled anti-M13 secondary antibody and, following the addition of TMB, the absorbance was read at 450nm using a Tecan Safire™ plate reader.

5.2.1.11 Soluble expression and monoclonal analysis of single clones by ELISA

Phage pools from round 2 and 4 were solubly expressed by transformation into the non-suppressor *E. coli* cell line Top10F'. The scFv-containing lysate was added to an ELISA plate coated with 1 µg/mL CD3ε. ***Figure 5.11*** shows the monoclonal ELISA results, three clones with absorbance above the determined 'cut-off' line were identified.

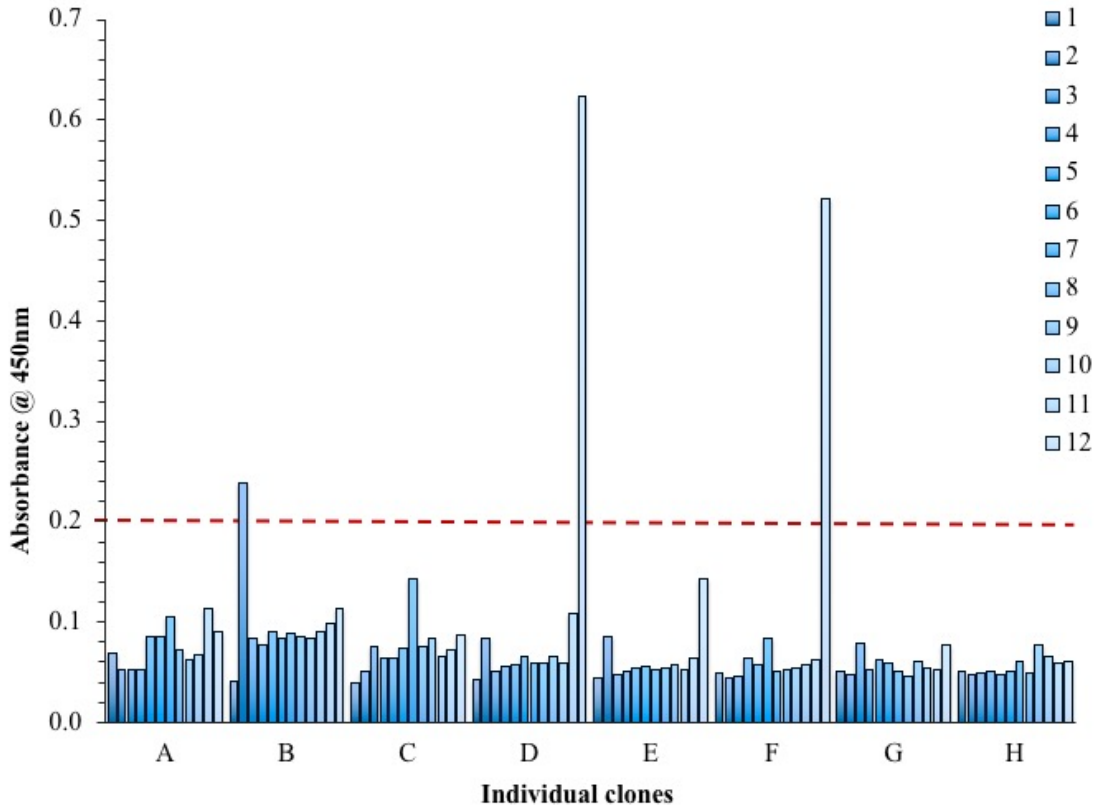

Figure 5.11 Soluble monoclonal ELISA screening for anti-CD3ε scFv from 96 randomly selected clones

Soluble monoclonal ELISA screening for anti-CD3ε scFv from 96 randomly selected clones from panning rounds 2 and 4. Periplasmic lysates were applied to the CD3ε-coated plate (1 µg/mL) and any specific scFv were detected using a HRP-labelled anti-HA antibody. The red dashed line represents the "cut-off" value (x 3 the background optical density).

Positive clones, selected by observed absorbance above the determined "cut-off" value, were taken forward for a lysate titration against the CD3ε protein to confirm specificity for the antigen. Doubling dilutions from neat – 1/128 were performed of the scFv-enriched lysate and added to the CD3ε (1 µg/mL) - coated ELISA plate (***Figure 5.12***). The observed results indicate the 12D and 12F clones successfully bind to the CD3ε protein and were taken forward for expression studies and characterization. The 7C clone shows limited specificity for the CD3ε protein and was not further investigated.

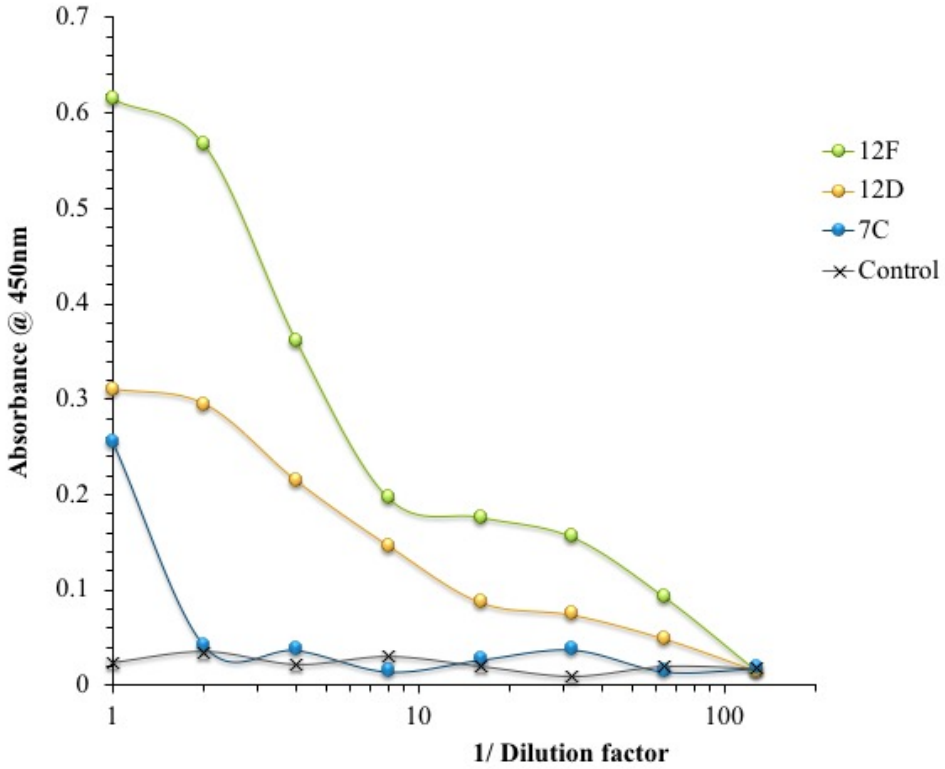

Figure 5.12 Titration of selected scFv lysate by ELISA against CD3ε protein

The scFv-containing lysate was applied to an antigen-coated ELISA plate. The bound scFv were detected using an HRP-labelled anti-HA antibody. Control – ELISA performed without the addition of scFv lysate.

5.2.1.12 Optimisation of 12F and 12D scFv expression

The optimum expression conditions of the clones were investigated by varying the temperature and IPTG-induction concentration. The cultures were centrifuged at 4,000*g* (Eppendorf™ centrifuge fixed angle rotor (F-45-30-11)) for 20 min and the cell pellets resuspended in buffer and lysed by sonication (25% amplitude, 2 sec on pulse, 2 sec off pulse for 2 min) . The lysate was applied to a CD3ε-coated ELISA plate (1 μg/mL) and bound scFv detected using a HRP-labelled anti-HA antibody. The levels of soluble expression produced were compared and the highest absorbance indicated the optimum expression conditions. The expression levels observed in ***Figure 5.13*** remained continuously low with no significant expression noted. An alternative expression vector was employed to increase expression levels.

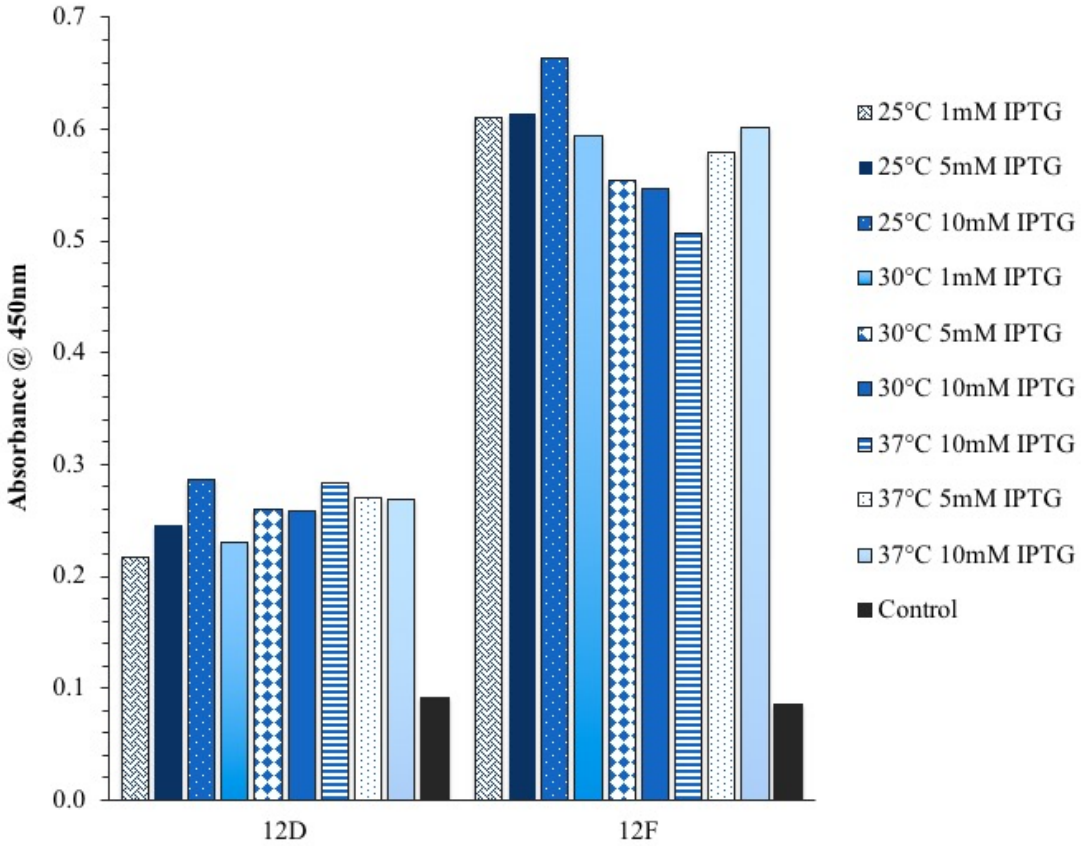

Figure 5.13 Optimisation of expression of the selected scFv

The expression of the scFv were induced with different IPTG concentrations (1 mM – 10 mM) and incubated at a range of temperatures (25°C, 30°C and 37°C). The lysate was tested in indirect ELISA format and bound antibody was detected by the addition of a HRP-labelled anti-HA antibody. Control – ELISA performed without the addition of lysate.

5.2.1.13 Sequencing analysis of the anti-CD3ε clones

Bacterial stocks of each clone were grown and the plasmid was isolated, as described in *Section 2.10.7,* and were sent for sequencing by Source BioSciences. On receiving the DNA sequence results, the sequences were translated to amino acid sequences using ExPasy translation program and aligned using MultAlin alignment program.

The scFv structure is composed of the variable heavy and light domains which have three hypervariable loops primarily involved in antigen binding, known as the CDR regions, which are supported by the framework regions that determine the structure of the domains (Herold *et al.,* 2017). The binding of the antibody-antigen complex within the CDR is dictated by electrostatic interactions, hydrogen bonds, van der Waals forces and

hydrophobic interactions (Sinha *et al.,* 2002). The amino acid side chains within the CDR, however, determine the specificity and affinity of the interaction.

The amino acids tyrosine, tryptophan and arginine, are involved in intermolecular interactions (Koide and Sidhu *et al.,* 2009). Amphipathic amino acids such as alanine, aid in tolerating an environmental change from hydrophilic to hydrophobic which occurs during antibody-antigen binding (Wang *et al.,* 2015). Larger residues participate in van der Waals forces and electrostatic interactions when binding to various proteins. The amino acids with flexible side-chains generate a region with the capability to mould around the antigen and improve the binding region complementarities (Mian *et al.,* 1991). Those with large side chains, such as tyrosine and tryptophan, are advantageous as they do not interact with other groups on the antibody, but will bind with other molecules (Robbins *et al.,* 2008).

Table 5.2 Sequencing analysis of the anti-CD3ε clones 12F and 12D.

The gene sequences were translated into amino acid sequences using the ExPasy Translate tool and aligned using MultAlin alignment program. The aligned sequences were analysed and the complementary determining regions (CDR) were identified for variations.

	CDR-L1	***CDR-L2***	***CDR-L3***
12F	**SGSSGSY**	**SNNQKP**	**GSYEGNTHVGI**
12D	**-**	**TNDKRP**	**AKFDSSS--G**
	CDR-H1	***CDR-H2***	***CDR-H3***
12F	**GFTIFSGYAYM**	**VGNTGSSTDYGSAV**	**TAG--HCVSCTEDIDA**
12D	**GFSISSYEYTM**	**IRSAGSWTNTGSAV**	**STAIDYDWYAAGSIDA**

The results from sequencing analysis indicated that these are two different scFvs, as the corresponding CDR regions show many variations. The 12F scFv was dominated by serine, glycine, aspartic acid, tyrosine, threonine, alanine and valine and the 12D scFv by

serine, aspartic acid, glycine, tyrosine and alanine, which are predominantly small amino acids. These smaller residues are beneficial as they confer greater conformational flexibility, required for antigen-antibody binding. Through sequencing, it was determined that that the 12D scFv is a truncated antibody, lacking a CDRL1 region. While it has been found that only 20-33% of the residues within the CDR participate in antigen-binding, the lack of an entire CDRL1 was deemed unacceptable when identifying potential scFv as this region could house vital residues (Polonelli *et al.,* 2008). The loss of this region may result in reduced binding capabilities, therefore, it is hypothesised that this is the responsible factor for the limited binding capacity, observed in ***Figure 5.12*** and ***Figure 5.13***. Consequently, this scFv was not brought forward for further expression studies.

5.1.2.14 Anti-CD3ε scFv gene amplification from the pComb3XSS plasmid

The pET system is deemed one of the most powerful systems for recombinant protein expression in *E. coli* (Wurm *et al.,* 2016). The expression of genes within the pET plasmid is under the control of strong bacteriophage T7 transcription. When fully induced, the majority of the cell resources are employed for gene expression. The total cell protein can comprise of almost 50% of the protein of interest, after only a few hours post-induction (Jia and Jeon, 2016). For this work, the translation vector, pET-26b(+), was employed. The "b" suffix in this vector denotes the reading frame relative to *BamH*I cloning recognition site GGATCC, in this case it expresses from the GAT triplet. This vector has attractive attributes such as, a kanamycin resistance gene, a C-terminal HIS-Tag for protein identification and purification, and a signal sequence for periplasmic localisation, which is the preferred location for folding and disulphide bond formation (Dewi *et al.,* 2016). This vector contains the T7 *lac* promoter which helps to control basal expression in DE3 lysogens. The *lac* repressor acts at the *lacUV* 5 promoter in the host chromosome which represses the transcription on the T7 RNA polymerase. It also acts at the T7*lac* promoter in the vector which stops transcription of the target gene by any T7 RNA polymerase (Rosano and Ceccarelli, 2014) (***Figure 5.14***).

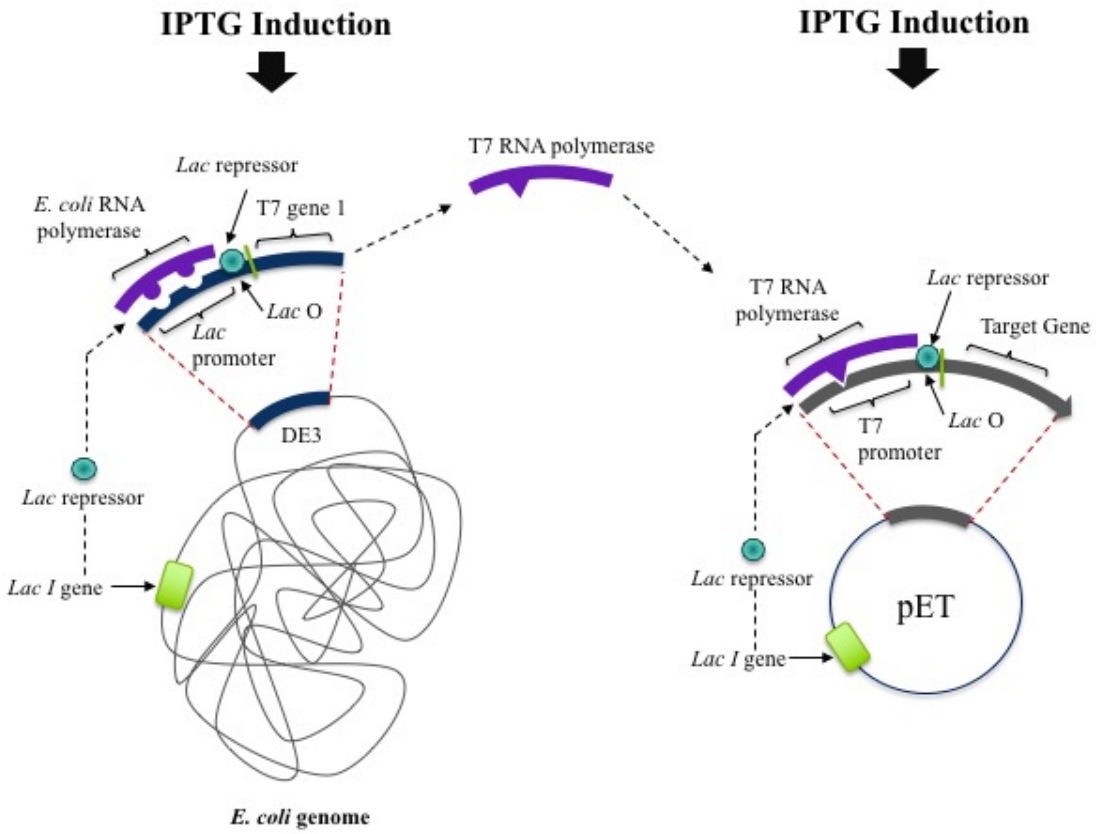

Figure 5.14 Control of the T7 lac promoter

A binding site is present on the lac operon in the E. coli genome complementary to E. coli RNA polymerase. In the absence of an inducer, the lac repressor binds to the lac operon, preventing transcription of T7 RNA polymerase. Upon induction with IPTG, the lac repressor no longer binds, due to a conformational change, and the E. coli RNA polymerase transcribes the T7 gene to generate T7 RNA polymerase. This T7 RNA polymerase results in the transcription of the target gene.

Digestion sites were incorporated by PCR into the scFv gene for cloning into the pET-26b(+) vector. The sequences of these primers are shown in ***Table 2.13,*** the forward primer is labelled 'scFv 2 Forward' and the reverse primer 'scFv 1 Back'. The pComb3XSS plasmid, harbouring the 12F scFv gene, was purified as per *Section 2.10.7* and incorporated into a large-scale 10 X PCR for amplification of the target gene (***Figure 5.15 (i)***). The amplified gene was resolved on a 1.5% (w/v) agarose gel and purified as per *Section 2.15.8.*

The pET-26b(+) vector was transformed into BL21(DE3) chemically competent cells using a heat-shock protocol described in *2.13.1*. A single colony was grown, the plasmid purified as described in *2.10.7* and the yield quantified using the NanoDrop™.

The pET-26b(+) vector and the scFv gene were digested with *Eco*RI and *Hind*III restriction enzymes, as described in *Section 2.18.4.* The digested pET-26b(+) vector was dephosphorylated through Antarctic phosphatase treatment to decrease the non-recombinant background that can result from incomplete digestion (Yao *et al.,* 2016). The digested scFv gene and vector were analysed on a 1.5% (w/v) and 0.6% (w/v) agarose gels, respectively. An undigested vector sample was analysed in conjunction with the digested vector as a control. The two bands observed in the undigested plasmid lane which represent two stable, circular conformations of the vector (supercoiled and nicked), however, once the vector was cut these conformations were destroyed, causing the vector to linearise (***Figure 5.15 (ii, b)***) (Iqbal *et al.,* 2014) .

The digested products were excised from the gels and purified as per *Section 2.15.8*. The purified digested products were ligated as described in *Section 2.18.4.1.* The ligation was ethanol precipitated and resuspended in MGH_2O. Two µL of the ligation was removed and diluted with 8 µL of MGH_2O and 4 X loading dye for analysis on an agarose gel (***Figure 5.16 (i)***). The ligation was transformed into One Shot BL21(DE3) chemically competent cells through a heat-shock protocol described in *2.13.1.* To determine the ligation and transformation efficiency, a colony-pick PCR was performed using the primers employed for the 12F gene amplification. All of the randomly selected colonies were positive for the 12F gene insert (***Figure 5.16 (ii)***).

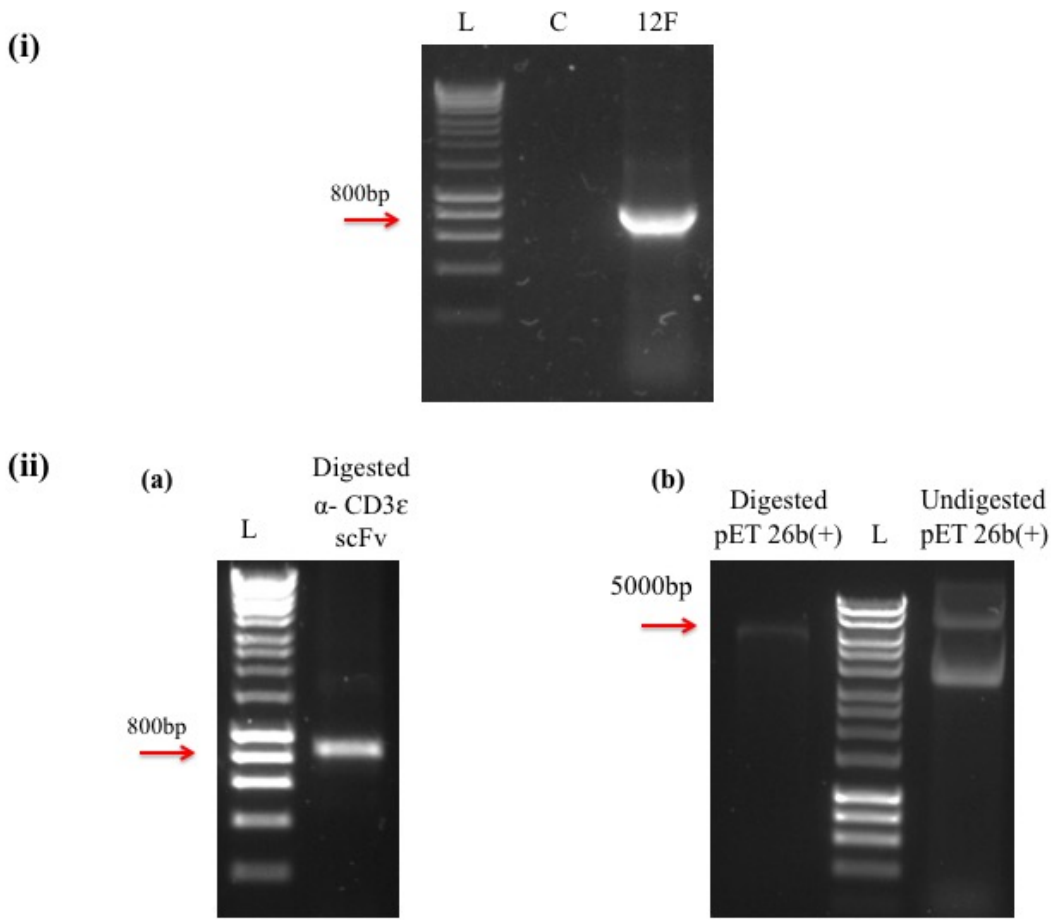

Figure 5.15 Preparation of the scFv gene and pET-26b(+) vector for ligation

(i) *Large-scale amplification of the 12F scFv gene was performed using specifically designed primers that incorporate specific restriction digest sites. C = All the necessary PCR components without the addition of plasmid DNA L = 1kb Ladder (Bioline HyperLadder™).**(ii) (a)** The amplified 12F scFv gene was digested with the restriction enzymes EcoRI and HindIII for directional cloning into the pET-26b(+) vector. L = 1kb Ladder (Bioline HyperLadder™).**(b)** The pET-26b(+) vector was digested with EcoRI and HindIII. The undigested vector was also analysed on the 0.6% (w/v) agarose gel to ensure digestion had occurred. L = 1kb Ladder (Bioline HyperLadder™).*

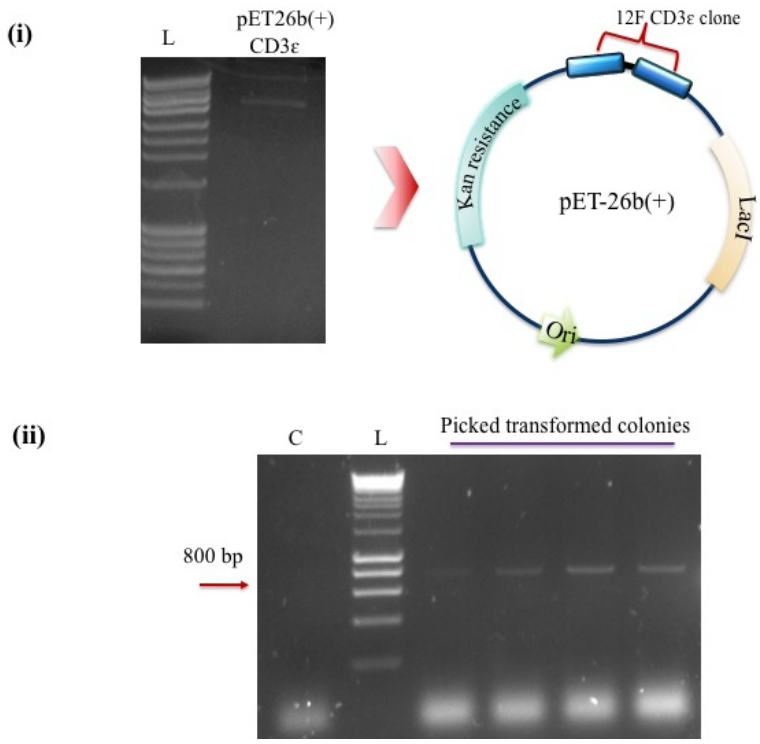

Figure 5.16 Analysis of ligation of the pET-26b(+) vector and scFv gene

(i) *Agarose gel electrophoresis (0.6% w/v) analysis showing the successful ligation of the vector with the 12F gene insert. L = 1kb Ladder (Bioline HyperLadder™).* ***(ii)*** *Visualisation of a colony-pick PCR performed on 4 randomly selected colonies. These products were resolved on a 1.5% (w/v) agarose gel. C = All the necessary PCR components without the addition of colony. L = 1kb Ladder (Bioline HyperLadder™).*

5.1.2.15 Analysis of anti-CD3ε scFv by indirect and competitive ELISA

A single colony was grown O/N, subcultured into fresh media and induced with 1 mM IPTG and grown O/N at 30°C. A sample of the culture was taken and pelleted by centrifugation at 4,000*g* (Eppendorf™ centrifuge fixed angle rotor (F-45-30-11)) for 20 min and the bacterial cell pellet lysed as outlined in *Section 2.16.7*. The clarified lysate was analysed by ELISA through the addition of the scFv-enriched lysate, in doubling dilutions, to the antigen-coated plate (1 µg/mL) (***Figure 5.17***). Furthermore, the ability of the scFv '12F' to bind to CD3ε in solution was investigated by competitive ELISA. Here, the scFv-containing lysate was incubated with free antigen and added to the CD3ε-coated plate. The assay was performed in triplicate and the standard deviations were calculated and are indicated by error bars. These results illustrate that the scFv exhibited specificity for the CD3ε protein in solution (***Figure 5.18***).

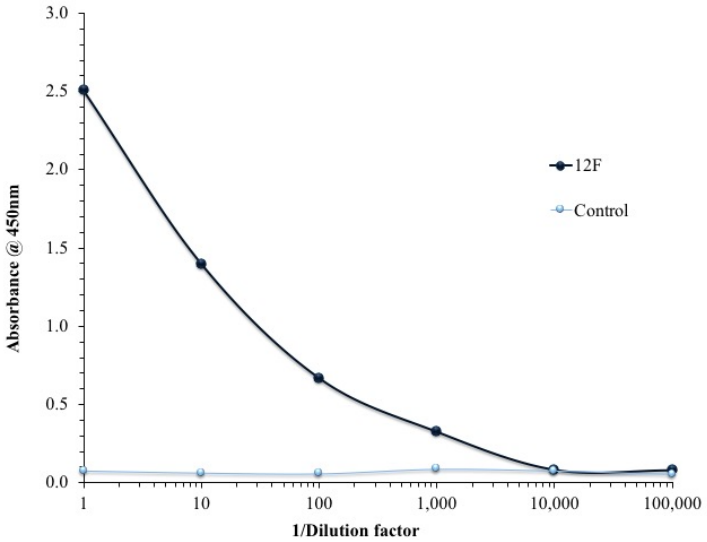

Figure 5.17 Titration of scFv lysate by ELISA against CD3ε protein

Titration of anti-CD3ε scFv 12F against CD3ε protein. The lysate was applied to a CD3ε-coated ELISA plate. The bound scFv were detected using a HRP-labelled anti-HA antibody. Control – ELISA performed against BSA as the coated protein (1 μg/mL).

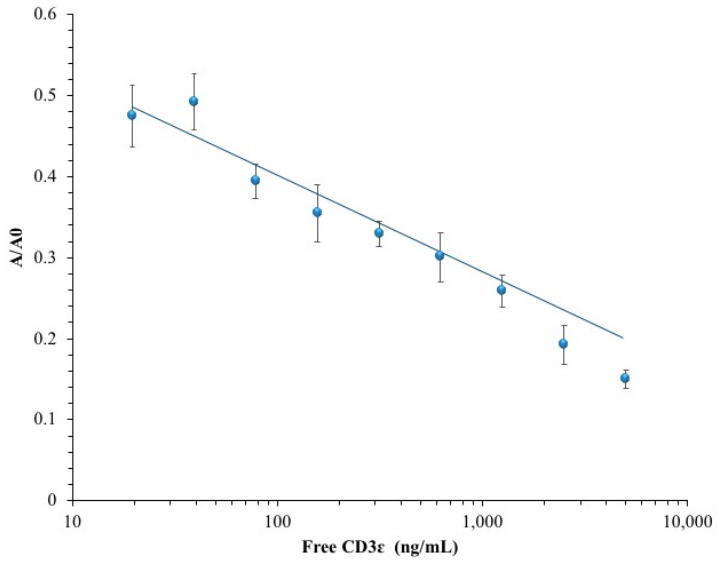

Figure 5.18 Competitive analysis of purified 12F scFv

The scFv was incubated with decreasing concentrations of CD3ε. Bound scFv were detected using a HRP-labelled anti-HA antibody. One μg of the CD3ε protein was coated on the surface of a Nunc MaxiSorp™ ELISA plate. The purified scFv was incubated with free CD3ε and added to the plate where competition occurs between the immobilized and free antigen. Bound antibody was detected using a HRP-labelled anti-HA antibody. The results are shown as A/A0, where the absorbance values of the evaluated samples (A), are normalised by expressing them as a function of the blank standard (A0).

5.2.1.16 Optimisation of scFv expression and purification of the 12F scFv from the pET-26b(+) expression system

Expression studies were performed, as outlined in *Section 5.2.1.13,* investigating the effects of various temperatures and IPTG concentrations. For recombinant protein expression in the pET vector the recommended induction concentration is 1 mM, consequently 1, 2, 5 and 10 mM IPTG induction concentrations were analysed (Sadeghi *et al.,* 2011). Each culture was then induced with the appropriate concentration of IPTG and incubated at one of the three temperatures under investigation. The following day the cultures were centrifuged at 4,000*g* (Eppendorf™ centrifuge fixed angle rotor (F-45-30-11)) for 20 min, resuspended in 1 mg/mL lysozyme and subjected to three cycles of freeze-thawing. The lysed cultures were centrifuged at 9,000*g* (Eppendorf™ centrifuge fixed angle rotor (F-45-30-11)) and the scFv-containing supernatant analysed by ELISA. The supernatant was added to a CD3ε-coated ELISA plate (1 µg/mL). ***Figure 5.19*** shows a high level of expressed anti-CD3ε scFv present in all samples, with a particularly high absorbance noted when expression occurs at 30°C. The determined optimum conditions for this scFv in the pET-26b(+) vector were 2 mM IPTG induction and incubation at 30°C.

Using the determined optimum conditions the anti-CD3ε 12F scFv was expressed large-scale (1L) and purified by IMAC. The efficiency of the purification was analysed by SDS-PAGE and WB. The WB shown in ***Figure 5.20*** was probed with a HRP-labelled anti-HA antibody which yielded strong bands at the expected size ~25kDa, confirming successful purification of the scFv. The eluted fraction was concentrated to 1 mL in 1 X PBS using a Vivaspin column, and the yield of 2.45 mg/mL was determined on the Nanodrop™.

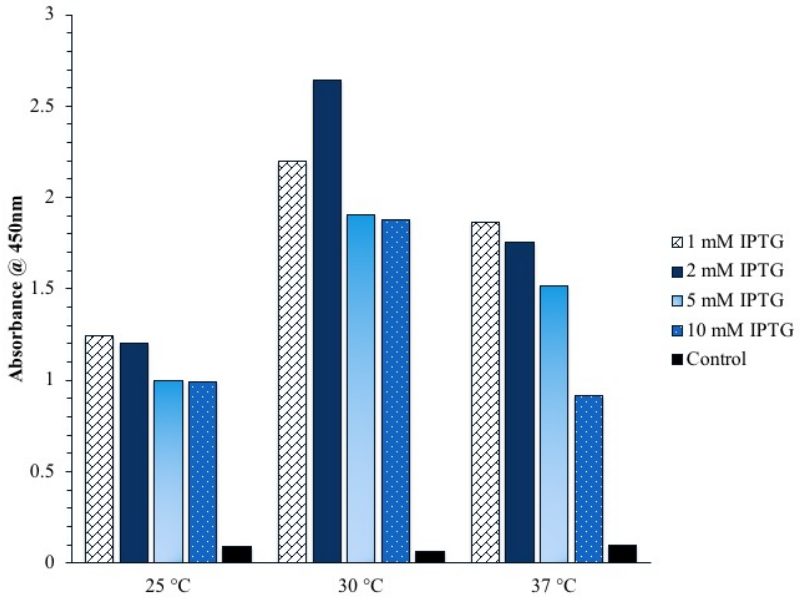

Figure 5.19 Analysis of optimal IPTG concentration and expression temperature for anti-CD3ε scFv 12F in the pET-26b(+) vector

Expression of the scFv was induced with different IPTG concentrations (1 mM – 10 mM) and grown at temperatures, 25°C, 30°C and 37°C. The lysate was tested in indirect ELISA format and bound antibody was detected following the addition of a HRP-labelled anti-HA antibody. Control – ELISA performed without the addition of lysate.

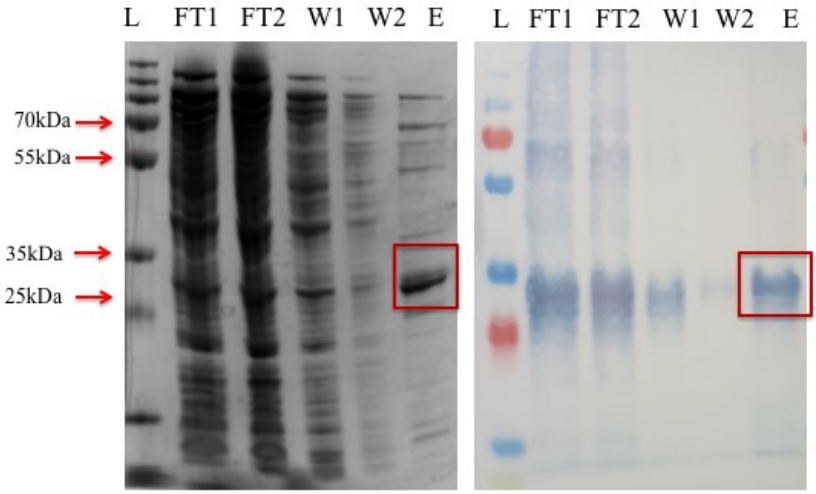

Figure 5.20 SDS-PAGE and western blot analysis of IMAC-purified scFv

SDS-PAGE and western blot analysis of the fractions obtained during IMAC purification of the scFv. The WB was probed with a HRP-labelled anti-HA antibody. L = PageRuler™ Plus Prestained Protein Ladder. FT1 = Flow through 1; FT2 = Flow through 2; W1 = Wash 1; W2 = Wash 2; E = Elution.

5.1.2.17 Checkerboard ELISA for the determination of the optimum antibody dilution and coating concentration of CD3ε protein

A checkerboard ELISA was performed to identify the appropriate antibody dilution and coating concentration for the immunoassay. Varying dilutions of 10 µg/mL to 0 µg/mL of CD3ε were coated on a MaxiSorp™ ELISA plate and dilutions (1/5 -1/640) of the purified antibody added to each antigen concentration. The optimal coating concentration was determined to be 8 µg/mL with an antibody dilution of 1/40 (***Figure 5.21***).

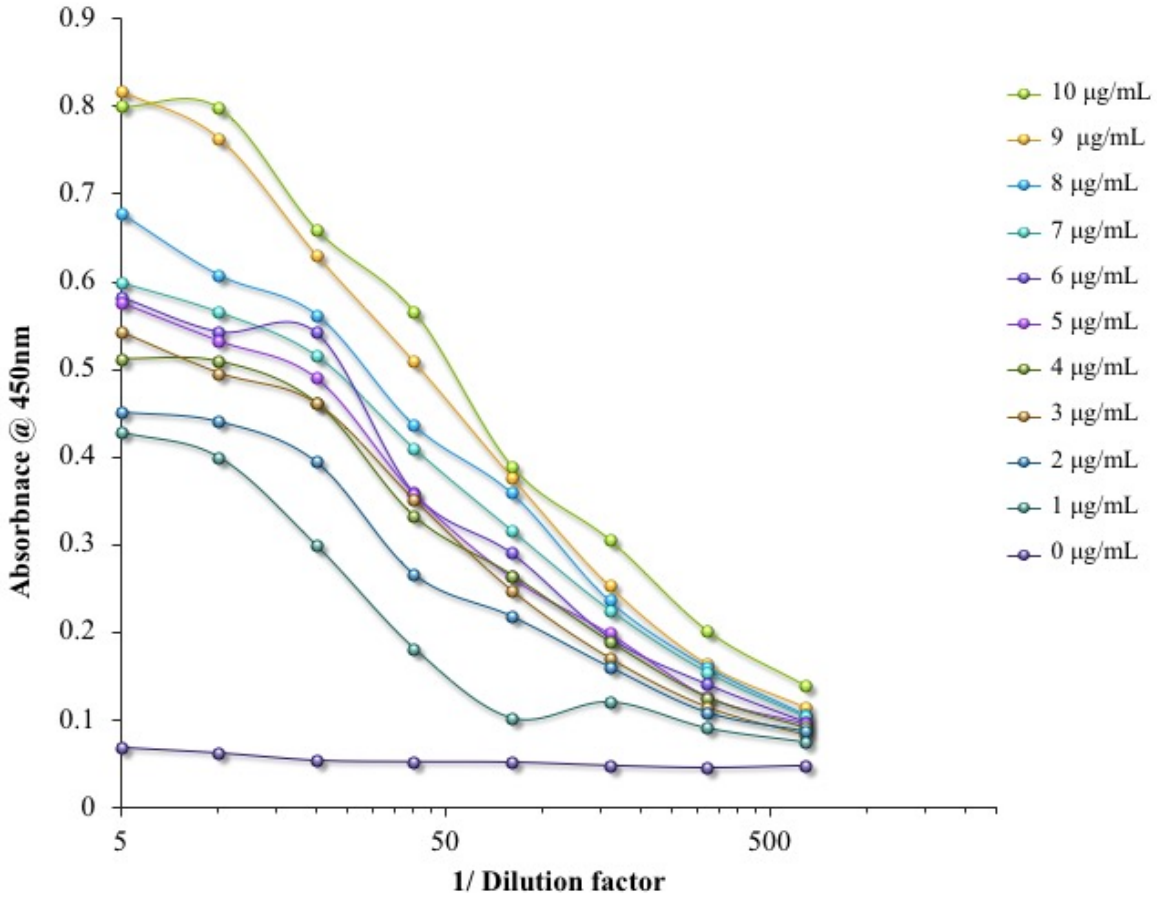

Figure 5.21 Checkerboard ELISA for the determination of the optimal CD3ε coating concentration and scFv dilution for use in a competitive ELISA

Antigen concentrations of 10 µg/mL to 0 µg/mL were used in an indirect ELISA with varying dilutions of antibody ranging from 1/5 to 1/640. Bound antibody was detected using a HRP-labelled anti-HA antibody.

5.1.2.18 Intra- / Inter-assay variability studies of the competitive ELISA of anti-CD3ε and anti-HER2 scFv in PBS

An avian anti-HER2 scFv previously generated (data not shown) by Dr. Julia Zapatero Rodríguez within the Applied Biochemistry Group (ABG), was employed as the TAA-specific arm of the BiTE. Inter- and intra-day assays were carried out on the anti-HER2 and anti-CD3ε scFv in PBS and normal human serum to evaluate the performance of the assay over a period of days and the assay repeatability in physiological conditions. By employing the optimum conditions determined by the checkerboard ELISA, inter- and intra-day assays in PBS were initially performed. Using BiaEvaluation^{TM} software, calibration curves were generated based on a 4-parameter sigmoidal equation. The standard deviation, coefficient variation (CV) and percentage accuracies for the inter- and intra-day assays for both the anti-CD3ε and anti-HER2 scFv were calculated and shown in ***Tables 5.3*** and ***5.4.***

Both the inter- and intra-day % CV observed for the anti-CD3ε and anti-HER2 scFv displayed acceptable reproducibility, as they fell within the recommended precision level of 20% with the highest percentages of 7.7% and 9.5% noted. While the % accuracy values were primarily within the acceptable limits of 80-120%, there are some inaccuracies found, however, these primarily fall outside of the linear ranges (Findlay *et al.,* 2000). It can be observed in the inter-day assay in ***Figure 5.22*** that the linear range of the anti-CD3ε was not fully defined. This is evident by the lack of a sigmoidal curve that results from plateauing of signal at either end of the curve which indicates the antigen concentration range at which the antibody can detect. To overcome this, the concentration range of assessed CD3ε was increased for the intra-/inter-day assays in normal human serum.

Table 5.3 Intra – and inter-day assay CV and percentage accuracies for the anti-CD3ε scFv 12F in PBS.

Coefficient of variation (CV) was calculated by % CV=(S.D/Mean) x 100. The standard deviation (S.D) for intra-day analysis was calculated from 3 replicate analyses within a single assay, whereas the S.D for inter-day analyses was calculated from 3 replicates over 3 assays on 3 separate days. Table cells that contain a "-" represent that no value could be extrapolated as the data point did not fit the calibration curve.

	Intra-day			**Inter-day**		
CD3ε Conc. (pg/mL)	**CV (%)**	**Back Calculated Conc. (pg/mL)**	**Accuracies (%)**	**CV (%)**	**Back Calculated Conc. (pg/mL)**	**Accuracies (%)**
12,000,000	5.5	6,557,900	55	3.4	7,319,420	61
4,000,000	2.1	5,875,600	147	3.3	5,561,560	140
1,333,333	1.2	1,439,810	108	5.1	1,523,850	114
444,444	2.5	514,066	115	4.1	503,658	113
148,148	1.3	136,552	92	1.7	128,925	87
49,382	2.1	48,511	98	4.3	47,523	96
16,460	3.9	15,581	95	1.5	16,461	100
5,487	5.9	6,221	113	6.8	5,487	100
1,828	1.3	1,687	92	1.7	1,838	101
609	6.9	563	92	3	517	85
203	5.8	-	-	7.7	-	-

Table 5.4 Intra – and inter-day assay CV and percentage accuracies for the anti-HER2 scFv in PBS.

Coefficient of variation (CV) was calculated by % CV=(S.D/Mean) x 100. The standard deviation (S.D) for intra-day analysis was calculated from 3 replicate analyses within a single assay, whereas the S.D for inter-day analyses was calculated from 3 replicates over 3 assays on 3 separate days. Table cells that contain a "-" represent that no value could be extrapolated as the data point did not fit the calibration curve.

	Intra-day			**Inter-day**		
HER2 Conc. (pg/mL)	**CV (%)**	**Back Calculated Conc. (pg/mL)**	**Accuracies (%)**	**CV (%)**	**Back Calculated Conc. (pg/mL)**	**Accuracies (%)**
20,000,000	2.2	6,482,630	32	5.4	7,614,620	38
4,000,000	2.1	3,674,960	92	2.9	4,000,000	100
800,000	9.2	938,760	117	5.6	788,850	99
160,000	9.1	181,072	113	3.4	179,305	112
32,000	3.9	28,311	88	9.5	27,809	87
6,400	2.5	6,027	94	4.5	6,830	106
1,280	5.8	1,156	90	2.7	1,172	92
256	4.3	326	127	4.5	272	106
51	8.1	57	112	3.5	52	102
10	2.4	10.2	100	3.1	8.9	89
2	1.4	-	-	3.5	-	-

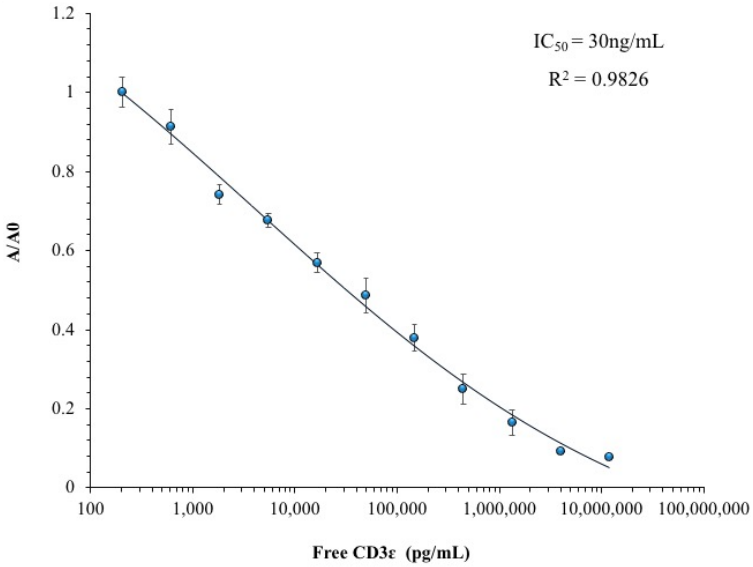

Figure 5.22 Inter-day assay calibration curve of anti-CD3ε scFv in PBS

The calibration curve was constructed using a 4-parameter equation in BiaEvaluation™. The inter-day assay means and CV are tabulated in ***Table 5.3.*** *Each point on the curve is the mean of 3 replicate measurements analysed over 3 days. The absorbance of the evaluated samples was normalised by expressing the absorbance as a function of the blank standard (A/A0).*

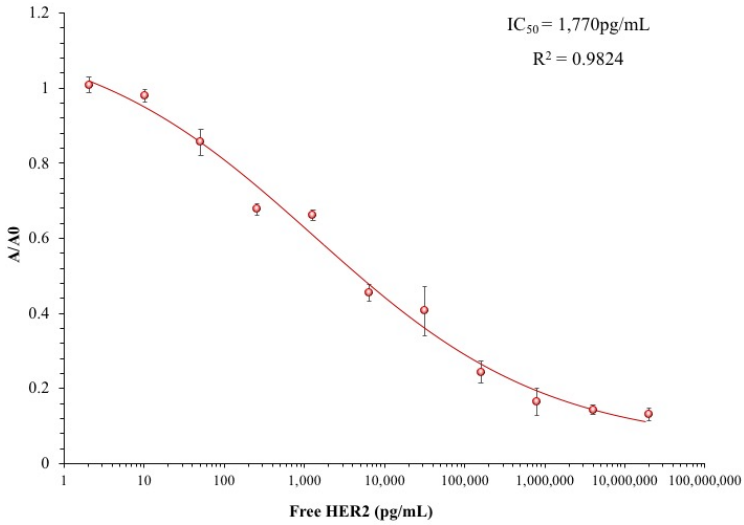

Figure 5.23 Inter-day assay calibration curve of anti-HER2 scFv in PBS

The calibration curve was constructed using a 4-parameter equation in BiaEvaluation™. The inter-day assay means and CV are tabulated in ***Table 5.4.*** *Each point on the curve is the mean of 3 replicate measurements analysed over 3 days. The absorbance of the evaluated samples was normalised by expressing the absorbance as a function of the blank standard (A/A0).*

5.2.1.19 Intra- / Inter-assay variability studies of the competitive ELISA of anti-CD3ε and anti-HER2 scFv in normal human serum

The intra- and inter-day assays were repeated, as per *Section 2.17.3.1,* in normal human serum to investigate the feasibility of the generated scFv for detection of the appropriate antigen in clinical samples. To assess a more appropriate dynamic range, the concentration of CD3ε protein was increased to 12 µg/mL - 1.2 pg/mL. Calibration curves were created using the BiaEvaluation™ software and the detection capabilities were extrapolated from the resulting curves. The coefficients of variation (CV), shown in ***Table 5.5*** and ***5.6***, were determined to assess the precision of the assay. The highest % CV observed for the anti-CD3ε scFv was 14.5% and 14.9% for the anti-HER2 scFv. The average % CV calculated from the intra-day assay increased from 3.9-6.3% and from 4.4-6.5% in normal human serum for the anti- CD3ε and anti-HER2 scFv respectively. This increase may be a result of the human error or variability between assays, however the increase remains substantially below the recommended % CV of 20 % for validated assays. (Andreasson *et al.,* 2015).

Potential matrix inference effects were investigated by comparison of spike and recovery percentages from standards analysed in PBS and normal human serum. The recoveries were estimated from the calibration curves for each standard. From these, the % accuracies (shown in ***Tables 5.3, 5.4, 5.5*** and ***5.6***) were calculated by dividing the actual recovery by the theoretical recovery and multiplied by 100. All average recoveries fell within the acceptable limits of 80-120% with averages increasing from 99.7 – 109% and 93-101% for anti-CD3ε and anti-HER2 scFv, respectively. While a minor increase can be observed the results indicate less than a 10 % deviation from the actual concentrations suggesting no significant matrix interference was occurring within the assay in normal human serum. (Ong *et al.,* 2013).

Table 5.5 Intra – and inter-day assay CV and percentage accuracies for the anti-CD3ε scFv 12F in normal human serum.

Coefficient of variation (CV) was calculated by % CV=(S.D/Mean) x 100. The standard deviation (S.D) for intra-day analysis was calculated from 3 replicate analyses within a single assay, whereas the S.D for inter-day analyses was calculated from 3 replicates over 3 assays on 3 separate days.

	Intra-day			***Inter-day***		
CD3ε Conc. (pg/mL)	**CV (%)**	**Back Calculated Conc. (pg/mL)**	**Accuracies (%)**	**CV (%)**	**Back Calculated Conc. (pg/mL)**	**Accuracies (%)**
12,000,000	5.1	7,404,410	62	11.5	8,024,880	67
2,400,000	7	2,831,900	118	3	2,816,270	117
480,000	10.5	520,223	108	14.5	442,887	92
96,000	9.1	91,117	95	12.5	84,655	88
19,200	8.7	17,716	92	1.36	16,346	85
3,840	9.1	4,223	109	7	4,442	115
768	4.3	817	106	3.7	885	115
154	2.6	137	89	5.5	149	97
31	3.5	28	90	5.3	27	87
6.1	4.7	6.7	110	3.8	5.6	92
1.2	3.7	1.6	133	1.2	1.7	142

Table 5.6 Intra – and inter-day assay CV and percentage accuracies for the anti-HER2 scFv in normal human serum.

Coefficient of variation (CV) was calculated by % CV=(S.D/Mean) x 100. The standard deviation (S.D) for intra-day analysis was calculated from 3 replicate analyses within a single assay, whereas the S.D for inter-day analyses was calculated from 3 replicates over 3 assays on 3 separate days. Table cells that contain a "-" represent that no value could be extrapolated as the data point did not fit the calibration curve.

	Intra-day			***Inter-day***		
HER2 Conc. (pg/mL)	**CV (%)**	**Back Calculated Conc. (pg/mL)**	**Accuracies (%)**	**CV (%)**	**Back Calculated Conc. (pg/mL)**	**Accuracies (%)**
20,000,000	6.9	-	-	8.5	-	-
4,000,000	3.2	3,690,720	92	14.9	4,698,480	117
800,000	11.8	867,039	108	9.5	750,540	94
160,000	10.2	158,244	99	5.9	183,627	115
32,000	8.3	28,193	88	9.6	35,510	111
6,400	5.3	5,449	85	5.1	5,905	92
1,280	3.6	1,189	92	3.3	1,120	88
256	1.8	301	117	2.5	238	93
51	5	60	118	6.9	58	114
10	2.1	8.3	83	3.1	8.1	81
2	1.4	3	140	2.3	2.2	110

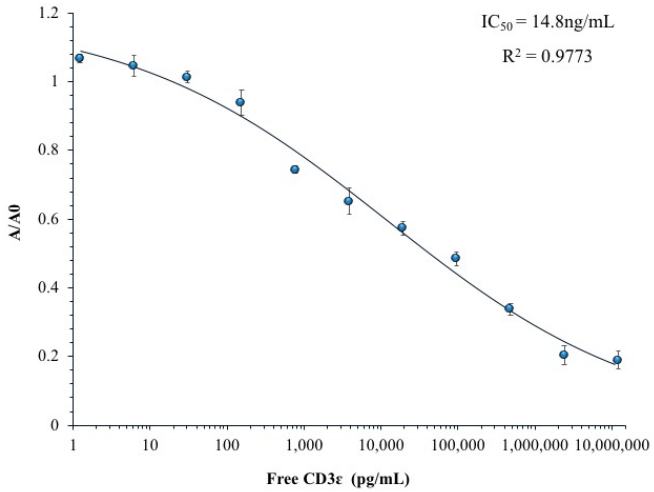

Figure 5.24 Inter-day assay calibration curve for the anti-CD3ε scFv 12F in normal human serum.

The calibration curve was constructed using a 4-parameter equation in BiaEvaluation™ software. The inter-day assay means and CV are shown in ***Table 5.5.*** *Each point on the curve is the mean of 3 replicate measurements analysed over 3 days. The absorbance of the evaluated samples was normalised by expressing the absorbance as a function of the blank standard (A/A0).*

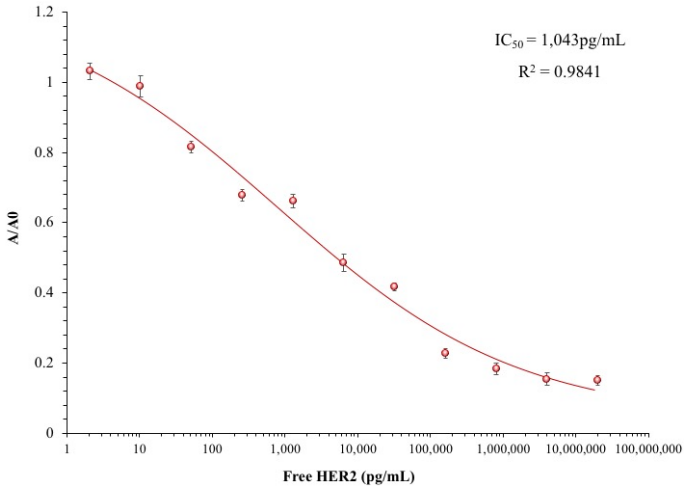

Figure 5.25 Inter-day assay calibration curve for the anti-HER2 scFv in normal human serum

The calibration curve was constructed using a 4-parameter equation in BiaEvaluation™ software. The inter-day assay means and CV are shown in ***Table 5.6.*** *Each point on the curve is the mean of 3 replicate measurements analysed over 3 days. The absorbance of the evaluated samples was normalised by expressing the absorbance as a function of the blank standard (A/A0).*

5.2.1.20 Determination of analytical limits

The limit of detection (LOD) values for the anti-CD3ε and anti-HER2 scFv were calculated by selecting the mean normalised absorbance minus three standard deviations of the blank standard (Şengül, 2016). The overall LOD were calculated as 20 pg/mL, and 10 pg/mL for the anti-CD3ε scFv and anti-HER2 scFv, respectively. Experimental confirmation of the extrapolated limits of detection were performed as described in *Section 2.17.4.* The confirmed lowest concentration of analyte that could be detected with 95% certainty above the blank sample was 20 pg/mL for the anti-CD3Ɛ scFv and 10 pg/mL for the anti-HER2 scFv. These are shown in ***Figure 5.26*** and ***Figure 5.27*** from which it can be observed that each scFv could correctly distinguish 19 out of 20 samples containing the LOD 'spiked' concentration of analyte when compared to the blank standard.

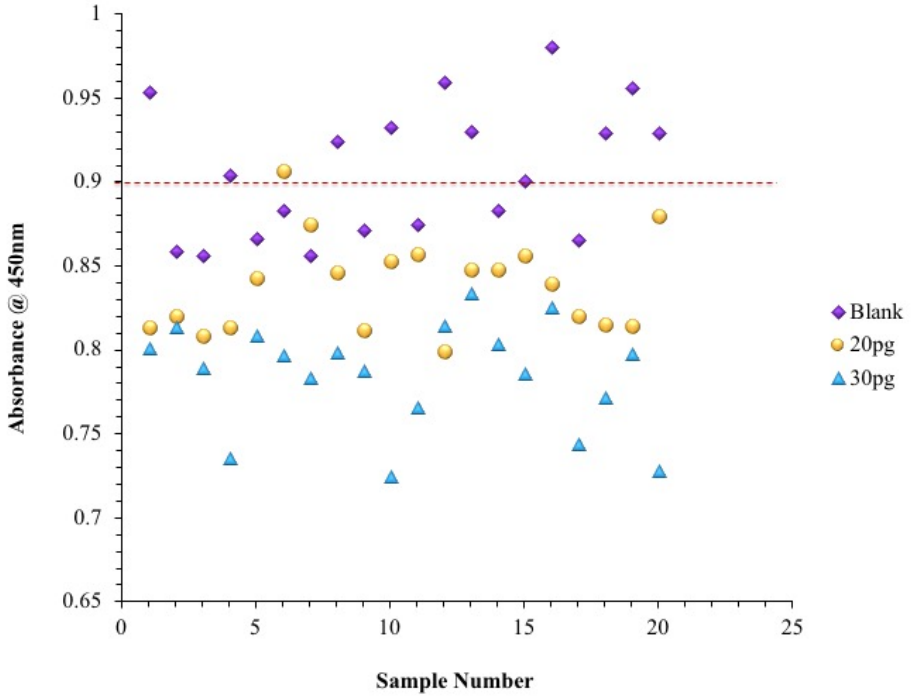

Figure 5.26 Precision assay for experimental verification of the CD3ε-specific scFv
The functional LOD is determined using 20 replicates of the blank standard, 20 replicates of 20 pg/mL CD3ε and 20 replicates of 30 pg/mL in a competitive ELISA format with 1 µg/mL CD3ε coated on the immunosorbent plate. A HRP-labelled anti-HA antibody was used to detect bound scFv. The dashed line indicates 95% compliance. This denotes the ability of the scFv to detect 95% of the samples as positive for CD3ε when compared to the blank standard. The dashed line was determined by the mean of the blank standards.

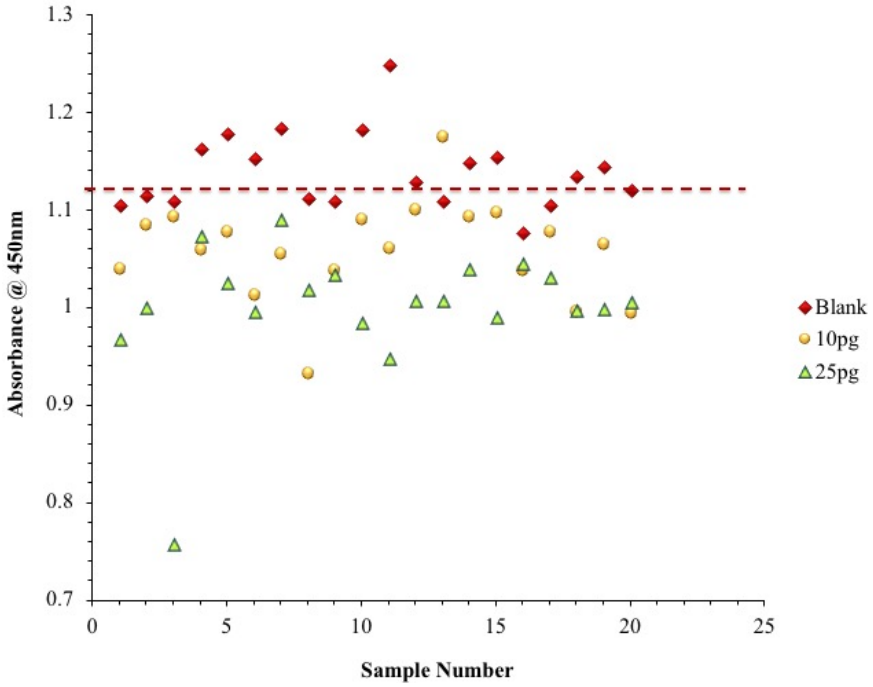

Figure 5.27 Precision assay for experimental verification of the HER2-specific scFv *The functional LOD is determined using 20 replicates of the blank standard, 20 replicates of 10 pg/mL HER2 and 20 replicates of 25 pg/mL in a competitive ELISA format with 1 µg/mL HER2 coated on the immunosorbent plate. HRP-labelled anti-HA antibody was used to detect bound scFv. The dashed line indicates 95% compliance. This denotes the ability of the scFv to detect 95% of the samples as positive for HER2 when compared to the blank standard. The dashed line was determined by the mean of the blank standards.*

5.2.1.21 Cross reactivity studies of the anti-HER2 and anti-CD3ε scFv

For reliable analysis of the BiTEs dual binding functionality, it was crucial that there was no cross reactivity of the two scFv. This arises from shared or overlapping epitopes or poor specificity of the antibody to the cognate antigen and was investigated herein through competitive ELISA (O'Kennedy *et al.,* 2017). The cross reactivity of the HER2 antibody against CD3ε antigen was analysed by coating a Nunc MaxiSorp plate with 1 µg/mL HER2 antigen and incubating the antibody with free CD3ε protein to determine its specificity for the CD3ε antigen. The CD3ε scFv was analysed in the same manner but against immobilised CD3ε and free HER2. The cross-reactivity profile of the HER2 scFv showed 0.32% cross reactivity with CD3ε antigen, and the CD3ε scFv showed a cross reactivity of -1.78% against the HER2 antigen. Both percentages are negligible indicating no cross reactivity, subsequently confirming these scFv ideal for bispecific pairing.

5.2.2 Generation of a Bispecific T-cell engager (BiTE)

A method for the generation of a bispecific T-cell engager was devised whereby designed primers were employed to amplify the scFv genes and incorporate desired restriction digestion sites. These sites allow the genes to be digested and directionally cloned into the pET-26b (+) vector.

5.2.2.1 Design of pET-specific primers for the amplification of the anti- CD3ε and anti- HER2 scFv genes

pET-specific primers were designed to incorporate the specific restriction sites for *EcoR*I, *Asc*I and *Hind*III into the appropriate scFv gene. The anti-HER2 scFv was termed 'scFv 1' and the anti-CD3ε 'scFv 2'. As illustrated in ***Figure 5.28***, the scFv 1 forward primer was designed to contain, an *EcoR*I site (blue), an *Asc*I site (green) and the initial eight codons from the N-terminus of the avian scFv gene which includes the *Sfi*I site (red). The inclusion of the *Asc*I site allows for the directional cloning of the second scFv. The scFv 1 back primer contains the *Hind*III site (purple) and the codons which encode for a HA-tag.

The scFv 2 forward primer contains the *EcoR*I site (blue), the N-terminus codons and *Sfi*I site (red) and the scFv 2 back primer is designed to contain an *Asc*I site to allow for cloning of the scFv upstream of the first scFv. Codons encoding a glycine and serine were added to provide a flexible linker between the scFv.

scFv 1 – Forward

5' AT CCG AAT TCG AGC GGC GCG CCG GTG GCC CAG GCG GCC CTG ACT CAG 3'

Translated primer

AT CCG AAT TCG AGC GGC GCG CCG GTG GCC CAG GCG GCC CTG ACT CAG
P N S V G A P V A Q A A L T Q

scFv 1 – Back

5' CAT GGC GCA TAC CCG TAC GAC GTT CCG GAC GAC TAC GCT TCT AAG CTT GCG G 3'

Translated primer

CAT GGC GCA TAC CCG TAC GAC GTT CCG GAC GAC TAC GCT TCT AAG CTT GCG G
H G A Y P Y D V P D D Y A S K L A

scFv 2 – Forward

5' AT CCG AAT TCG GTA GTG GCC CAG GCG GCC CTG ACT CAG 3'

Translated primer

AT CCG AAT TCG GTA GTG GCC CAG GCG GCC CTG ACT CAG
P N S V V A Q A A L T Q

scFv 2– Back

5' TCC TCC ACT AGT GGC CAG GCC GGC CAG GGT TCG GGC GCG CCG GTG 3'

Translated primer

TCC TCC ACT AGT GGC CAG GCC GGC CAG GGT TCG GGC GCG CCG GTG
S S T S G Q A G Q G S G A P V

= *Sfi*I site = *EcoR*I site

= *Asc*I site = *Hind*III site

Figure 5.28 Primers designed for the amplification and subcloning of the CD3ε and HER2 scFv genes.

These specifically designed primers incorporate 3 digestion sites that allow for directional cloning of both scFv into the pET-26b(+) vector with a flexible linker to provide the necessary space between the two scFv.

5.2.2.2 Generation of a BiTE construct by ligation into the pET-26b(+) vector

Cultures containing plasmids harbouring the anti-CD3ε scFv and anti-HER2 scFv and pET-26b(+) vector were grown and the plasmids purified, as described in *Section 2.10.7.* Two large-scale 10 X PCR were carried out to amplify the anti-HER2 scFv gene and the anti-CD3ε scFv gene with the incorporated digestion sites. The PCR were performed, as described in *Section 2.18.3,* using the purified plasmids as the DNA templates and the appropriate primer combination. ***Figure 5.29*** shows the amplification of the two scFv genes with both yielding strong bands at ~800bp when resolved on a 1.5% (w/v) agarose gel. The anti-HER2 scFv product is a slightly larger as the primers were designed to include more modifications, such as the codons required for the HA-tag and the two restriction sites added into the gene sequence.

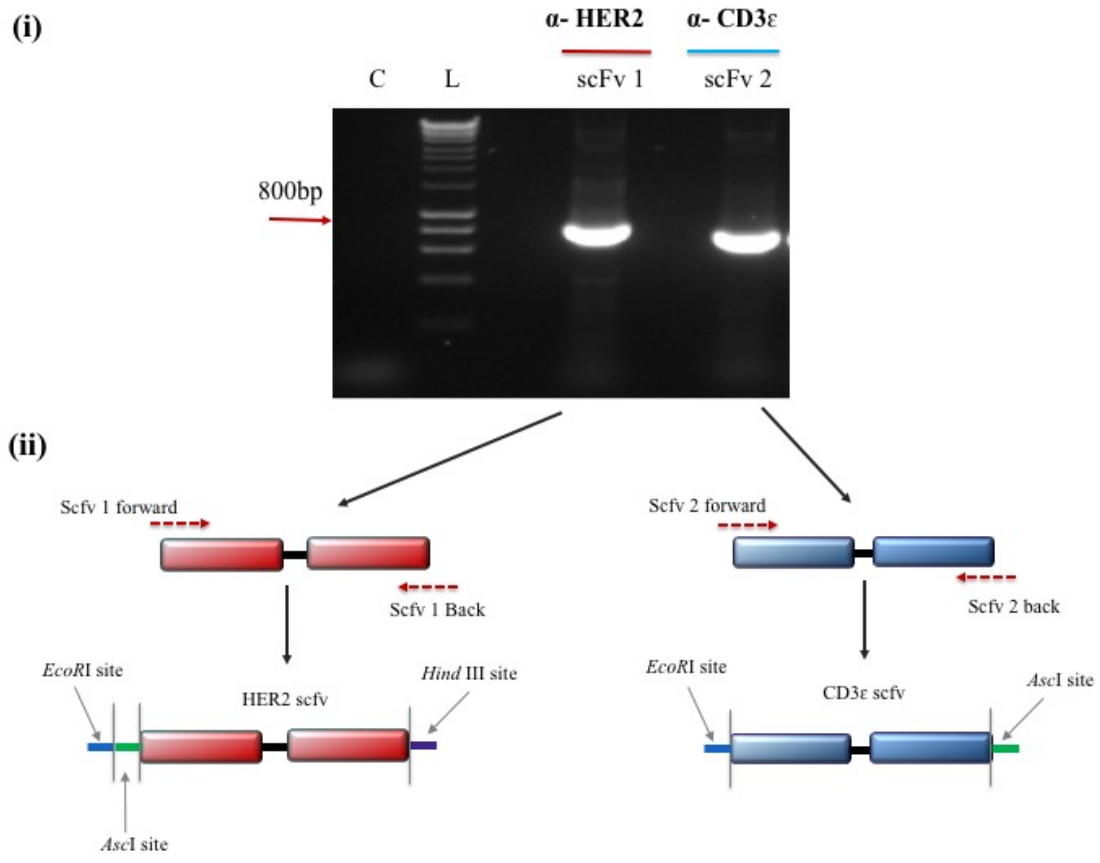

Figure 5.29 Large-scale amplification of the CD3ε scFv and HER2 scFv genes

(i) *Large-scale amplification of the anti-CD3ε and anti-HER2 scFv genes using primers that incorporate specific restriction digest sites (EcoRI, HindIII and AscI). C = A negative control was carried out consisting of all the necessary PCR components without the addition of plasmid DNA, to ensure no contamination was present. L = 1kb Ladder (Bioline HyperLadder™).* ***(ii)*** *Simplistic schematic of subcloning process.*

The amplified scFv genes were gel-purified, as described in *Section 2.15.8,* and quantified on the NanoDrop™. The HER2 scFv gene and the pET-26b(+) vector were double digested with *EcoR*I and *Hind*III to create complementary ends for ligation of the scFv gene into the pET -26b(+) vector (*Section 2.18.4*). The digested vector was dephosphorylated with Antarctic phosphatase to hinder any self-ligation of the digested ends. The digested anti-HER2 scFv product and vector were resolved on 1.5% (w/v) and 0.6% (w/v) agarose gels, respectively (***Figure 5.30***).

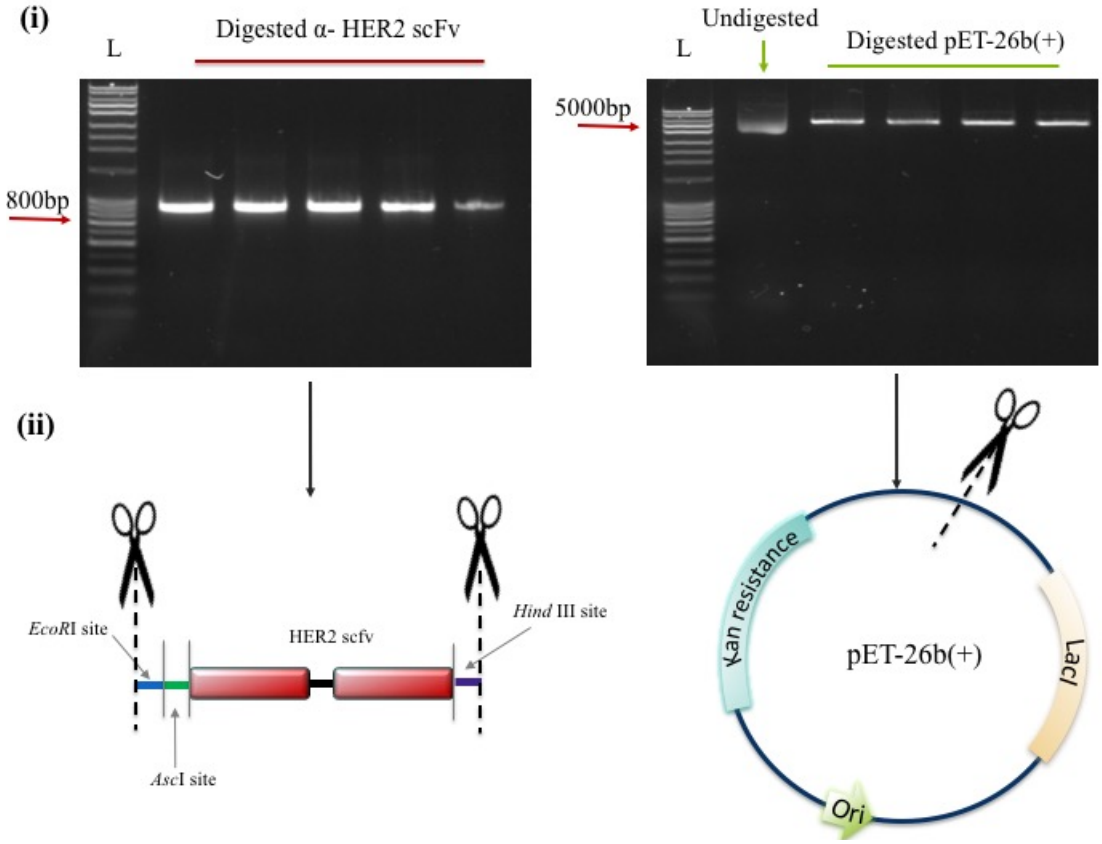

Figure 5.30 Digestion of the anti-HER2 scFv gene and pET-26b(+) vector

The amplified anti-HER2 gene and pET-26b(+) vector were digested using EcoRI and HindIII. ***(i)*** *The anti-HER2 scFv digested gene was analysed on a 1.5% (w/v) agarose gel. A non-digested sample of the pET-26b(+) vector was analysed with the digested vector on a 0.6% (w/v) agarose gel to determine successful digestion. L = 1kb Ladder (Bioline HyperLadder™).****(ii)*** *Simplistic schematic of digestion events occurring.*

For comparison, a non-digested sample of the vector was analysed. Plasmid DNA presents in three different conformations. These are supercoiled, which is how the plasmid is found *in vivo* to fit inside the cell, open-circular or nicked, which can occur when nicks are created causing supercoils to be released, and as a linear conformation as

a result of digestion by enzymes. The undigested sample appears on the gel as a smaller band than the digested due to its supercoiled conformation as it sustains less friction when running through the agarose gel (Levy, 2000).

Subsequently, both digested products were purified from the respective gels as per *Section 2.15.8.* A ligation was performed overnight at RT using T4 DNA ligase. The ligation was then ethanol precipitated overnight to remove excess salt and enzymes and to concentrate the ligation sample. A small sample of ligation was analysed on a 0.6% (w/v) agarose gel (***Figure 5.31*).**

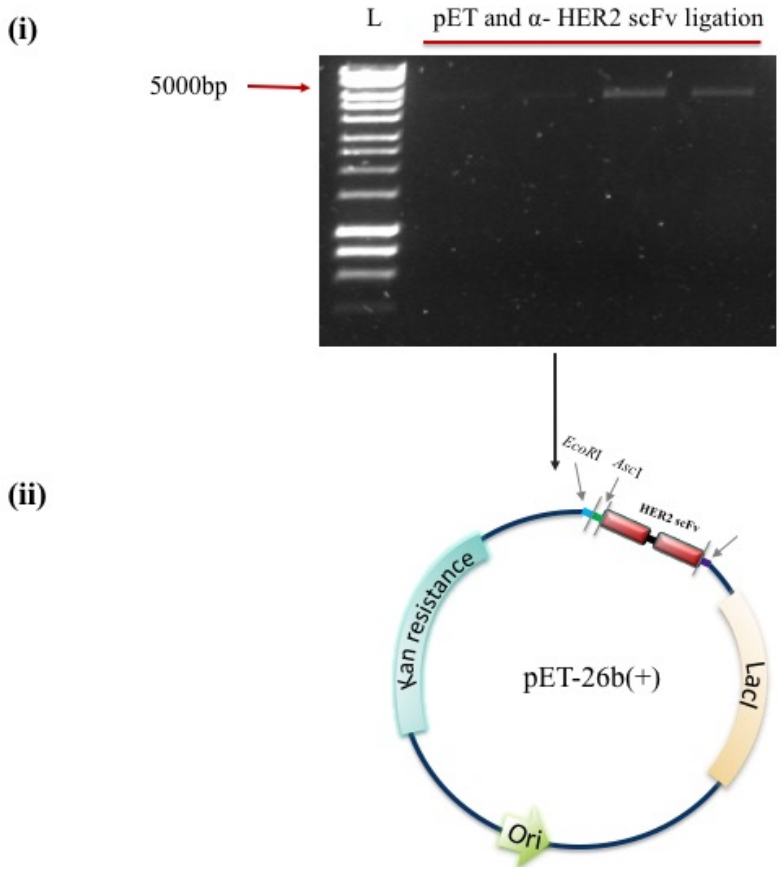

Figure 5.31 Ligation of the digested anti-HER2 scFv gene and pET-26b(+) vector.
(i) The digested scFv gene and vector were ligated using T4 DNA ligase and analysed on a 0.6% (v/v) agarose gel. L = 1kb Ladder (Bioline HyperLadder™). ***(ii)*** *Simplistic schematic of ligation described.*

To clone the anti-CD3ε scFv upstream of the HER2 scFv within the pET-26b(+) vector, the pET-26b(+) vector containing the HER2 scFv gene and the anti-CD3ε scFv gene were

double-digested with *EcoR*I and *Asc*I, resolved on agarose gels and purified (***Figure 5.32***).

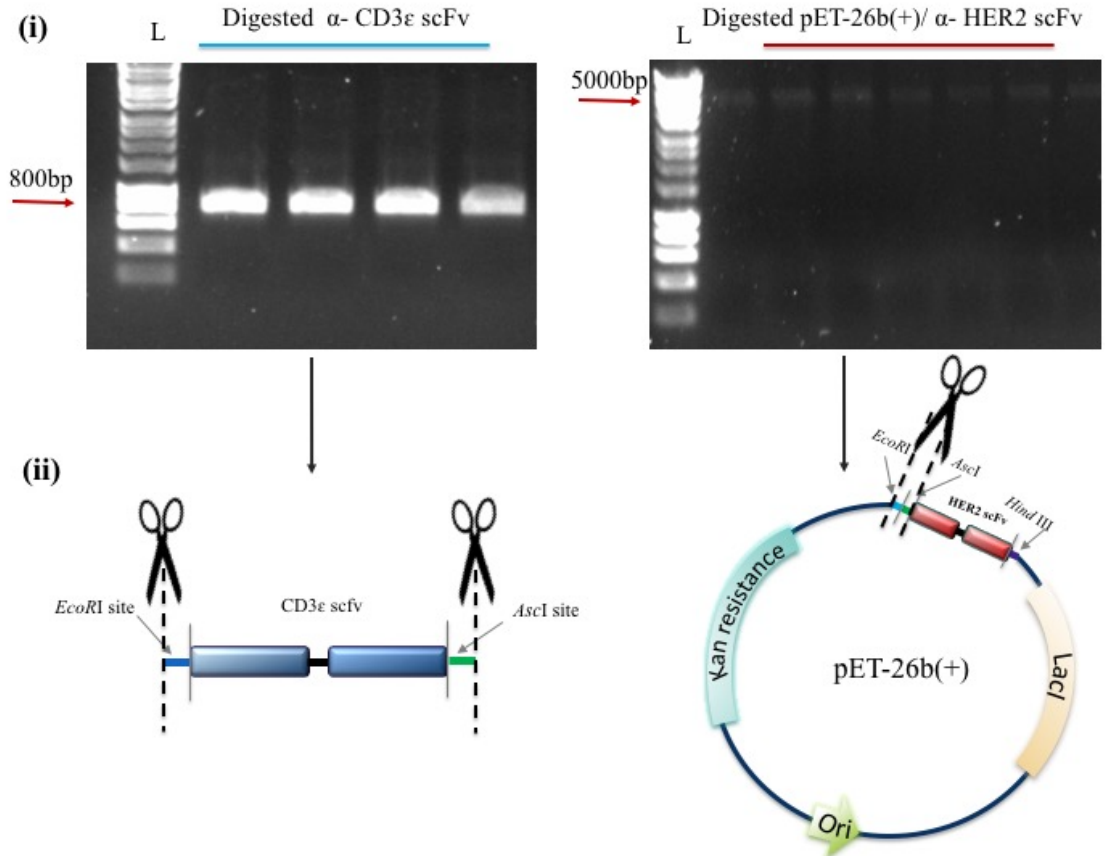

Figure 5.32 Digestion of the anti-CD3ε scFv gene and pET-26b(+)-anti-HER2 scFv vector

The amplified anti-CD3ε gene and pET-26b(+) vector containing the anti-HER2 scFv gene were digested using EcoRI and AscI restriction enzymes. ***(i)*** *The anti-CD3ε scFv digested gene was analysed on a 1.5% (w/v) agarose gel and the pET-26b(+) vector containing the anti-HER scFv gene was analysed on a 0.6% (w/v) agarose gel. L = 1kb Ladder (Bioline HyperLadder™).* ***(ii)*** *Simplistic schematic of the digestion event described.*

The scFv and the pET-scFv construct were ligated and analysed on a 0.6% (v/v) agarose gel (***Figure 5.33***). The final ligation was ethanol precipitated and resuspended in MGH_2O prior to transformation into BL21 (DE3) *E. coli* cells. The transformation was carried out by heat-shock as described in *Section 2.13.1.*

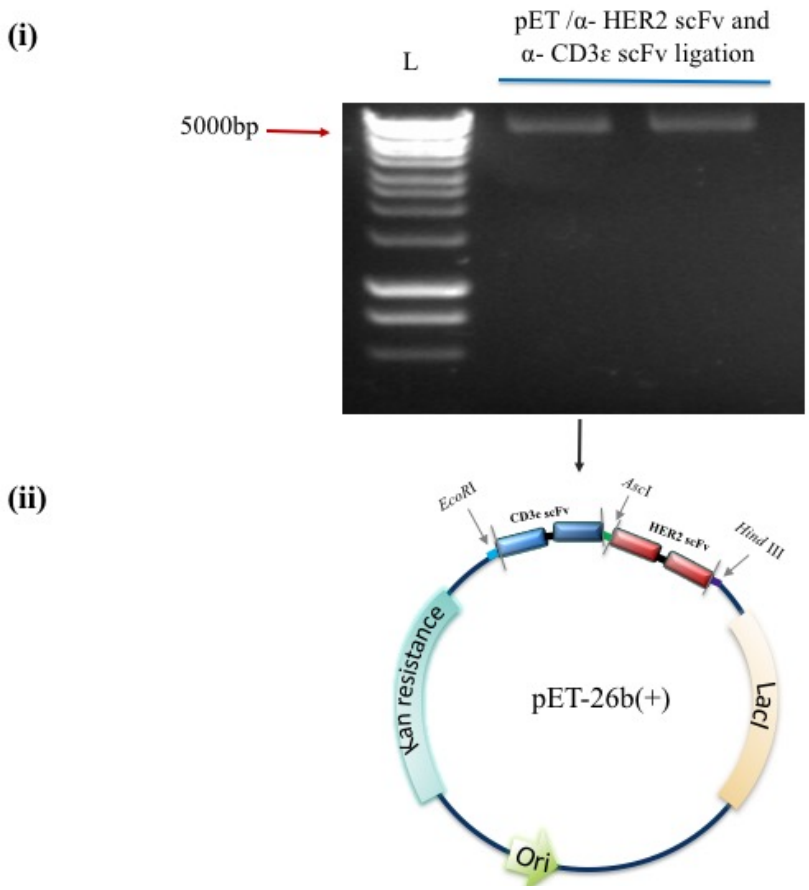

Figure 5.33 Ligation of the digested anti-CD3ε scFv gene and pET-26b(+) vector containing the anti-HER2 scFv gene

(i) *The digested scFv gene and vector were ligated using T4 DNA ligase and resolved on a 0.6% (v/v) agarose gel. L = 1kb Ladder (Bioline HyperLadder™).* ***(ii)*** *Simplistic schematic of ligation described.*

5.2.2.3 Expression and purification of a bispecific T-cell engager (BiTE)

A small-scale purification was performed to determine if a full ~55-60kDa antibody was successfully expressed. Expression of the recombinant BiTE was induced by the addition of 1 mM IPTG and grown overnight at 30°C. Purification of the BiTE was performed by IMAC and evaluated by SDS-PAGE and WB analysis. ***Figure 5.34*** shows the successful purification of the BiTE protein as is confirmed by a WB probed with a HRP-labelled anti-HA antibody yielding a band at ~60kDa. The eluted fraction was concentrated and a yield of 0.25 mg/mL was obtained according to the NanoDrop™ and employed for subsequent evaluation of the binding capabilities of the produced protein.

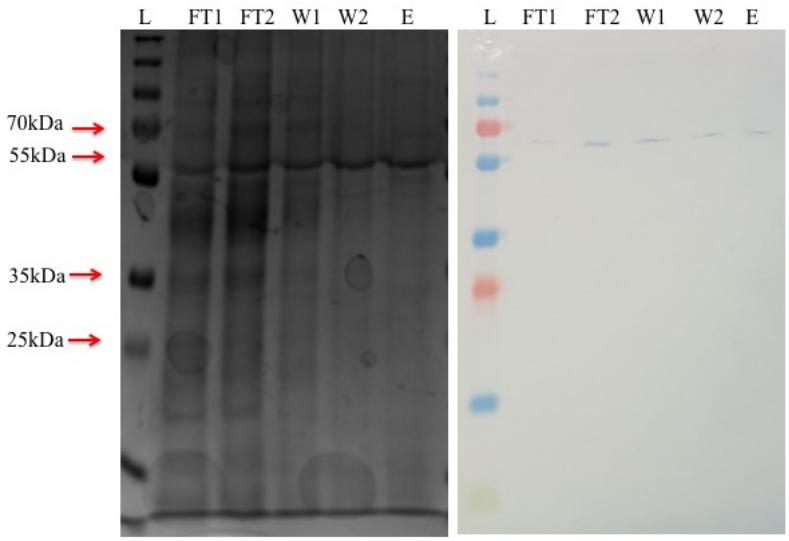

Figure 5.34 SDS PAGE and western blot analysis of the IMAC-purified BiTE

SDS-PAGE and WB analysis of the fractions obtained during IMAC purification of the BiTE antibody. The WB was probed with a HRP-labelled anti-HA antibody. L = PageRuler™ Plus Prestained Protein Ladder. FT1 = Flow through 1; FT2 = Flow through 2; W1 = Wash 1; W2 = Wash 2; E = Elution.

5.2.2.4 ELISA format for evaluation of the BiTEs functional binding capacity

Testing the dual binding capabilities of the purified BiTE required a complex ELISA format. The HER2 antigen (1 µg/mL) was used to coat the MaxiSorp™ ELISA plate and blocked with 3% (w/v) BSA in 1 X PBS. The purified BiTE antibody was then added to the plate and wash steps performed to remove unbound antibody. Free CD3ε (8 µg/mL) was added and allowed to bind to the anti-CD3ε arm of the BiTE. To detect bound CD3ε, a mouse monoclonal anti-CD3ε antibody was added followed by a HRP-labelled anti-mouse antibody (***Figure 5.35***).

Initially, an ELISA was performed to ensure the anti-CD3ε scFv and commercial anti-CD3ε antibody bound to different epitopes on the CD3ε protein. Using a sandwich format ELISA, the CD3ε protein was added to the anti-CD3ε scFv-coated plate. The commercial mouse monoclonal anti-CD3ε antibody was added and detected using a HRP-labelled anti-mouse antibody. The results were plotted on the below graph (***Figure 5.36***) where it can be observed that both antibodies can simultaneously bind to the CD3ε protein and can therefore be used in the ELISA format for the investigation of the dual binding capabilities of the BiTE.

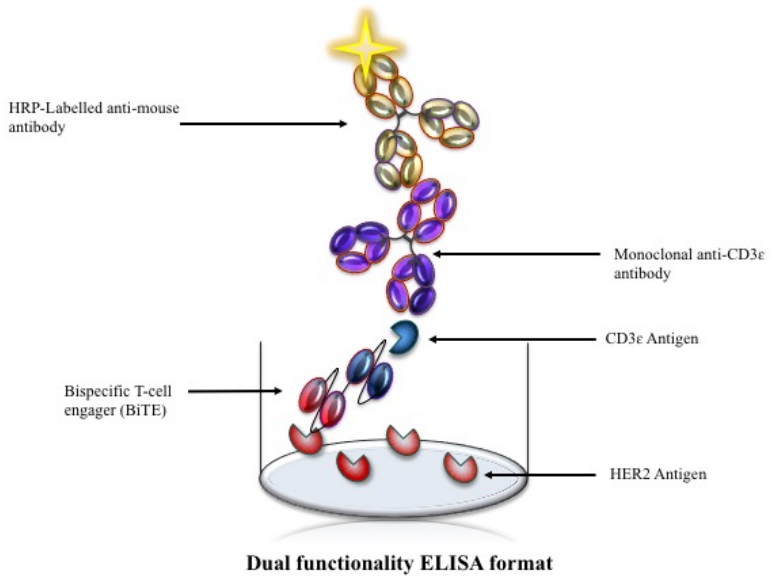

Figure 5.35 Schematic representation of the proposed ELISA format to evaluate and confirm the dual binding abilities of the BiTE

The dual binding abilities of the BiTE was investigated using the above ELISA format.

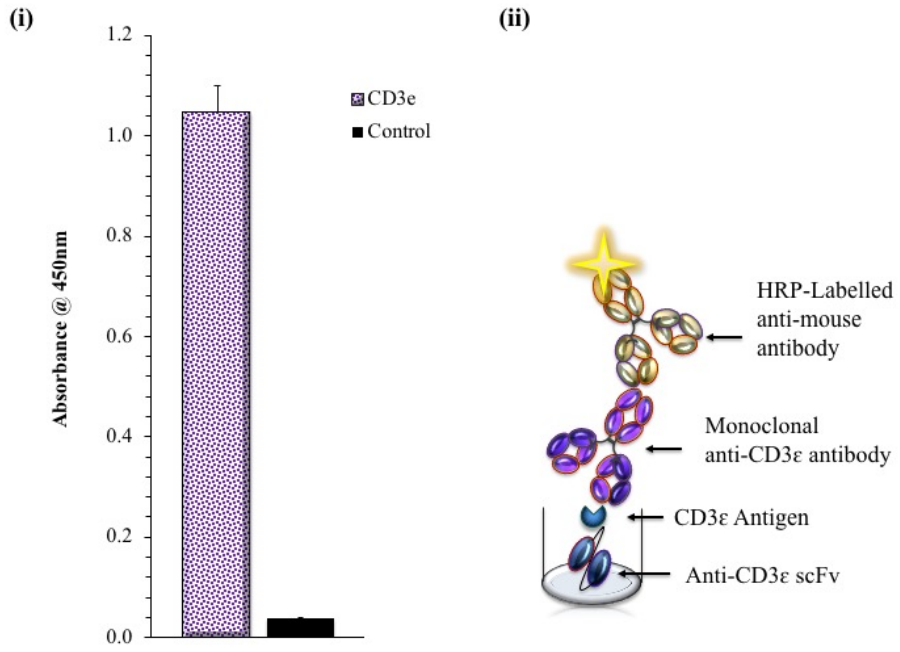

Figure 5.36 Simultaneous binding of the CD3ε scFv and commercial monoclonal anti-CD3ε antibody to bind to CD3ε antigen

(i) *The notable increased absorbance over the control indicates that both antibodies have the ability to bind simultaneously to the CD3ε antigen. Control = ELISA performed without the addition of CD3ε antigen.* ***(ii)*** *Simplistic schematic of the detection format.*

5.2.2.5 Investigation into the BiTEs functional binding capacity

Initial analysis was carried out to ensure that both scFv within the BiTE retained the ability to bind to the cognate antigen when expressed in tandem. An indirect ELISA was performed and the purified BiTE added to wells coated with either CD3ε (8 µg/mL) protein or HER2 (1 µg/mL) protein. Bound BiTE was detected by the addition of a HRP-labelled anti-HA antibody. It can be observed in ***Figure 5.37*** that both scFv retained the binding ability for each antigen when expressed in tandem.

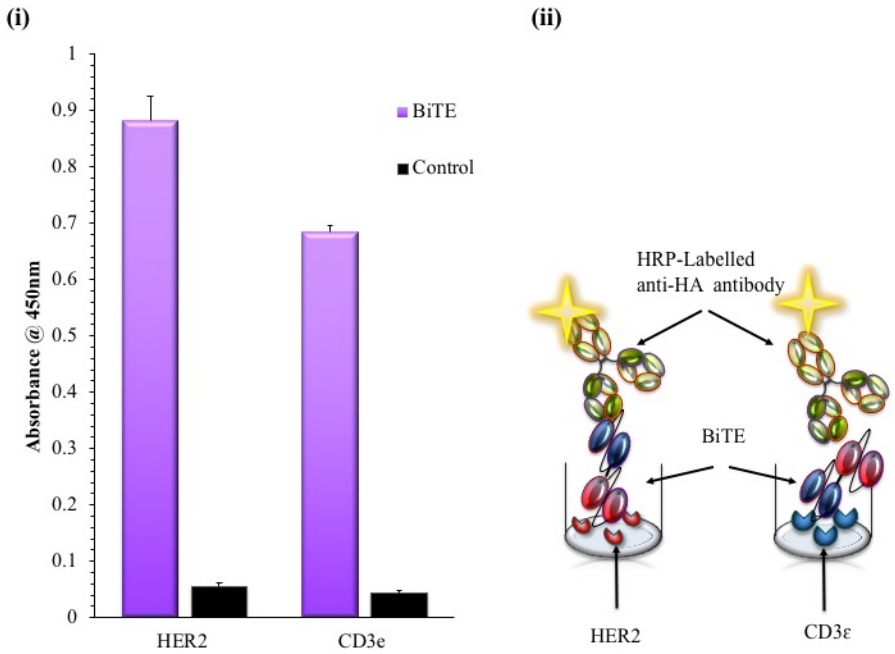

Figure 5.37 Investigating the binding abilities of the BiTE to each antigen separately ***(i)*** *This graph indicates that expressed and purified BiTE antibody retains the ability to bind to both antigens individually. Bound BiTE was detected by the addition of a HRP-labelled anti-HA antibody C= ELISA performed without the addition of the BiTE antibody.* ***(ii)*** *Simplistic schematic of the detection format.*

Subsequently, the dual binding capabilities of the purified BiTE was investigated by employing the ELISA format described in ***Figure 5.35***. Despite the low absorbance observed, the BiTE is significantly higher than the control as it exceeds 3 times the standard deviation (***Figure 5.38***). It is possible the simultaneous dual binding abilities are compromised due to scFv proximity resulting in steric hindrance. Steric effects, first proposed over 130 years ago by Hofmann (1872), often arise from steric bulk whereby large groups within a molecule prevent chemical reactions. These effects are important in antibody-antigen binding as they can result in limited antigen accessibility (Hlavacek

et al., 1999; Metz *et al.,* 2012). A study carried out by Watanabe and colleagues (2011) performed *in vitro* and *in vivo* experiments on bispecific antibodies and encountered issues with T-cell direction due to steric hindrance. Other work that has encountered problems with steric hindrance limiting antigen binding of bispecific antibodies, employed optimisations of linker length and construction to circumvent this issue, as it was found too short a linker can result in spatial steric hindrance (Orcutt *et al.,* 2010; Hao *et al.,* 2015). In this research, the linker incorporated into the BiTE was composed of two serine amino acids, however, according to the literature the flexible linker within a BiTE is primarily constructed of approximately five serine or glycine amino acids (Huehls *et al.,* 2015). It was decided that increasing the linker size could relieve this issue by creating more space and flexibility to accommodate dual binding and elevate any steric interference (Ahmad *et al.,* 2012; Vauquelin and Charlton, 2013).

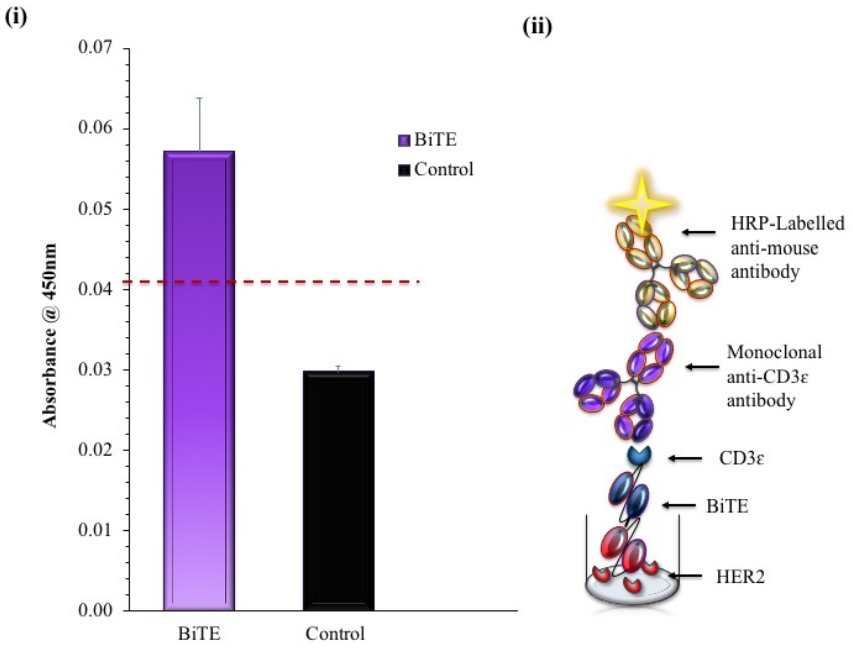

Figure 5.38 Investigating the dual binding capabilities of the BiTE

(i) *An indirect ELISA was performed using the format illustrated in* ***Figure 5.34****. The purified BiTE was added to a plate coated with 1 µg/mL HER2 antigen. Five µg/mL free CD3ε antigen was added and a monoclonal anti-CD3ε antibody employed to bind to the bound CD3ε. A HRP-labelled anti-mouse antibody was then added to detect the monoclonal anti-CD3ε antibody. Control = ELISA performed without the addition of the BiTE. The red dashed line represents 3 times the standard deviation.* ***(ii)*** *Simplistic schematic of the detection format.*

5.2.2.6 Generation of a BiTE construct by increasing the length of the linker to facilitate binding

The linker was extended by the addition of two serine and glycine residues to the scFv 2 back primer, shown in ***Figure 5.39*** (the additional codons are highlighted in yellow). This expanded the flexible linker to four serine and two glycine which are small amino acids that provide optimum flexibility and the necessary distance between the scFv for optimal binding conditions (Huehls *et al.,* 2015).

The scFv genes were re-amplified by PCR using the newly designed primers. The method for BiTE construction by cloning the two scFv into the pET-26b(+) was identical to that performed in *Section 5.2.2.1*. ***Figure 5.40*** shows the various agarose gels of each step carried out. The final ligation was ethanol precipitated and transformed into BL21 (DE3) *E. coli* cells. The transformation was grown on LB agar plates supplemented with kanamycin and grown O/N at 37°C.

All single colonies obtained from the transformation of the pET-26b(+) vector containing the BiTE gene construct were picked and grown overnight at 37°C. The following day, these were subcultured into fresh media and induced with 2 mM IPTG and grown O/N at 30°C. The lysate from each culture was obtained as described in *Section 2.12.3.* The lysate was applied to a HER2-coated (1 μg/mL) ELISA plate and the dual binding functionality of each clone was analysed via the ELISA format outlined in ***Figure 5.35***. Each clone was analysed in triplicate and the standard deviation calculated and shown in the graph through error bars (***Figure 5.41***). Three times the standard deviation was applied as the cut-off value indicating a significant difference between the wells containing the BiTE and the control well. In order to correctly determine the effects of the inclusion of a longer linker, the H11 clone yielded the highest absorbance with the most minimal error bar, was taken forward for expression studies.

scFv 1 – Forward

5' AT CCG AAT TCG AGC GGC GCG CCG GTG GCC CAG GCG GCC CTG ACT CAG 3'

Translated primer

AT CCG AAT TCG AGC GGC GCG CCG GTG GCC CAG GCG GCC CTG ACT CAG
P N S V G A P V A Q A A L T Q

scFv 1 – Back

5' CAT GGC GCA TAC CCG TAC GAC GTT CCG GAC GAC TAC GCT TCT AAG CTT GCG G 3'

Translated primer

CAT GGC GCA TAC CCG TAC GAC GTT CCG GAC GAC TAC GCT TCT AAG CTT GCG G
H G A Y P Y D V P D D Y A S K L A

scFv 2 – Forward

5' AT CCG AAT TCG GTA GTG GCC CAG GCG GCC CTG ACT CAG 3'

Translated primer

AT CCG AAT TCG GTA GTG GCC CAG GCG GCC CTG ACT CAG
P N S V V A Q A A L T Q

scFv 2– Back

5' TCC TCC TCC TCC GGC GGC ACT AGT GGC CAG GCC GGC CAG GGT TCG GGC GCG CCG GTG 3'

Translated primer

TCC TCC TCC TCC GGC GGC ACT AGT GGC CAG GCC GGC CAG GGT TCG GGC GCG
S S S S G G T S G Q A G Q G S G A
CCG GTG
P V

= *Sfi*I site = *EcoR*I site

= *Asc*I site = *Hind*III site

Figure 5.39 Primers designed for the amplification of the scFv genes with a longer serine-glycine linker.

Re-designed primers for the amplification and cloning of the anti-CD3ε and-HER2 scFv into the pET 26-b(+) vector. The additional codons are highlighted in yellow.

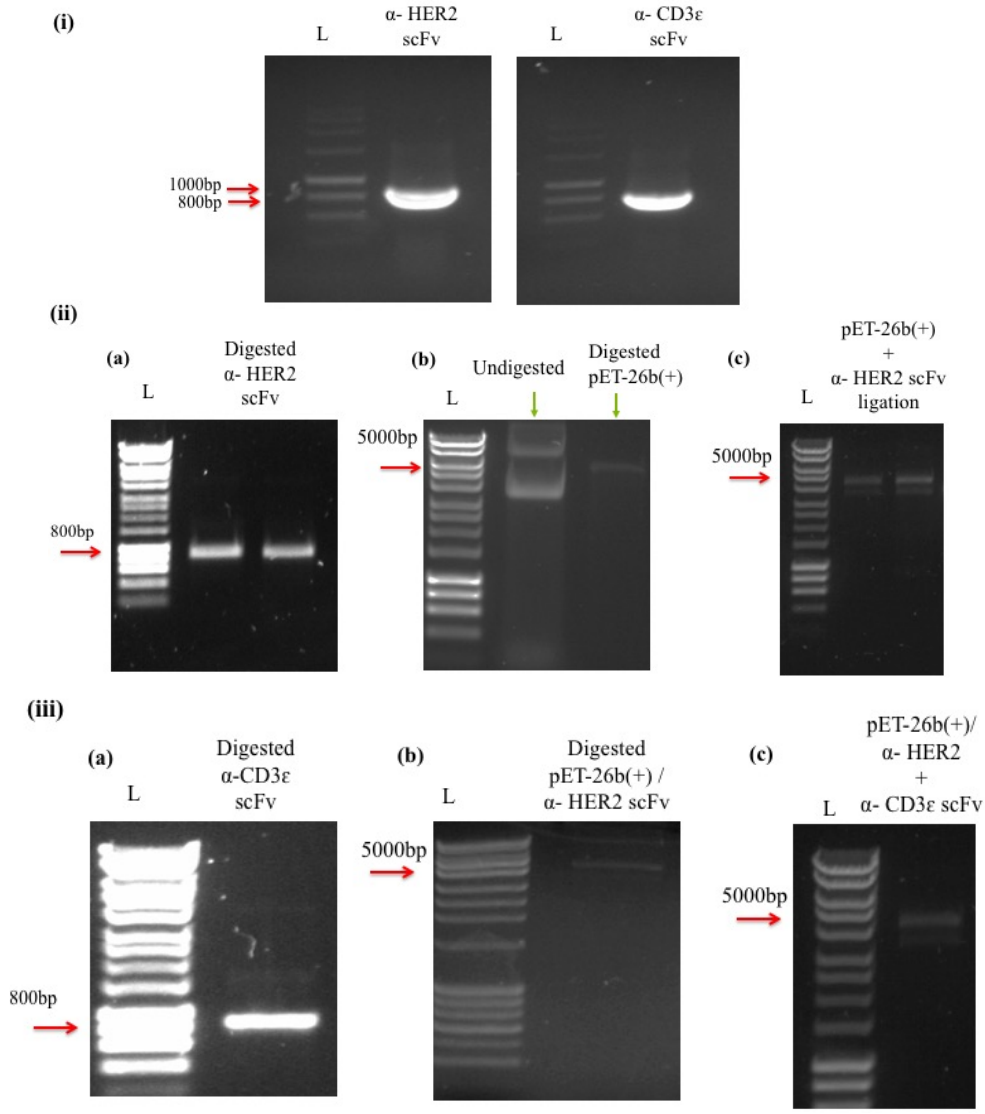

Figure 5.40 Generation of BiTE construct containing a longer linker

(i) *Large-scale amplification of the anti-CD3ε and anti-HER2 scFv genes was performed using primers to incorporate a longer linker.* ***(ii) (a)*** *The amplified anti-HER2 scFv gene and* ***(b)*** *pET-26b(+) vector were digested using EcoRI and HindIII. The digested anti-HER2 scFv was analysed on a 1.5% (w/v) agarose gel. An undigested sample of the pET-26b(+) vector was analysed with the digested vector on a 0.6% (w/v) agarose gel.* ***(c)*** *The digested scFv gene and vector were ligated and analysed on a 0.6% (v/v) agarose gel.* ***(iii) (a)*** *The amplified anti-CD3ε scFv gene and* ***(b)*** *pET-26b(+)-HER2 scFv vector were digested using EcoRI and AscI. The digested anti-CD3ε scFv gene was analysed on a 1.5% (w/v) agarose gel. The pET-26b(+)-HER2 scFv vector was analysed on a 0.6% (w/v) agarose gel.* ***(c)*** *The digested scFv gene and vector were ligated using T4 DNA ligase and analysed on a 0.6% (v/v) agarose gel. L = 1kb Ladder (Bioline HyperLadder™)*

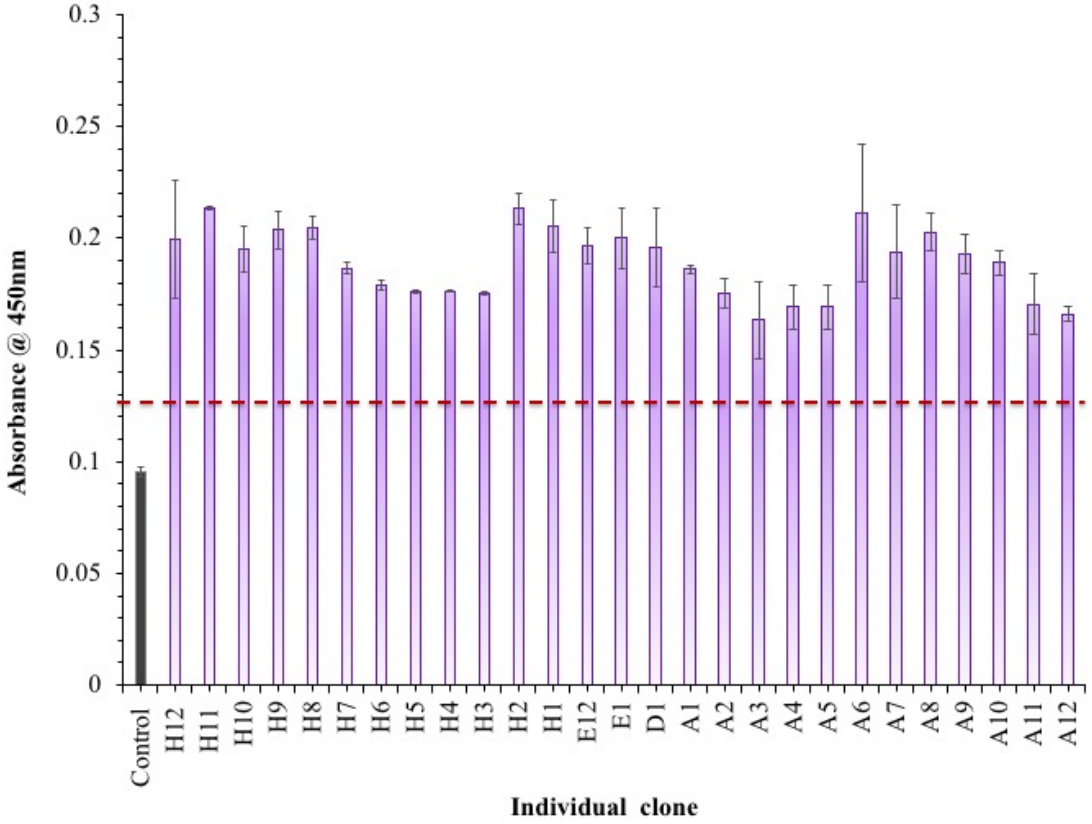

Figure 5.41 Analysis of transformed single colonies for the presence of a BiTE with dual binding abilities

Periplasmic lysates were applied to the HER2-coated plate and the ELISA performed as per ***Figure 5.35*** *whereby CD3ε protein was added followed by a monoclonal anti-CD3ε antibody to bind to the bound CD3ε. A HRP-labelled anti-mouse antibody was then added to detect the monoclonal anti-CD3ε antibody. Red dashed line represents 3 times the standard deviation.*

5.2.2.7 Expression and purification of the BiTE antibody from the pET-26b(+) vector

Expression studies were carried out on the H11 clone and analysed using the dual binding ELISA format (***Figure 5.42***). These results suggest that 1 mM IPTG and an incubation temperature of 30°C are the optimum conditions for BiTE expression. This temperature was expected as it promotes solubility and improved protein folding which is imperative for the retention of the BiTE antibody's abilities (Sørensen and Mortensen, 2005).

The BiTE was expressed in a 1L culture using the optimum conditions determined. The lysate was obtained by sonication of the cells to release the recombinant protein from the periplasmic space as described in *Section 2.12.5.* The lysate was subjected to IMAC purification and the purification analysed by SDS-PAGE and WB. Both the SDS-PAGE and WB support the conclusion that the BiTE was successfully purified as there is a strong band present at the expected ~60kDa band (***Figure 5.43***). The eluted fractions were pooled and concentrated in 1 X PBS to 1 mL with a resulting yield of 1.2 mg/mL.

Following IMAC purification of the BiTE, the purified antibody was titred against the HER2 antigen in ELISA using the BiTE-specific format to determine the working concentration for further assays (***Figure 5.44***). The cumulative data to this point confirms a functional BiTE was generated that successfully binds to both antigens. Future assay development and validation would require a more extensive means of characterization through surface plasmon resonance (SPR) or fluorescence-activated cell sorting (FACS) analysis. Once fully characterised, this BiTE could be applied as a therapeutic against PDAC or any disease target of interest due to its design flexibility.

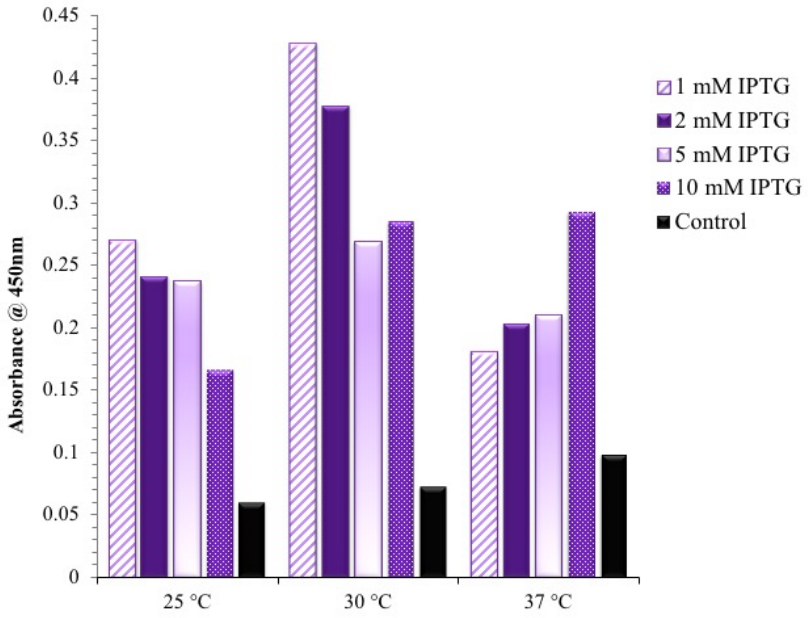

Figure 5.42 Analysis of optimal IPTG concentration and temperature for BiTE expression in the pET-26b(+) vector.

Expression of the BiTE was induced with different IPTG concentration (1 mM – 10 mM) and temperatures (25°C, 30°C and 37°C). The lysate was tested in the BiTE-specific ELISA format. Control – ELISA performed without the addition of BiTE lysate

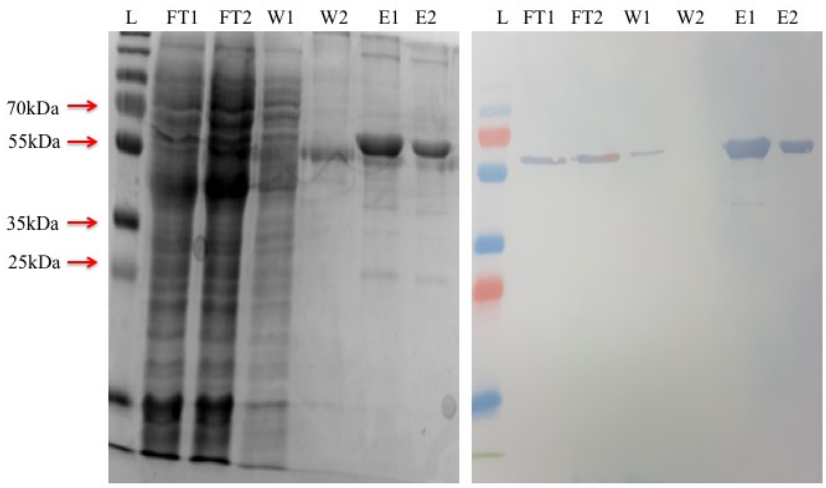

Figure 5.43 SDS PAGE and Western blot analysis of IMAC purified BiTE

SDS-PAGE and WB analysis of the fractions obtained during IMAC purification of BiTE. The WB was probed with a HRP-labelled anti-HA antibody. L = PageRuler™ Plus Prestained Protein Ladder. FT1 = Flow through 1; FT2 = Flow through 2; W1 = Wash 1; W2 = Wash 2; E = Elution.

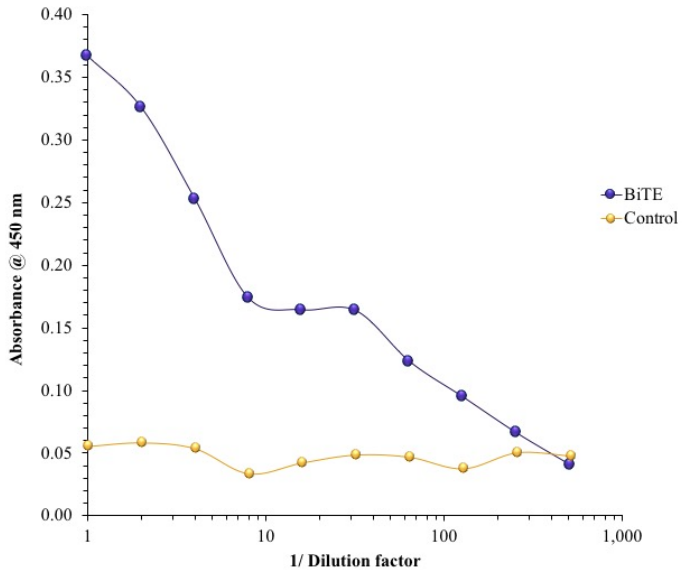

Figure 5.44 Titration of IMAC-purified BiTE using ELISA format shown in Figure 5.35

Titration of the purified BiTE against immobilised HER2 (1 µg/mL). Dilutions from 'neat' to 1/512 of the purified BiTE were performed, and applied to a HER2-coated ELISA plate. Free CD3ε (8 µg/mL) was added and bound antigen detected by the addition the anti-CD3ε mouse monoclonal antibody followed by a HRP-labelled anti-mouse antibody. Control – ELISA performed without the addition of BiTE antibody.

5.3 Discussion and conclusion

Over the past few years our understanding of the mechanisms of tumour cells evading immune surveillance has improved significantly. This has promoted research into novel T-cell based immunotherapies. Bispecific antibodies (bsAb) have become a popular and promising method to directly target cancer by engaging immune cells. Two such bsAbs have been approved for therapeutic use in patients, catumaxomab (anti-EpCAM x CD3) and blinatumomab (anti-CD19 x anti-CD3) with a variety more in clinical trials (Chen *et al.,* 2016). Various T-cell based cancer immunotherapeutic approaches are reported in the literature, among which is the bsAb format, the BiTE. As previously described, their mechanism of action links the tumour cell to the T-cell, leading to T-cell activation and tumour cell lysis (Stieglmaier *et al.,* 2015). Blinatumomab is the first BiTE antibody approved in the U.S and the E.U. and has resulted in long-term remission in many patients with CD19-expressing refractory or relapsed acute B-lymphocytic leukaemia (Ross *et al.,* 2017).

The aim within this chapter was to create a bispecific T-cell engager using a 'proof-of-concept' strategy which could serve as a targeted therapy for treatment of PDAC, infamous for its poor survival rates and limited treatment options. However, the resulting BiTE was created targeting HER2 rendering it applicable as a therapeutic approach to cancers that overexpress this antigen, most specifically, HER2+ breast cancers. Furthermore, the strategy employed has great design flexibility which allows the method to be used for the generation of a BiTE against a TAA to target any cancer. BiTEs are particularly beneficial for cancers that are not appropriately sensitive to standard chemotherapeutic approaches. Cancer cells use a multitude of methods to evade detection such as the creation of an immune suppressive environment and loss of MHC 1 molecules. When tested against cells with known involvement in tumour cell evasion, promising results with limited resistance to the BiTE was observed (Yuraszeck *et al.,* 2017). As chemoresistance is a devastating issue associated with pancreatic cancer, this format of bispecific antibody was selected for the generation of a targeted therapy to treat this malignancy. Furthermore, a humanized BiTE was created by Gohil and colleagues (2017) against receptor tyrosine kinase-like orphan receptor 1 (ROR1) which is present on the surface of a variety of cancer-initiating cells. Gohil and colleagues research

focused on the BiTEs applicability in PDAC and showed that it resulted in T-cell mediated and antigen-specific cytotoxicity when applied to PDAC cancer cell lines at a concentration of 0.1 ng/mL. Furthermore, it reduced the size of PDAC tumours in mice. This work highlights the exciting potential of BiTEs as a promising immunotherapeutic approach for the targeted treatment of PDAC. Other work carried out has illustrated the potential of BiTEs for PDAC cancer treatment. For example, some studies have shown that the MT110 (solitomab) BiTE specific for EpCAM on tumour cells, could potentially eradicate PDAC primary cancer cells and circulating cancer cells *in vivo* and *in vitro* (Cioffi *et al.,* 2012). Advantageously, the permeability of a BiTE is greater than many formats of bispecific antibody due to its small molecular mass, making it an attractive candidate for PDAC treatment, as this could potentially aid in its penetrance into the desmoplastic stromal environmental (Shengnan *et al.,* 2017). This array of promising data described led to the conception of the 'proof-of-concept' strategy for the creation of a BiTE described herein.

The strategy devised in this work involves the use of PCR and cloning techniques. It allows for both scFv within the BiTE to be incorporated into the expression vector individually through digestion sites which provides the flexibility of incorporating scFv specific to any target of interest. Considerations must be made when selecting for a target antigen. The TAA must be homogenously expressed across cancer cells as the heterogeneity of TAA expression can become problematic by potential resistance as the treatment will only eliminate TAA-expressing tumour cells (Ross *et al.,* 2017). While the anti-CD3ε scFv of the BiTE was generated herein, it was decided to employ a previously isolated and characterized scFv against HER2 as the TAA-specific arm. This decision was made as the anti-AGR2 scFv, originally envisioned as the anti-TAA scFv, had not been fully characterized prior to initiation of the work on the BiTE antibody. According to the literature, there are a plethora of strategies employed for the generation of BiTEs. Most commonly, the full BiTE construct (V_H - V_L - V_H - V_L) is created through molecular DNA techniques, primarily through SOE-PCR, and expressed in *E. coli* or mammalian systems (Choi *et al.,* 2013; Schmohl *et al.,* 2016). When generating the anti-ROR1 BiTE, Gohil *et al.,* created the anti-ROR1 scFv from hybridomas acquired through rat immunizations, which was coupled with an anti-CD3 scFv by SOE-PCR. The disadvantage associated with this method is the finality of the anti-TAA arm. A change in target requires removal of the entire construct and further PCR steps, unless restriction

sites are previously incorporated. Other work carried out by Kim and colleagues (2012) constructed an anti-HER2 X CD3 BiTE through genetically encoded unnatural amino acids and orthogonal chemical reactivity. This construct reported impressive yields and homogenous products. Most similar to the method described herein was the construction of an anti-CD19 X CD3 BiTE. The antibody was generated by obtaining a vector which contained an anti-17-1A X CD3 BiTE and replacing the anti-17-1A region with an anti-CD19 scFv fragment (Löffler *et al.,* 2000). This method offers the design flexibility envisioned for the strategy herein. By employing this method, the two scFv constructs were successfully amplified and cloned into the expression vector.

Initially, issues were encountered with the dual binding abilities of the BiTE as a result of steric hindrance which can often arise during the creation of bispecific antibodies, yet it was shown to disappear when an appropriately long flexible linker is incorporated (Orcutt *et al.,* 2010; Watanabe *et al.,* 2011; Hao *et al.,* 2015) Lack of appropriate linkers, or short linkers can cause misfolding, low yield in production and impaired activity (Li *et al.,* 2014). Consequently, a longer linker, constructed with serine and glycine amino acids ,was incorporated. These small non-immunogenic amino acids were selected for the linker as they create flexible linkers employed when the fused domains require additional movement. Moreover, the addition of small amino acids ensures that distance between the tumour cell and T-cell remains appropriate for the potency of the BiTE, and formation of the immunological synapse (Horn *et al.,* 2017). This is evident in the construction of the BiTE blinatumomab where extra-long linkers are incorporated between the V_H and V_L domains and a shorter linker of 4 glycine and a serine fuses the two scFv (Brinkmann and Kontermann, 2017; Zhang *et al.,* 2017). Upon incorporation of a longer linker, the resulting antibody showed the ability to bind to both antigens simultaneously. These results clearly show that the strategy created for this work can be successfully employed to create a functional bispecific antibody.

The determined affinity of blinatumomab for CD3 and CD19 is low with K_d values noted in the range of 10^{-7}M and 10^{-9} M, respectively. It is however, highly potent with cytotoxic effects as low as 10 pg/mL (1.8×10^{-13}M) (Yuraszeck *et al.,* 2017). Comparably, the limits of detection for the scFv within the BiTE described in this chapter are 20 pg/mL and 10 pg/mL for the anti- CD3ε and anti-HER2 scFv, respectively. However, for complete direct comparison, the affinities of each scFv arm must be determined by SPR. By

employing such an approach, the complete binding abilities of the BiTE can be elucidated. Additionally, a vast amount of further investigations would be required to fully characterize the BiTE antibody and its effects. Cell viability assays should be performed with unstimulated T-cells and a cancer cell line in the presence of the BiTE to investigate the antibodies ability to elicit antigen-specific cytotoxic responses. The capability of the BiTE to induce T-cell activation must also be explored through the use of co-cultures and employing flowcytometry to determine the expression of T-cell activation markers (Cioffi *et al.,* 2012). It is common practice to characterize a BiTE antibody using a T-cell dependent cellular cytotoxicity (TDCC) assay. It measures the cytotoxicity induced from a BiTE binding to a T-cell and redirecting it to TAA expressing tumour cells (Compte *et al.,* 2014; Nazarian *et al.,* 2015). Long-term analysis would include investigation of the anti-tumor response of the BiTE antibody in animal models using xenograft mice (Gohil *et al.,* 2017).

In its current form, the anti-HER2 X CD3ε BiTE would potentially be applicable as a immunotherapy for breast cancer as HER2 is overexpressed in 25-30% of breast cancers. HER2 has served as a target for a variety of breast cancer therapies (Wang *et al.,* 2013). Most notable is the recombinant monoclonal antibody, trastuzumab, employed for patients with HER2+ breast cancer, as it inhibits the proliferation of cancer cells and has a reported low K_D value of 0.1 nM (Carter *et al.,* 1992). Recently, bsAbs have become a popular choice for HER2+ cancer therapies. A study in 2013 by Wang and colleagues, created a bsAb called FcabCD3 by fusing an anti-CD3 scFv with a Fcab (Fc antigen binding) with a mutant Fc fragment specific against HER2. The results indicated the antibody had the ability to kill HER2+ cells *in vitro.* The Fcab has a reported affinity of ~8.6 nM to HER2, comparably, the anti-HER2 specific arm of the BiTE created here, yielded a LOD of 10 pg/mL and with further investigation using SPR technology could prove superior to the described FcabCD3 (Wozniak-Knopp *et al.,* 2010). Another antibody specific for HER2 is ertumaxomab, an anti-HER2 X CD3ε trifunctional bsAb, composed of a unique isotype combination (mouse IgG2a and rat IgG2b) that can recruit an activate cells such as natural killer cells and macrophages. It was found to recognize a different epitope to that detected by trastuzumab and thus has been proposed as potentially beneficial as a combination therapy with trastuzumab. However, this antibody encountered immunogenicity issues relating to HAMA/ HARA responses (Jäger *et al.,* 2009). In comparison, the BiTE created within this chapter is avian derived. This can be

very beneficial due to phylogenetic distance from humans meaning high responses to immunised mammalian protein antigens (Conroy *et al.,* 2014). Furthermore, the higher avian core temperature of 41°C results in more stable antibodies and a longer half-life (Conroy *et al.,* 2012). These superior attributes render the avian BiTE herein an attractive therapeutic option when treating cancers found to be HER2+.

Further characterisation of this BiTE could elucidate the therapeutic potential of this research. Initially *in vitro* analysis should be carried out using cell lines, such as the Jurkat E.6.1 clone T-lymphocyte and the Capan-1 adenocarcinoma cell line in the ELISA format previously described that analyses the dual binding capabilities of the BiTE. Such an experiment will determine if the BiTE has the ability to bind to both proteins when presented on a cell surface. Furthermore it will provide data on any possible steric hindrance that could result from the bulk size of the cells. Additionally, the BiTEs kinetic binding abilities to each antigen would need to be evaluated using surface plasmon resonance. This is of particular importance as it has been shown in studies that the BiTEs affinity for CD3ε should be inferior to its affinity for the tumour associated antigen. This ensures the BiTE preferentially binds the TAA resulting in improved tumor targeting while sufficiently recruiting T-cells (Bortolletto *et al.,* 2002). A variety of other *in vitro* testing on the BiTE functionalities would also be required. For example, proliferation assays would be performed to ensure the BiTE has the capability to activate T-cells. This requires measuring the cytokine response, such as interferon gamma levels, from T-cells that have and have not been exposed to the BiTE in the presence of adenocarcinoma cells. Additionally, activation markers on T-cells such as CD64 and CD25 can be measured. The generation of the immunological synapse can also be tested by measuring the levels of accumulated actin (Ross *et al.,* 2017). It is of the utmost importance that a cytotoxicity assay is carried out to ensure that the BiTE can kill the target tumor cells. The most common of the cytotoxicity test is the chromium release (^{51}Cr) assay whereby the target tumor cells are packed with ^{51}Cr and tumor cells that are undergoing T-cell mediated death will release this ^{51}Cr which is subsequently measured and quantified (Nazarian *et al.,* 2014). Following *in vitro* studies, *in vivo* analysis of the BiTE in a mouse xenograft model would be required. *In vivo* analysis of the BiTE blinatumomab, indicated that sub-microgram doses would prevent the growth of xenografts and was curative when administered to early tumor stage. The BiTE generated herein should, in the future, be analysed in the same manner. Immunocompromised mice, such as SCID mice are

employed as a result of their T-cell and B-cell deficiency. Pancreatic adenocarcinoma cells should be mixed with peripheral blood mononuclear cells (PBMC) and injected subcutaneously with one group of mice injected with an irrelevant BiTE as a control group. Tumor sizes should be measure twice weekly (Dreier *et al.,* 2003). Only with the data that can be provided by *in vitro* and *in vivo* analysis of the BiTE generated within will its full therapeutic ability be established.

In conclusion, the work within this chapter offers a potentially promising contribution to tackling the therapeutic problems surrounding PDAC. The chemoresistant nature of this disease requires potent targeted treatment options, which BiTEs have the ability to provide. Within this chapter an anti-CD3ε scFv was successfully isolated from an avian-derived anti-Jurkat scFv library. Subsequently, two immunoassays were qualitatively validated for the detection of HER2 and CD3ε using an anti-HER2 scFv and the anti-CD3ε generated herein. This chapter also describes the successful generation of an anti-HER2 X CD3ε BiTE that has shown successful functional dual-binding capacity. Furthermore, without requiring additional steps involving the removal of the current anti-TAA scFv within the BiTE, the anti-HER2 X CD3ε antibody provides a targeted method of treatment for any cancer known to overexpress the HER2 antigen such as, ovarian, bladder, endometrial, prostate and non-small-cell lung cancer (Wang *et al.,* 2013).

Chapter 6

Overall conclusions

6.1 Overall conclusions

PDAC has an almost 100% mortality rate as a direct result of poor detection methods and limited treatment options (Ramos *et al.,* 2017). Thus, PDAC is a disease that would greatly benefit from the discovery and development of new and superior methods for both detection and treatment. The overall aims of this research were to exploit the applications of recombinant antibodies to provide an improved means of PDAC diagnosis using a panel of scFv antibodies and to demonstrate a potential antibody-based strategy for targeted treatment to counteract its chemoresistant nature. It is envisioned that the antibodies generated herein could, in the future, provide clinicians with analytical tools for PDAC detection and possible alternative means of treatment. The approach employed includes the construction of scFv immune libraries, the generation, and characterization of specific recombinant antibody fragments to selected biomarkers, the development of associated ELISA assays and the exploitation of the design flexibilities associated with antibodies to create a bispecific antibody tailored for treatment of solid malignancies less sensitive to standard chemotherapies.

The initial phase of this research was the construction of a communal murine Capan-1 - specific library described in *Chapter 3* for the isolation of the three scFv proposed for the diagnostic panel. Despite extensive work, the communal library was only successfully employed for the isolation of anti-MSLN scFv. The resulting anti-MSLN scFv were characterized by ELISA which showed the limited abilities of the antibody fragments to bind to the antigen in solution. From the onset on this chapter, it had been envisioned that the anti-MSLN scFv could be used for detection of MSLN in serum and tissue. The future application of the scFv was altered as lack of free antigen recognition rendered the scFv inappropriate for use as serum MSLN detectors. Consequently, further characterization focused on elucidating the scFvs abilities to detect MSLN through linear and conformational epitopes using western and dot blotting techniques. Despite being inferior to anti-MSLN primary antibodies available, these investigations indicated the potential of these scFv for applications in IHC and further work to increase the antibodies performance characteristics, for example, by highly directed genetic engineering approaches could prove very beneficial. Due to time constraints, improvements by altering the functionality to improve the specificity of the scFv was not performed.

The generation of the remaining scFv of the proposed diagnostic panel are described in *Chapter 4.* As mentioned, it was intended that anti-Capan-1 scFv library generated in *Chapter 3* would serve as a communal pool of anti-PDAC scFv for selection of antibody fragments specific to the markers targeted within this research. However, attempts to isolate AGR2- and MUC1-specific antibody fragments were ineffective and alternative routes were explored. The naïve synthetic Tomlinson library was employed for isolation of specific scFv which resulted in the identification of two anti-AGR2 scFv and an anti-MUC1 scFv which were subsequently incorporated into an ELISA. Competitive ELISAs were developed with all three antibodies in PBS and normal human serum. Inter- and intra-day studies were carried out to evaluate the precision and reproducibility of the assays. With maximum observed CV percentages of 15.8% the assays were found to be accurate and reproducible. Spiked serum calibration curves were employed for the calculation limits of detection (LOD) of the three antibodies. The anti-AGR2 scFv B11 and anti-MUC1 scFv A5 calculated LODs were found to be 40 pg/mL and 20 pg/mL, respectively, which were verified by precision analysis. The combined data of *Chapter 4* confirmed that both scFv have promising potential as members of the suggested diagnostic panel as each scFv has shown impressive sensitivity for the cognate antigen. The detection capabilities of both scFv were found to be in the picogram range. The potential application of the proposed panel offers the promise of a more accurate and earlier diagnosis that will generate valuable information on the optimum therapeutic route that could be implemented. Extensive further clinical work to verify this would be necessary. The work described in *Chapter 3* and *Chapter 4* provides a fundamental basis for additional research on panel to demonstrate its utility in a clinical setting.

In addition to improving diagnosis of PDAC, the work in this thesis investigated a potential means for the targeted therapy of PDAC using a bispecific T-cell engager. *Chapter 5* focuses on the generation of an anti-CD3ε antibody fragment and its incorporation into a functional bispecific T-cell engager. Despite issues encountered with the murine immune library generated in this chapter, an anti-CD3ε scFv was successfully isolated from an anti-Jurkat avian immune library previously generated within the Applied Biochemistry Group (data not shown). Initially, it was hypothesized that the anti-AGR2 scFv would be used as the tumour associated arm for the generated BiTE as this marker is a well-established therapeutic target as it plays a vital role in PDAC initiation and progression (Dumartin *et al.,* 2017). However, on account of issues associated with

the murine anti-Capan-1 library, the anti-AGR2 scFv was not sufficiently characterized prior to initiation of the BiTE formation. Therefore, a previously generated avian anti-HER2 scFv was employed. Both the anti-HER2 and -CD3ε scFv were first incorporated into competitive ELISAs, initially in PBS and subsequently in normal human serum. The generated competitive assays showed good intra- and inter-day CV percentages confirming the accuracy and reproducibility of the assays. Through calibration curve and experimental validation using precision assays, the LOD of the anti-HER2 and -CD3ε scFv were confirmed to be 10 pg/mL and 20 pg/mL, respectively.

The initial strategy for generating the BiTE construct in *Chapter 5* utilised specifically designed primers used for the amplification of both scFv genes with incorporated digestion sites for ligation into the pET-26b(+) expression vector. This successfully yielded a bispecific product, confirmed by SDS-PAGE and WB that had the ability to bind to each antigen individually, however, issues arose during attempts to bind to both antigen simultaneously. It was decided the short linker incorporated between the two scFv did not allow for the necessary space and flexibility to allow both scFv to bind to the antigen simultaneously. The second attempt employed the same strategy with alterations to one primer that incorporated a longer flexible linker. This was successful and a BiTE capable of dual binding was obtained, expressed and purified, as confirmed by SDS-PAGE, WB and ELISA. The generation of this antibody has great promise for the targeted treatment of PDAC. However, significant further work using more complex screening methods such as FACS and SPR is required.

In conclusion, the work in this thesis has generated recombinant scFv against three different targets proposed for a novel diagnostic panel, and that they have been successfully characterized in the appropriate manner for their future application. It is envisioned that this panel could improve the current methods of diagnosis and provide valuable information on the optimum therapeutic route to be taken. Furthermore, this work describes the successful generation of a putative therapeutic bsAb, using two extensively characterized scFv, constructed by a flexible and highly applicable 'proof-of-concept' strategy. Successful dual binding of the BiTE was shown and further work on this could elucidate its full therapeutic potential.

Chapter 7

Bibliography

Aavula, S.M., Nimmagadda, S.V., Biradhar, N., Sula, S., Chandran, D., Lingala, R., & Villuppanoor, S.A. Generation and characterization of an scFv directed against site II of rabies glycoprotein. *Biotechnol. Res. Int.* 2011; 652147.

Adamczyk, B., Tharmalingam, T., & Rudd, P.M. Glycans as cancer biomarkers. *BBA-Gen. Subjects.* 2012; **1820** (9): 1347-1353.

Aghamaliyev, U., Hajiyeva, Y., & Rückert, F. Desmoplastic reaction in pancreatic ductal adenocarcinoma. *Pancreas. Open. J.* 2016; **1** (2): 22-29.

Ahmad, ZA., Yeap, S.W., Ali, A.M., Ho, W.Y., Alitheen, N.B., & Hamid, M. scFv antibody: Principles and clinical application. *Clin. Dev. Immunol.* 2012; **980250**: 1-15.

Albrecht, H., Denardo, G.L., & Denardo, S.J. Development of anti-MUC1 di-scFvs for molecular targeting of epithelial cancers, such as breast and prostate cancers. *Q. J. Nucl. Med. Mol. Imaging.* 2007; **51** (4): 304-313.

Alcover, A., Alarcón, B., & Di Bartolo, V. Cell biology of T cell receptor expression and regulation. *Ann. Rev. Immunol.* 2018; **36**: 103-125.

Amato, E., dal Molin, M., Mafficini, A., Yu, J., Malleo, G., Rusev, B., Fassan, M., Antonello, D., Sadakari, Y., Castelli, P., Zamboni, G., Maitra, A., Salvia, R., Hruban, R.H., Bassi, C., Capelli, P., Lawlor, R.T., Goggins, M., & Scarpa, A. Targeted next-generation sequencing of cancer genes dissects the molecular profiles of intraductal papillary neoplasms of the pancreas. *J. Pathol.* 2014; **233:** 217-227.

Andersson, G., Wennersten, C., Borgquist, S., & Jirström, K. Pancreatic cancer risk in relation to sex, lifestyle factors and pre-diagnostic anthropometry in the Malmö diet and cancer study. *Biol. Sex. Differ.* 2018; **7**: (66): 1-11.

Andreasson, U., Perret-Liaudet, A., van Waalwijk van Doorn, L.J.C., Blennow, K., Chiasserini, D., Engelborghs, S., Fladby, T., Genc, S., Kruse, N., Kuiperij, H.B., Kulic, L., Lewczuk, P., Mollenhauer, B., Mroczko, B., Parnetti, L., Vanmechelen, E., Verbeek,

N.M., Winblad, B., Zetterberg, H., Koel-Simmelink, M., & Teunissen, C.E. A practical guide to immunoassay method validation. *Front. Neurol.* 2015; **6** (179): 1-8.

Andris-Widhopf, F., Rader, C., Steinberger, P., Fuller, R., & Barbas III, C.F. Methods for the generation of chicken monoclonal antibody fragments by phage display. *J. Immunol. Methods.* 2000; **242:** (1-2): 159-181.

Argani, P., Iacobuzio-Donahue C., Ryu, B., Rosty, C., Goggins, M., Wilentz, R.E., Murugesan, S.R., Leach, S.D., Jaffee, E., Yeo, C.J., Cameron, J.L., Kern, S.E., & Hruban, R.H. Mesothelin is overexpressed in the vast majority of ductal adenocarcinomas of the pancreas: identification of a new pancreatic cancer marker by serial analysis of gene expression (SAGE). *Clin. Cancer Res.* 2001; **7:** 3862-3868.

Armbruster, D.A., Tillman, M.D., & Hubbs, L.M. Limit of detection (LOD)/limit of quantification (LOQ): comparison of the empirical and the statistical methods exemplified with GC-MS assays of abused drugs. *Clin. Chem.* 1994; **40** (7): 1233-1238.

Asghari, S., Khaniani, M.S., Darabi, M., & Derakhshan, S.M. Cloning of soluble human stem cell factor in pET-26b(+) vector. *Adv. Pharm. Bull.* 2014; **4** (1): 91-95.

Attard, C.L., Brown, S., Alloul, K., & Moore, M.J. Cost-effectiveness of FOLFIRNOX for first-line treatment of metastatic pancreatic cancer. *Curr. Oncol.* 2014; **21** (1): e41-e51.

Bahara, N.H.H., Chin. S.T., Choong, Y.S., & Lim, T.S. Construction of a semisynthetic human VH single-domain antibody library selection of domain antibodies against α-crystalline of *Mycobacterium tuberculosis*. *J. Biomol. Screen.* 2015; **21** (1): 35-43.

Bai, X., Kim, J., Kang, S., Kim, W., & Shim, H. A novel human scFv library with non-combinatorial synthetic CDR diversity. *PLos One.* 2015; **10** (10): e0141045.

Ballehaninna, U.K., & Chamberlain, R.S. The clinical utility of serum CA 19-9 in the diagnosis, prognosis and management of pancreatic adenocarcinoma: An evidence based appraisal. *J. Gastrointestinal Oncol.* 2012; **3** (2):105-119.

Ballehaninna, U.K., & Chamberlain, R.S. Biomarkers for pancreatic cancer: Promising new markers and options beyond CA 19-9. *Tumor Biol.* 2013; **34** (6): 3279-3292.

Balmaña, M., Duran, A., Gomes, C., Liop, E., Lopez-Martos, R., Ortiz, M.R., Barrabes, S., Reis, C.A., & Peracaula, R. Analysis of sialyl-Lewis x on MUC5AC and MUC1 mucins in pancreatic cancer. *Int. J. Biol. Macromol.* 2018; **112**: 33-45.

Barbas III, C.F., Burton, D.R., Scott, J.K, & Silverman, G.J. Phage Display: A Laboratory Manual, 1st edition, 736pp, Cold Spring Harbour Laboratory Press, 2001.

Barbas III, C.F., & Wagner, J. Synthetic human antibodies: Selecting and evolving functional proteins. *Methods.* 1995; **8** (2): 94-103.

Barbazán, J., Muinelo-Romay, L., Vieito, M., Candamio, S., Díaz-López, A., Cano, A., Gómez-Tato, A., Casares de Cal Mde, L., Abal, M., & López-López, R. A multimarker panel for circulating tumor cells detection predicts patient outcome and therapy response in metastatic colorectal cancer. *Int. J. Cancer.* 2014; **135** (11): 2633-2643.

Bashiri, S., Vikström, D., & Ismail, N. Optimization of protein expression in *Escherichia coli. BioPharm. International.* 2015; **28** (5): 42-44.

Bastarache, J.A., Koyama, T., Wickersham, N.E., Mitchell., D.B., Mernaugh, R.L., & Ware, L.B. Accuracy and reproducibility of a multiplex immunoassay platform: A validation study. *J. Immunol. Methods.* 2011; **367** (1-2): 33-39.

Bazan, J., Całkosiński, I., & Gamian, A. Phage display—A powerful technique for immunotherapy: 1. Introduction and potential of therapeutic applications. *Hum. Vaccin. Immunother.* 2012 **8** (12): 1817-1828.

Beauchemin, N., & Arabzadeh, A. Carcinoembryonic antigen-related cell adhesion molecules (CEACAMs) in cancer progression and metastasis. *Cancer Metast. Rev.* 2013; **32** (3-4): 643-671.

Benini, L., Cavallini, G., Zordan, D., Rizzotti., P., Rigo, L., Brocco, G., Perobelli, L., Zanchetta, M., Pederzoli, P., & Scuro, L.A. A clinical evaluation of monoclonal (CA19-9, CA50, CA12-5) and polyclonal (CEA, TPA) antibody-defined antigens for the diagnosis of pancreatic cancer. *Pancreas.* 1988; **3** (1): 61-66.

Bharadwaj, U., Li, M., Chen, C., & Yao, Q. Mesothelin-induced pancreatic cancer cell proliferation involves alteration of cyclin E via activation of Stat3. *Mol. Cancer. Res.* 2008; **6** (11): 1755-1765.

Billiau, A., & Matthys, P. Modes of action of Freund's adjuvants in experimental models of autoimmune diseases. *J. Leukoc. Biol.* 2001; **70** (6): 849-860.

Birnbaum, ME., Berry, R., Hsiao, Y.S., Chen, Z, Shingu-Vazquez, MA., Yu, X., Waghray, D., Fischer, S., McClusky, J., Rossjohn, J., Walz, T., & Garcia, K.C. Molecular architecture of the αβ T cell receptor-CD3 complex. *Proc. Natl. Acad. Sci. USA.* 2014; **111** (49): 17576-17581.

Bissolati, M., Sandri, M.T., Burtulo, G., Zorzino, L., Balzano, G., & Braga, M. Portal vein-circulating tumor cells predict liver metastases in patients with resectable pancreatic cancer. *Tumor Biol.* 2014; **36** (2): 991-996.

Blackford, A., Serrano, O.K., Wolfgang, C.L., Parmigiani, G., Jones, S., Zhang, X., Parsons, D.W., Lin, J.C., Leary, R.J., Eshleman, J.R., Goggins, M., Jaffee, E.M., Iacobuzio-Donahue, C.A., Maitra, A., Cameron, J.L., Olino, K., Schulick, R., Winter, J., Herman, J.M., Laheru, D., Klein, A.P., Vogelstein, B., Kinzler, K.W., Velculescu, V.E., & Hruban, R.H. *SMAD4* gene mutations are associated with poor prognosis in pancreatic cancer. *Clin. Cancer Res.* 2009; **15** (14): 4674-4679.

Bloomston, M., Frankel, W.L., Petrocca, F., Volinia, S., Alder, H., Hagan, J.P., Liu, C.G., Bhatt, D., Taccioli, C., & Croce, C.M. MicroRNA expression patterns to differentiate pancreatic adenocarcinoma from normal pancreas and chronic pancreatitis. *JAMA.* 2007; **297:** 1901-1908.

Boeck, S., Jung, A., Laubender, R.P., Neumann, J., Egg, R., Goritschan, C., Vehling-Kaiser, U., Winkelmann, C., Fischer von Weikersthal, L., Clemens, M.R., Gauler, T.C., Märten, A., Klein, S., Kojouharoff, G., Barner, M., Geissler, M., Greten, T.F., Mansmann, U., Kirchner, T., & Heinemannn, V. EGFR pathway biomarkers in erlotinib-treated patients with advanced pancreatic cancer: translational results from the randomised, crossover phase 3 trial AIO-PK0104. *Br. J. Cancer.* 2013; **108** (2): 469-476.

Bornhorst, J.A., & Falke, JJ. Purification of proteins using polyhistidine affinity tags. *Methods Enzymol.* 2000; **326**: 245-254.

Bortoletto, N., Scotet, E., Myamoto, Y., D'Oro, U & Lanzavecchia, A. Optimizing anti-CD3 affinity for effective T cell targeting against tumor cells. *Eur. J. Immunol.* 2002; **32** (11): 3102-3107.

Bosma, M.J., & Carroll, A.M. The SCID mouse mutant: definition, characterization, and potential uses. *Annu. Rev. Immunol.* 1991; **9:** 323-350.

Boulter-Bitzer, J.I., Lee, H., & Trevors, J.T. Single-chain variable fragment antibodies selected by phage display against the sporozoite surface antigen P23 of *Cyrptosporidium parvum*. *J. Parasitol.* 2009; **95** (1): 75-81.

Brand, R.E., Nolen, B.M., Zeh, H.J., Allen, P.J., Eloubeidi, M.A., Goldberg, M., Elton, E., Arnoletti, J.P., Christein, J.D., Vickers, S.M., Langmead, C.J., Landsittel, D.P., Whitcomb, D.C., Grizzle, W.E., & Lokshin, A.E. Serum biomarker panels for the detection of pancreatic cancer. *Clin. Cancer Res.* 2011; **17** (4): 805-816.

Brinkmann, U., & Kontermann, R.E. The making of bispecific antibodies. *MAbs.* 2017; **9** (2): 182-212.

Brischwein, K., Schlereth, B., Guller, B., Steiger, C., Wolf, A., Lutterbueses, R., Offner, S., Locher, M., Urbig, T., Raum, T., Kleindienst, P., Wimberger, P., Kimmig, R., Fichtner, I., Hofmeister, R., da Silva, A.J., & Baeuerle, P.A. MT110: A novel bispecific single-chain antibody construct with high efficacy in eradicating established tumors. *Mol. Immunol.* 2006; **43** (8): 1129-1143.

Brischwein, K., Parr, L., Pflanz, S., Volkland, J., Lumsden, J., Klinger, M., Locher, M., Hammond, S.A., Kiener, P., Kufer, P., Schlereth, B., & Baeuerle, P.A. Strictly target cell-dependent activation of T cells by bispecific single-chain antibody constructs of the BiTE class. *J. Immunother.* 2007; **30** (8): 798-807.

Brozy, J., Schlaepfer, E., Mueller, C.K.S., Rochat, M.A., Rampini, S.K., Myburgh, R., Raum, T., Kufer, P., Baeuerle, P.A., Muenz, M., & Speck, R.F. Antiviral activity of HIV gp120 targeting bispecific T cell engager (BiTE®) antibody constructs. *J. Virol.* 2018; **92** (14): 1-18.

Brunner, D., Frank, J., Appl, H., Schöffl, H., Pfaller, W., & Gstraunthaler G. Serum-free cell culture: The serum-free media interactive online database. *ALTEX.* 2010; **21**(1): 53-62.

Brychtova, V., Vojtesek, B., & Hrstka, R. Anterior gradient 2: A novel player in tumor cell biology. *Cancer Lett.* 2011; **304:** 1-7.

Brychtova, V., Hermanova, M., Karasek, P., Lenz, J., Selingerova, I., Vojtesek, B., Kala, K., & Hrstka, R. Anterior gradient 2 and mucin 4 expression mirrors tumor cell differentiation in pancreatic adenocarcinomas, but aberrant anterior gradient 2 expression predicts worse patient outcome in poorly differentiated tumors. *Pancreas.* 2014*;* **43** (1): 75-81.

Buchsbaum, D.J., & Croce, C.M. Will detection of microRNA biomarkers in blood improve the diagnosis and survival of patients with pancreatic cancer? *JAMA.* 2014; **311** (4): 363-365.

Bünger, S., Laubert, T., & Roblick, U.J. Serum biomarkers for improved diagnostic of pancreatic cancer: a current overview. *J. Cancer Res. Clin. Oncol.* 2011; **137:** 375-389.

Burkovitz, A., & Ofran, Y. Understanding differences between synthetic and natural antibodies can help improve antibody engineering. *Mabs.* 2016; **8** (2): 278-287.

Byrne, H., Conroy, P.J., Whisstock, J.C., O'Kennedy, R.J. A tale of two specificities; bispecific antibodies for therapeutic and diagnostic applications. *Trends. Biotechnol.* 2013; **31** (11): 621-632.

Carter, P., Presta, L., Gorman, C.M., Ridgeway, J.B.B., Henner, D., Wong, W.L., Rowland, A.M., Kotts, C., Carver, M.E., & Shepard, H.M. Humanization of an anti-p185HER2 antibody for human cancer therapy. *Proc. Natl. Acad. Sci. USA.* 1992; **89** (10): 4285-4289.

Carrera, S., Sancho, A., Azkona, E., Azkuna, J., & Lopez-Vivanco, G. Hereditary pancreatic cancer: related syndromes and clinical perspective. *Hered. Cancer Clin. Prac.* 2017; **15**: (9): 1-9.

Cascio, S., Finn, O.J. Intra- and extra-cellular events related to altered glycosylation of MUC1 promote chronic inflammation, tumor progression, invasion, and metastasis. *Biomolecules.* 2016; **6** (4): 39.

Chames, P., & Baty, D. Bispecific antibodies for cancer therapy: The light at the end of the tunnel? *mAbs.* 2009; **1** (6): 539-547.

Chames, P., Kerfelec, B., & Baty, D. Therapeutic antibodies for the treatment of pancreatic cancer. *Sci. World J.* 2010; **10:** 1107-1120.

Chan, A., Prassas, I., Dimitromanolakis, A., Brand, R.E., Serra, S., Diamandis, R.P., & Blasutig, I.M. Validation of biomarkers that complement CA19.9 in detecting early pancreatic cancer. *Clin. Cancer Res.* 2014; **20** (22): 5787-5795.

Chang, M.C., Chen, C.A., Hsieh, C.Y., Lee, C.N., Su, Y.N., Hu, Y.H., & Cheng, W.F. Mesothelin inhibits paclitaxel-induced apoptosis through the PI3K pathway. *Biochem. J.* 2009; **424:** 449-458.

Chang, J.C., & Kundranda, M. Novel diagnostic and predictive biomarkers in pancreatic adenocarcinoma. *Int. J. Mol. Sci.* 2017; **18** (3): 1-14.

Chen, L., & Flies, D.B. Molecular mechanisms of T cell co-stimulation and co-inhibition. *Nat. Rev. Immunol.* 2014; **13** (4): 227-242.

Chen, R., Pan, S., Duan, X., Nelson, B.H., Sahota, R.A., de Rham, S., Kozarek, R.A., McIntosh, M., & Brentnall, T.A. Elevated level of anterior gradient-2 in pancreatic juice from patients with pre-malignant pancreatic neoplasia. *Mol. Cancer.* 2010; **9** (149): 1-12.

Chen, R., Dawson, D.W., Pan, S., Ottenhof, N.A., de Wilde, R.F., Wolfgang, C.L., May, D.H., Crispin, D.A., Lai, L.A., Lay, A.R., Waghray, M., Wang, S., McIntosh, M.W., Simeone, D.M., Maitra, A., & Brentnall, T.A. Proteins associated with pancreatic cancer survival in patients with resectable pancreatic ductal adenocarcinoma. *Lab. Invest.* 2015; **95** (1): 43-55.

Chen, S., Hung, W., Wang, P., Paul, C., & Konstantopoulos, K. Mesothelin binding to CA125/MUC16 promotes pancreatic cancer cell motility and invasion via MMP-7 activation. *Sci. Rep.* 2013; **(**1870) :1-10

Chen, S., Li, J., Li, Q., & Wang, Z. Bispecific antibodies in cancer immunotherapy. *Hum. Vaccin. Immunother.* 2016; **12** (12): 2491-2500.

Chen, S., Na, N., & Jian, Z. Pretreatment platelet count as a prognostic factor in patients with pancreatic cancer: A systematic review and meta-analysis. *OncoTargets. Ther.* 2018; **11**: 59-65.

Chen, X., Zaro, J., & Shen, W.C. Fusion protein linkers: Property, design and functionality. *Adv. Drug Deliv. Rev.* 2012; **65** (10): 1357-1369.

Chen, Y., Wang, X., Zhao, P., & Cao, B. Development and characterization of monoclonal antibodies against pancreatic cancer marker hippocalcin-like 1 protein. *Monocl. Antib. Immunodiagn. Immunother.* 2014; **33** (1): 20-27.

Cheng, W.F., Huang, C.Y., Chang, M.C., Hu, Y.H., Chiang, Y.C., Chen, Y.L., Hsieh., & Chen, C.A. High mesothelin correlates with chemoresistance and poor survival in epithelial ovarian carcinoma. *Br. J. Cancer.* 2009; **100:** 1144-1153.

Chesher, D. Evaluating assay precision. *Clin. Biochem. Rev.* 2008; **29** (Suppl 1): S23-S26.

Chevet, E., Fessart, D., Delom, F., Mulot, A., Votesek, B., Hrstka, R., Murray, E., Gray, T & Hupp, T. Emerging roles for the pro-oncogenic anterior gradient-2 in cancer development. *Oncogene*. 2013; **32** (20): 2499-2509.

Chiramel, J., Backen, A.C., Pihlak, R., Lamarca, A., Frizziero, M., Tariq, N.U., Hubner, R.A., Valle, J.W., Amir, E., & McNamara, M.G. Targeting the epidermal growth factor receptor in addition to chemotherapy in patients with advanced pancreatic cancer: A systematic review and meta analysis. *Int. J. Mol. Sci.* 2017; **18** (909): 1-14.

Choi, B.D., Kuan, C.T., Cai, M., Archer, G.E., Mitchell, D.A., Gedeon, P.C., Sanchez-Perez, L., Pastan, I., Bigner, D.D., & Sampson, J.H. Systemic administration of a bispecific antibody targeting EGFRvIII successfully treats intracerebral glioma. *Proc. Natl. Acad. Sci. USA.* 2014; **110** (1): 270-275.

Chu, L.C., Goggins, M.G., & Fishman, E.K. Diagnosis and detection of pancreatic cancer. *Cancer J.* 2017; **23** (6): 333-342.

Cicenas, J., Kvederaviciute, K., Meskinyte, I., Meskinyte-Kausiliene, E., Skeberdyte, A., & Cicenas Jr., J. KRAS, TP53, CDKN2A, SMAD4, BRAC1, and BRAC2 mutations in pancreatic cancer. *Cancers (Basel).* 2017; **9** (42): 1-8.

Cioffi, M., Dorado, J., Baeuerle, P.A., & Heeschen, C. EpCAM/CD3-Bispecific T-cell engaging antibody MT110 eliminates primary human pancreatic cancer stem cells. *Clin. Cancer Res.* 2012; **18** (2): 465-474.

Cochran, J.R., Cameron, T.O., & Stern, L.J. The relationship of MHC-peptide binding and T cell activation probed using chemically defined MHC class II oligomers. *Immunity.* 2000; **12** (3): 241-250.

Collins, M.A., & di Magliano, M.P. Kras as a key oncogene and therapeutic target in pancreatic cancer. *Front. Physiol.* 2014; **4** (407): 1-8.

Collins, A.M., Wang, Y., Roskin, K.M., Marquis, C.P., & Jackson, K.J. The mouse antibody heavy chain repertoire is germline-focused and highly variable between inbred strains. *Philos. Trans. R. Soc. Lond. B. Biol. Sci.* 2015; **370** (1676): 1-16.

Compte, M., Álvarez-Cienfuegos, A., Nuñez-Prado, N., Sainz-Pastor, N., Blanco-Toribio, A., Pescador, N., Sanz, L., & Álvarez-Vallina, L. Functional comparison of single-chain and two-chain anti-CD3-based bispecific antibodies in gene immunotherapy applications. *Oncoimmunol.* 2014; **3**: e28810.

Conroy, P., Hearty, S., Leonard, P., O'Kennedy, R.J. Antibody production, design and use for biosensor-based applications. *Semin. Cell Dev. Biol.* 2009; **20** (1): 10-26.

Conroy, P., O'Kennedy, R.J., & Hearty, S. Cardiac troponin I: a case study in rational antibody design for human diagnostics. *Protein Eng. Des. Sel.* 2012; **25** (6): 295-305.

Conroy, P., Law, R.H.P., Gilgunn, S., Hearty, S., Caradoc-Davies, T.T., Lloyd, G., O'Kennedy, R., & Whisstock, J.C. Reconciling the structural attributes of avian antibodies. *J. Biol. Chem.* 2014; **289** (22): 15384-15392.

Coulson, A., Levy, A., & Gossell-Williams, M. Monoclonal antibodies in cancer therapy: Mechanisms, successes and limitations. *West. Indian Med. J.* 2014; **63** (6): 650-654.

Cunningham, D., Chau, I., Stocken, D.D., Valle, J.W., Smith, D., Steward, W., Harper, P.G., Dunn, J., Tudur-Smith, C., West, J., Falk, S., Crellin, A., Adab, F., Thompson, J., Leonard, P., Ostrowski, J., Eatock, M., Scheithauer, W., Hermann, R., & Neoptolemos, J.P. Phase III randomized comparison of gemcitabine versus gemcitabine plus

capecitabine in patients with advanced pancreatic cancer. *J. Clin. Oncol.* 2009; **27** (33): 5513-5518.

Dahl, M.K., & Manson, M.D. Interspecific reconstitution of maltose transport and chemotaxis in *Escherichia coli* with maltose-binding protein from various enteric bacteria. *J. Bacteriol.* 1985; **164** (3): 1057-1063.

Dahlén, E., Veitonmäki, N., & Norlén, P. Bispecific antibodies in cancer immunotherapy. *Ther. Adv. Vaccines.* 2018; **6** (1): 3-17.

Dantas-Barbosa, C., De Macedi Brigido, M., & Maranhao, A.Q. Antibody phage display libraries: Contributions to oncology. *Int. J. Mol. Sci.* 2012; **13** (5): 5420-5440.

De Boer, H.A., Comstock, L.J., & Vasser, M. The tac promoter: a functional hybrid derived from the trp and lac promoters. *Proc. Natl. Acad. Sci. USA.* 1983; **80** (1): 21-25.

de Sousa Cavalcante, L., & Monteiro, G. Gemcitabine: Metabolism and molecular mechanisms of action, sensitivity and chemoresistance in pancreatic cancer. *Eur. J. Pharmacol.* 2014; **741:** 8-16.

Denton, G., Sekowski, M., Spencer, D.I., Hughes, O.D., Murray, A., Denley, H., Tendler, S.J., & Price, M.R. Production and characterization of a recombinant anti-MUC1 scFv reactive with human carcinomas. *Br. J. Cancer.* 1997; **76** (5): 614-621.

Dewi, K.S., Retnoningrum, D.S., Riani, C., & Faud, A.M. Construction and periplasmic expression of the anti-EGFRvIII scFv antibody gene in *Escherichia coli. Sci. Pharm.* 2016; **84** (1): 141-152.

di Magliano, M.P., & Logsdon, C.D. Roles for KRAS in pancreatic tumor development and progression. *Gastroenterology.* 2013; **144:** 1220-1229.

Ding, Z., Wu, H., Zhang, J., & Ji, D. MicroRNAs as novel biomarkers for pancreatic cancer diagnosis: a meta-analysis based on 18 articles. *Tumor. Biol.* 2014; **35:** 8837-8848.

Distler, M., Aust, D., Weitz, J., Pilarsky, C., & Grützmann, R. Precursor lesions for sporadic pancreatic cancer: PanIN, IPMN, and MCN. *BioMed. Res. International.* 2014; Article ID: 474905

DocNet; http://docplayer.net/30268507-Human-single-fold-scfv-libraries-i-j-tomlinson-i-j.html. Accessed on the 25th June 2018.

Dodson, L.F., Hawkins,W.G., & Goedegebuure, P. Potential targets for pancreatic cancer immunotherapeutics. *Immunotherapy.* 2011; **3**(4): 517-537.

Doiron, B., & DeFronzo, R.A. A novel experimental model for human mixed acinar-ductal pancreatic cancer. *Carcinogenesis.* 2018; **39** (2): 180-190.

Drakaki, A., & Iliopoulos, D. MicroRNA-gene signaling pathways in pancreatic cancer. *Biomed. J.* 2013; **36** (5): 200-208.

Dreier, T., Baeuerle, P.A., Fichtner, I., Grün, M., Schlereth, B., Lorenczewski, G., Kufer, P., Lutterbüse, R., Riethmüller, G., Gjorstrup, P., & Bargou, R.C. T cell costimulus-independent and very efficacious inhibition of tumor growth in mice bearing subcutaneous or leukemic human B cell lymphoma xenografts by a CD19-/CD3-bispecific single-chain construct. *J. Immunol.* 2003; **170** (8): 4397-4402.

Duffy, M.J., Sturgeon, C., Lamerz, R., Haglund, C., Holubec, V.L., Klapdor, R., Nicolini, A., Topoclan, O., & Heinemann, V. Tumor markers in pancreatic cancer: A European group on tumor markers (EGTM) status report. *Ann. of Oncol.* 2010; **21:** 441-447.

Duffy, M.J. Tumor markers in clinical practice: A review focusing on common solid cancers. *Med. Princ. Pract.* 2013; **22:** 4-11.

Dumartin, L., Whiteman, H.J., Weeks, M.E., Hariharan, D., Dmitrovic, B., Iacobuzio-Donahue, C.A., Brentnall, T.A., Bronner, M.P., Freakins, R.M., Timms, J.F., Brennan, C., Lemoine, N.R., & Crnogorac-Jurcevic, T. AGR2 is a novel surface antigen that

promotes the dissemination of pancreatic cancer cells through regulation of cathepsins B and D. *Cancer Res.* 2011. **71** (22): 7091-7102.

Dumartin, L., Alarwashdeh, W., Trabulo, S.M., Radon, T.P., Steiger, K., Feakins, R.M., di Magliano, M.P., Heeschen, C., Esposito, I., Lemoine, N.R., & Crnogorac-Jurcevic, T. ER stress protein AGR2 precedes and is involved in the regulation of pancreatic cancer initiation. *Oncogene.* 2017; **36** (22): 3094-3103.

Duong-Ly, K.C., & Gabelli, S.B. Affinity purification of a recombinant protein expressed as a fusion with the maltose-binding protein (MBP) tag. *Methods Enzymol.* 2015; **559**: 17-16.

Dupin, M., Fortin, T., Larue-Triolet, A., Surault, I., Beaulieu, C., Gouel-Chéron, A., Allaouchiche, B., Asehnoune, K., Roquilly, A., Venet, F., Monneret, G., Lacoux, X., Roitsch, C.A., Pachot, A., Charrier, J.P., & Pons, S. Impact of serum and plasma matrices on the titration of human inflammatory biomarkers using analytically validated SRM assays. *J. Proteome Res.* 2016; **15**: 2366-2378.

Edge, S., & Compton, C.C. The American joint committee on cancer: The 7th edition of the AJCC cancer staging manual and the future of TNM. *Ann. Surg. Oncol.* 2010; **17** (6): 1471-1474.

Edgell, T., Martin-Roussety, G., Barker, G., Autelitano, D.J., Allen, D., Grant, P., & Rice, G.E. Phase II biomarker trail of a multi-marker diagnostic for ovarian cancer. *J. Cancer Res. Clin. Oncol.* 2010; **136** (7): 1079-1088.

Eteshola, E. Isolation of scFv fragments specific for monokine induction by interferon-gamma (MIG) using phage display. *J. Immunol. Methods.* 2011; **358** (1-2): 104-110.

Fantini, M., Pandolfini, L., Lisi, S., Chirichella, M., Arisi, I., Terrigno, M., Goracci, M., Cremisi, F., & Cattaneo, A. Assessment of antibody library diversity through next generation sequencing and technical error compensation. *PLoS One.* 2017; **12** (5): e0177574.

FDA: Development Tools Qualification Programs. DDT Glossary. Available at http://www.fda.gov/Drugs/DevelopmentApprovalProcess/DrugDevelopmentToolsQualificationProgram/ucm284395.htm Accessed on the 28th May 2018.

Felder, M., Kapur, A., Gonzalez-Bosquet, J., Horibata, S., Heintz, J., Albrecht, R., Fass, L., Kaur, J., Hu, K., Shojaei, H., Whelan, R.J., & Patankar, M.S. MUC16 (CA125): tumor biomarker to cancer therapy, a work in progress. *Mol. Cancer.* 2014; **13** (129): 1-15.

Fenwick, N., Griffin, G., & Gauthier., C. The welfare of animals used in science: How the "Three Rs" ethic guides improvemens. *Can. Vet. J.* 2009; **50** (5): 532-530.

Ferreira, R.M.M., Sancho, R., Messal, H.A., Nye, E., Spencer-Dene, B., Stone, R.K., Stamp, G., Rosewell, I., Quaglia, A., & Behrens, A. Duct- and acinar-derived pancreatic ductal adenocarcinomas show distinct tumor progression and marker expression. *Cell. Rep.* 2017; **21**: 966-978.

Ferrer-Miralles, N., & Villaverde, A. Bacterial cell factories for recombinant protein production; expanding the catalogue. *Microb. Cell Fact.* 2013; **12**: 113.

Finlay, J.W.A., Smith, W.C., Lee, J., Nordblom, G.D., Das, I., DeSilva, B.S., Khan, M.N., & Bowsher, R.R. Validation of immunoassays for bioanalysis: a pharmaceutical industry perspective. *Pharmaceutical. Biomed. Anal.* 2000; **21:** 1249-1273.

Fiorino, S., Chili, E., Bacchi-Reggiani, L., Masetti, M., Deleonardi, G., Grondona, A.G., Silvestri, T., Magrini, E., Zanini, N., Cuppini, A., Nardi, R., & Jovine, E. Association between hepatitis B or hepatitis C virus infection and risk of pancreatic adenocarcinoma development: a systemic review and meta-analysis. *Pancreatology.* 2013; **13:** 147-160.

Fitzgerald, J., Leonard, P., Darcy, E., Danaher, M., & O'Kennedy, R. Light-chain shuffling from an antigen-biased phage pool allows 185-fold improvement of an anti-halofuginone single-chain variable fragment. *Anal. Biochem.* 2011; **410** (1): 27-33.

Fitzgerald, T.L., & McCubrey, J.A. Pancreatic stem cells: Association with cell surface markers, prognosis, resistance, metastasis and treatment. *Adv. Biol. Regul.* 2014; **56:** 45-50.

Fong, Z.V., & Winter, J.M. Biomarkers in pancreatic cancer: Diagnostic, prognostic, and predictive. *Cancer J. (United States).* 2012; **18** (6): 530-538.

Forsström, B., Axnäs, B.B., Rockberg, J., Danielsson, H., Bohlin, A., & Uhlen, M. Dissecting antibodies with regards to linear and conformational epitopes. *PLoS One.* 2015; **10** (3): e0121673.

Fox, B.G., & Blommel, P.G. Autoinduction of Protein Expression. *Curr. Protoc. Protein Sci.* 2009; Chapter 5: Unit-5.23.

Frankel, S.R., & Baeuerle, P.A. Targeting T cells to tumor cells using bispecific antibodies. *Curr. Opin. Chem. Biol.* 2013; **17:** 385-392.

Fu, X., Deng, J., Yang, H., Masuda, T., Goto, F., Yoshihara, T., & Zhao, G. A novel EP-involved pathway for iron release from soya bean seed ferritin. *Biochem. J.* 2010; **427** (2): 313-321.

Gąciarz, A., & Ruddock, L.W. Complementarity determining regions and framework contribute to the disulfide bond independent folding of intrinsically stable scFv. *PLoS One.* 2017; **12** (12): e0189964.

Garcia-Contreras, M., Ricordi, C., Robbins, P.D., & Oltra, E. Exosomes in the pathogenesis, diagnosis and treatment of pancreatic diseases. *CellR4.* 2014; **2** (1): e807.

Garnock-Jones, K.P., Keating, G.M., & Scott, L.J. Trastuzumab: A review of its use as adjuvant treatment in human epidermal growth factor receptor 2 (HER2)-positive early breast cancer. *Drugs.* 2010; **70** (2): 215-239.

Garzon, R., Calin, G.A., & Croce, C.M. MicroRNAs in cancer. *Annu. Rev. Med.* 2009; **60:** 167-179.

Gay, G., Wagner, D.T., Keatinge-Clay, A.T., & Gay, D.C. Rapid modification of the pET-28 expression vector for ligation independent cloning using homologous recombination in *Saccharomyces cerevisiae. Plasmid.* 2014; **76** : 66-71.

Gayral, M., Jo, S., Hanoun, N., Vignolle-Vidoni, A., Lulka, H., Delpu, Y., Meulle, A., Dufresne, M., Humeau, M., Chalret du Rieu, M., Bournet, B., Sèlves, J., Guimbaud, R., Carrère, N., Buscail, L., Torrisani, J., & Cordelier, P. MicroRNAs as emerging biomarkers and therapeutic targets for pancreatic cancer. *World J. Gastroenterol.* 2014; **20** (32): 11199-11209.

Gascoigne, N.J.R. Do T cells need endogenous peptides for activation? *Nat. Rev. Immunol.* 2008; **8**: 895-900.

Ghazale, A., Chari, S.T., Smyrk, T.C., Levy, M.J., Topazian, M.D., Takahashi, N., Clain, J.E., Pearson, R.K., Pelaez-Luna, M., Petersen, B.T., Vege, S.S., & Farnell, M.B. Value of serum IgG4 in the diagnosis of autoimmune pancreatitis and in distinguishing it from pancreatic cancer. *Am. J. Gastronenterol.* 2007; **102:** 1646-1653.

Gittes, G.K. Developmental biology of the pancreas: A comprehensive review. *Developmental Biology.* 2009; **326** (1): 2-35.

Gnanamony, M., & Gondi, C.S. Chemoresistance in pancreatic cancer: Emerging concepts. *Oncol. Lett.* 2017; **13** (4): 2507-2513.

Goel, G., & Sun, W. Novel approaches in the management of pancreatic ductal adenocarcinoma: potential promises for the future. *J. Hematol. & Oncol.* 2015; **8** (44): 1-16.

Gohil, S.H., Paredes-Moscosso, S.R., Harrasser, M., Vezzalini, M., Scarpa, E., Morris, E., Davidoff, AM., Sorio, C., Nathwani, A.C., & Della Peruta, M. An ROR1 bi-specific T-cell engager provides effective targeting and cytotoxicity against a range of solid tumors. *Oncoimmunol.* 2017; **6** (7): e1326437.

Goonetilleke, K.S., & Siriwardena, A.K. Systematic review of carbohydrate antigen (CA 19-9) as a biochemical marker in the diagnosis of pancreatic cancer. *EJSO.* 2007; **33:** 266-270.

Gore, J., & Korc, M. Pancreatic cancer stroma: Friend or foe? *Cancer Cell.* 2014; **25** (6): 711-712.

Goyos, A., Li, C., Deegen, P., Bogner, P., Thomas, O., Wahl, J., Goldstein, R., Friedrich, M., Coxon, A., Balazs, M., & Arvedson, T. Abstract LB-299: Cynomolgus monkey plasma cell gene signature to quantify the *in vivo* activity of a half-life extended anti-BCMA BiTE ® for the treatment of multiple myeloma. *Cancer Res.* 2018; **78** (13).

Gretts, D.R., Gretts, M,T., McCarthy, D.P., Chastain, E.M.L., & Miller, S.D. Have we overestimated the benefit of human(ized) antibodies? *MAbs.* 2010; **2** (6): 682-694.

Groff, K., Brown, J., & Clippinger, A.J. Modern affinity reagents: Recombinant antibodies and aptamers. *Biotechnol. Adv.* 2015; **33** (8): 1787-1798.

Güngör, C., Hofmann, B.T., Wolters-Eisfeld, G., & Bockhorn, M. Pancreatic cancer. *Br. J. Pharmacol.* 2014; **171:** 849-858.

Guo, H., Chen, H., Zhu, Q., Yu, X., Rong, R., Merugu, S.B., Mangukiya, H.B., & Li, D. A humanized monoclonal antibody targeting secreted anterior gradient 2 effectively inhibits the xenograft tumor growth. *Biochem. Biophys. Res. Commun.* 2016; **475** (1): 57-63.

Guo, L., Wang, L., Yang, R., Feng, R., Li, Z., Zhou, X., Dong, Z., Ghartney-Kwansah, G., Xu, M., Nishi, M., Zhang, Q., Isaacs, W., Ma, J., & Xu, X. Optimizing conditions for calcium phosphate-mediated transient transfection. *Saudi. J. Biol. Sci.* 2017; **24** (3): 622-629.

Habisch, H., Zhou, S., Siech, M., Bachem, M.G. Interaction of stellate cells with pancreatic carcinoma cells. *Cancers.* 2010; **2:** 1661-1682.

Hammers, C.M., & Stanley, J.R. Antibody phage display: Technique and applications. *J. Invest. Dermatol.* 2014. **134** (2): 1-5.

Hao, C.H., Han, Q.H., Shan, Z.J., Hu, J.T., Zhang, N., & Zhang, X.P. Effects of different interchain linkers on biological activity of an anti-prostate cancer single-chain bispecific antibody. *Theor. Biol. Med. Model.* 2015; **12** (14): 1-10.

Harder, J., Ihosrt, G., Heinemann, V., Hofheniz, R., Moehler, M., Buechler, P., Kloeppel, ., Röcken, C., Bitzer, M., Boeck, S., Endlicher, E., Reinacher-Schick, A., Schmoor, C., & Geissler, M. Multicentre phase II trial of trastuzumab and capecitabine in patients with HER2 overexpressing metastatic pancreatic cancer. *Br. J. Cancer.* 2012; **106** (6): 1033-1038.

Harding, F.A. Stickler, M.M., Razo, J., & DuBridge, R.B. The immunogenicity of humanized and fully human antibodies: Residual immunogenicity resides in the CDR regions. *MAbs.* 2010; **2** (3): 256-265.

Hassan, R., Tapan, B., & Pastan, I. Mesothelin: A new target for immunotherapy. *Clin. Cancer Res.* 2004; **10:** 3937-3942.

Hassan, R., Laszik, Z.G., Lerner, M., Raffeld, M., Postier, R., & Brackett, D. Mesothelin is overexpressed in pancreaticobiliary adenocarcinomas but not in normal pancreas and chronic pancreatitis. *Am. J. Clin. Pathol.* 2005; **124:** 838-845.

Hassan, R., & Ho., M. Mesothelin targeted cancer immunotherapy. *Eur. J. Cancer.* 2008; **44** (1): 46-53.

Hassan., R., Thomas, A., Alewine, C., Le., D.T., Jaffee, E.M., & Pastan, I. Mesothelin immunotherapy for cancer: Ready for prime time? *J. Clin. Oncol.* 2016; **34** (34): 4171-4179.

Hayhurst A., Happe S., Mabry, R., Koch, Z., Iverson, B.L., & Georgiou, G. Isolation and expression of recombinant antibody fragments to the biological warfare pathogen *Brucella melitensis*. *J. Immunol. Methods.* 2003; **276** (1-2): 185-96.

Hearty, S., & O'Kennedy, R. Exploiting recombinant antibodies in point-of-care (POC) diagnostics: The combinatorial advantage. *Bioeng. Bugs.* 2011; **2** (3): 182-186.

Heinemann, V., Haas, M., & Boeck, S. Systemic treatment of advanced pancreatic cancer. *Cancer Treat. Rev.* 2012; **38:** 843-853.

Henderikx, P., Kandilogiannaki, M., Petrarca, C., von Mensdorff-Pouilly, S., Krambovitis, E., Arends, J.W., & Hoogenboom, H.R. Human single-chain Fv antibodies to MUC1 core peptide selected from phage display libraries recognize unique epitopes and predominantly bind adenocarcinoma. *Cancer Res.* 1998; **58** (19): 4324-4332.

Hermann, P.C., Huber, S.L., Herrler, T., Aicher, A., Ellwart, J.W., Guba, M., Bruns, C.J., & Heeschen, C. Distinct populations of cancer stem cells determine tumor growth and metastatic activity in human pancreatic cancer. *Cell Stem. Cell.* 2007; **1** (3): 313-323.

Hernandez, J.M., Cowgill, S.M., Al-Saadi, S., Collins, A., Ross, S.B., Cooper, J., Villadolid, D., Zervos, E., & Rosemurgy, A. CA19-9 velocity predicts disease-free survival and overall survival after pancreatectomy of curative intent. *J. Gastrointest. Surg.* 2009; **13:** 349-353.

Herold, E.M., John, C., Weber, B., Kremser, S., Eras, J., Berner, C., Deubler, S., Zacharias, M., & Buchner, J. Determinants of the assembly and function of antibody variable domains. *Sci. Rep.* 2017; **7** (12276): 1-17..

Herreros-Villanueva, M., Gironella, M., Castells, A., & Bujanda, L. Molecular markers in pancreatic cancer diagnosis. *Clin. Chim. Acta.* 2013; **418:** 22-29.

Heussner, A.H., Altaner, S., Kamp, L., Rubio, F., & Dietrich, D.R. Pitfalls in microcystin extraction and recovery from human blood serum. *Chem. Biol. Interact.* 2014; **223**: 87-94.

Hidalgo, M. Pancreatic cancer. *N. Engl. J. Med.* 2010; **362:** 1605-1617.

Hinoda, Y., Ikematsu, Y., Horinochi, M., Sato, S., Yamamoto, K., Nakano, T., Fukui, M., Suehiro, Y., Hamanaka, Y., Nishikawa, T., Kida, H., Waki, S., Oka, M., Imai, K., & Yonezawa, S. Increased expression of MUC1 in advanced pancreatic cancer. *J. Gastroenterol.* 2003; **28** (12): 1162-1166.

Hlavacek, W.S., Posner, R.G., & Perelson, A.S. Steric effects on multivalent ligand-receptor binding: Exclusion of ligand sites by bound cell surface receptors. *Biophys. J.* 1999; **76** (96): 3031-3043.

Ho, M., Feng, M., Fisher, R.J., Rader, C., & Pastan, I. A novel high-affinity human monoclonal antibody to mesothelin. *Int. J. Cancer.* 2011; **128** (9): 2020-2030.

Hofmann, A.W. Synthese aromatischer monamine durch atomwanderung im molecule. *Ber. Dtsch. Chem. Ges.* 1872; **5** (20): 704.

Horn, L.A., Ciavattone, N.G., Atkinson, R., Woldergerima, N., Wolf, J., Clements, V.K., Sinha, P., Poudel, M., & Ostrand-Rosenberg, S. CD3xPDL1 bi-specific T cell engager (BiTE) simultaneously activates T cells and NKT cells, kills $PDL1^{+}$ tumor cells, and extends the survival of tumor-bearing humanized mice. *Oncotarget.* 2017; **8** (35): 57964-57980.

Hosoda, W., Chianchiano, P., Griffen, J.F., Pitman, M.E., Brosens, L.A., Noë, M., Yu, J., Shindo, K., Suenaga, M., Rezaee, N., Yonehara, R., Ning, Y., Albores-Saavedra, J., Yoshizawa, N., Harada, K., Yoshizawa, A., Hanada, K., Yonehara, S., Shimizu, M., Uehara, T., Samra, J.S., Gill, A.J., Wolfgang, C.L., Goggins, M.G., Hruban, R.H., & Wood, L.D. Genetic analyses of isolated high-grade pancreatic intraepithelial neoplasia (HG-PanIN) reveal paucity of alterations in *TP53* and *SMAD4. J. Pathol.* 2017; **242** (1): 16-23.

Hou, Y.C., Chao, Y.J., Tung, H.L., Wang, H.C., & Shan, Y.S. Coexpression of CD44-positive/CD33-positive cancer stem cells and CD204-positive tumor-associated macrophages in a predictor of survival in pancreatic ductal adenocarcinoma. *Cancer.* 2014; **120** (17): 2766-2777.

Hu, D., Hu, S., Wan, W., Xu, M., Du, R., Zhao, W., Gao, X., Liu, J., Liu, H., & Hong, J. Effective optimization of antibody affinity by phage display integrated with high-throughput DNA synthesis and sequencing technologies. *PLoS One.* 2015; **10** (6): e0129125.

Huang, W., Samata, M., Crawford, S.E., Estes, M.K., Neill, F.H., Atmar, R.L., & Palzkill, T. Identification of human single-chain antibodies with broad reactivity for noroviruses. *Protein Eng. Des. Sel.* 2014; **27** (10): 339-349.

Huang, Z., & Buchsbaum, D.J. Monoclonal antibodies in the treatment of pancreatic cancer. *Immunotherapy.* 2009; **1** (2): 223-239.

Huang, Z., & Liu, F. Diagnostic value of serum carbohydrate antigen 19-9 in pancreatic cancer: a meta-analysis. *Tumor Biol.* 2014; **35:** 7459-7465.

Huehls, A.M., Coupet, T.A., & Sentman, C.L. Bispecific T cell engagers for cancer immunotherapy. *Immunol. Cell Biol.* 2015; **93** (3): 290-296.

Humar, M., Kern, I., Vlacic, G., Hadzic, V., & Cufer, T. Insulin-like growth factor 1 receptor expression in advanced non-small-cell lung cancer and its impact on overall survival. *Radiol. Oncol.* 2017; **51** (2): 195-202.

Inaguma, S., Wang, Z., Lasota, J., Onda, M., Czapiewski, P., Langfort, R., Rys, J., Szpor, J., Waloszczyk, P., Okoñ, K., Ikeda, H., Schrump. D.S., Hassan, R., Pastan, I., & Miettinen, M. Comprehensive immunohistochemical study of mesothelin (MSLN) using different monoclonal antibodies 5B2 and MN-1 in 1562 tumors with evaluation of its prognostic value in malignant pleural mesothelioma. *Oncotarget.* 2017; **8** (16): 26744-26754.

Iqbal, M., Li, K., Reading, D., & Shahtaheri, K. Attempted construction of an arabinose-inducible pBAD28 recombinant expression vector containing *acr*D, an *Escherichia coli* aminoglycoside efflux porin. *JEMI.* 2014; **18:** 134-138.

Jäger, M., Schoberth, A., Ruf, P., Hess, J., & Lindhofer, H. The trifunctional antibody ertumaxomab destroys tumor cells that express low levels of human epidermal growth factor receptor 2. *Cancer Res.* 2009; **69** (10): 4270-4276.

Janeway, C.A., Jr., Travers, P., Walport, M., & Capra, J. The recognition of antigen in Immunology: the immune system in health and disease, 4th edition, p79-113, Austin, P. and Lawrence, E. (eds.). Garland publishing, 1999.

Jazieh, K.A., Foote, M.B., & Diaz, L.A. The clinical utility of biomarkers in the management of pancreatic adenocarcinoma. *Semin. Radiat. Oncol.* 2014; **24** (2): 67-76.

Jelliffe, R.W., Schumitzky, A., Bayard, D., Fu, X., & Neely, M. Describing assay precision-reciprocal of variance is correct, not CV percent: its use should significantly improve laboratory performance. *Ther. Drug Monit.* 2015; **37** (3): 389-394.

Jensen, M.A., Fukushima, M., & Davis, R. DMSO and betaine greatly improve amplification of GC-rich constructs in *de novo* synthesis. *PLoS One.* 2010; **5** (6): e11024.

Jia, B., & Joen, C.O. High-throughput recombinant protein expression in *Escherichia coli:* current status and future perspectives. *Open. Biol.* 2016; **6** (8): 1-17.

Jimeno, A., & Hidalgo, M. Molecular biomarkers: Their increasing role in the diagnosis, characterization, and therapy guidance in pancreatic cancer. *Mol. Cancer Ther.* 2006; **5:** 787-796.

Johnston, F.M., Tan, M.C.B., Tan, B.R, Jr., Porembka, M.R., Brunt, E.M., Linehan, D.C., Simon, P.O, Jr., Plambeck-Suess, S., Eberlein, T.J., Hellstrom, I., Hawkins, W.G., & Goedegebuure, P. Circulating mesothelin protein and cellular anti-mesothelin immunity in patients with pancreatic cancer. *Clin. Cancer Res.* 2009; **15:** 6511-6518.

Jones, M.L., Alfaleh, M.A., Kumble, S., Zhang, S., Osborne, G.W., Yeh, M., Arora, N., Hou, J.J.C., Howard, C.B., Chin, Y.D., & Mahler. S.M. Targeting membrane proteins for antibody discovery using phage display. *Sci. Rep.* 2016; **6**: 1-11.

Jones, R.J., & Brown, J. Circulating biomarkers in cancer care: What possible use? *Practical Lab. Med.* 2017; **7** : 45-48.

Kaltsas, S., Syrigos, K.N., & Saif, M.W. Pancreatic cancer in 2014. *JOP. J. Pancreas (Online).* 2014; **15** (2): 84-86.

Kaku, Y., Noguchi, A., Okutani, A., Inoue, S., Tanabayashi, K., Yamamoto, Y., Hotta, A., Suzuki, M., Sugiura, N., & Yamada, A. Altered specificity of single-chain antibody fragments bound to pandemic H1N1-2009 influenza virus after conversion of the phage-bound to the soluble form. *BMC. Res. Notes.* 2012; **5** (483): 1-7.

Kawa, S., Tokoo, M., Hasebe, O., Hayashi, K., Imai, H., Oguchi, H., Kiyosawa, K., Furuta, S., & Homma, T. Comparative study of CA242 and CA19-9 for the diagnosis of pancreatic cancer. *Br. J. Cancer.* 1994; **70:** 481-486.

Kendrick, Z.W., Firpo, M.A., Repko, R.C., Scaife, C.L., Adler, D.G., Boucher, K.M., & Mulvihill, S.J. Serum IGFBP2 and MSLN as diagnostic and prognostic biomarkers for pancreatic cancer. *HPB.* 2014; **16** (7): 670-676.

Kenner, B.J. Early detection of pancreatic cancer: The role of depression and anxiety as a precursor for disease. *Pancreas.* 2018; **47** (4): 363-367.

Kent, S.P., Ryan, K.H., & Siegel, A.L. Steric hindrance as a factor in the reaction of labeled antibody with cell surface antigenic determinants. *J. Histochem. Cytochem.* 1978; **26** (8): 618-621.

Khow, O., & Santrarachun, S. Strategies for production of active eukaryotic proteins in bacterial expression system. *Asian. Pac. J. Trop. Biomed.* 2012; **2** (2): 159-162.

Kikuyama, M., Kamisawa, T., Kuruma, S., Chiba, K., Kawaguchi, S., Terada, S., & Satoh, T. Early diagnosis to improve the poor prognosis of pancreatic cancer. *Cancers (Basel).* 2018; **10** (48): 1-9.

Kim, C.H., Axup, J.Y., Dubrovska, A., Kazane, S.A., Hutchins, B.A., Wold, E.D., Smider, V.V., & Schultz, P.G. Synthesis of bispecific antibodies using genetically encoded unnatural amino acids. *J. Am. Chem. Soc.* 2012; **134** (24): 9918-9921.

Kim, M.V., & Ahuja, N. Early detection of pancreatic cancer. *Chin. J. Cancer. Res.* 2015; **27** (4): 321-331.

Kim, J.E., Lee, K.T., Lee, J.K., Paik, S.W., Rhee, J.C., Choi, K.W. Clinical usefulness of carbohydrate antigen 19-9 as a screening test for pancreatic cancer in an asymptomatic population. *J. Gastroenterol. Hepatol.* 2004; **19** (2): 182-186.

Kindler, H.L., Niedzwiecki, D., Hollis, D., Oraefo, E., Schrag, D., Hurwitz, H., McLeod, H.L., Mulcahy, M.F., Schilsky, R.L., & Goldberg, R.M. A double-blind, placebo-controlled, randomized phase III trial of gemcitabine (G) plus bevacizumab (B) versus gemcitabine plus placebo (P) in patients (pts) with advanced pancreatic cancer (PC): a preliminary analysis of cancer and Leukemia group B (CALGB). *J. Clin. Oncol.* 2007; **25** (18S): Abstract 4508.

Kjer-Nielsen, L., Dunstone, M.A., Kostenko, L., Ely, L.K., Beddoe, T., Mifsud, N.A., Purcell, A.W., Brooks, A.G., McCluskey, J., & Rossjohn, J. Crystal structure of the human T cell receptor CDE εγ heterodimer complexed to the therapeutic mAb OKT3. *Proc. Natl. Acad. Sci. USA.* 2004; **101** (20): 7675-7680.

Kleeff, J., Korc, M., Apte, M., La Vecchia, C., Johnson, C.D., Biankin, A.V., Neale, R.E., Tempero, M., Tuveson, D.A., Hruban, R.H., & Neoptolemos, J.P. Pancreatic cancer. *Nat. Rev. Dis. Primers.* 2016; **2**: Article 16022.

Klein, A.P., Wolpin, B.M., Risch, H.A., Stolzenberg-Solomon, R.Z., Mocci, R., Zhang, M., Canzian, F., Childs, E.J., Hoskins, JW., Jermusyk, A., Zhong, J., Chen, F., Albanes, D., Andreotti, G., Arslan, AA., Babic, A., Bamlet, W.R., Beane-Freeman, L., Berndt, S.I.,, Blackford, A., Borges, M., Borgida, A., Bracci, P.M., Brais, L., Brennan, P., Brenner, H., Bueno-de-Mesquita, B., Bruing, J., Campa, D., Capurso, G., Cavestro, G.M., Chaffee, K.G., Chung, C.C., Cleary, S., Cotterchio, M., Dijk., F., Duell, E.J., Foretova, L., Fuchs, C., Funel, N., Gallinger, S., M Gaziano, J.M., Gazouli, M., Giles, G.G.,

Giovannucci, E., Goggins, M., Goodman, G.E., Goodman, P.J., Hacket, Y., Haiman, C., Hartge, P., Hasan, M., Hegyi, P., Helzlsouer, K.J., Herman, J., Holcatova, I., Holly, E.A., Hovver, R., Hung, R.J., Jacobs, E.J., Jamroziak, K.J., Janout, V., Kaaks, R., Khaw, K.T., Klein, E.A., Kogevinas, M., Kooperberg, C., Kulke, M.H., Kupcinskas, J., Kurtz, R.J., Laheru, D., Landi, S., Lawlor, R.T., Lee, I.M., LeMarchand, L., Lu. L., Malats, N., Mambrini, A., Mannisto, S., Milne, R.L., Mohelníkoví- Duchñová, B., Neale, R.E., Neotolemos, J.P., Oberg, A.L., Olson, S.H., Orlow, I., Pasquali, C., Patel, A.V., Peters, U., Pezzilli, R., Porta, M., Real, F.X., Rothman, N., Scelo, G., Sesso, H.D., Severi, G., Shu, X.O., Silverman, D., Smith, J.P., Soucek, P., Sund, M., Talar-Wojnarowaska, R., Tavano, F., Thornquist, M.D., Tobias, G.S., Van Den Eeden, S.K., Vashist, Y., Visvanathan, K., Vodicka, P., Wactawski-Wende, J., Wang, Z., Wentzensen, N., White, E., Yu, H., Yu, K., Zelenuich-Jacquotte, A., Zheng, W., Kraft, P., Li, D., Chanock, S., Obazee, O., Peterson, G.M., & Amundadottir, L.T. Genome-wide meta-analysis identifies five new susceptibility loci for pancreatic cancer. *Nat. Commun.* 2018; **9** (556): 1-11.

Koide, S., & Sidhu, S.S. The importance of being tyrosine: Lessons in molecular recognition from minimalist synthetic binding proteins. *ACS. Chem. Biol.* 2009; **4** (5): 325-334.

Koohapitagtam, M., Rungpragayphan, S., Hongprayoon, R., Kositratana, W., & Sirinarumitr, T. Efficient amplification of light and heavy chain variable regions and construction of a non-immune phage scFv library. *Mol. Biol. Rep.* 2010; **37** (4): 1677-1683.

Köhler, G., & Milstein C. Continuous cultures of fused cells secreting antibody of predefined specificity. *Nature.* 1975; **256:** 495-497.

Kontermann, R.E. Dual targeting strategies with bispecific antibodies. *mAbs.* 2012; **4** (2): 182-197.

Kotlan, B., Simsa, P., Teillaud, J., Fridman, W.H., Toth, J., McKnight, M., & Glassy, M.C. Novel ganglioside antigen identified by B cells in human medullary breast

carcinomas: The proof of principle concerning the tumor-infiltrating B lymphocytes. *J. Immunol.* 2005; **175**: 2278-2285.

Kovalyov, C.I., Shishkin, S.S., Khasigov, P.Z., Dzeranov, N.K., Toropygin, I.I.U., & Mamykina, S.V. Identification of AGR2 protein, a novel potential cancer marker, using proteomics technologies. *Appl. Biochem. Microbiol.* 2006; **42** (4): 424-427.

Koyama, Y., Wang, P., Liang, S., Iwaisako, K., Liu, X., Xu, J., Zhang, M., Sun, M., Cong, M., Karin, D., Taura, K., Benner, C., Heinz, S., Bera, T., Brnner, D.A., & Kisseleva, T. Mesothelin / mucin 16 signalling in activated portal fibroblasts regulates cholestatic liver fibrosis. *J. Clin. Invest.* 2017; **127** (4): 1254-1270.

Krasnoslobodtsev, A.V., Torres, M.P., Kaur, S., Vlassiouk, I.V., Lipert, R.J., Jain, M., Batra, S.K., & Lyunchenko, Y.L. Nano-immunoassay with improved performance for detection of cancer biomarkers. *Nanomed. Nanotech. Biol. Med.* 2015; **11:** 167-173.

Krauss, J., Arndt, M.A.E., Zhu, Z., Newton, D.L., Vu, B.K., Choudhry, V., Darbha, R., Ji, X., Courtenay-Luck, N.S., Deonarain, M.P., Richards, J., & Rybak, S.M. Impact of antibody framework residue V_H-71 on the stability of a humanised anti-MUC1 scFv and derived immunoenzyme. *Br. J. Cancer.* 2004; **90:** 1863-1870.

Krishnamurthy, A., & Jimeno, A. Bispecific antibodies for cancer therapy: A review. *Pharmacol. Ther.* 2018; **185:** 122-134

Krška, Z., Šváb., J., Hoskovec, D., & Ulrych, J. Pancreatic cancer diagnostics and treatment- Current state. *Prague Med. Rep.* 2015; **116** (4): 253-267.

Kulis, M., & Esteller, M. DNA methylation and cancer. *Adv. Genet.* 2010. **70:** 27-56.

Kushwaha, R., Schäfermeyer, K.R., & Downie, A.B. A protocol for phage display and affinity selection using recombinant protein baits. *J. Vis. Exp.* 2014; **84**: 1-13.

Laffly, E., & Sodoyer, R. Monoclonal and recombinant antibodies, 30 years after… *Hum. Antibodies.* 2005; **14** (1-2): 33-55.

Lago, S., Nadai, M., Rossetto, M., & Richter, S.N. Surface plasmon resonance kinetic analysis of the interaction between G-quadruplex nucleic acids and an anti-G-quadruplex monoclonal antibody. *Biochim Biophys Acta Gen Subj.* 2018; **1862** (6): 1276-1282.

Lau, C., Kim, Y., Chia, D., Spielmann, N., Eibl, G., Elashoff, D., Wei, F., Lin, Y.L., Moro, A., Grogan, T., Chiang, S., Feinstein, E., Schafer, C., Farrell, J., & Wong, D.T. Role of pancreatic cancer-derived exosomes in salivary biomarker development. *J. Biol. Chem.* 2013; **288** (37): 26888-26897.

Le, D.T., Ko, A.H., Wainberg, Z.A., Picozzi, V.J., Kindler, H.L., & Wang-Gillam, A. Results from a phase 2b, randomized, multicentre study of GVAX pancreas and CRS-207 compared to chemotherapy in adults with previously-treated metastatic pancreatic adenocarcinoma (ECLIPSE Study). *J. Clin. Oncol.* 2017; **35;** 4_suppl, 345.

Lee, H.S., Jang, C.Y., Kim, S.A., Park, S.B., Jung, D.E., Kim, B.O., Kim, H,Y, Chung, M.J., Park, J.Y., Bang, S., Park, S.W., & Song, S.Y. Combined use of CEMIP and CA19-9 enhances diagnostic accuracy for pancreatic cancer. *Sci. Rep.* 2018; **8** (1): Article 3383.

Lee, J.C., Dosch, J., & Simeone, D.M. Pancreatic cancer stem cells. *J. Clin. Oncol.* 2008; **26** (17): 2806-2812.

Leonard, P., Hearty, S., Ma, H., & O'Kennedy, R. Measuring protein-protein interactions using Biacore. *Methods Mol. Biol.* 2017; **1485**: 339-354.

Lerner, R.A. Combinatorial antibody libraries: new advances, new immunological insights. *Nat. Rev. Immunol.* 2016; **16:** 498-508.

Levi, E., Kilmstra, D.S., Adsay, N.V., Andea, A., & Basturk, O. MUC1 and MUC2 in pancreatic neoplasia. *J. Clin. Pathol.* 2004; **57:** 456-462

Levy, M.S., Lotfian, P., O'Kennedy, R., Lo-Yim, M.Y., & Shamlou, P.A. Quantitation of supercoiled circular content in plasmid DNA solutions using fluorescence-based method. *Nucleic Acids Res.* 2000; **28** (12): i-vii.

Li, D., Wu, Z., Zhu, Q., Guo, H., Gao, G., Mashausi, D.S., & Chen, H.. Abstract 4320: Agtuzumab, a humanized monoclonal antibody, blocks AGR2 function through conformational epitopes around its catalytic center. *Cancer Res.* 2013; **73** (8 Suppl): 4320.

Li, D., Xie, K., Wolff, R., & Abbruzzese, J.L. Pancreatic cancer. *Lancet.* 2004; **363:** 1049-1057.

Li, H.Y., Cui, Z.M., Chen, J., Guo, X.Z., & Li, Y.Y. Pancreatic cancer: diagnosis and treatments. *Tumour Biol.* 2015; **36:** 1375-1384.

Li, Y., Hu, X., Zhang, X., Liu, Z., Ding, X., Xia, L., & Hu, S. *Photorhabdus luminescens* PirAB-fusion protein exhibits both cytotoxicity and insecticidal activity. *FEMS. Microbiol. Lett.* 2014; **356** (1): 23-31.

Liang, W.S., Craig, D.W., Carpten, J., Borad, M.J., Demeure, M.J., Weiss, G.J., Izatt, T., Sinari, S., Christoforides, A., Aldrich, J., Kurdoglu, A., Barrett, M., Philips, L., Benson, H., Tembe, W., Braggion, E., Kiefer, J.A., Legendre, C., Posner, R., Hostetter. G.H., Baker, A., Egan, J.B., Han, H., Lake, D., Sitites, E.C., Ramanathan, R.K., Fonseca, R., Stewart, A.K., & Von Hoff, D. Genome-wide characterization of pancreatic adenocarcinoma patients using next generation sequencing. *PLoS ONE.* 2012; **7** (10): e43192.

Lianidou, E.S., Strati, A., & Markou, A. Circulating tumor cells as promising novel biomarkers in solid cancers. *Crit. Rev. Clin. Lab.* 2014; **51** (3): 160-171.

Lim, T.S., & Chan, S.K. Immune antibody libraries: Manipulating the diverse immune repertoire for antibody discovery. *Curr. Pharm. Des.* 2016; **22** (43): 6480-6489.

Lin, J., Li, J., Huang, B., Liu, L., Chen, X., Chen, X.M., Xu, Y.M., Huang, L.F., & Wang, X.Z. Exosomes: Novel biomarkers for clinical diagnosis. *Sci. World J.* 2015; Article ID: 657086.

Lin, H.J., & Lin, J. Seed-in-Soil: Pancreatic cancer influenced by tumor microenvironment. *Cancers (Basel).* 2017; **9** (93): 1-13.

Lin, Y., Benqiang, L., Wang, M., Jia, R., Wang, J., Zhang, Y., & Zhu, J. Improved affinity of a chicken single-chain antibody to avian infectious bronchitis virus by site-directed mutagenesis of complementarity-determining region H3. *Afr. J. Biotechnol.* 2011; **10** (79): 18294-18302.

Liu, F., Li, C., Zhu, J., Ren, L., & Qi, X. ABO blood type and risk of hepatocellular carcinoma: a meta-analysis. *Expert Rev*. *Gastroenterol*. *Hepatol*. 2018; **12** (9): 927-933.

Liu, J., Gao, J., Du, Y., Li, Z., Ren, Y., Gu, J., Wang, X., Gong, Y., Wang, W., & Kong, X. Combination of plasma microRNAs with serum CA19-9 for early detection of pancreatic cancer. *Int. J. Cancer.* 2012; **131** (3): 683-691.

Liu, R., Chen, X., Du, Y., Yao, W., Shen, L., Wang, C., Hu, Z., Zhuang, R., Ning, G., Zhang, C., Yuan, Y., Li, Z., Zen, K., Ba, Y., & Zhang, C.Y. Serum microRNA expression profile as a biomarker in the diagnosis and prognosis of pancreatic cancer. *Clin. Chem.* 2012; **58** (3): 610-618.

Liu, Q.G., Li, Y.J., & Yao, L. Knockdown of AGR2 induces cell apoptosis and reduces chemotherapy resistance of pancreatic cancer cells with the involvement of ERK/AKT axis. *Pancreatology.* 2018; **18** (6): 678-688.

Löffler, A., Kufer, P., Lutterbüse, R., Zettl, F., Daniel, P.T., Schwenkenbecher, J.M., Reithmüller, G., Dörken, B., & Bargou, R.C. A recombinant bispecific single-chain antibody, CD19 X CD3, induces rapid and high lymphoma-directed cytotoxicity by unstimulated T lymphocytes. *Blood.* 2000; **95:** 2098-2103.

Loosen, S.H., Neumann, U.P., Trautwein, C., Roderburg, C., & Luedde, T. Current and future biomarkers of pancreatic adenocarcinoma. *Tumour Biol.* 2017; **39** (6): 1-11.

Lorenz, T.C. Polymerase chain reaction: Basic protocol plus troubleshooting and optimization strategies. *J. Vis. Exp.* 2012; **63** (3998): 1-15.

Louis, K.S., & Siegel, A.C. Cell viability analysis using trypan blue: manual and automated methods. *Methods Mol. Biol.* 2011; **740**: 7-12.

Lowery, M.A., & O'Reilly, E.M. Pancreatic cancer: The role of molecular markers in diagnosis and management. *Clin. Adv. Hematol. & Oncol.* 2011; **9** (12): 900-908.

Lucas, A.L., Frado, L.E., Hwang, C., Kumar, S., Khanna, L.G., Levinson, E.J., Chabot, J.A., Chung, W.K., & Frucht, H. BRCA1 and BRCA2 germline mutations are frequently demonstrated in both high-risk pancreatic cancer screening and pancreatic cancer cohorts. *Cancer.* 2014; **120** (13): 1960-1967.

MacPhee, D.J. Methodological considerations for improving Western blot analysis. *J Pharmacol. Toxicol. Methods.* 2010; **61**: 171-177.

Madhavan, B., Yue, S., Galli, U., Rana, S., Gross, W., Müller, M., Glese, N.A., Kalthoff, H., Becker, T., Büchler, M.W., & Zöller, M. Combined evaluation of a panel of protein and miRNA serum-exosome biomarkers for pancreatic cancer diagnosis increases sensitivity and specificity. *Int. J. Cancer.* 2015; **136:** 2616-2627.

Maisonneuve, P., & Lowenfels, A. Epidemiology and Prospects for Prevention of Pancreatic Cancer. In: Neoptolemos J., Urrutia R., Abbruzzese J., Büchler M. (eds) Pancreatic Cancer, 2nd Edition, 3-18pp, Springer, New York, NY, 2018.

Maisonneuve, P., & Lowenfels, A. Epidemiology of pancreatic cancer: An update. *Dig. Dis.* 2010; **28** (4-5): 645-656.

Maitra, A., & Hruban, R.H. Pancreatic cancer. *Annu. Rev. Pathol.* 2008; **3:** 157-188.

Malati, T. Tumour markers: An overview. *Indian J. Clin. Biochem.* 2007; **22** (2): 17-31.

Mallbris, L., Davies, J., Glasebrook, A., Tang, Y., Glaesner, W., & Nickoloff, B.J. Molecular insights into fully human and humanized monoclonal antibodies. *J. Clin. Aesthet. Dermatol.* 2016; **9** (7): 13-15.

Mardis, E.R. Applying next-generation sequencing to pancreatic cancer treatment. *Nat. Rev. Gastroenterol. & Hepatol.* 2012; **9:** 477-486.

Marks, J.D., Bradbury, A. Selection of human antibodies from phage display libraries. *Methods Mol. Biol.* **248:** 161-176.

Matsubayashi, H., Canto, M., Sato, N., Klein, A., Abe, T., Yamashita, K., Yeo, C.J., Hruban, R., & Goggins, M. DNA Methylation alterations in the pancreatic juice of patients with suspected pancreatic disease. *Cancer Res.* 2006; **66** (2): 1208-1217.

Matsusaki, M., Komeda, M., Mura, S., Tanaka, H.Y., Kano, M.R., Couvreur, P., & Akashi, M. Desmoplastic reaction in 3D-pancreatic cancer tissues suppresses molecular permeability. *Adv. Healthc. Mater.* 2017; **6** (15): 1-7.

McCullum, E.O., Williams, B.A., Zhang, J., & Chaput, J.C. Random mutagenesis by error-prone PCR. *Methods Mol. Biol.* 2010; **634**: 103-109.

Mc. Johnston, F., Tan, M.C.B., Tan, B.R.Jr., Porembka, M.R., Brunt, E.M., Linehan, D.C., Simon, P.O. Jr., Plambeck-Suess, S., Eberlein, T.J., Hellstrom, K.E., Hellstrom, I., Hawkins, W.G., & Goedegebuure, P. Circulating mesothelin protein and cellular anti-mesothelin immunity in patients with pancreatic cancer. *Clin. Cancer Res.* 2009; **15** (21): 6511-6518.

Meldrum, C., Doyle, M.A., & Tothill, R.W. Next-generation sequencing for cancer diagnostics: A practical perspective. *Clin. Biochem. Rev.* 2011; **32:** 177- 195.

Merika, E.E., Syrigos, K.N., & Saif, M.W. Desmoplasia in pancreatic cancer. Can we fight it? *Gastroenterol. Res. Pract.* 2012; **2012** (781765): 1-10.

Metz, S., Panke, C., Haas, A.K., Schanzer, J., Lau, W., Croasdale, R., Hoffmann, E., Schneider, B., Auer, J., Gassner, C., Bossenmaier, B., Umana, P., Sustmann, C., & Brinkmann, U. Bispecific antibody derivatives with restricted binding functionalities that are activated by proteolytic processing. *Protein Eng. Sel.* 2012; **25** (10): 571-580.

Mezencev, R., & McDonald, J.F. Subcutaneous xenografts of human T-lineage acute lymphoblastic leukemia Jurkat cells in nude mice. *In Vivo.* 2011; **25** (4): 603-607.

Mian, IS., Bradwell, AR., & Olson, A.J. Structure, function and properties of antibody binding sites. *J. Mol. Biol.* 1991; **217** (1): 133-151.

Michl, P., & Gress, T.M. Current concepts and novel targets in advanced pancreatic cancer. *Gut.* 2013; **62:** 317-326.

Mizuuchi, Y., Aishima, S., Ohuchida, K., Shindo, K., Fujino, M., Hattori, M., Miyazaki, T., Mizumoto, K., Tanaka, M., & Oda, Y. Anterior gradient 2 downregulation in a subset of pancreatic ductal adenocarcinoma is a prognostic factor indicative of epithelial-mesenchymal transition. *Lab. Invest.* 2015. **95** (2): 193-206.

Moniaux, N., Andrianifahana, M., Brand, R.E., & Batra, S.K. Multiple roles of mucins in pancreatic cancer, a lethal and challenging malignancy. *Br. J. Cancer.* 2004; **91:** 1633-1683.

Müller, S., Raulefs, S., Bruns, P., Afonsp-Grunz, F., Plötner, A., Thermann, R., Jäger, C., Schlitter, A.M., Kong, B., Regel, I., Roth, W.K., Rotter, B., Hoffmeier, K., Kahl, G., Theis, F.J., Kleeff, J., Winter, P., & Michalski, C.W. Next-generation sequencing reveals novel differentially regulated mRNAs, IncRNAs, miRNAs, sdRNAs and a piRNA in pancreatic cancer. *Mol. Cancer.* 2015; **14** (94): 1-18.

Nagai, K., & Thøgersen, H.C. Generation of *β*-globin by sequence-specific proteolysis of a hybrid protein produced in *Escherichia coli. Nature.* 1984; **309:** 810-812.

Narat, M. Production of antibodies in chickens. *Food Technol. Biotechnol.* 2003; **41**: 259-267.

Nath, S., Daneshvar, K., Roy, L.D., Grover, P., Kidiyoor, A., Mosely, L., Sahraei, M., & Mukherjee, P. MUC1 induces drug resistance in pancreatic cancer cells via upregulation of multidrug resistance genes. *Oncogenesis.* 2013; **2**: e51.

Nazarian, A.A., Archibeque, I.L., Nguyen, Y.H., Wang, P., Sinclair, A.M., & Powers, D.A. Characterization of bispecific T-cell Engager (BiTE) antibodies with a high-capacity T-cell dependent cellular cytotoxicity (TDCC) assay. *J. Biomol. Screen.* 2015; **20** (4): 519-527.

Neale, R.E., Clark, P.J., Fawcett, J., Fritschi, L., Nagler, B.N., Risch, H.A., Walters, R.J., Crawford, W.J., Webb, P.M., Whiteman, D.C., & Buchanan, D.D. Association between hypermethylation of DNA repetitive elements in white blood cell DNA and pancreatic cancer. *Cancer Epidemiol.* 2014; **38:** 576-582.

Neissi, A., Shapouri, M.S.A., Najafabadi, M.G., & Jaydary, A. Using rice flour for purification of maltose binding fusion proteins expressed in *Escherichia coli. Jundishapar. J. Microbiol.* 2013; **6** (3): 227-229.

Ngoenkam, J., Schamel, W.W., & Pongcharoen, S. Selected signalling proteins recruited to the T-cell receptor-CD3 complex. *Immunology.* 2017; **153** (1): 42-50.

Niv, Y. Mucin expression and the pancreas: A systematic review and a meta-analysis. *World J. Meta-Anal.* 2017; **5** (2): 63-70.

Nivebrant, J., & Sidhu, S.S. Construction of synthetic antibody phage-display libraries. *Methods Mol. Biol.* 2018; **1701**: 45-60.

Nolen, B.M., Brand, R.E., Prosser, D., Velikokhatnaya, L., Allen, P.J., Zeh, H.J., Grizzle, W.E., Huang, Y., Lomakin, A., & Lokshin, A.E. Prediagnostic serum biomarkers as early detection tools for pancreatic cancer in a large prospective cohort study. *PLoS ONE.* 2014; **9** (4): e94928.

Norris, A.M., Gore, A., Balboni, A., Young, A., Longnecker, D.S., & Korc, M. AGR2 is a SMAD4-suppressible gene that modulates MUC1 levels and promotes the initiation and progression of pancreatic intraepithelial neoplasia. *Oncogene.* 2013; **32**: 3867-3876.

O'Kennedy, R., Fitzgerald, S., & Murphy, C. Don't blame it all on the antibodies – The need for exhaustive characterisation, appropriate handling, and addressing the issues that affect specificity. *Trends. Anal. Chem.* 2017; **89**: 53-59.

Omar, N., Yan, B., & Salto-Tellez, M. HER2: An emerging biomarker in non-breast and non-gastric cancers. *Pathogensis.* 2015; **2** (3): 1-9.

Ong, J., Harris, D., Jeffers, G., Watson, L., Ballantine, L., & Beresford, M. THU0296 Matrix interference of IL-6, IL-17, IL-21 and TNF-alpha measurement in juvenile-onset systemic lupus erythematosus serum and plasma. *Ann. Rheum. Dis.* 2013; **71**: 255-256.

O'Reilly, J.A., Fitzgerald, J., Fitzgerald, S., Kenny, D., Kay, E.W., O'Kennedy, R., & Kijanka, G.S. Diagnostic potential of zinc finger protein-specific autoantibodies and associated linear B-cell epitopes in colorectal cancer. *PLoS One.* 2015; **10** (4): e0123469.

Orcutt, K.D., Ackerman, M.E., Cieslewicz, M., Quiroz, E., Slusarczyk, A.L., Frangioni, J.V., & Wittrup, K.D. A modular IgG-scFv bispecific topology. *Protein Eng. Des. Sel.* 2010; **23** (4): 221-228.

Osada, T., Patel, S.P., Hammond, S.A., Osada, K., Morse, M.A., & Lyerly, H.K. CEA/CD3-bispecific T cell-engaging (BiTE) antibody-mediated T lymphocyte cytotoxicity maximized by inhibition of both PD1 and PD-L1. *Cancer. Immunol. Immunother.* 2015; **64** (4): 677-688.

Ossysek, K., Uchański, T., Kulesza, M., Bzowska, M., Klaus, T., Wos, K., Madej, M., & Bereta, J. A new expression vector facilitating production and functional analysis of scFv antibody fragments selected from Tomlinson I + J phagemid libraries. *Immunol. Lett.* 2015; **167** (2): 95-102.

Papayannidis, C., & Martinelli, G. Blinatumomab in Ph+ B-ALL: Present and perspectives. *Oncotarget.* 2017; **8** (55): 93309-93310.

Pan, B., Guo, J., Liao, Q & Zhao, Y. β 1 and β3 integrins in breast, prostate and pancreatic cancer: A novel implication. *Oncol. Lett.* 2018; **15** (4): 5412-5416.

Pang, S., & Cowen, S. A generic standard additions based method to determine endogenous analyte concentrations by immunoassays to overcome complex biological matrix interference. *Sci. Rep.* 2017; **7** (17542): 1-10.

Pansri, P., Jaruseranee, N., Rangnoi, K., Kristensen, P., & Yamabhai, M. A compact phage display human scFv library for selection of antibodies to a wide variety of antigens. *BMC. Biotechnol.* 2009; **9** (6): 1-16.

Park, J.Y., Hiroshima, Y., Lee, J.Y., Maawy, A.A., Hoffman, R.M., & Bouvet, M. MUC1 selectively targets human pancreatic cancer in orthotopic nude mouse models. *PLoS One.* 2015; **10** (3): e0122100

Park, J., Choi, Y., Yi, S.G., Kim, H., Yu, J., Kim, Y., Kwon, M.S., Kwon, W., Oh, D.Y., Kim, S.W., Jeong, S.Y., Han, W., Lee, K.E., Heo, J.S., Park, J.O., Park, J.K., Kim, S.C., Kang, C.M., Lee, W.J., Lee, S., Han, S., Park, T., Jang, J,Y., & Kim, Y. Diagnostic performance enhancement of pancreatic cancer using proteomic multimarker panel. *Oncotarget.* 2017; **8** (54): 93117-93130.

Park, Y., Lim, YA., Kim, K., Jung, J.H., Lee, S., Lim, O.J., Lee, Y.J., Lim, S., Lee, J., Kim, S., Kwon, H.N., & Won, J. MSLN-targeting bispecific T-cell engaging antibody, MG1122, for treatment of solid tumors. *J. Clin. Oncol.* 2018; 15_suppl, e14500-e14500

Parkinson, N.J., Roddis, M., Ferneyhough, B., Zhang, G., Marsden, A.J., Maslau, S., Sanchez-Pearson, Y., Barthlott, T., Humphreys, I.R., Ladell, K., Price, D.A., Ponting, C.P., Hollander, G., & Fischer, M.D. Violation of the 12/23 rule of genomic V(D)J recombination is common in lymphocytes. *Genome Res.* 2015; **25** (2): 226-234.

Passerini, R., Cassatella, M.C., Boveri, S., Salvatici, M., Radice, D., Zorzino, L., Galli, C., & Sandri, M.T. The pitfalls of CA19-9: Routine testing and comparison of two automated immunoassays in a reference oncology center. *Am. J. Clin. Pathol.* 2012; **138:** 281-287.

Patra, K.C., Bardeesy, N., & Mizukami, Y. Diversity of precursor lesions for pancreatic cancer: The genetics and biology of intraductal papillary mucinous neoplasm. *Clin. Transl. Gastroenterol.* 2017; **8** (4): e86.

Pegg, D.E. Principles of cryopreservation. *Methods Mol. Biol.* 2007; **368**: 39-57.

Philips, P.A., Benedetti, J., Corless, C.L., Wong, R., O'Reilly, E.M., Flynn, P.J., Rowland, K.M., Atkins, J.N., Mirtsching, B.C., Rivkin, S.E., Khorana, A.A., Goldman, B., Fenogolio-Preiser, C.M., Abbruzzese, J.L., & Blanke, C.D. Phase III study of gemcitabine [G] plus cetuximab [C] versus gemcitabine in patients with locally advanced or metastatic pancreatic adenocarcinoma [PC]: SWOG S0205 study. *J. Clin. Oncol.* 2007; **25:** 4509.

Pilarsky, C., & Grützmann, R. Analysis of DNA methylation in pancreatic cancer: An update. *Methods Mol. Biol.* 2015; **1238:** 173-181.

Platonova, N., Miquel, G., Chiu, L.Y., Taouji, S., Moroni, E., Colombo, G., Chevet, E., Sue, S.C., & Bikfalvi, A. Dimerization capacities of FGF2 purified with or without heparin-affinity chromatography. *PLoS One.* 2014; **9** (10): e110055.

Plunkett, W., Huang, P., Xu, Y.Z., Heinemann, V., Grunewald, R., & Gandhi, V. Gemcitabine: metabolism, mechanisms of action, and self potentiation. *Semin. Oncol.* 1995; **22**: 3-10.

Polonelli, L., Pontón, J., Elguezabal, N., Elguezabal, N., Moragues, M.D., Casoli, C., Pilotti, E., Ronzi, P., Dobroff, A.S., Rodrigues, E.G., Juliano, M.A., Maffei, D.L., Magliani, W., Conti, S., & Travassos, L.R. Antibody complementarity-determining regions (CDRs) can display differential antimicrobial, antiviral and antitumor activities. *PLoS One.* 2008; **3** (6): e2371.

Ponsel, D., Neugebauer, J., Ladetzki-Baehs, K., & Tissot, K. High affinity, developability and functional size: The holy grail of combinatorial antibody library generation. *Molecules.* 2011; **16:** 3675-3700.

Poruk, K.E., Firpo, M.A., Adler, D.G., & Mulvihill, S.J. Screening for pancreatic cancer: Why, how and who? *Ann. Of. Surg.* 2013; **257** (1): 17-26.

Poruk, K.E., Firpo, M.A., Scaife, C.L., Adler, D.G., Emerson, L.L., Boucher, K.M., & Mulvihill, S.J. Serum osteopontin and TIMP-1 as diagnostic and prognostic biomarkers for pancreatic adenocarcinoma. *Pancreas.* 2013; **42** (2):193-197.

Poruk, K.E., Gay, D.Z., Brown, K., Mulvihill, J.D., Boucher, K.M., Scaife, C.L., Firpo, M.A., & Mulvihill, S.J. The clinical utility of CA 19-9 in pancreatic adenocarcinoma: Diagnostic and prognostic updates. *Curr. Mol. Med.* 2015; **13** (3): 340- 351.

Puri, V., Streaker, E., Prabakaran, P., Zhu, Z., & Dimitrov, D.S. Highly efficient selection of epitope specific antibody through competitive yeast display library sorting. *MAbs.* 2013; **5** (4): 533-539.

Qudsia, S., Merugu, S.B., Mangukiya, H.B., Hema, N., Wu, Z., & Li, D. A novel lentiviral scFv display library for rapid optimization and selection of high affinity antibodies. *Biochem. Biophys. Res. Commun.* 2018; **449** (1): 71-77.

Rachagani, S., Torres, M.P., Kumar, S., Haridas, D., Baine, M., Macha, M.A., Kaur, S., Ponnusamy, M.P., Dey, P., Seshacharyulu, P., Johansson, S.L., Jain, M., Wagner, K.U., & Batra, S.K. Mucin (Muc) expression during pancreatic cancer progression in spontaneous mouse model: potential implications for diagnosis and therapy. *J. Hematol. Oncol.* 2012; **5** (68): 1-12.

Rahbarizadeh, F., Rasaee, M.J., Forouzandeh-Moghadam, M., & Allameh, A.A. High expression and purification of the recombinantcamelid anti-MUC1 single-domain antibodies in *Escherichia coli*. *Protein Expr. Puriff.* 2005; **44** (1): 32-38.

Rajput, R., Sharma, G., Rawat, V., Gautam. A., Kumar, B., Pattnaik, B., Pradhan, H.K., & Khanna, M. Diagnostic potential of recombinant scFv antibodies generated against hemagglutinin protein of influenza A virus. *Front. Immunol.* 2015; **6** (440): 1-9.

Ramachandran, V., Arumugam, T., Wang, H., & Logsdon, C.D. Anterior gradient 2 is expressed and secreted during the development of pancreatic cancer and promotes cancer cell survival. *Cancer Res.* 2008; **68** (19): 7811-7818.

Rami, A., Behdani, M., Yardehnavi, N., Habibi-Anbouhi, M., & Kazemi-Lomedasht, F. An overview on application of phage display technique in immunological studies. *Asian Pac. J. Trop. Biomed.* 2017; **7** (7): 599-602.

Rao, C.V., Janakiram, N.B., Madka, V., Kumar, G., Scott, E.J., Pathuri, G., Bryant, T., Kutche, H., Zhang, Y., Biddick, L., Gali, H., Zhao, Y.D., Lightfoot, S., & Mohammed, A. Small-molecule inhibition of GCNT3 disrupts mucin biosynthesis and malignant cellular behaviors in pancreatic cancer. *Cancer Res.* 2016; **76** (7): 1965-1974.

Raran-Kurussi, S., Keefe, K., & Waugh, D.S. Positional effects of fusion partners on the yield and solubility of MBP fusion proteins. *Protein Expr. Purif.* 2015; **110:** 159-164.

Raran-Kurussi, S., & Waugh, D.S. The ability to enhance the solubility of its fusion partners is an intrinsic property of maltose-binding protein but their folding is either spontaneous or chaperone-mediated. *PLoS One.* 2013; **7** (11): e49589.

Reed, G.F., Lynn, F., & Meade, B.D. Use of coefficient of variation in assessing variability of quantitative assays. *Clin. Diagn. Lab. Immunol.* 2002; **9** (6): 1235-1239.

Regel, I., Kong, B., Raulefs, S., Erkan, M., Michalski, C.W., Hartel, M., & Kleeff, J. Energy metabolism and proliferation in pancreatic carcinogenesis. *Langenbecks Arch. Surg.* 2012; **397:** 507-512.

Ren Y.R., Patel, K., Paun, B.C., & Kern, S.E. Structural analysis of cancer-specific promoter in mesothelin and in other genes overexpressed in cancers. *J. Biol. Chem.* 2011; **286** (14): 11960-11969.

Riener, M., Pilarsky, C., Gerhardt, J., Grützmann, R., Fritzsche, F.R., Bahra, M., Weichert, W., & Kristiansen, G. Prognostic significance of AGR2 in pancreatic ductal adenocarcinoma. *Histol. Histopathol.* 2009; **24** (4): 1121-1128.

Riethmüller, G. Symmetry breaking: bispecific antibodies, the beginnings, and 50 years on. *Cancer Immunity.* 2012; **12** : p.12.

Rio, D.C., Ares, M Jr., Hannon G.J., & Nilsen, T.W. Purification of RNA using TRIzol (TRI reagent). *Cold. Spring. Harb. Protoc.* 2010; **6**: 5439.

Rivlin, N., Brosh, R., Oren, M., & Rotter, V. Mutations in the p53 tumor suppressor gene: Important milestones at the various steps of tumorigenesis. *Genes. Cancer.* 2011; **2** (4): 466-474.

Robin, G., & Martineau, P. Synthetic customized scFv libraries. *Methods Mol. Biol.* 2014; **907**: 109-122.

Robbins, P.F., Li., Y.F., El-Gamil, M., Zhao, Y., Wargo, J.A., Zheng, Z., Xu, H., Morgan, R.A., Feldman, S.A., Johnson, L.A., Bennett, A.D., Dunn, S.M., Mahon, T.M., Jakobsen, B.K., & Rosenberg, S.A. Single and dual amino acid substitutions in TCR CDRs can enhance antigen-specific T cells functions. *J. Immunol.* 2008; **180** (9): 6116-6131.

Roberts, A.S., Campa, M.J., Gottlin, E.B., Jiang, C., Owzar, K., Kindler, H.L., Venook, A.P., Goldberg, E.M., O'Reilly, E.M., & Patz, E.F. Jr. Identification of potential prognostic biomarkers in patients with untreated, advanced pancreatic cancer from a phase 3 trial (cancer and Leukemia group B 80303). *Cancer.* 2012; **118** (2): 571-578.

Root, A., Allen, P., Tempst, P., & Yu, K. Protein biomarkers for early detection of pancreatic ductal adenocarcinoma: Progress and challenges. *Cancers (Basel).* 2018; **10** (67): 1-12.

Rosano, G.L., & Ceccareilli, E.A. Recombinant protein expression in *Escherichia coli*: Advances and challenges. *Front. Microbiol.* 2014; **5** (172): 1-17.

Rosenberg-Hasson, Y., Hansmann, L., Liedtke, M., Herschmann, I., & Maecker, H.T. Effects of serum and plasma matrices on multiplex immunoassays. *Immunol. Res.* 2014; **58** (0): 224-233.

Rosner, K., Winter, D.B., Tarone, R.E., Skovgaard, G.L., Bohr, V.A., & Gearhart, P.J. Third complementarity-determining region of mutated V_H immunoglobulin genes contains shorter V, D, J, P, and N components than non-mutated genes. *Immunology.* 2001; **103** (2): 179-187.

Ross, S.L., Sherman, M., McElroy, P.L., Lofgren, J.A., Moody, G., Baeuerle, P.A., Coxon, A., & Arvedson, T. Bispecific T cell engager (BiTE®) antibody constructs can mediate bystander tumor cell killing. *PLoS One.* 2017; **12** (8): e0183390.

Rückert, F., Pilarsky, C., & Grützmann, R. Serum tumor markers in pancreatic cancer-Recent discoveries. *Cancers.* 2010; **2**: 1107-1124.

Sadeghi, H.M.M., Rabbani, M., Rismani, E., Moazen, F., Khodabakhsh, F., Dormiani, K., & Khazaei, Y. Optimization of the expression of reteplase in *Escherichia coli. Res. Pharm. Sci.* 2011; **6** (2): 87-92.

Sadofsky, M.J. The RAG proteins in V(D)J recombination: more than just a nuclease. *Nucleic Acids Res.* 2001; **29** (7) : 1399-1409.

Saggy, I., Wine, Y., Shefet-Carasso, L., Nahary, L., Georgiou, G., & Benhar, I. Antibody isolation from immunized animals: comparison of phage display and antibody discovery via V gene repertoire mining. *Protein Eng. Des. Sel.* 2012; **25** (10): 539-549.

Sahraei, M., Roy, L.D., Curry, J.M., Teresa, T.L., Nath, S., Besmer, D., Kidiyoor, A., Dalia, R., Gendler, S.J., & Mukherjee, P. MUC1 regulates PDGFA expression during pancreatic cancer progression. *Onocogene.* 2012; **31** (47): 4935-4945.

Saif, M.W. Advancements in the management of pancreatic cancer: 2013. *JOP.* 2013; **14** (2): 112-118.

Saif, M.W. Advanced stage pancreatic cancer: Novel therapeutic options. *Expert. Rev. Clin. Pharmacol.* 2014; **7** (4): 487-498.

Saiki, Y., & Horii, A. Molecular pathology of pancreatic cancer. *Pathol. Int.* 2014; **64:** 10-19.

Säll, A., Walle, M., Wingren, C., Müller, S., Nyman, T., Vala, A., Ohlin, M., Borrebaeck, C.A.K., & Persson, H. Generation and analyses of human synthetic antibody libraries and their application for protein microarrays. *Protein Eng. Des. Sel.* 2016; **29** (10): 427-437.

Satake, K., Takeuchi, T., Homma, T., & Ozaki, H. CA19-9 as a screening and diagnostic tool in symptomatic patients: The Japanese experience. *Pancreas.* 1994; **9:** 703-706.

Schmohl, J.U., Gleason, .K., Dougherty, P.R., Miller, J.S., & Vallera, D.A. Heterodimeric bispecific single chain variable fragments (scFv) killer engagers (BiKEs) enhance NK-cell activity against CD133+ colorectal cancer cells. *Target Oncol.* 2016; **11** (3): 353-361.

Schultz, N.A., Werner, J., Wilenbrock, H., Roslind, A., Giese, N., Horn, T., Wøjdemann, M., & Johansen, J.S. microRNA expression profiles associated with pancreatic adenocarcinoma and ampullary adenocarcinoma. *Mod. Pathol.* 2012; **25** (12): 1609-1622.

Schultz, N.A., Dehlendorff, C., Jenson, B.V., Bjerregaard, J.K., Nielsen, K.R., Bojesen, S.E., Calatayud, D., Nielsen, S.E., Yilmaz, M., Holländer, N.H., Andersen, K.K., & Johansen, J.S. MicroRNA biomarkers in whole blood for detection of pancreatic cancer. *JAMA.* 2014; **311** (4): 392-404.

Schwimmer, L.J., Huang, B., Glang, H., Cotter, R.L., Chemia-Vogel, D.S., Dy, F.V., Tam, E.M., Zhang, F., Toy, P., Bohmann, D.J., Watson, S.R., Beaber, J.W., Reddy, N., Kuan, H.F., Bedinger, D.H., & Rondon, I.J. Discovery of diverse and functional antibodies from large human repertoire antibody libraries. *J. Immunol. Methods.* 2013; **391** (1-2): 60-71.

Sedykh, S.E., Prinz, V.V., Buneva, V.N., & Nevinsky, G.A. Bispecific antibodies: design, therapy, perspectives. *Drug Des. Devel. Ther.* 2018; **12** : 195-208.

Sela-Culang, I., Vered, K., & Ofran, Y. The Structural Basis of Antibody-Antigen Recognition. *Front. Immunol.* 2013; **4** (302): 1-13.

Selleck, M.J., Senthil, M., & Wall, N.R. Making meaningful clinical use of biomarkers. *Biomark. Insights.* 2017; **12**: 1-7.

Şengül, Ü. Comparing determination methods of detection and quantification limits for aflatoxin analysis in hazelnut. *J. Food Drug Anal.* 2016; **24** (1): 56-62.

Sharma, S. Tumor markers in clinical practice: General principles and guidelines. *Indian J. Med. Paediatr. Oncol.* 2009; **30** (1): 1-8.

Sharma, S., Crawley, A., & O'Kennedy, R. Strategies for overcoming challenges for decentralised diagnostics in resource-limited and catastrophe settings. *Expert Rev. Mol. Diagn.* 2017; **17** (2): 109-118.

Shaw, V.E., Lane, B., Jenkinson, C., Cox, T., Greenhalf, W., Halloran, C.M., Tang, J., Sutton, R., Neoptolemos, J.P., & Costello, E. Serum cytokine biomarker panels for discriminating pancreatic cancer from benign pancreatic disease. *Mol. Cancer.* 2014; **13** (114): 1-13.

Shengnan, Y., Li, A., Liu, Q., Yuan, X., Xu, H., Jiao, D., Pestell, R.G., Han, X., & Wu, K. Recent advances of bispecific antibodies in solid tumors. *J. Hematol. Oncol.* 2017; **10** (155): 1-16.

Shi, X.-H., Li, X., Zhang, H., He, R.Z., Zhao, Y., Zhou, M., Pan, S.T., Zhao, C.L., Feng, Y.C., Wang, M., Guo, X.J., & Qin, R.Y. A five-microRNA signature for the survival prognosis in pancreatic adenocarcinoma based on TCGA data. *Sci. Rep.* 2018; **8** (1): 7638.

Shukra, A.M., Sridevi, N.V., Chandran, D., & Maithal, K. Production of recombinant antibodies using bacteriophages. *Eur. J. Microbiol. Immunol. (Bp).* 2014; **4** (2): 91-98.

Siegel, R., Ma, J., Zou, Z., & Jemal, A. Cancer statistics, 2014. *Ca. Cancer J. Clin.* 2014; **64:** 9-29.

Silacci, M., Brack, S., Schirru, G., Marlind, J., Ettore, A., Merlo, A., Viti, F., & Neri, D. Design, construction, and characterization of a large synthetic human antibody phage display library. *Proteomics.* 2005; **9**: 2340-2350.

Sinha, N., Mohan, S., Lipschultz, C.A., & Smith-Gill, S.J. Differences in electrostatic properties at antibody-antigen binding sites: Implications for specificity and cross-reactivity. *Biophys. J.* 2002; **83** (6): 2946-2968.

Singh, S., Chitkara, D., Kumar, V., Behrman, S.W., & Mahato, R.I. MiRNA profiling in pancreatic cancer and restoration of chemosensitivity. *Cancer Lett.* 2013; **334:** 211-220.

Sivashanmugam, A., Murray, V., Cui, C., Zhang, Y., Wang, J., & Li, Q. Practical protocols for production of very high yields of recombinant proteins using *Escherichia coli. Protein Sci.* 2009; **18** (5): 936-948.

Sjoquist, K.M., Chin, V.T., Chantrill, L.A., O'Connor, C., Hemmings, C., Chang, D.K., Chou, A., Pajic, M., Johns, A.L., Nagrial, A.M., Biankin, A.V., & Yip, D. Personalising pancreas cancer treatment; when tissue is the issue. *World J. Gastroenterol.* 2014; **20** (24): 7849-7863.

Smith, G.P. Filamentous fusion phage: novel expression vectors that display cloned antigens on the virion surface. *Science.* 1985; **228:** 1315-1317.

Smits, N.C., & Sentman, C.L. Bispecific T-cell engagers (BiTEs) as treatment of B-cell lymphoma. *J. Clin. Oncol.* 2016; **34** (10): 1131-1133.

Sørensen, H.P., & Mortensen, K.K. Soluble expression of recombinant proteins in the cytoplasm of *Escherichia coli. Microb. Cell Fact.* 2005; **4** (1): 1-8.

Stengel, K.R., Barnett, K.R., Wang, J., Liu, Q., Hodges, E., Hiebert, S.W., & Bhaskara, S. Deacetylase activity of histone deacetylase 3 is required for productive VDJ recombination and B-cell development. *Proc. Natl. Acad. Sci. USA.* 2017; **114** (32): 8608-8613.

Steinberg, W. The clinical utility of the CA 19-9 tumor associated antigen. *Am. J. Gastroenterol.* 1990; **85:** 350-355.

Stieglmaier, J., Benjamin, J., & Nagorsen, D. Utilizing the BiTE (bispecific T-cell engager) platform for immunotherapy of cancer. *Expert Opin. Biol. Ther.* 2015; **15** (8): 1093-1099.

Stoita, A., Penman, I.D., & Williams, D.B. Review of screening for pancreatic cancer in high risk individuals. *World J. Gastroenterol.* 2011; **17** (19): 2365-2371.

Studier, F.W. Stable expression clones and auto-induction for protein production in *E. coli. Methods Mol. Biol.* 2014; **1091**: 17-32.

Sturm, P.D., Hruban, R.H., Ramsoekh, T.B., Noorduyn, L.A., Tytgat, G.N., Gouma, D.J., & Offerhaus, G.J. The potential diagnostic use of K-ras codon 12 and p53 alterations in brush cytology from the pancreatic head region. *J. Pathol.* 1998; **186** (3): 247-253.

Taieb, J., Pointet, A.-L., Van Laethem, J.L., Laquente, B., Pernot, S., Lordick, F., & Reni, M. What treatment in 2017 for inoperable pancreatic cancers? *Ann. Oncol.* 2017; **28** (7): 1473-1483.

Takadate, T., Onogawa, T., Fukuda, T., Motoi, F., Suzuki, T., Fujii, K., Kihara, M., Mikami, S., Bando, Y., Maeda, S., Ishida, K., Minowa, T., Hanagata, N., Ohtsuka, H., Katayose, Y., Egawa, S., Nishimura, T., & Unno, M. Novel prognostic protein markers of resectable pancreatic cancer identified by coupled shotgun and targeted proteomics using formalin-fixed paraffin-embedded tissues. *Int. J. Cancer.* 2013; **132:** 1368-1382.

Tamm, E.P., Balachandran, A., Bhosale, P.R., Katz, M.H., Fleming, J.B., Lee, J.H., & Varadhachary, G.R. Imaging of pancreatic adenocarcinoma: update on staging/resectability. *Radiol. Clin. North Am.* 2012; **50:** 407-428.

Tang, Z., Qian, M., & Ho, M. The role of mesothelin in tumor progression and targeted therapy. *Anticancer Agents Med. Chem.* 2013; **13** (2): 276-280.

Tanase, C.P., Neagu, A.I., Necula, L.G., Mambet, C., Enciu, A.M., Calenic, B., Cruceru, M.L., Albulescu, R. Cancer stem cells : Involvement in pancreatic cancer pathogenesis and perspectives on cancer therapeutics. *World J. Gastroenterol.* 2014; **20** (31): 10790-10801.

Tate, J., & Ward, G. Interferences in immunoassay. *Clin. Biochem. Rev.* 2004; **25** (2): 105-120.

Thie, H., Toleikis, L., Li, J., von Wasielewski, R., Bastert, G., Schirrmann, T., Esteves, I.T., Behrens, C.K., Fournes, B., Fournier, N., de Romeuf, C., Hust, M., & Dübel, S. Rise and fall of an anti-MUC1 specific antibody. *PLoS One.* 2011; **6** (1): e15921.

Thway, T., & Salimi-Moosavi, H. Evaluating the impact of matrix effects on biomarker assay sensitivity. *Bioanalysis.* 2014; **6** (8): 1081-1091.

Thomas, P., & Smart, T.G. HEK293 cell line: A vehicle for the expression of recombinant proteins. *J. Pharmacol. Toxicol. Methods.* 2005; **51** (3): 187-200.

Thomsson, O., Ström-Holst, B., Sjunnesson, Y., & Bergqvist, A.S. Validation of an enzyme-linked immunosorbent assay developed for measuring cortisol concentration in human salvia and serum for its applicability to analyse cortisol in pig saliva. *Acta. Vet. Scand.* 2014; **56** (55): 1-5.

Tian, S.B., Tao, K.X., Hu, J., Liu, Z.B., Ding, X.L., Chu, Y.N., Cui, J.Y., Shuai, X.M., Gao, J.B., Cai, K.L., Wang, J.L., Wang, G.B., Wang, L., & Wang, Z. The prognostic value of AGR2 expression in solid tumours: a systematic review and meta-analysis. *Sci. Rep.* 2017; **7** (15500): 1-10.

Tjensvoll, K., Nordgård, O., & Smaaland, R. Circulating tumor cells in pancreatic cancer patients: Method of detection and clinical implications. *Int. J. Cancer.* 2014; **134:** 1-8.

Torres, M.P., Chakraborty, S., Souchek, J., & Batra, S.K. Mucin-based targeted pancreatic cancer therapy. *Curr. Pharm. Des.* 2012; **18** (17): 2472-2481.

Trivedi, A., Stienen, S., Zhu, M., Li, H., Yuraszeck, T., Gibbs, J., Heath, T., Loberg, R., & Kasichayanula, S. Clinical pharmacology and translational aspects of bispecific antibodies. *Clin. Transl. Sci.* 2017; **10** (3): 147-162.

Tur, M.K., Huhn, M., Sasse, S., Engert, A., & Barth, S. Selection of scFv phages on intact cells under low pH conditions leads to a significant loss of insert-free phages. *BioTechniques.* 2001; **30:** 404-413.

Ujiki, M.B., & Talamonti, M.S. Surgical management of pancreatic cancer. *Semin. Radiat. Oncol.* 2005; **15** (4): 218-225.

Van der Merwe, P.A., & Dushek, O. Mechanisms for T cell receptor triggering. *Nat. Rev. Immunol.* 2011; **11:** 47-55.

Vauquelin, G., & Charlton, S.J. Exploring avidity: understanding the potential gains in functional affinity and target residence time of bivalent and heterobivalent ligands. *Br. J. Pharmacol.* 2013; **168** (8): 1771-1785.

Vrijenhoek, T., Kraaijeveld, K., Elferink, M., de Ligt, J., Kranendonk, E., Santen, G., Nijman, I.J., Butler, D., Claes, G., Costessi, A., Dorlijin, W., van Eyndhoven, W., Halleym D.J., van den Hout, M.C., van Hove, S., Johansson, L.F., Jongbloed, J.D., Kamps, R., Kockx, C.E., de Koning, B., Kriek, M., Lekanne Dit Deprez, R., Lunstroo, H., Mannens., M., Mook, O.R., Nelen, M., Ploem, C., Rijnen, M., Saris, J.J., Sinke, R., Sistermans, E., van Slegtenhorst, M., Sleutels, F., van der Stoep, N., van Tienhoven, M., Vermaat, M., Vogel, M., Waisfisz, Q., Marjan, Weiss, J., van der Wijingaard, A., van Workum, W., Ijntema, H., van der Zwaag, B., van IJcken, W.F., den Dunnen, J., Veltman, J.A., Hennekam, R., & Cuppen, E. Next-generation sequencing-based genome diagnostics across clinical genetics centers: implementation choices and their effects. *Eur. J. Hum. Genet.* 2015; **23** (9): 1142-1150.

Vu, N.X., Pruksametanan, N., Srila, W., Yuttavanichalkul, W., Teamtisong, K., Teaumroong, N., Boonkerd, N., Tittabutr, P., & Yamabhai, M. Generation of a rabbit single-chain fragment variable (scFv) antibody for specific detection of Bradyrhizobium sp. DOA9 in both free-living and bacteriod forms. *PLoS One.* 2017; **12** (6): e0179983.

Waaijer, S.J.H., Warnders, F.J., Stienen, S.K., Friedrich, M., Sternjak, A., Cheung, H.K., Terwisscha van Scheltinga, A.G.T., Schröder, C.P., de Vries, E,G., & Lub-de Hooge, M.N. Molecular imaging of radiolabeled bispecific T-cell Engager 89Zr-AMG211 targeting CEA-positive tumors. *Clin. Cancer Res.* 2018; doi: 10.1158/1078-0432

Walsh, N., Clynes, M., Crown, J., & O'Donovan, N. Alterations in integrin expression modulates invasion of pancreatic cancer cells. *J. Exp. Clin. Cancer Res.* 2009; **28** (140): 1-12.

Watanabe, Y., Asano, R., Arai, K., Shimomura, I., Ogata, H., Kawaguchi, H., Hayashi, H., Ohtsuka, H., Yoshida, H., Katayose, Y., Egawa, S., Nakanishi, T., Umetsu, M., Yasui, H., Ishida, T., Imai, K., Kudo, T., Unno, M., & Kumagai, I. *In vitro* and *in vivo* antitumor effects of recombinant bispecific antibodies based on humanized anti-EGFR antibody. *Oncol. Rep.* 2011; **26** (4): 949-955.

Wang, J., Chen, J., Chang, P., LeBlanc, A., Li, D., Abbruzzesse, J.L., Frazier, M.L., Killary, A.M., & Sen, S. MicroRNAs in plasma of pancreatic ductal adenocarcinoma patients as novel blood-based biomarkers of disease. *Cancer Prev. Res. (Phila).* 2009; **2** (9): 807-813.

Wang, J., Paris, P.L., Chen, J., Ngo, V., Yao, H., Frazier, M.L., Killary, A.M., Liu, C.G., Liang, H., Mathy, C., Bondada, S., Kirkwood, K., & Sen, S. Next generation sequencing of pancreatic cyst fluid microRNAs from low grade-benign and high grade-invasive lesions. *Cancer Lett.* 2015; **356:** 404-409.

Wang, L., He, Y., Zhang, G., Ma, J., Liu, C., He, W., Wang, W., Han, H., Boruah, B.M., & Gao, B. Retargeting T cells for HER2-positive tumor killing by a bispecific Fv-Fc antibody. *PLoS One.* 2013: **8** (9): e75589.

Wang, M.H., Sun, R., Zhou, X.M., Zhang, M.Y., Lu, J.B., Yang, Y., Zeng, L.S., Yang, X.Z., Shi, L., Xiao, R.W., Wang, H.Y., & Mai, S.J. Epithelial cell adhesion molecule overexpression regulates epithelial-mesenchymal transition, stemness and metastasis of

nasopharyngeal carcinoma cells via the PTEN/ALT/mTOR pathway. *Cell Death Dis.* 2018; **9** (2): 1-16.

Wang, S., Huang, S., & Ling Sun, Y. Epithelial-mesenchymal transition in pancreatic cancer: A review. *BioMed. Res. Int.* 2017; Article ID 2646148.

Wang, S., Zhang, N., Hu, T., Dai, W., Feng, X., Zhang, X., & Qian, F. Viscosity-lowering effect of amino acids and salts on highly concentrated solutions of two IgG1 monoclonal antibodies. *Mol. Pharm.* 2015; **12** (12): 4478-4487.

Wang, Y., Duan, H., Yang, X., & Guo, J. Cigarette smoking and the risk of pancreatic cancer: a case-control study. *Med. Oncol.* 2014; **31** (10): 184.

Weber, M., Bujak, E., Putelli, A., Villa, A., Matasci, M., Gualandi, L., Hemmerle, T., Wulhfard, S., & Neri, D. A highly functional synthetic phage display library containing over 40 billion human antibody clones. *PLoS One.* 2014; **9** (6): e100000.

Whatcott, C.J., Posner, R.G., Von Hoff, D.D., & Han, H. Desmoplasia and chemoresistance in pancreatic cancer. In: Grippo PJ, Munshi, HG, editors. Pancreatic Cancer and Tumor Microenvironment, 1st Edition, Trivandrum (India): Transworld Research Network, 2012.

White, M., Freistaedter, A., Jones, G.J.B., Zervos, E., & Roper, R.L. Development of improved therapeutic mesothelin-based vaccines for pancreatic cancer. *PLoS One* 2018; **13** (2): e0193131.

Wiemik, A., Foley, B., Zhang, B., Verneris, M.R., Warlick, E., Gleason, M.K., Ross, J.A., Luo, X., Weisdorf, D.J., Walcheck, B., Vallera, D.A., & Miller, J.S. Targeting natural killer cells to acute myeloid leukemia in vitro with a CD16 x 33 bispecific killer cell engager and ADAM17 inhibition. *Clin. Cancer Res.* 2013; **19** (14): 3844-3855.

Winter, J.M., Yeo, C.J., & Brody, J.R. Diagnostic, prognostic and predictive biomarkers in pancreatic cancer. *J. Surg. Oncol.* 2013; **107:** 15-22.

Witkiewicz, A.K., McMillan, E.A., Balaji, U., Baek, G., Lin, W.C., Mansour, J., Mollaee, M., Wagner, K.U., Koduru, P., Yopp, A., Choti, M.A., Yeo, C.J., McCue, P., White, M.A., & Knudsen, E.S. Whole-exome sequencing of pancreatic cancer defines genetic diversity and therapeutic targets. *Nat. Commun.* 2015; **6** (6744): 1-11.

Wodziak, D., Dong, A., Basin, M.F., & Lowe, A.W. Anterior gradient 2 (AGR2) induced epidermal growth factor receptor (EGFR) signaling is essential for murine pancreatitis-associated tissue regeneration. *PLoS One.* 2016; **11** (10): e0164968.

Wolfgang, C.L., Herman, J.M., Laheru, D.A., Klein, A.P., Erdek, M.A., Fishman, E.K., & Hruban, R.H. Recent progress in pancreatic cancer. *Ca. Cancer J. Clin.* 2013; **63:** 318-348.

Wolpin, B.M., Chan, A.T., Hartge, P., Chanock, S.J., Kraft, P., Hunter, D.J., Giovannucci, E.L., & Fuchs, C.S. ABO blood group and the risk of pancreatic cancer. *J. Natl. Cancer Inst.* 2009; **101:** 424-431.

Wöll, S., Schlitter, A.M., Dhaene, K., Roller, M., Esposito, I., Sahin, U., & Türeci, Ö. Claudin 18.2 is a target for IMAB362 antibody in pancreatic neoplasms. *Int. J. Cancer.* 2014; **134**: 731-739.

Wozniak-Knopp, G., Bartl, S., Bauer, A., Mostageer, M., Woisetschläger, M., Antes, B., Ettl, K., Kainer, M., Weberhofer, G., Wiederkum, S., Himmler, G., Mudde, G.C., & Rüker, F. Introducing antigen-binding sites in structural loops of immunoglobulin constant domains: Fc fragments with engineered HER2/neu-binding sites and antibody properties. *Protein Eng. Des. Sel.* 2010; **23** (4): 289-297.

Wu, S.T., Williams, C.D., Grover, P.A., Moore, L.J., & Mukherjee, P. Early detection of pancreatic cancer in mouse models using a novel antibody, TAB004. *PLoS One.* 2018; **13** (2): e0193260.

Wu, Z.H., Zhu, Q., Gao, G.W., Zhou, C.C., & Li, D.W. [Preparation, characterization and potential application of monoclonal antibody 18A4 against AGR2]. 2010; **26** (1): 49-51.

Wurm, D.J., Veiter, L., Ulonska, S., Eggenreich, B., Herwig, C., & Spadiut, O. The *E. coli* pET expression system revisited- mechanistic correlation between glucose and lactose uptake. *Appl. Microbiol. Biotechnol.* 2016; **100** (20): 8721-8729.

Xia, J., Zhang, Y., Qian, J., Zhu, X., Zhang, Y., Zhang, J., & Zhao, G. Isolation, identification and expression of specific human CD133 antibodies. *Sci. Rep.* 2013; **3** (3320): 1-9.

Xie, D., & Xie, K. Pancreatic cancer stromal biology and therapy. *Genes. Dis.* 2015; **2:** 133-143.

Xu, Z., Pothula, S.P., Wilson, J.S., & Apte, M.V. Pancreatic cancer and its stroma: A conspiracy theory. *World J. Gastroenterol.* 2014; **20** (32): 11216-11229.

Xue, X., Fei, X., Hou, W., Zhang, Y., Liu, L., & Hu, R. miR-342-3p suppresses cell proliferation and migration by targeting AGR2 in non-small cell lung cancer. *Cancer Lett.* 2018; **412** : 17-178.

Yan, J.P., Ko, J.H., & Qi, Y.P. Generation and characterization of a novel single-chain antibody fragment specific against human fibrin clots from phage display antibody library. *Thromb. Res.* 2004; **114** (3): 205-211.

Yang, H.Y., Kang, K.J., Chung, J.E., & Shim, H. Construction of a large synthetic human scFv library with six diversified CDRs and high functional diversity. *Mol. Cells.* 2009; **27** (2): 225-235.

Yang, W., Hu, Q., Xu, Y., Liu, H., & Zhong, L. Antibody fragment-conjugated gemcitabine and paclitaxel-based liposome for effective therapeutic efficacy in pancreatic cancer. *Mat. Sci. Eng. C.* 2018; **89**: 328-335.

Yang, Z.Y., Yuan, J.Q., Zheng, D.Y., Chen, J.Z., Ding, H., Wu, X.Y., Huang, Y.F., Mao, C., & Tang, J.L. Gemcitabine plus erlotinib for advanced pancreatic cancer: a systematic review with meta-analysis. *PLoS ONE.* 2013; **8** (3): e57528.

Yao, F., Sun, M., Dong, M., Jing, F., Chen, B., Xu, H., & Wang, S. NPTX2 hypermethylation in pure pancreatic juice predicts pancreatic neoplasms. *Am. J. Med. Sci.* 2013; **346** (3): 175-180.

Yao, S., Hart, D.J., & An, Y. Recent advances in universal TA cloning methods for use in function studies. *Protein Eng. Des. Sel.* 2016; **11**: 551-556.

Yokoyama, S., Kitamoto, S., Higashi, M., Goto, Y., Hara, T., Ikebe, D., Yamaguchi, T., Arisaka, Y., Niihara, T., Nishimata, H., Tanaka, S., Takaori, K., Batra, S.K., & Yonezawa, S. Diagnosis of pancreatic neoplasms using a novel method of DNA methylation analysis of mucin expression in pancreatic juice. *PLoS ONE.* 2014; **9** (4): e93760.

Yu, D.A., Yu, Y.D., Kim, W.B., Han, H.J., Choi, S.B., Kim, D.S., Choi, S.Y., Kim, J.Y., Chang, H., & Kim, B.H. Clinical significance of pancreatic intraepithelial neoplasia in resectable pancreatic cancer on survivals. *Ann. Surg. Treat. Res.* 2018; **94** (5): 247-253.

Yu, I.S., & Cheung, W.Y. A contemporary review of the treatment landscape and the role of predictive and prognostic biomarkers in pancreatic adenocarcinoma. *Can. J. Gastroenterol. Hepatol.* 2018; Article ID 1863535.

Yuraszeck, T., Kasichayanula, S., & Benjamin, J.E. Translation and clinical development of bispecific T-cell engaging antibodies for cancer treatment. *Clin. Pharmacol. Ther.* 2017; **101** (5): 634-645.

Yurkovetsky, Z., Ta'asan, S., Skates, S., Rand, A., Lomakin, A., Linkov, F., Marrangoni, A., Velikokhatnaya, L., Winans, M., Gorelik, E., Lu, K., Maxwell, G.L., & Lokshin, A. Development of multimarker panel for the early detection of endometrial cancer. High diagnostic power of prolactin. *Gynecol. Oncol.* 2007; **107** (1): 58-65.

Zervos, E., Agle, S., Freistaedter, A.G., Jones, G.J., & Roper, R.L. Murine mesothelin: characterization, expression, and inhibition of tumor growth in a murine model of pancreatic cancer. *J. Exp. Clin. Cancer Res.* 2016; **35** (39): 1-13.

Zhang, L., Farrell, J.J., Zhou, H., Elashoff, D., Akin, D., Park, N.H., Chia, D., & Wong, D.T. Salivary transcriptomic biomarkers for detection of resectable pancreatic cancer. *Gastroenterology.* 2010; **138** (3): 949-957.

Zhang, L., Ni, X., & Jin, D. Clinical Significance of Mesothelin in Pancreatic Cancer. *Curr. Signal. Transd. Ther,* 2016; **11** (1): 9-12.

Zhang, L., Sanagapalli, S., & Stoita, A. Challenges in diagnosis of pancreatic cancer. *World J. Gastroenterol.* 2018; **24** (19): 2047-2060.

Zhang, Y., Yang, J., Li, H., Wu, Y., Zhang, H., & Chen, W. Tumor markers CA19-9, CA242 and CEA in the diagnosis of pancreatic cancer: a meta-analysis. *Int. J. Clin. Exp. Med.* 2015; **8** (7): 11683-11691.

Zhang, Y., Yang, C., Cheng, H., Fan, Z., Huang, Q., Lu, Y., Fan, K., Luo, G., Jin, K., Wang, Z., Liu, C., & Yu, X. Novel agents for pancreatic ductal adenocarcinoma: emerging therapeutics and future directions. *Int. J. Hematol. Res.* 2018; **11** (14): 1-17.

Zhang, X., Yang, Y., Fan, D., & Xiong, D. The development of bispecific antibodies and their applications in tumor immune escape. *Exp. Hematol. Oncol.* 2017; **6** (12): 1-6.

Zhao, J. Cancer stem cells and chemoresistance: The smartest survives the raid. *Pharmacol. Ther.* 2016; **160**: 145-158.

Zhao, X., Li, G., & Liang, S. Several affinity tags commonly used in chromatographic purification. *J. Anal. Methods Chem.* 2013; **2013**: 581093.

Zhong, X., Coukos, G., & Zhang, L. miRNAs in human cancer. *Methods Mol. Biol.* 2012; **822**: 295-306.

Zhu, L., Liu, Y., & Chen, G. Diagnostic value of mesothelinin pancreatic cancer: A meta-analysis. *Int. J. Clin. Exp. Med.* 2014; **7** (11): 4000-4007.

Chapter 8

Appendices

APPENDIX A

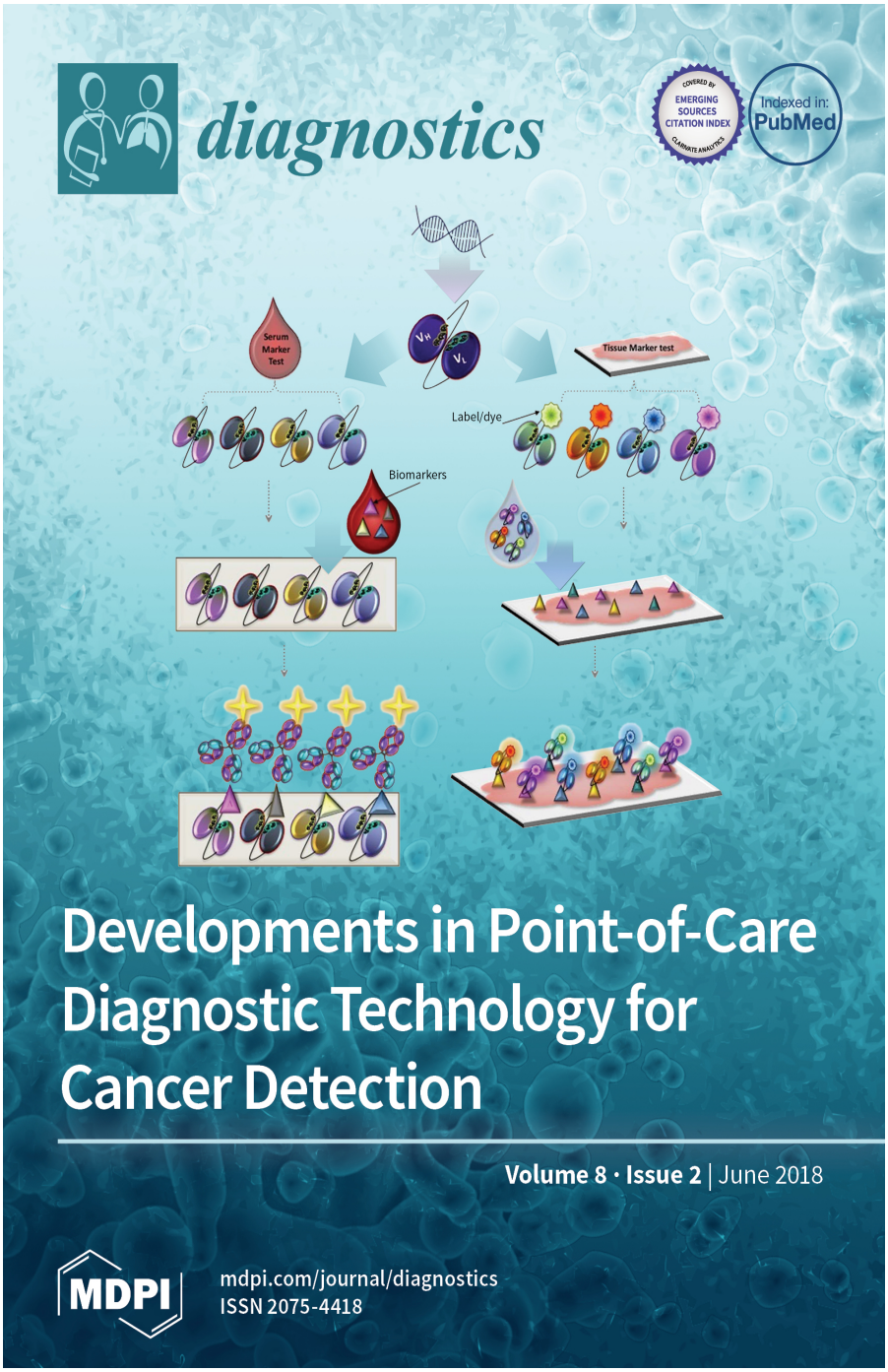

Figure 8.1 Cover illustration for Diagnostics, Volume 8, Issue 2 June 2018

APPENDIX B

Table 8.1 Avian scFv (pComb3XSS vector) SOE-PCR Primer sequences

Primer	Sequence
SOE Sense Primer	
CSC-F	5` GAG GAG GAG GAG GAG GAG GTG GCC CAG GCG GCC CTG ACT CAG 3`
SOE Reverse Primer	
CSC-B	5` GAG GAG GAG GAG GAG GAG GAG CTG GCC GGC CTG GCC ACT AGT GGA GG 3`

APPENDIX C

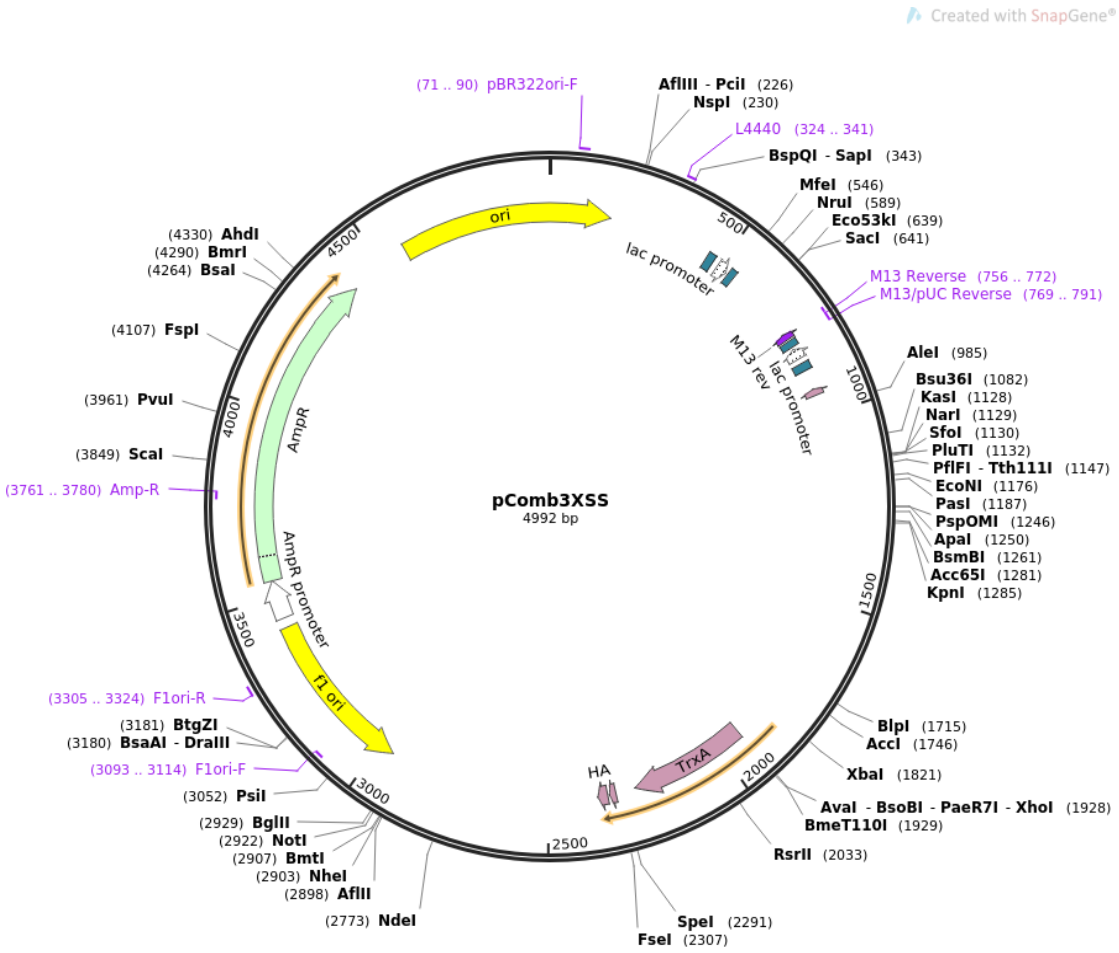

Figure 8.2 Map of pComb3XSS vector

This vector was employed for the construction of the anti-Capan-1 and anti-Jurkat libraries described in Chapters 3 and 5. From this map the amber stop codon , HIS tag, HA tag, SfiI digestion sites and ampicillin resistance gene can be observed. (https://www.addgene.org/63890/)

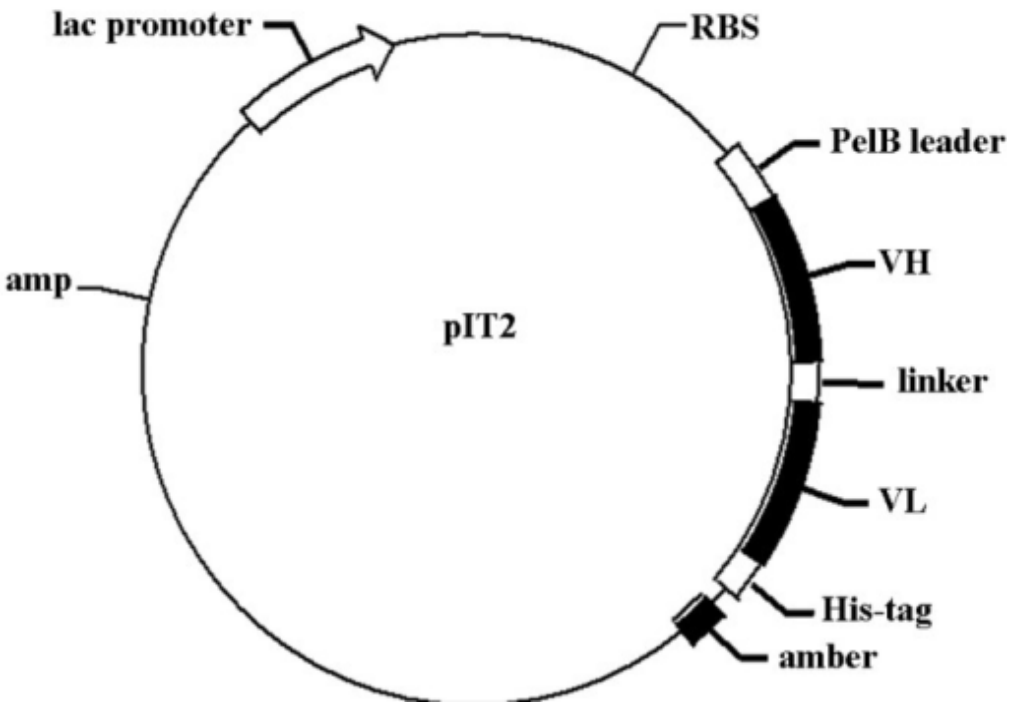

Figure 8.3 Map of pIT2 vector

The pIT2 phagemid vector harboured the synthetic naïve human Tomlinson I and J libraries employed in Chapters 4. From this map the variable domain genes, linker, PelB leader sequence, amber stop codon , HIS tag, and ampicillin resistance gene can be observed.

(https://openi.nlm.nih.gov/detailedresult.php?img=PMC3786976_ETM-06-02-0552-g00&req=4)

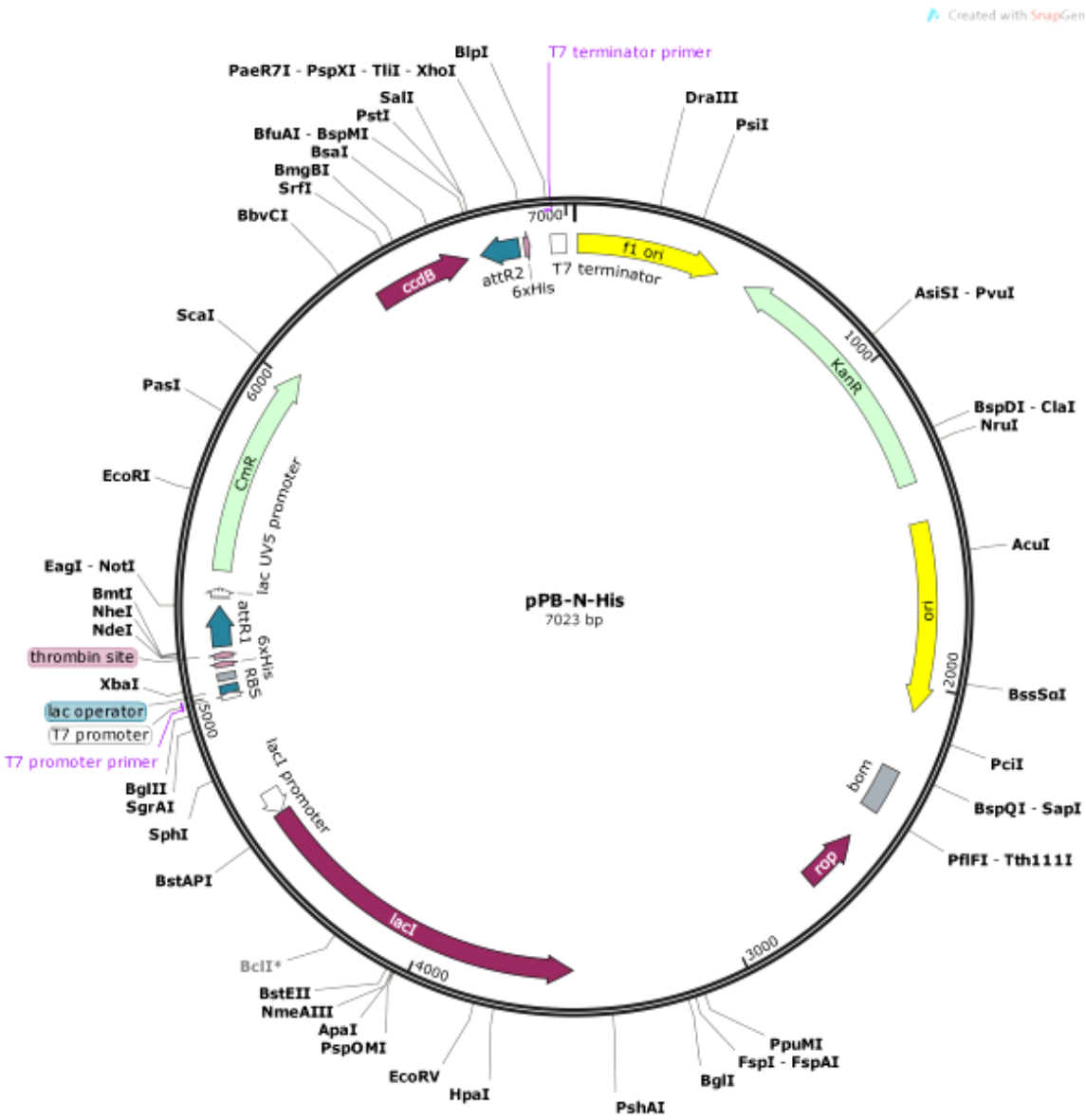

Figure 8.4 Map of pPB-N-His vector

Two pPB-N-His vectors were purchased containing the recombinant protein MUC1 and MSLN genes. The pPB-MSLN-N-His vector was used in Chapter 3 to attempt to express the recombinant MSLN protein in E. coli. The pPB-MUC1-N-His vector was successfully employed for the expression of a recombinant MUC1 protein in Chapter 4. From this map the HIS tag, and kanamycin resistance gene can be observed. (https://www.genomics-online.com/vector-backbone/93/ppb-n-his/)

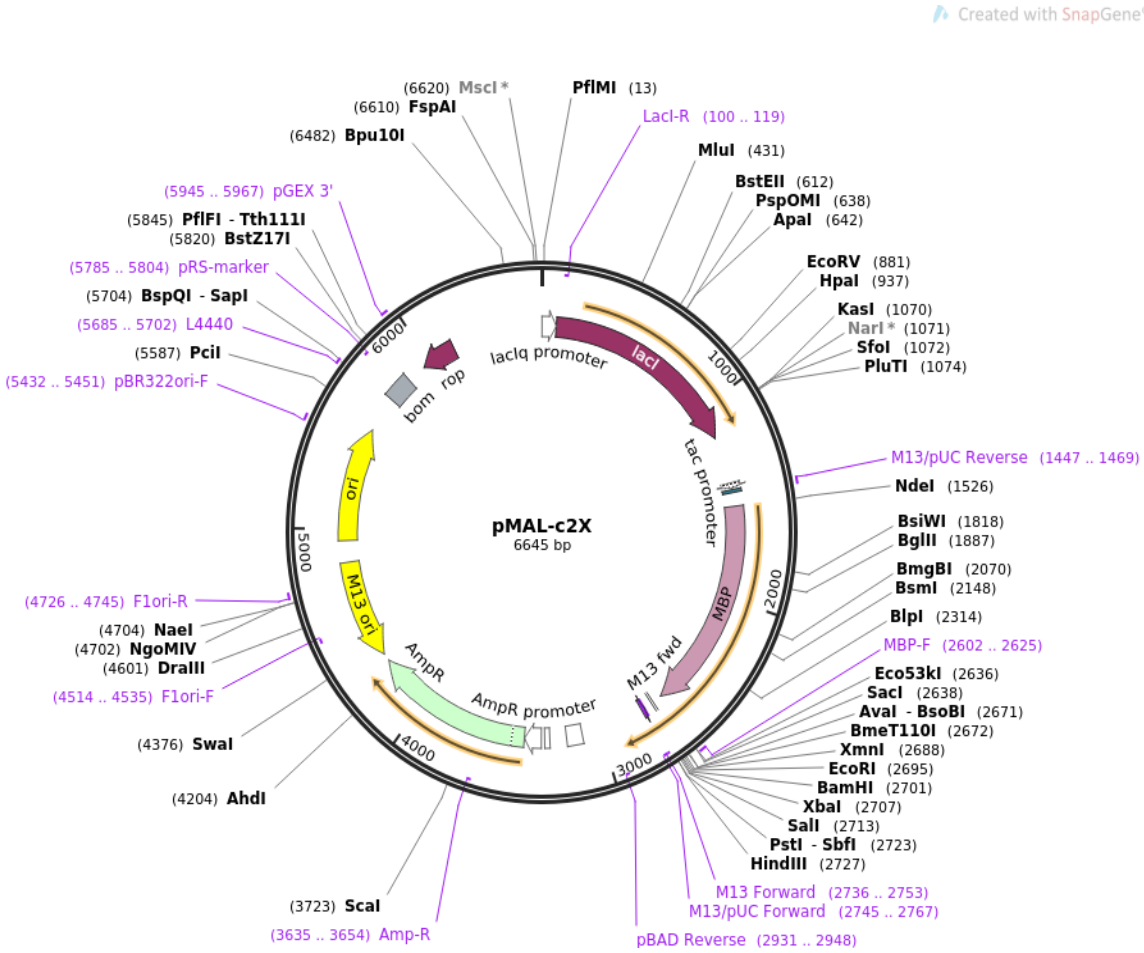

Figure 8.5 Map of pMAL-c2x vector

The pMal-AGR2-MBP vectors was purchased from Addgene for the expression of the AGR2 protein described in Chapter 4. From this map the MBP fusion partner and affinity tag and ampicillin resistance gene can be observed.

(https://www.addgene.org/75286/)

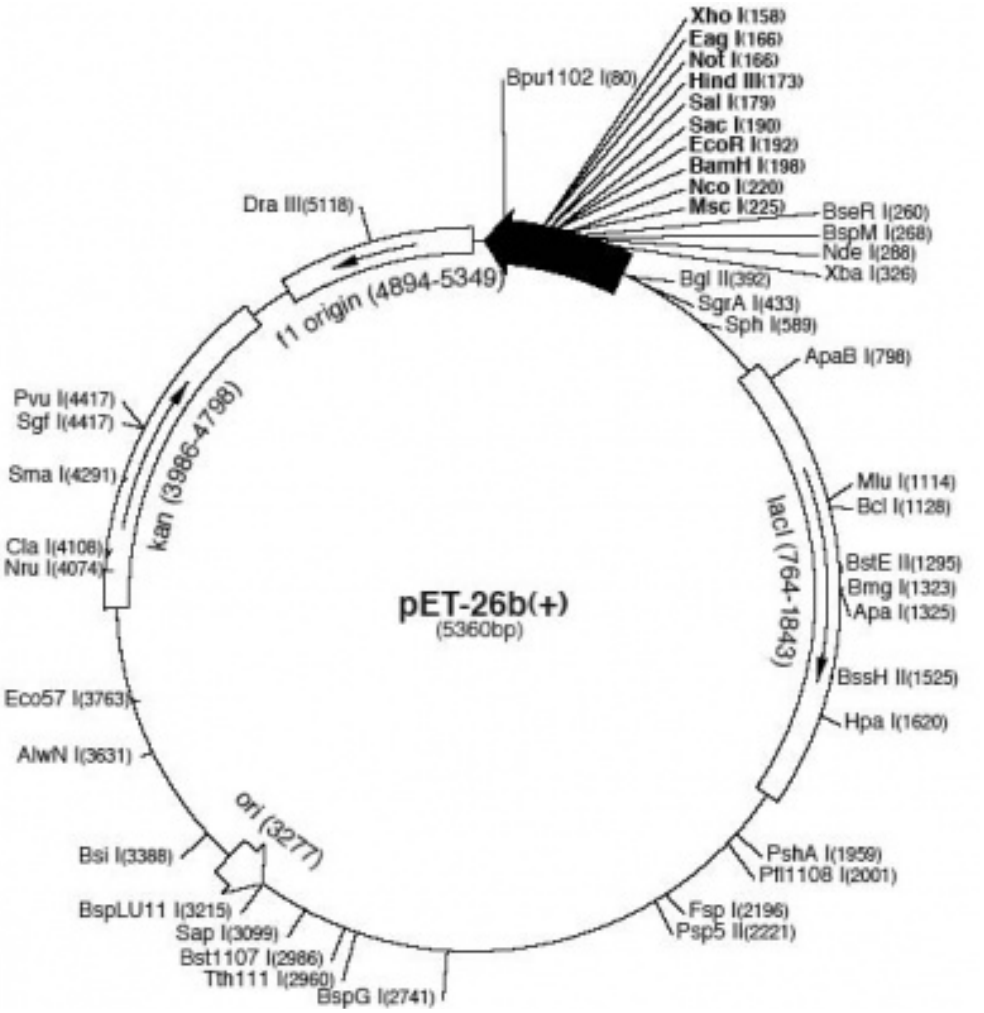

Figure 8.6 Map of pET-26b(+) vector

The pET-26b(+) vectors was sourced for improving the expression of the CD3e scFv described in Chapter 5. Furthermore, it was employed for the expression of the BiTE antibody created in Chapter 5. From this map the multiple cloning site and kanamycin resistance gene can be observed.

(http://www.merck-chemicals.se/life-science-research/vector-table-novagen-pet-vector-table/c_HdSb.s1O77QAAAEhPqsLdcab?PortalCatalogID=merck4biosciences&CountryName=Ireland)

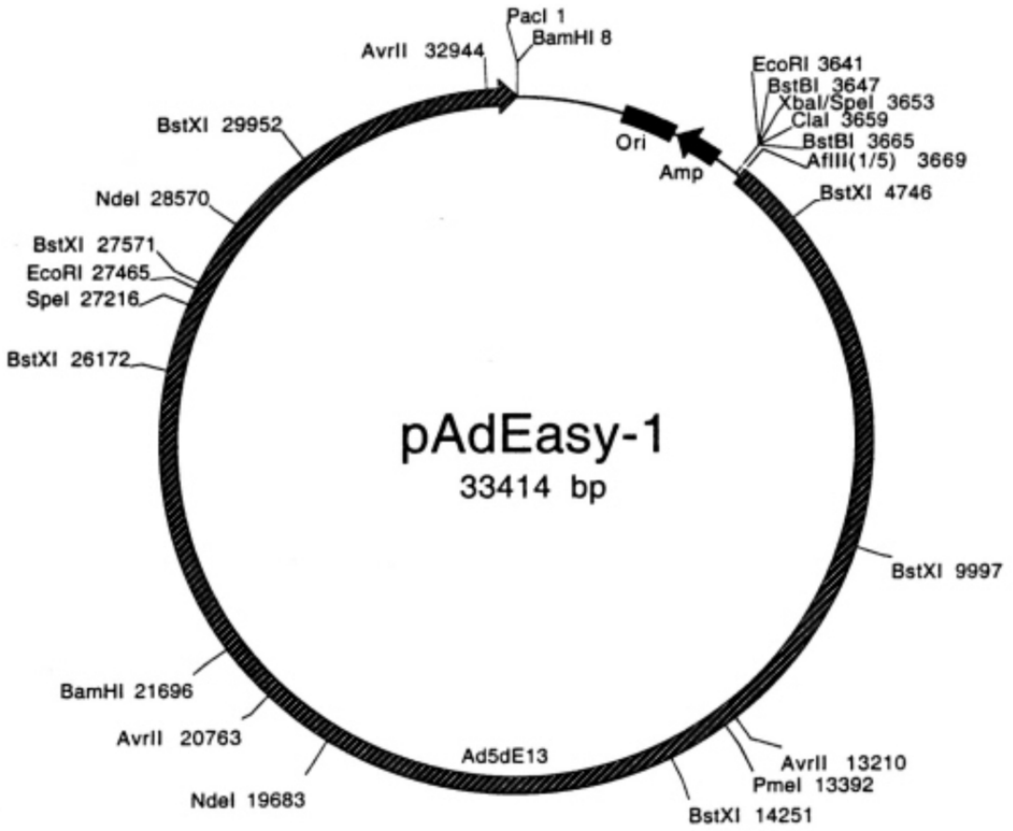

Figure 8.7 Map of pAdEasy-1 vector

The pAd-Easy-MSLN-iCre-HA-FLAG vector was purchased from Addgene for the mammalian expression of the recombinant MSLN protein described in Chapter 3. (https://www.addgene.org/16400/)

APPENDIX D

5.2 DNA extraction from agarose gels

Before starting the preparation:

- Check if Wash Buffer NT3 was prepared according to section 3.

1 Excise DNA fragment/ solubilize gel slice

Note: Minimize UV exposure time to avoid damaging the DNA. Refer to section 2.5 for more tips on agarose gel extraction.

Take a clean scalpel to excise the DNA fragment from an agarose gel. Remove all excess agarose.

Determine the weight of the gel slice and transfer it to a clean tube.

+ 200 µL NTI per 100 mg gel

For each **100 mg of agarose gel < 2 %** add **200 µL Buffer NTI**.

For gels containing > 2 % agarose, double the volume of Buffer NTI.

Incubate sample for **5–10 min** at **50 °C**. Vortex the sample briefly every 2–3 min until the gel slice is **completely** dissolved!

50 °C 5–10 min

2 Bind DNA

Load sample

Place a **NucleoSpin® Gel and PCR Clean-up Column** into a Collection Tube (2 mL) and load up to 700 µL sample.

11,000 x *g* 30 s

Centrifuge for **30 s** at **11,000 x *g***. Discard flow-through and place the column back into the collection tube.

Load remaining sample if necessary and repeat the centrifugation step.

3	**Wash silica membrane** Add **700 µL Buffer NT3** to the NucleoSpin® Gel and PCR Clean-up Column. Centrifuge for **30 s** at **11,000 x *g***. Discard flow-through and place the column back into the collection tube. <u>Recommended:</u> Repeat previous washing step to minimize chaotropic salt carry-over and low A_{260}/A_{230} (see section 2.7 for detailed information).	 **+ 700 µL NT3**  **11,000 x *g* 30 s**  **+ 700 µL NT3**  **11,000 x *g* 30 s**
4	**Dry silica membrane** Centrifuge for **1 min** at **11,000 x *g*** to remove Buffer NT3 completely. Make sure the spin column does not come in contact with the flow-through while removing it from the centrifuge and the collection tube. <u>Note:</u> *Residual ethanol from Buffer NT3 might inhibit enzymatic reactions. Total removal of ethanol can be achieved by incubating the columns for 2–5 min at 70 °C prior to elution.*	  **11,000 x *g* 1 min**
5	**Elute DNA** Place the NucleoSpin® Gel and PCR Clean-up Column into a **new** 1.5 mL microcentrifuge tube (not provided). Add **15–30 µL Buffer NE** and incubate at **room temperature** (18–25 °C) for **1 min**. Centrifuge for **1 min** at 11,000 x *g*. <u>Note:</u> *DNA recovery of larger fragments (> 1000 bp) can be increased by multiple elution steps with fresh buffer, heating to 70 °C and incubation for 5 min. See section 2.6 for detailed information.*	 **+ 15–30 µL NE RT 1 min**  **11,000 x *g* 1 min**

8.8 NucleoSpin Gel and PCR clean-up Kit taken directly from the manufacturers handbook.

6 NucleoSpin® Plasmid QuickPure protocol – isolation of high-copy plasmid DNA from *E.coli*

Before starting the preparation:

- Check if Wash Buffer AQ was prepared according to section 3.

1 Cultivate and harvest bacterial cells

Use **1–3 mL** of a saturated ***E.coli* LB culture**, pellet cells in a standard benchtop microcentrifuge for 30 s at **11,000 x *g***. Discard the supernatant and remove as much of the liquid as possible.

11,000 x *g*, 30 s

2 Cell lysis

Add **250 µL Buffer A1**. Resuspend the cell pellet completely by vortexing or pipetting up and down. Make sure no cell clumps remain before addition of Buffer A2!

+ 250 µL A1

Resuspend

Attention: Check Buffer A2 for precipitated SDS prior to use. If a white precipitate is visible, warm the buffer for several minutes at 30–40 °C until precipitate is dissolved completely. Mix thoroughly and cool buffer down to room temperature (18–25 °C).

+ 250 µL A2

Mix

RT, 5 min

Add **250 µL Buffer A2**. Mix gently by inverting the tube **6–8 times**. Do not vortex to avoid shearing of genomic DNA. Incubate at **room temperature** for up to **5 min** or until lysate appears clear.

+ 300 µL A3

Mix

Add **300 µL Buffer A3**. Mix thoroughly by inverting the tube **6–8 times** until blue samples turn colorless completely! Do not vortex to avoid shearing of genomic DNA!

Make sure to neutralize completely to precipitate all the protein and chromosomal DNA.

3 Clarification of lysate

Centrifuge for **5 min** at **11,000 x *g*** at room temperature.

11,000 x *g*, 5–10 min

4 Bind DNA

Place a NucleoSpin® Plasmid QuickPure Column in a Collection Tube (2 mL) and decant the supernatant from step 3 or pipette a maximum of 750 µL of the supernatant onto the column. Centrifuge for **1 min** at **11,000 x *g***. Discard flowthrough and place the NucleoSpin® Plasmid QuickPure Column back into the collection tube.

Repeat this step to load the remaining lysate.

Load supernatant

11,000 x *g*, 1 min

5 Wash silica membrane

Add **450 µL Buffer AQ** (supplemented with ethanol, see section 3). Centrifuge for **3 min** at **11,000 x *g***.

Very carefully discard the collection tube and the flowthrough and make sure the spin cup outlet does not touch the wash buffer surface. Otherwise repeat the centrifugation step.

+ 450 µL AQ

11,000 x *g*, 3 min

6 Dry silica membrane

The drying of the NucleoSpin® Plasmid QuickPure Column is performed by the 3 min centrifugation in step 5.

7 Elute DNA

Place the NucleoSpin® Plasmid QuickPure Column in a 1.5 mL microcentrifuge tube (not provided) and add **50 µL Buffer AE**. Incubate for 1 min at **room temperature**. Centrifuge for **1 min** at **11,000 x *g***.

Note: For more efficient elution procedures and alternative elution buffer (e.g., TE buffer or water) see section 2.5.

+ 50 µL AE

RT, 1 min

11,000 x *g*, 1 min

8.9 NucleoSpin Plasmid Purification Kit taken directly from the manufacturers handbook.

APPENDIX E

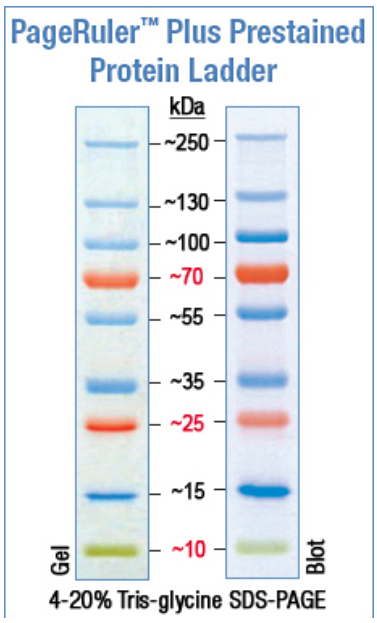

Figure 8.10 Page-Ruler^{TM} Plus Prestained Protein ladder

https://www.thermofisher.com/order/catalog/product/26619

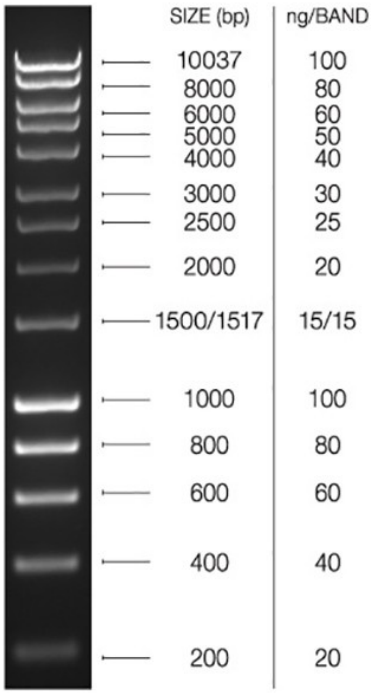

Figure 8.11 Bioline HyperLadder^{TM} 1Kb

https://www.bioline.com/hyperladder-1kb.html